ABSTRACT

Title of Dissertation: HARMONIC AND RANDOM VIBRATION DURABILITY INVESTIGATION FOR SAC305 (Sn3.0Ag0.5Cu) SOLDER INTERCONNECTS

Yuxun Zhou, Doctor of Philosophy, 2008

Dissertation directed by: Professor Abhijit Dasgupta

Department of Mechanical Engineering

Vibration loading is commonly encountered during the service life of electronic products. However, compared to thermal cycling durability, vibration durability is more complex and has been less investigated. In surface mount technology, solder joints are the primary mechanical, thermal and electrical interconnects between the component and the PWB. So the reliability of solder joints is very crucial for most electronic assemblies. The vibration durability of Pb-free solder joints is the focus of this dissertation.

The characteristics of the stress from vibration loading are low amplitude and high frequency, while those from cyclic thermal loading are high amplitude and low frequency. In this study, several exploratory vibration tests were conducted, using both narrow band and broad-band, step-stress excitation at several different isothermal and thermal cycling conditions. The effect of thermal pre-aging on solder joint vibration failures was also investigated.

Some of the vibration durability results were analyzed in detail, to obtain quantitative insights into the vibration fatigue behavior of the SAC305 solder material. A time-domain approach was

adopted to investigate the durability of solder interconnects under different kinds of vibration and quasi-static mechanical loading.

First, the solder interconnects were subjected to narrow-band (harmonic) vibration loading. The test were conducted at the first natural frequency of the test board using constant-amplitude excitation and solder fatigue properties were extracted with the help of a time-domain analysis that is based on quasi-static finite element simulation. Compared to broad-band step-stress vibration durability tests, the advantage of the harmonic constant-amplitude test is less complexity in the model extraction process, hence, less uncertainty in the desired fatigue constants. Generalized strain-based S-N curves have been obtained for both SAC305 and Sn37Pb solder materials. The strain-life model constants show that SAC305 solder material has superior fatigue properties compared to Sn37Pb solder material under low-cycle fatigue loading, while the reverse is true for high-cycle fatigue loading. These results are consistent with test results from other researchers. In actual application, SAC305 assemblies almost always fail before Sn37Pb assemblies under comparable vibration excitation because of (i) higher solder strain at a given excitation level; and (ii) multiple failure modes such as copper trace cracking.

Next, durability was investigated under step-stress, broad-band (random) excitation. These test results show that SAC305 interconnects are less durable than Sn37Pb interconnects under the random excitation used in this study, which agrees with the harmonic durability results. The random and harmonic durability results were quantitatively compared with each other in this study. Finite element simulation was used to investigate the stress-strain response in the interconnects. The output of this simulation is the strain transfer function due to the first flexural mode of the PWB. This transfer function is used to obtain the solder strain from the measured board strain. This fatigue assessment method demonstrated that the model constants obtained

from the harmonic test overestimate the fatigue life under random excitation by an order of magnitude. The causes for this discrepancy were systematically explored in this study.

The effects of cyclic loading and mean stress on the vibration durability were addressed and found to be minimal in this study. The stress-strain curves assumed for the solder material were found to have a very large effect on the durability constants, thus affecting the agreement between harmonic and random durability results. The transient response of the components on the test board under both harmonic and random excitation was also included in the strain transfer function with the help of dynamic implicit simulation, and found to have a much stronger effect on the vibration durability at the high frequencies used in broad-band excitation compared to the low frequency used in narrow-band test. Furthermore, the higher PWB vibration modes may play a strong role and may need to be included in the strain transfer-function. This study clearly reveals that the solder strain analysis for broad-band random excitation cannot be limited to the quasi-static strain transfer-function based on the first PWB flexural mode, that has been used in some earlier studies in the literature.

The time-domain approach used in this study provided fundamental and comprehensive insights into the key factors that affect vibration durability under different types of excitation, thus leading to a generalized S-N modeling approach that works for both harmonic and random vibration loading.

HARMONIC AND RANDOM VIBRATION DURABILITY INVESTIGATION FOR Sn3.0Ag0.5Cu SOLDER INTERCONNECTS

by

Yuxun Zhou

Dissertation submitted to the faculty of the Graduate School of the

University of Maryland, College Park in partial fulfillment

of the requirements for the degree of

Doctor of Philosophy

2008

Advisory Committee:

Professor Abhijit Dasgupta, Chair and Advisor

Professor Donald Barker

Professor Balakumar Balachandran

Professor Sung Lee

Associate Professor Patrick McCluskey

DEDICATION

To my mother and father, who gave me the freedom to pursue the knowledge and provided all the support I needed and stood with me in all circumstances during this period.

ACKNOWLEDGEMENTS

I would like to acknowledge the professors and staff of Mechanical Engineering Department and CALCE Electronic Products and Systems Center who supported me in the project.

I also would like to thank my lab-mates, Joe, Dan, Gayatri, Koustav, Lynn and so on. My acknowledgement is also given to other CALCE students, Yong, Jie, Gustavo…, for their valuable discussion and knowledge.

I would like to thank the students from the German exchange program, Kris, Stefan, Elma, for their help in the project.

I am grateful to Prof. Balachandran and all students in vibration lab, for providing the experimental equipment and consideration during my experiments.

In particular, I would like to acknowledge my dissertation committee: Dr. Barker, Dr. Balachandran, Dr. McCluskey and Dr. Lee for evaluating my dissertation and providing valuable suggestions.

Most of all, I would like to thank my advisor, Dr. Abhijit Dasgupta, for his valuable guidance and support. I deeply appreciate his patience, understanding, encouragement, and the time he spent discussing and explanaing the various technical issues in this study.

Chapter 1 Introduction

Pb-free soldering in the electronics industry is a part of the global environmental movement to transition to Pb-free products. The Pb-free transition advanced much more rapidly in the Japanese and European elecronics industries. Interestingly, Europe passed legislation to ban Pb-based solders by 2006, although the contribution of electronic products to global Pb contamination was estimated to be less than 1%. In fact, it is not even clear at this time whether the Pb-free replacements have a worse environmental impact because of higher energy consumption, higher material costs and a different set of toxicity impacts on the environment.

In the U.S. electronics industry, the transition to Pb-free solders was initiated in the early 1990's. Since then, research effort has gained significant momentum to identify new Pb-free materials, in order to keep up with business opportunities in an increasingly 'green' electronics market-place.

1.1 Background and motivation

The development of Pb-free solder materials will be introduced in this section, including the selection criteria of Pb-free alloys. The challenges in switching from eutectic SnPb to Pb-free alloys will also be reviewed here.

1.1.1 *Why Pb-free?*

Pb-based solders have been used for a few thousand years since they are inexpensive and have good process characteristics. Approximately 5 million tons of Pb is consumed globally every year, with 81% used in storage batteries. The toxicological effects of lead (Pb) have brought about the reduction or elimination of Pb use in many major industries. Historically, this has been fostered by legislation. Europe proposed the prohibition of Pb-

based solders [WEEE, 2001]. In July 2006, several European institutions, including European Commission (EC), Waste Electrical and Electronic Equipment (WEEE) and Restriction of Hazardous Substances (ROHS) legislated the ban of Pb in electronics. Furthermore, several Japanese electronics manufacturers have successfully created a market differentiation based on "green" products that use Pb-free solders. In recent years, industrial and research groups related to Pb-free solders have increased dramatically due to the prohibition of leaded solder by environmental and health concerns. AMD published the Pb-free strategy from 2000 to 2003 [Hayward, 2000] to transition from Pb-based to Pb-free materials. JEDEC defined Pb-free electronics in 2002 as electrical and electronic assemblies and components in which the Lead (Pb) level in any of the raw materials and the end product is less than or equal to 0.1% by weight and which also meets any Pb-fee requirements/definitions adopted by the ROHS Directive 2002/95/EC [JEDEC, 2002].

Finally the switch from Pb-based solder materials to Pb-free materials is the tread all over the world. There are several major drivers for this change [Zhang, 2004]

- Hazards of Pb-based materials

  Lead is one of the top seventeen chemicals having the greatest threat to human health. Medical studies have shown that lead can harm the kidney, liver, blood and central nervous system once absorbed in the body. The real risk of lead in the electronics industry doesn't come from the production environment but from the disposal of electronic products containing lead, which can leach into and contaminate underground water.

- Legislation

This driver is related to the first one. Since lead is poisonous, its application in many areas has been banned for many years in USA and Europe, such as plumbing, paint, gasoline and so on. Japan has passed seven laws and acts for collecting and recycling waste products, including household appliances and electronic products, to the producers of these products.

- Marketing and profit

  Pb-free products are labeled as "green" products, which provides an advantage to those segments of the market that are concerned about environmental damage. Market forces may become a major driver in the conversion to Pb-free soldering for the electronics industry. Their interest is also driven by the desire to increase the operating temperature of their products.

Another key issue and goal in Pb-free technology is sound metallurgy and long-term joint reliability. This is critical to ensure that future generations of electronic circuits don't fail in the field and result in catastrophe, especially, for example, electronics guidance systems in aerospace applications. Pb-free solders have significantly different microstructure and composition than Pb-based solders, thus resulting in different mechanical, electrical, and thermal properties. The effect of these different properties on the reliability of electronic products is a critical issue. Equivalent or better reliability of the Pb-free solder is critical to convince the electronics industry to make this transition. Among the failure mechanisms of Pb-free solder materials, fatigue is one of the most critical concerns. The reliability of Pb-free solder joints have been investigated under all kinds of life-cycle stress conditions, such as thermal cycling, vibration, shock, and so on, by researchers from all over the world.

Compared to the mechanical properties database for Pb-based solder materials, the information for Pb-free solder materials is still inadequate. The following data are needed for Pb-free solder materials in order to replace Pb-based solders:

- Mechanical and thermo-mechanical characterization: elastic-viscoplastic deformations and thermal expansion coefficients at the length scale of typical solder joints,
- Durability characterization: durability under thermal cycling, vibration, shock/drop, humidity cycling, and combinations of the above
- Failure mechanisms of Pb-free solder joints under different loading conditions: failure site, failure mode and microstructure evolution
- Solder-metallization interactions: characterization of the different intermetallic compounds (IMCs) that form between different Pb-free solder materials and different metallization materials on solderable surfaces of PWBs and components.

Populating this database will be very helpful in promoting Pb-free solder application and in the gradual elimination of Pb from electronics.

Zeng and Tu [Tu and Zeng, 2002] reviewed six aspects of reliability of Pb-free solders: (1) interfacial reactions between Pb-free solder and thick metallization of bond-pad on the substrate-side, (2) interfacial reactions between Pb-free solder and thin-film under-bump metallization on the chip-side, (3) the growth of a layered intermetallic compound (IMC) by ripening in solid state aging of solder joints, (4) a long range interaction between chip-side and substrate-growth on Pb-free finish on Cu leadframe (5)

electromigration in flip chip solder joints and finally (6) Sn whisker growth on Pb-free finish on Cu leadframe. Similar work has been conducted by Schubert and co-workers A [Schubert, et al 2002] on the characterization, testing and durability of Pb-free solders. The application of Pb-free solder to automotive electronics was discussed by Whitten [Whitten, 2000]. Kujala [Kujala, et al, 2002] presented techniques for the transition to Pb-free manufacturing using land grid array packaging.

1.2 Problem Statement and Objectives

Based on the data needed, and the background information described in previous Section, solder durability characterization is one of the critical issues that needs attention. Depending on the life-cycle application condition of electronic systems, the solder joints experience different kinds of loading, such as thermal cycling, vibration, shock, and so on. This study will focus on the vibration durability for SAC305 solder materials and interconnects. The corresponding vibration durability for Sn37Pb will also be investigated for purposes of comparison. Results will also be compared to baseline results in the literature. Vibration loading is important because it is commonly encountered during the service life of many classes of electronic products. However, compared to thermal cycling durability, analysis of vibration durability is more complex and has received less attention in the literature. The characteristics of the stress from vibration loading are low amplitude and high frequency, while those of thermal cycling loading are high amplitude and low frequency. In order to have a better understanding of Pb-free vibration durability, a generalized durability model is very helpful. Without a durability model, test results cannot be quantified and extrapolated to other components and other loading conditions. Literature review of related work shows that most of the

vibration durability testing by industry and institutional researchers has relied on step-stress random excitation. There are two reasons for this type of experiments:

- Similarity to life-cycle usage conditions: most vibration loading in actual application conditions include random vibration over a broad frequency band, rather than at a single frequency.
- Acceptable experiment time: compared to low cycle thermal cycling durability tests, vibration durability tests are characterized as high cycle durability test. In order to avoid overstress failures, the loading amplitude needs to be carefully limited. This may result in long time and high testing cost. In order to decrease the cost and experiment time, step-stressing during vibration durability testing is a well accepted method in industry.

However, the extraction of durability model constants from the random step-stress durability test results is very complex and difficult because of the random response history and varying damage accumulation rate. To overcome these complexities, a set of less complex and easily quantifiable durability tests have been conducted in this study. The objectives of this study are:

1) Obtain the generalized strain-life durability model for SAC305 and Sn37Pb solders from constant amplitude harmonic durability test using a time-domain approach
2) Verify the model constants and the time-domain durability modeling approach using random step-stress durability test results
3) Check the durability model sensitivity on the material stress-strain properties

4) Verify the relative importance of the inertial forces generated in the solder joint by transient response of components, relative to the PWB, under both harmonic and random excitation
5) Check the cyclic effect, mean stress effect to the vibration durability

1.3 Literature Review

The related work in the literature will be reviewed in this section, including quasi-static mechanical cycling durability and vibration durability. Quasi-static mechanical cyclic loading includes cyclic bending, cyclic shearing, at a relatively low loading rate compared to dynamic loading like vibration and repetitive shock loading. Commonly used durability models will also be examined, including the model will be used in this study.

In order to quantify the loading and response in random vibration tests, cycle counting techniques are needed to obtain range distribution functions. The cycle counting algorithm and damage superposition methods used in this study will also be briefly introduced.

1.3.1 *Constitutive properties*

The material property of new Pb-free materials is one of the critical focuses before the successful transition from lead-based alloys to Pb-free alloys. The Pb-free solder alloys have a very different microstructure compared to the traditional lead-based solder alloys, which results in different strength, time-independent plastic and time-dependent creep material properties. Darveaux [Darveaus, 1992] provided extensive data on 62Sn36Pb2Ag, 60Sn40Pb, 96.5Sn3.5Ag, 97.5Pb2.5Sn, and 95Pb5Sn solder. All the data were collected on actual soldered assemblies to properly account for the effects of grain

size and intermetallic compound distribution. Tensile and shear loading were employed in the strain rate range between 10^{-8} and 10^{-1} s^{-1} and temperature range between 25°C and 135°C. The creep model in this study is shown in Equation 1.1.

$$\gamma_c = \frac{d\gamma_s}{dt}t + \gamma_T\left(1 - \exp\left(-Bt\frac{d\gamma_s}{dt}\right)\right) \qquad 0.1$$

Where γ_c is the creep strain, $\frac{d\gamma_s}{dt}$ is the steady-strain creep rate, γ_T is the transient creep strain, and B is the transient creep coefficient.

The time-independent plastic strain component γ_p of the deformation is described with a power-law relationship, as shown in Equation 1.2, where C_2 and *m* are constants.

$$\gamma_p = C_2\left(\frac{\tau}{G}\right)^m \qquad 0.2$$

The elastic shear modulus *G* is temperature dependent:

$$G = G_0 - G_1 T' \left(^\circ C\right) \qquad 0.3$$

Where G_0 is the modulus at 0^oC, G_1 gives the temperature dependence, and T' is the temperature in ^oC. The total inelastic strain is given by the sum of creep strain and plastic strain.

$$\gamma_{in} = \gamma_c + \gamma_p \qquad 0.4$$

Darveaux's model constants were obtained from experiments on actual solder joints. The advantage of actual solder joint samples is that microstructural length-scale effects are preserved correctly in the test specimens. However, it does introduce some experimental error compared to testing bulk samples. First, the cross-sectional area of a controlled collapse joint varies slightly across its thickness, so the stress and strain distribution in

the material will not be perfectly uniform. Second, the solder material is constrained at the interfaces with the substrate and or IC chip, which also affects the stress and strain distribution. The final results from this paper are the material properties constants for different Pb-free solder alloys and SnPb baseline alloy. These material constants are very useful for the simulation of the Pb-free assemblies and for comparison of the results with baseline SnPb assemblies.

Table 1.1: Solder alloy material constants [Darveaus, 1992]

		Elastic		Steady State Creep				Transient Creep		Plastic	
solder		G_0 (10^6 lbf/in^2)	G_1 (10^3 lbf/in^2)	C_1 (k/s/lb f/in^2)	α	n	Q (eV)	B	γ_T	C_2	m
60Sn40Pb	Shear	1.9	8.1	0.198	1300	3.3	0.548	440	0.020	2.3 (10^{13})	5.6
	Tensile	5.0	22.0	0.114	751	3.3	0.548	762	0.012	6.1 (10^{11})	5.6
62Sn36Pb 2Ag	Shear	1.9	8.1	0.0989	1300	3.3	0.548	137	0.037	6.6 (10^7)	3.5
	Tensile	5.0	22.0	0.0571	751	3.3	0.548	237	0.021	5.6 (10^6)	3.5
96.5Sn3.5 Ag	Shear	2.8	10.0	4.89 (10^{-4})	1300	5.5	0.40	147	0.086	2.0 (10^{11})	4.4
	Tensile	7.6	28.0	2.82 (10^{-4})	751	5.5	0.40	255	0.050	1.0 (10^{10})	4.4
97.5Pb2.5 Sn	Shear	1.3	1.5	5.04 (10^7)	1200	7.0	1.20	137	0.115	2.8 (10^{10})	4.0
	Tensile	3.5	4.1	2.91 (10^7)	693	7.0	1.20	237	0.066	1.8 (10^9)	4.0

Similar mechanical characterization for Pb-free alloy has been carried out by many researchers after the appearance of Pb-free alloys, including [Amagai, 2002; Wiese, 2001; Zhang, 2003; Cuddalorepatta, 2005].

Amagai [Amagai, 2002] characterized the rate-dependent plasticity to represent the inelastic deformation behavior for Sn-Ag-based Pb-free solders. The material parameters in the constitutive models were determined by a direct method combining both rate-dependent and rate-independent plastic strains. This constitutive model unifies both rate-dependent creep behavior and rate-independent plastic behavior occurring concurrently at the same time in the solders.

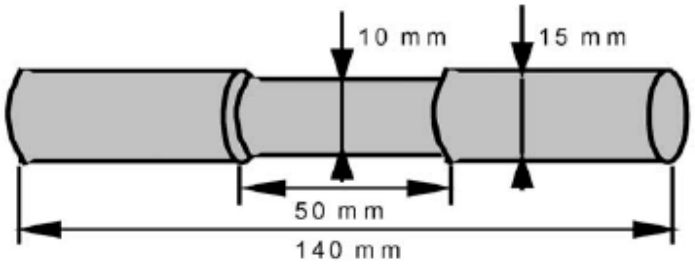

Figure 1.1: Specimen design of experimental tests [Amagai, 2002]

A bulk solder specimen, shown in Figure 1.1, was tested in a feedback controlled servo-electric testing machine, and a data acquisition system was used to record load and displacement. The constitutive models are mostly separated into rate-independent plastic deformations and time-dependent creep deformations. However, it's very difficult to separate the plastic strain from creep strain based on the mechanical experimental tests. A unified constitutive model proposed by Anand [Anand, 1985] is therefore used in Amagai's [Amagai, 2002] study as shown in equation 1.5.

$$\sigma^* = \frac{\bar{s}}{\varsigma}\left\{\frac{1}{A}\frac{d\varepsilon^p}{dt}\exp\left(\frac{Q}{R\theta}\right)\right\}^n \times \sinh^{-1}\left[\left\{\frac{1}{A}\frac{d\varepsilon^p}{dt}\exp\left(\frac{Q}{R\theta}\right)\right\}^m\right] \qquad 0.5$$

The obtained material constants are listed in following table.

Table 1.2: material parameters for different solder alloys [Amagai, M., 2002]

Parameter	63Sn37Pb	62Sn36Pb2Ag	Sn3.5Ag0.75Cu	Sn2.0Ag0.5Cu
Q/R (K^{-1})	9400	9400	8400	8400
A (s^{-1})	1.09×10^{7}	8.49×10^{6}	4.61×10^{6}	2.42×10^{7}
ζ	0.07	0.065	0.038	0.043
m	0.316	0.322	0.162	0.168
$\bar{s}\,(MPa)$	0.998	0.990	1.04	1.005
n	1.37×10^{-5}	6.71×10^{-4}	4.60×10^{-3}	8.10×10^{-4}

The author also checked the growth of intermetallic compound (IMC) layer for both Pb-free and SnPb alloys. The results in this study show that the thickness of IMC layers in Pb-based solders is typically higher than in Pb-free solders

Two Pb-free solder alloys (Sn96.5Ag3.5, Sn95.5Ag3.8Cu0.7) and two Pb-based solder alloys (Sn63Pb37, Sn59Pb40Ag1) were investigated and compared with each other by Wiese, S. et al [Wiese, 2001] in order to examine the reliability enhancement of the new Pb-free soldering technology. The mechanical and thermomechanical behavior (coefficient of thermal expansion, stress-strain corves at different strain-rates, ultimate strength) were examined by TMA, tensile tests, shear tests and creep tests. Two types of specimen were used in Wiese's study. The first type was a bulk dog-bone specimen. The second type was a flip chip joint. It's easy to derive stress-strain date from the force displacement data in case of bulk dog-bone specimens. While for the flip chip joints, where stress distribution is highly inhomogeneous, an FEA simulation was applied to evaluate the constitutive properties from the experimental raw data. Microstructural

analysis of SnPb, SnPbAg, SnAg, SnAgcu solders of near eutectic composition show significant differences between bulk and flip chip specimens. Therefore, the creep behavior of SnAg, SnAgCu solder in flip chip joints was found to be very different from that in bulk specimens.

1.3.2 *Mechanical cycling durability*

In addition to thermal cycling durability, cyclic mechanical durability is another critical issue for electronic assemblies, since they are subjected to cyclic mechanical loading during transportation, handling and operation. Compared with thermal cycling tests, mechanical cycling tests are inexpensive and easier to conduct in the laboratory. There are reasonable amounts of data in the literature for mechanical cycling durability of SnPb solder materials [Haswell, 2001; Haswell, Dasgupta, 2000; Vaynman, 1993; Zhang, 2004; Zhang, 2005; Kariya, et al., 2001, Krishna, 2002; Barker, 1994].

Zhang et al. [Zhang, 2004] investigated isothermal mechanical durability of three NEMI-.recommended Pb-free solders, 95.5Sn3.9Ag0.6Cu, 96.5Sn3.5Ag and 99.3Sn0.7Cu, which were tested on a thermal-mechanical-microscale (TMM) setup under two test conditions. The first test is under room temperature and relatively high strain rate, while the second test is under high temperature and low strain rate. Creep deformations dominate in the first test while rate-independent plastic deformations dominate in the second test. The damage metrics monitored in this study are total strain range (TSR), inelastic strain range (ISR) and cyclic work density. Failure is defined in this study when the load-carrying capacity of the specimen drops by 50%. The test data were presented in a power-law relationship in Equation 1.6 between all selected damage metrics.

$$D = C \cdot N_f^n \qquad 1.6$$

The power-law durability parameters for three Pb-free solders are listed in Table 1.3 for this test condition [Zhang, 2005].

Table 1.3: Power-law durability parameters for three Pb-free solders [Zhang, 2005]

Solder		Room temperature and high strain rate condition		
		n	C	R^2
Sn3.9Ag0.6Cu	TSR	-0.16	0.25	0.40
	ISR	-0.49	2.4	0.92
	W	-0.57	201	0.96
Sn3.5Ag	TSR	-0.23	0.33	0.61
	ISR	-0.56	3.2	0.86
	W	-0.68	371	0.92
Sn0.7Cu	TSR	-0.22	0.28	0.95
	ISR	-0.50	1.1	0.98
	W	-0.60	72.6	0.98

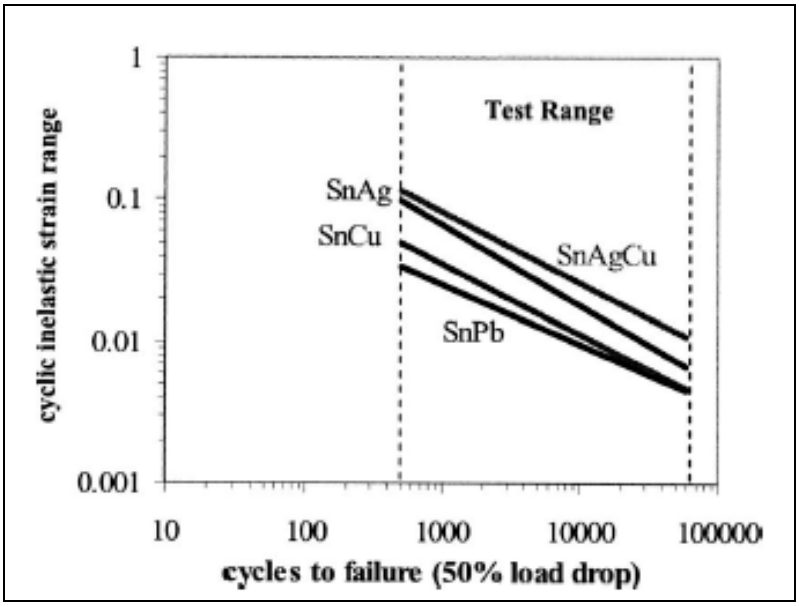

Figure 1.2: ISR-based damage relation comparison of four solder alloys at room temperature

The obtained durability properties were compared with those of eutectic 63Sn37Pb solder. At the second test condition (room temperature and high strain-rate) 95.5Sn3.9Ag0.6Cu and 96.5Sn3.5Ag solders show better mechanical durability than Sn37Pb solder, while the 99.3Sn0.7Cu solder performs worse than Sn37Pb solder. This comparison can be graphically seen in Figure 1.2 which shows the ISR-based damage relations for three Pb-free solder alloys and for eutectic Sn37Pb solder alloy. The results show that it's possible to design Pb-free electronics for mechanical cycling environments.

Kariya et al investigated the fatigue lives and damage mechanisms of Sn-Ag-X (X = Bi and Cu) solder alloys under creep-fatigue interaction mode. The strain-range partitioning approach [Kariya, 2001] was used to characterize the creep-fatigue interactions in these alloys.

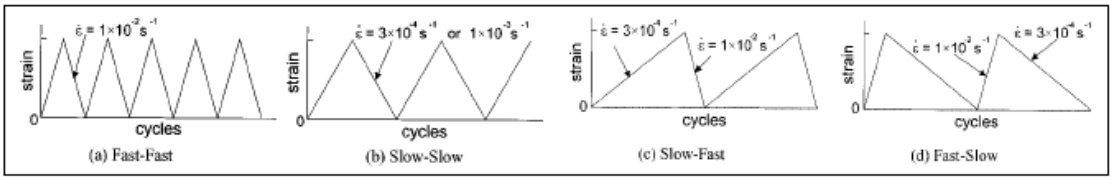

Fig. 1. Strain profiles.

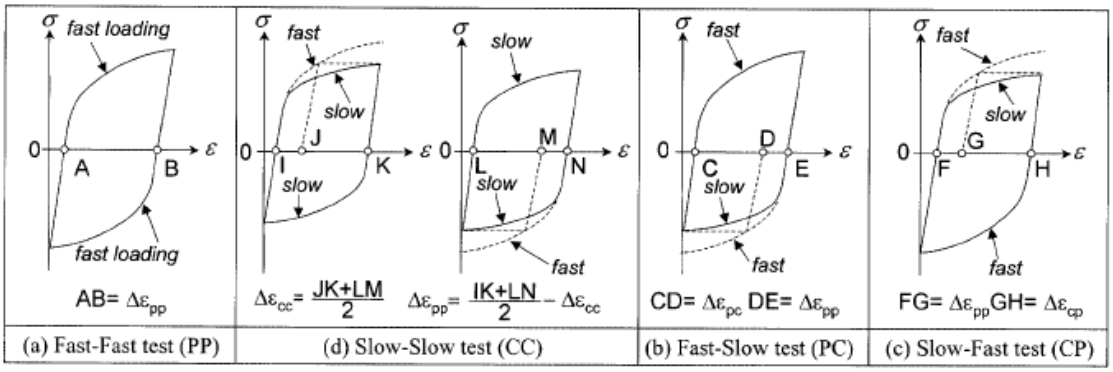

Figure 1.3: Typical hysteresis loops for different strain waveforms

The author conducted strain-controlled isothermal quasi-static fatigue tests in air at room temperature, using a servo-controlled electro-hydraulic testing machine. The total strain range, $\Delta\varepsilon_{total,}$ was chosen to be in the range between 0.3 and 1.3 percent. A fast ramp rate of 10^{-2}/s and a slow ramp rate of 3×10^{-4}/s were used in asymmetrical cycling. Fatigue life was defined as the number of cycles to 50 percent load reduction. The basic concept of strain range partitioning (SRP) method is that the entire reversed inelastic strain range can be partitioned into four generic components identified with cyclic creep strain (cc), cyclic plastic strain (pp), tensile creep strain reversed with plastic strain (cp) and tensile plastic strain reversed with creep strain (pc). Figure 1.3 shows schematic illustrations of the four typical hysteresis loops and the strain-range partitioning concept. Equation 1.7 expresses the power law relationship between number of cycles to failure and the partitioned strain ranges.

$$\frac{1}{N_f} = \left(\frac{\Delta\varepsilon_{pp}}{A_{pp}}\right)^{n_{pp}} + \left(\frac{\Delta\varepsilon_{cc}}{A_{cc}}\right)^{n_{cc}} + \left(\frac{\Delta\varepsilon_{cp}}{A_{cp}}\right)^{n_{cp}} + \left(\frac{\Delta\varepsilon_{pc}}{A_{pc}}\right)^{n_{pc}} \quad 0.7$$

The obtained model constants are listed in Table 1.5. It shows that the fatigue life of eutectic Sn3.5Ag binary alloy markedly decreases with increasing content of bismuth, withd additions of bismuth over 2% reducing the fatigue life by 90%.

Table 1.4: strain based durability model constants for Pb-free solder alloys [Kariya, 2001]

Model Constants	**Sn3.5Ag**	**Sn3.5Ag1Cu**	**Sn3.5Ag2Bi**	**Sn3.5Ag5Bi**
n_{pp}	1.92	1.82	1.85	2.50
A_{pp}	1.06	1.47	0.51	0.1
n_{cc}	1.56	1.22	2.27	2.44
A_{cc}	0.24	7.46	0.24	0.03
n_{cp}	1.67	0.71	1.41	1.03
A_{cp}	1.92	140.2	0.74	0.63
n_{pc}	0.98	0.65	2.43	0.88
A_{pc}	4.76	565.6	0.04	4.39

Creep damage is cancelled in a reversible symmetric strain cycling such as slow-slow test as shown in Figure 1.3. Therefore the strain rate doesn't have a dramatic effect on fatigue lives of all alloys tested in symmetrical cycling, while the creep damage is the dominant failure mechanism in slow-fast strain cycling for all alloys.

Among the various Pb-free solders, the SnAgCu family of solders has emerged as one of the leading candidates for high volume implementation. Krishna, et al [Krishna, Mahesh, and Andrew, 2002] examined the mechanical fatigue reliability of SnAgCu PBGAs on FR4 boards. Mechanical bending fatigue durability is a critical performance metric for applications such as repeated quasi-static key-press in key-pads, handling and drop induced flexure in portable electronics, vibration of electronic assemblies, etc . The Pb-free reliability data are compared with Sn37Pb alloy, as shown in Figure 1.4.

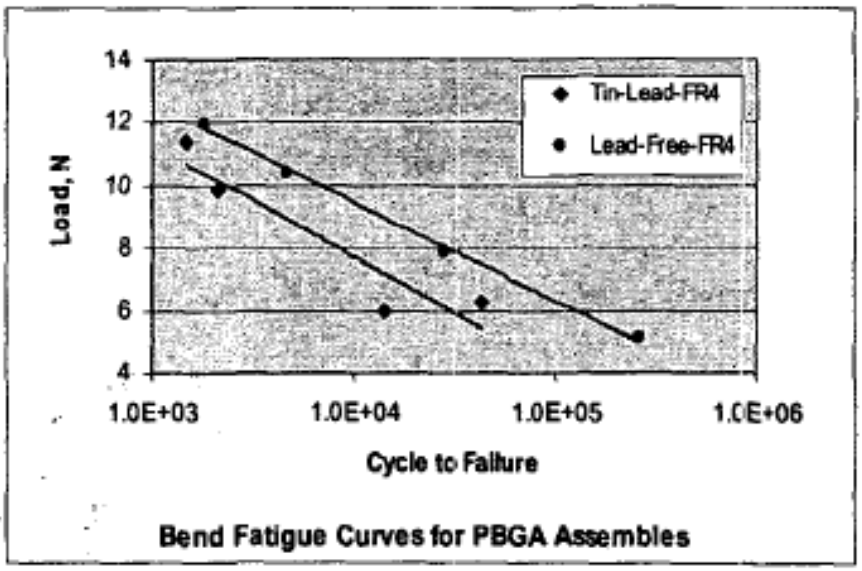

Figure 1.4: Fatigue curves for PBGA assemblies with various solder pastes [Krishna, 2002]

The number of cycles to failure increases exponentially as the load decreases. This behavior is characteristic of material fatigue. Overall, the data from this study indicates that across the spectrum, the mechanical bending fatigue durability of Pb-free PBGAs is significantly superior to that of Sn37Pb PBGAs under quasi-static cycling. These results demonstrate that in addition to the obvious environmental and product differentiation benefits, migrating to Pb-free solder assemblies could actually enhance the reliability of portable products.

Park and Lee [Park and Lee 2002] investigated the isothermal mechanical low cycle fatigue for both 63Sn/37Pb and Sn/3.5Ag/0.75Cu solder joints. The test was conducted under several loading phases with constant displacement control. Morrow energy model was examined and found to be a proper low cycle fatigue model for solder joints from this study. The different loading case was shown in **Figure 1.5** from pure tension to pure shear.

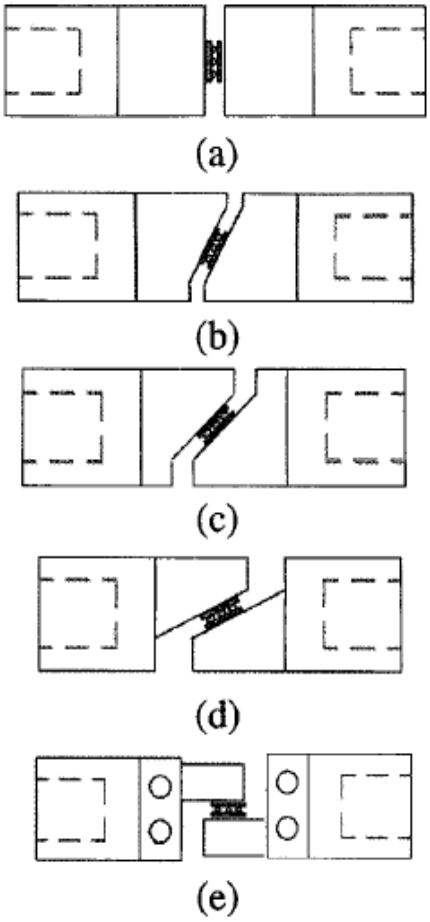

Figure 1.5: Test grip configuration. Loading phase of each specimen is (a) 0^{o} (pure tension) (b) 27^{o} (c) 45^{o} (d) 63^{o} (e) 90^{o} (pure shear)

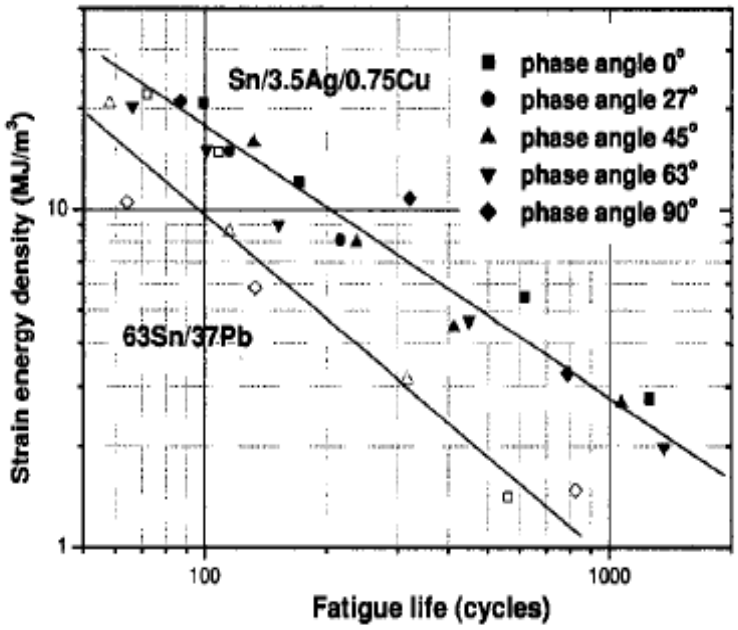

Figure 1.6: Fatigue life versus strain energy density

The low cycle fatigue test results for both SAC and SnPb was plotted in **Figure 1.6** with respect to the strain energy density. Throughout the whole test condition, Sn/3.5Ag/0.75Cu solder ally has longer fatigue life than 63Sn/37Pb alloy.

1.3.3 ***Vibration Durability***

Electronic assemblies can experience vibration loading during storage, transportation and operation, depending on the application. Compared to thermal cycling durability, the fatigue data for vibration is much less. In order to have a full understanding of the vibration fatigue properties, durability test and simulation have been conducted for Pb-free assemblies and compared with Pb-based solder alloy benchmark.

Among all the empirical work in vibration fatigue, Steinberg [Steinberg, 1998], who is probably the best known in the area of PWB vibration fatigue, proposed a simple rule of thumb for designing PWB's in a vibration environment. If the maximum deflection of the PWB is less than

a critical value, d, the component mounted at the center of the board has a life of at least 10^7 cycles under sinusoidal vibration or 2×10^7 cycles under random vibration.

$$d = \frac{0.00022\ B}{ct\sqrt{L}} \qquad 0.8$$

Where:

B = the length of the PWB edge parallel to the component located at the center of the board (in.)

L = length of component (in.)

t = thickness of PWB (in.)

c = 1.0 for standard DIP, 1.26 for DIP with side brazed leads, 1.0 for pin-grid array with four rows of pin (one row extending along the perimeter of each edge), and 2.25 for a leadless chip carrier.

Barker [Barker et al, 1994] discussed the assumptions and details of the stress analysis required to predict the fatigue life of quad leaded surface mount components operating in a vibration environment. A simple approximate stress analysis is presented that doesn't require complex finite element modeling, nor does it reduce the problem to a simple empirical equation or rule of thumb. Three steps were used in this study for the calculation of the vibration fatigue life of components mounted on a PWB: modal analysis of the PWB, a dynamic analysis of the PWB, and a stress analysis of the individual component interconnects.

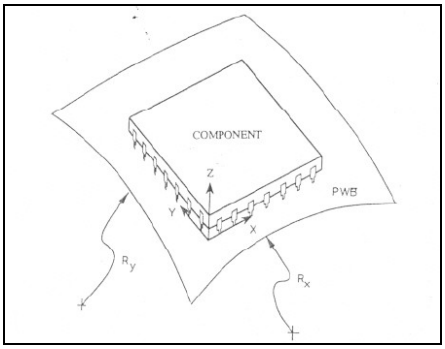

Figure 1.7: Deformation of local region of PWB can be described with two radii of curvature

The local deformation of the PWB can be modeled with two radii of curvature, as shown in Figure 1.7, based on the small-deformation assumption.

$$\kappa_x = \frac{1}{R_x} = -\frac{M_x - vM_y}{D\left(1-v^2\right)} \tag{1.9}$$

$$\kappa_y = \frac{1}{R_y} = -\frac{M_y - vM_x}{D\left(1-v^2\right)} \tag{1.10}$$

The κ_i in Eq. 1.9-1.10 is the curvature, R_i is the radius of curvature, and M_i is the moment applied in the i^{th} coordination direction. The plate rigidity, D, is:

$$D = \frac{Et^3}{12\left(1-v^2\right)} \tag{0.11}$$

Figure 1.8 is a schematic of a rigid component supported with simple linear springs above the deflected PWB.

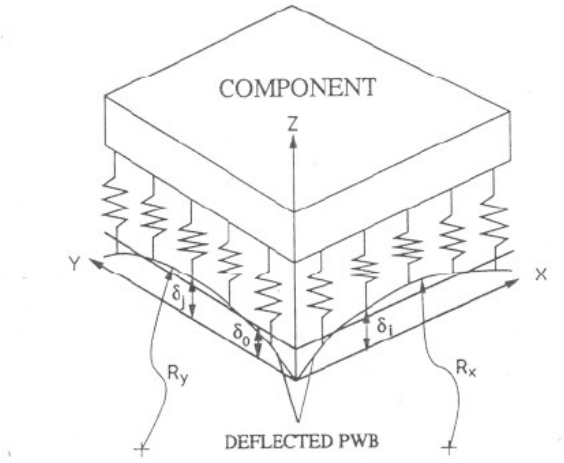

Figure 1.8: Schematic of rigid component mounted above PWB with simple linear springs

The force in each lead can be solved from this simple parallel-springs model from the equilibrium equation. Finite element analysis was used to verify the results of the simple

approximate solution. The rigidity ratio between component and PWB was the input to the FEA simulation. The FEA model is shown in Figure 1.9.

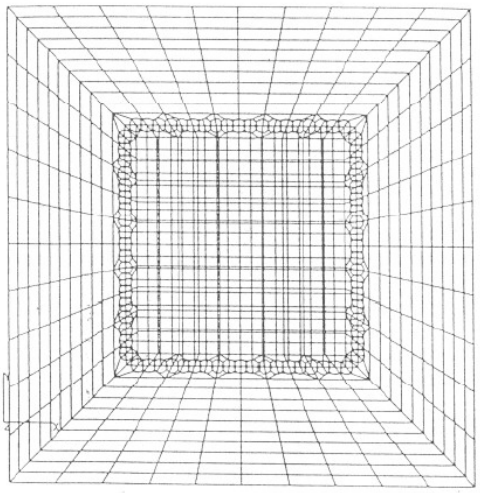

Figure 1.9: The full finite element model for a square component mounted on a local section of the PWB

The maximum interconnect force from FEA simulation is about 80% of the value predicted from the simple approximate analytic solution for radius of curvature ratios of 0.5 or greater. For smaller radius of curvature ratios, the maximum attached force is about 40 to 50 percent of that predicted by the approximate solution.

Then the fatigue life in cycles to failure, N_f, is calculated for the component attach with the highest stress, using the high cycle fatigue (HCF) power-law relation [Basquin, 1910],

$$\sigma\left(N_f\right)^b = constant \qquad 0.12$$

Of course, the use of Basquin's relation to model vibration fatigue is not limited to electronic systems and many examples can be found in the literature. For example, Dhar [Dhar et al, 2004] conducted similar transient stress analysis of a turbine blade taking into account the combined effects of centrifugal stresses, vibratory stresses and thermal stresses. In another example,

Susmel [Susmel et al, 2004] used the nominal stress to predict the fatigue strength of welded joints under biaxial loading. Hamblin [Hamblin, 2003] presented a simple robust method of calculating vibration induced stress for cantilevered fittings.

Similar work has been conducted to estimate the vibration fatigue for Pb-free and Pb-based solder alloys, for many different kinds of components. Barker [Barker, et al 1993] estimated the vibration fatigue life of quad leaded surface mount components. Barasan [Barasan, et al, 1998] investigated the mechanics of Sn40Pb near-eutectic solder alloy subjected to vibrations. Che [Che, et al., 2003] conducted vibration fatigue test and analysis for flip chip solder joints. Dynamic characterizations of flip chip on board (FCOB) assemblies were evaluated using accelerometer and high speed camera during vibration tests. A sinusoidal sweep test within a narrow band near the fundamental resonant frequency was used. Solder joint failure detection was made by daisy chained resistance monitoring during the test. 50% increase of resistance was used as a rule to determine the threshold setting. The cumulative damage was calculated with Miner's rule. The fatigue model was obtained based on G-N curve (G-level vs MTTF) for FCOB assembly. Displacement results measured by high speed camera have a good agreement with the theoretical results.

Liu [Liu, et al. 2006] and Wong [Wong, 2000] performed experiments and analysis for vibration HCF in BGA package. Their experimental system provides controls for varying the cycling frequency and magnitude of the applied load. The failure of solder interconnects in BGA specimens were recorded by direct visual monitoring method. In all test cases, BGA interconnect failure was observed to be the result of crack initiation and propagation along the nickel/solder interface between the BGA solder ball and the ENIG plating on the copper pads of the PBGA substrate.

Figure 1.10: Photograph of component BGA

A primary crack developed at one edge of the interconnect and progressed stably until a secondary crack initiated from the opposite edge. The test specimen and solder joint geometry are shown in Figure 1.10 and Figure 1.11.

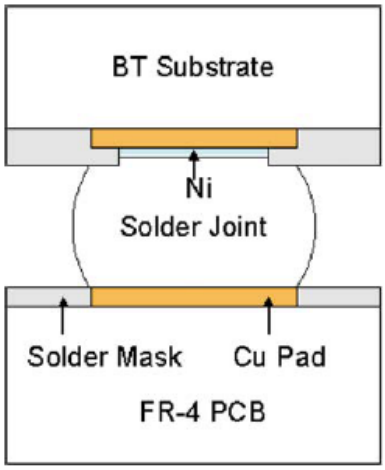

Figure 1.11: Schematic of the detailed structure around a PBGA solder interconnect

Figure 1.12 shows the apparatus used for testing and image acquisition. The loading system consists of a cyclic curvature-controlled cantilever device, which can apply high cycle vibration up to 300 Hz and control the magnitude of the applied load. The specimen is clamped at the clamped end of the cantilever, while the hinged end of the cantilever rests in a notch on link 3. Deformations imparted through this link impose a sinusoidal deformation onto the specimen, at

frequencies up to 300 Hz. The image acquisition system for recording crack propagation includes a stroboscope with an optical sensor, a CCD camera for video acquisition and data post-processing software. The CCD camera is focused on the critical solder joint, which is the one located near the highest curvature (end closest to the clamped side).

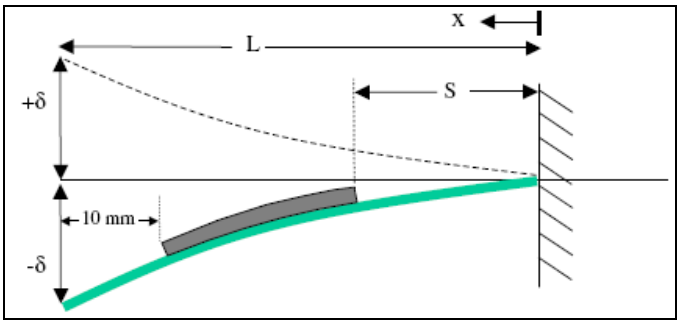

Figure 1.12: Deflection of specimen during a typical loading cycle

The distance (S) between the clamped edge and the adjacent end of the BT substrate (as shown in Figure 1.12) was chosen as the loading parameter. To study the effect of various strain levels and vibration frequencies, the tests were carried out for S = 6mm at 50 Hz and S = 7.5mm at 50 Hz, 75 Hz and 100 Hz. The maximum amplitude of the oscillating displacement a the free end , d, was fixed at 2mm and was applied 10mm away from the adjacent end of BT substrate in all tests. As expected, cracks formed first in the solder joints closest to the fixed end of the specimen. The primary solder crack always started at the inner corner of the component side. The secondary crack always started at the outer corner of the joint, usually after the primary crack passes half of the total width as shown in Figure 1.13.

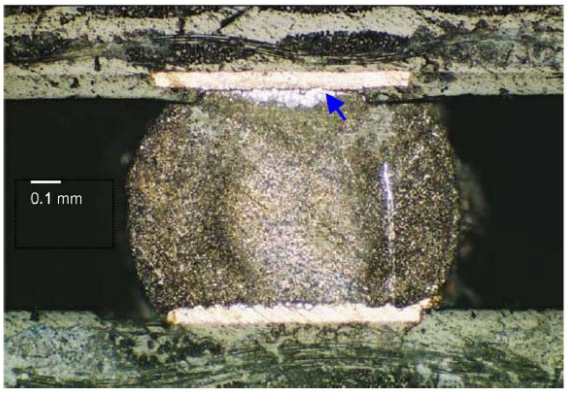

Figure 1.13: micrograph of solder ball cross-section, with blue arrow showing crack parallel to the solder/nickel interface

The test results showed that the crack growth rate was not sensitive to the frequency variations in the range tested, implying that within the interval of 50-100 Hz and the strain ranges imposed in this study: (a) creep variations are negligible, due to the relatively rapid vibration, and (b) the strain-rate variations in the solder joint did not significantly alter its fatigue life.

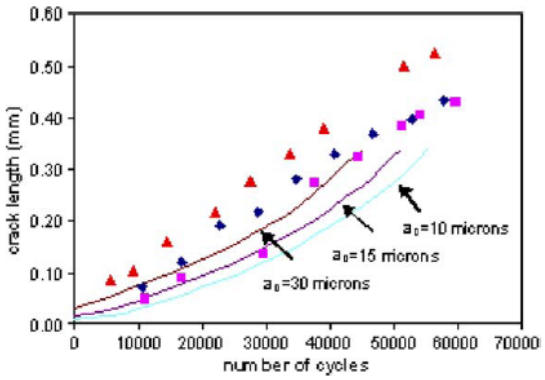

Figure 1.14: Predicted fatigue life using Paris-law compared with the test data (50Hz, S=6mm)

The recorded failure process shows that crack initiation time accounts for about 15% of the total fatigue life, and the majority of the fatigue life is spent in a stable crack growth stage, followed by an accelerated crack growth stage. The primary crack (from inner corner) growth rate remains nearly linear until the secondary crack (from outer corner) begins to grow. Fatigue life was

observed to decrease with increasing strain. The number of cycles to failure was not sensitive to variations in the frequency of vibration in the range of 50-100 Hz.

Yang et al [Yang et al 1997, 2000, 2002] conducted several studies on PBGA vibration reliability, including modal analysis of board, vibration reliability characterization under out-of-plane excitation. Yu [Yu, et al 2002] and Shah [Shah, 2004] simulated the dynamic behavior of electronic package and reliability of BGA solder joints. Tu [Tu et al. 2001] examined the effect of intermetallic compounds on vibration fatigue of μBGA solder joint. Kim et al [Kim, Noguchi, Amagai 2003] proposed a new method for evaluating the high-cycle fatigue strength of BGA packages with Pb-free and Pb solder due to vibration. Attaching a weight induced mixed mode stress (more than $\sigma_n/\tau_n = 1$ where σ_n and τ_n are the maximum normal and shear stresses respectively) in the solder ball of a package. To consider the effect of a stress ratio, the four kinds of weight (2, 4, 5 and 6) were investigated. The test frequency used in this study within a range 15- 25*Hz*. However, the test frequency didn't affect the fatigue strength of the solder joint.

Andrade, et al [Andrade, 2001] proposed a new time-domain approach for early identification of spur gear tooth fatigue crack under vibration loading condition, namely the Kolmogorov-Smirnov test. This test works on the null hypotheses that the cumulative density function (CDF) of a target distribution is statistically similar to the CDF of a reference distribution. This is a time-domain signal processing technique that compares two signals, and returns the likelihood that the two signals have the same probability distribution function. It's not a moment technique as it uses the whole CDF, instead of sections of the cumulative density function. The test and combined simulation shows that the KS method effectively distinguishes vibration signature by comparing their CDFs, and can be used for the identification of tooth fatigue cracks on gears.

Dynamic response of solder PWB and solder joint is another research area to understand the solder behavior under vibration loading. Haterbouch, Benamar and Moussaoui [Haterbouch, and Benamar, 2004; Moussaoui et al, 2000] checked the effects of large vibration amplitude on the mode shapes and natural frequencies of thin elastic shells. A nonlinear theoretical model from Hamilton's principle and spectral analysis was developed based on beam theory, in order to determine the effect of large vibration amplitudes on the first and second coupled transverse-circumferential mode shapes and their corresponding natural frequency. The second part of the paper determined the effects of large vibration amplitudes on the first and second axisymmetric mode shapes and their corresponding natural frequencies and associated membrane and bending stress distribution. Compared to the theoretical method, experiment and simulation are more applicable since theoretical solution is only available for fairly simple structures. The vibration loading can be grouped as random vibration and harmonic vibration. The detail of random vibration theory can be found in several text-books [Soong, Grigoriu and Mircea, 1993; Wirsching et al, 1995]. He [He and Fulton, 2000] used nonlinear laminate theory for PWB dynamic response modeling and analysis. Equations of motion for isotropic laminates were derived for free and forced vibration response analysis of simply supported printed wiring boards. Results show that a nonlinear system has higher frequency oscillations and lower magnitude than that of the linear system. Low K. H [Low et al, 1998] compared experimental and theoretical frequencies for rectangular plates with various boundary conditions and added masses. An analytical procedure based on the Rayleigh-Ritz approach was adopted, in which each of single and multiple trigonometric series terms were used to represent the shape function. Two experimental methods, a spectrum analyzer and a TV-holographic system, were used to study the behavior of the plate vibrations. The experimental results showed good agreement with

the analytical model. Pitarresi [Pitarresi, 1993] developed a theoretical formulation for random vibration analysis of surface mounted devices. Finite element implementation of the approach and experimental measurements were used to investigate the response of a surface mount lead/solder joint to out-of-plane random excitation. A finite element sub-modeling approach is used in the paper to determine the effective stiffness of the connection. Resonant behavior of Pb-free solders is a big concern for the solder fatigue since resonant response is much bigger than expected. Song J. M. [Song et al 2003] investigated the resonant vibration fatigue characteristics of some potential Pb-free solders, including SnZn, SnAgCu, and SnBi alloys. It shows that, under a fixed vibration force, the damping capacity and vibration-fracture resistance of SnCu and SnAg eutectic alloys with an off-eutectic structure are higher than SnPb and are also higher than SnBi and SnZn. The striated deformation in the Sn-rich phase can be regarded as an effective mechanism for absorbing vibration energy. The tensile test specimen used in this study is shown in Figure 1.15.

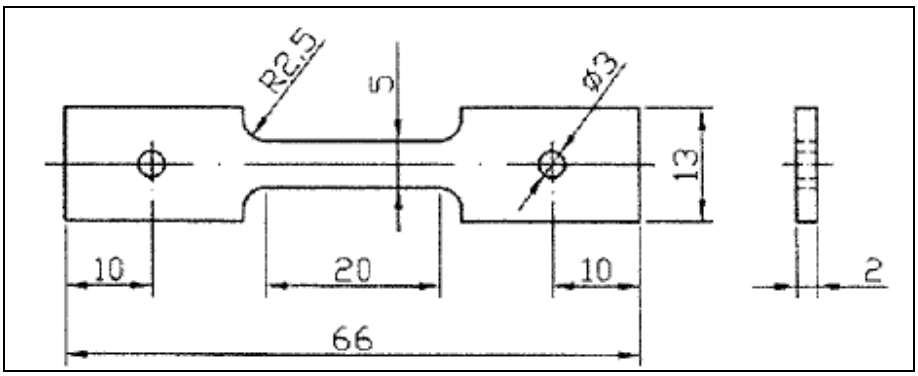

Figure 1.15: Specimen shape and dimension for tensile test [Song et al 2003]

A simple cantilever-beam vibration system, as shown schematically in Figure 1.16, was used for the vibration experiment.

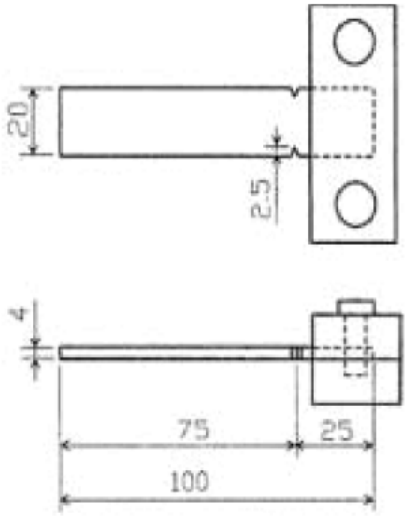

Figure 1.16: Vibration test setup

The test specimens were clamped on the end of the vibration shaker. Resonant vibration tests were conducted at either a fixed vibration force or a fixed initial deflection under resonant vibration condition. The variation in deflection amplitude against cyclic number was recorded. Each datum was the average result of three samples. The damping capacity was measured in terms of logarithmic decrement value, which was derived from the deflection-amplitude decay of a specimen under free vibration.

$$\delta = \frac{1}{n} \ln\left(\frac{A_i}{A_{i+n}}\right) \qquad 0.13$$

Where A_i and A_{i+n} are the deflection amplitude of the i^{th} cycle and the $(i+n)^{th}$ cycle separated by n periods of oscillation. The natural frequencies of different test specimen are shown in Table 1.8.

Table 1.5: natural frequency of different test specimen

Sample	Resonant Frequency (Hz)	δ Value	Tortuosity (Constant Force)
Sn-37Pb	73 ± 1	0.215	1.16
Sn-0.7Cu	74 ± 1	0.268	1.40
Sn-58Bi	73 ± 1	0.185	1.06
Sn-3.5Ag	79 ± 1	0.220	1.32
Sn-9Zn	83 ± 1	0.157	1.11
Sn-Zn-0.5Ag	82 ± 1	0.159	1.16
Sn-Zn-1.0Ag	80 ± 1	0.200	1.18
Sn-Zn-1.5Ag	80 ± 1	0.273	1.22
Sn-Zn-2.5Ag	80 ± 1	0.284	1.23
Sn-Zn-3.5Ag	80 ± 1	0.292	1.28

The test results of five Pb-free solder alloy are plotted in Figure 1.17.

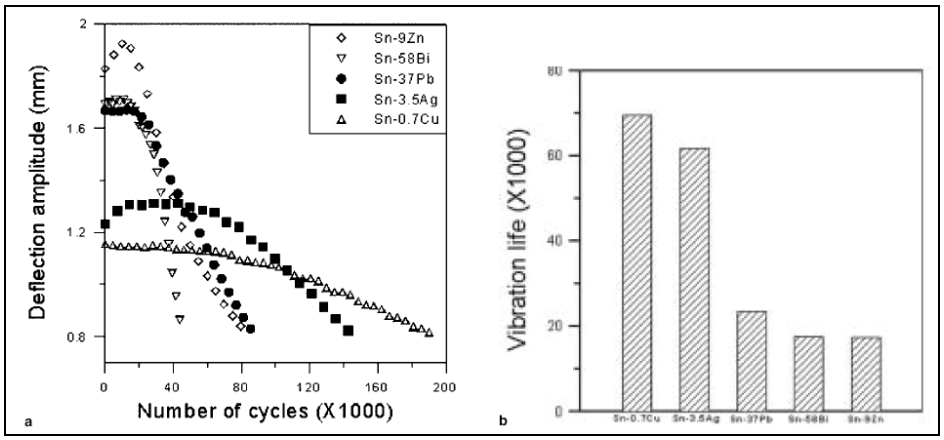

Figure 1.17: (a) The D-N curves and (b) vibration life of the samples under a fixed vibration force of 3.5g

The dependence of deflection amplitude on the number of vibration cycles (D-N curve) for the fixed vibration force of 3.5g is shown in Figure 1.17a. According to this figure, the deflection amplitude initially increased, then remained nearly constant for a while and subsequently decreased with increasing vibration cycles because of the deviation of the actual vibration frequency from the resonant frequency caused by the inward propagation of major cracks.

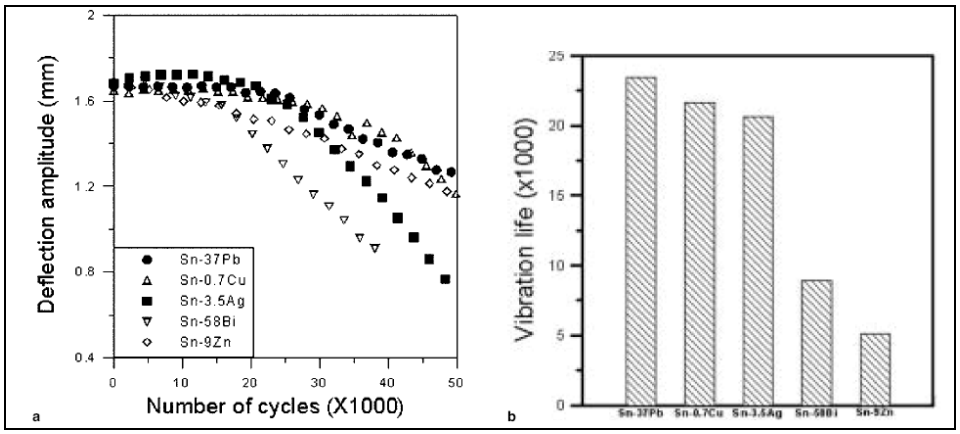

Figure 1.18: (a) The D-N curves and (b) vibration life of the samples under a fixed ID of 1.7mm

The results of vibration testing performed under constant initial deflection (ID) amplitude are shown in Figure 1.18, indicating that the critical cyclic number to failure of SnPb, SnCu and SnAg were similar, but all were significantly higher than SnBi and SnZn. The vibration life under constant ID conditions seems to be related to the strength of the materials, except for the SnBi and SnZn. The lower vibration-fracture resistance of these two alloys can be ascribed to the crack-growth morphology.

1.3.4 ***Solder joint fatigue models***

The commonly used durability models will be reviewed in this section, including the proper usage condition. Unfortunately, there is no one universally applicable model that can be used in all cases. So fully understanding the validity and limitations of each durability model is very necessary for a correct choice. Darveaux, R. [Darveaux, 1997] developed a model to predict

solder joint fatigue life for surface mounted components. He focused on aspects of the finite element analysis that affect the fatigue life prediction, such as time and temperature dependent material properties, element size, singularities, load step size and so on. A detailed procedure was given so that any skilled analyst should be able to use the model. Dasgupta, A. [Dasgupta, 1999] introduced four simple conceptual models for failure: stress-strength, damage endurance, challenge-response, and tolerance-requirement. The specific failure mechanisms depend on material or structural defects, damage induce during manufacture and assembly, and on conditions during storage and field use. The effects of stresses are influenced by geometry, constitutive and damage properties of the materials, manufacturing parameters and the application environment. Table 1.8 lists generic mechanisms which can serve as potential agents of failure.

Table 1.6: List of Failure Mechanisms in Microelectronic Packages [Dasgupta, 1999]

List of Failure Mechanisms	
Overstress Failure	Wear-out Failures
Brittle Fracture	Wear
Ductile Fracture	Corrosion
Yield	Dendritic Growth
Buckling	Interdiffusion
Large elastic deformation	Fatigue crack propagation
Interfacial De-adhesion	Diffusion Radiation Fatirue crack initiation creep

Lee, [Lee, 2000] reviewed fourteen solder joint fatigue models with an emphasis on summarizing the features and applications of each fatigue model. The models are classified into five categories, based on the metric used to quantify durability: stress, plastic strain, creep strain, energy, and damage. Fatigue models falling outside these categories are categorized as "other empirical models".

- *Stress-based model*

The stress-based classification is based on the application of a force or stress to a component that causes damage in the material. Typically, stress-based fatigue applies when the deformations are predominantly elastic, and are used for vibrational or physically shocked or stressed components.

- *Plastic strain-based model*

Plastic strain-based models are useful when the deformations are dominated by plastic deformation. These models are used to predict durability (cycles to failure) based on calculation or experimental determination of the applied plastic shear strain. The coffin-Manson fatigue model is perhaps the best known and most widely used approach today. The relationship of this model is described in Equation 1.14 [Coffin 1954, Manson 1965].

$$\frac{\Delta\varepsilon_p}{2} = \varepsilon_f^{'}\left(2N_f\right)^c \qquad 0.14$$

The fatigue ductility coefficient, $\varepsilon_f^{'}$, is approximately equal to the true fracture ductility, ε_f. The fatigue ductility exponent, c, varies between -0.5 and -0.7. This model was originally proposed to predict the fatigue life of metals in the aircraft industry. Because the Coffin-Manson equation considers only plastic deformations, it is commonly combined with Basquin's equation to account for elastic deformation as well, as shown in Equation 1.15.

$$\frac{\Delta\varepsilon}{2} = \frac{\sigma_f^{'}}{E}\left(2N_f\right)^b + \varepsilon_f^{'}\left(2N_f\right)^c \qquad 0.15$$

$\Delta\varepsilon$ is the strain range, $\sigma_f^{'}$ is the fatigue strength coefficient, $\varepsilon_f^{'}$ is the fatigue ductility, b is the fatigue strength exponent, and c is the fatigue ductility exponent. This fatigue model is an improvement over the Coffin-Manson equation in that it also accounts for the elastic contribution to fatigue failure. As can be seen in Figure 1.19, the low cycle fatigue (LCF) region to the left of N_f is governed by the plastic-strain amplitude (Coffin-Manson equation), and the high cycle fatigue (HCF) region to the right of N_f is governed by the elastic-strain amplitude (Basquin's equation).

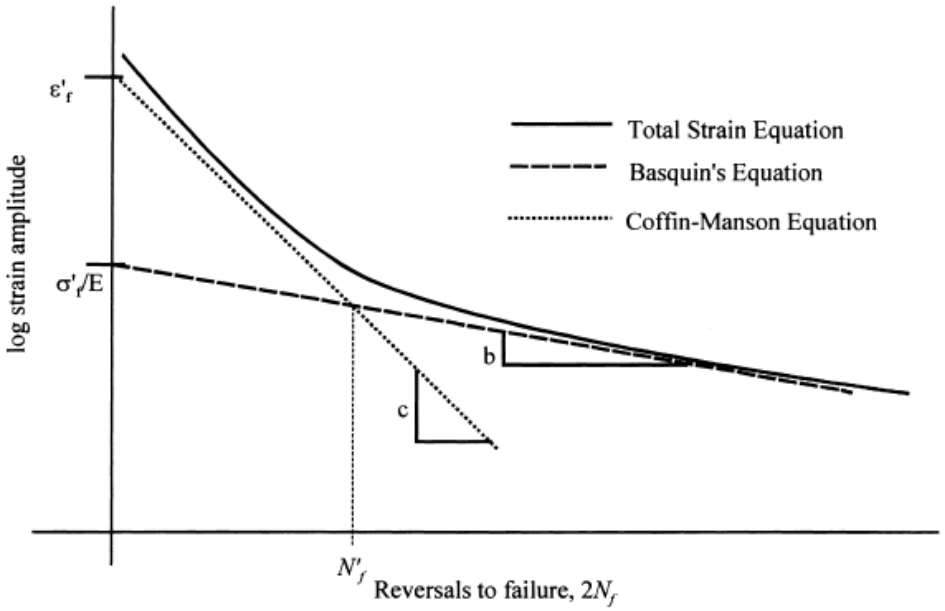

Figure 1.19: Total strain versus life relation

1.3.5 ***Cycle counting algorithm***

The rainflow-counting algorithm (also known as the "rain-flow counting method") is used in the analysis of fatigue data in order to reduce a variable-amplitude strain history into blocks of constant-amplitude strain reversals. Its importance is that it allows the application of Miner's rule

in order to assess the fatigue life of a structure subject to complex loading. Matsuiki and Endo [Matsuiski and Endo, 1969] and Downing [Downing, 1982] have introduced the cycle counting concept and procedure. In this study, the procedure of rain-flow cycle counting used in current study is listed here:

1. Reduce the time history to a sequence of (tensile) peaks and (compressive) troughs.
2. Imagine that the time history is a template for a rigid sheet (pagoda roof).
3. Turn the sheet clockwise 90° (earliest time to the top).
4. Each tensile peak is imagined as a source of water that "drips" down the pagoda.
5. Count the number of half-cycles by looking for terminations in the flow occurring when either:
    1. It reaches the end of the time history;
    2. It merges with a flow that started at an earlier tensile peak; or
    3. It flows opposite a tensile peak of greater magnitude.
6. Repeat step 5 for compressive troughs.
7. Assign a magnitude to each half-cycle equal to the stress difference between its start and termination.

Pair up half-cycles of identical magnitude (but opposite sense) to count the number of complete cycles. Typically, there are some residual half-cycles. The following example signal, plotted in Figure 1.20, is used to demonstrate the rainflow cycle counting procedure.

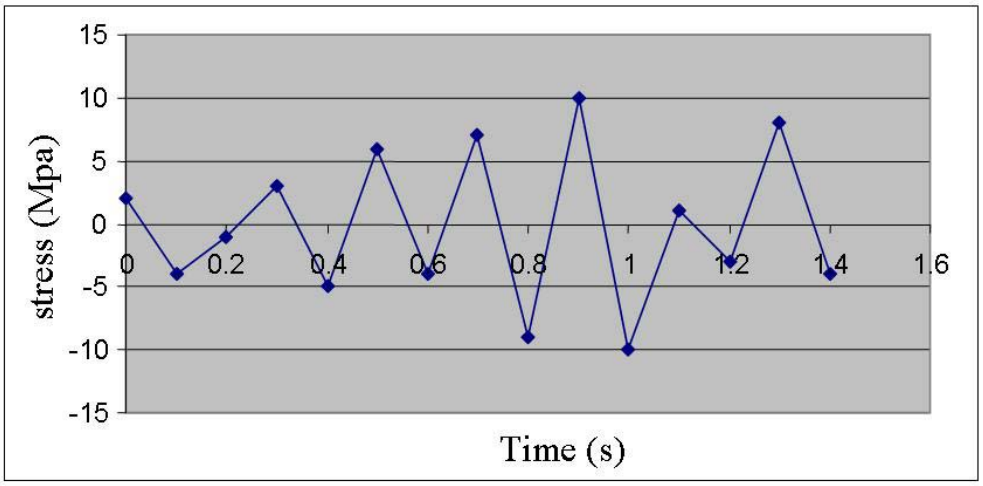

Figure 1.20: Example stress history used for cycle counting algorithm

The rain-flow cycle counting results including the half cycle and full cycle reversal, together with corresponding mean stress and time interval of each cycle, are shown in Table 1.11.

Table 1.7: Full cycle results from rainflow cycle counting algorithm

Whole cycle		
Stress Range (MPa)	mean	Interval
10	1	0.1
4	-1	0.1

Table 1.8: half cycle results from rainflow cycle counting algorithm

Half cycle		
Stress Range (MPa)	mean	Interval
6	-1	0.1
8	-1	0.1
16	-1	0.1

20	0	0.1
12	2	0.1
7	-0.5	0.2
12	1	0.3
19	0.5	0.1
18	-1	0.3

In this study, the rainflow cycle counting algorithm is used to quantify the random strain history to obtain the strain range distribution functions (RDFs). This facilitates damage quantification for each cycle, and subsequent superposition, using Miner's rule, to estimate the total damage.

1.4 Overview of Dissertation

Each of the Chapters 2-5 of this dissertation consist of a journal paper that is either accepted or in review. As a result, there is some overlap of technical content between the different chapters. There is a small introduction and summary presented for each of these sections, to provide continuity and transitions. Additional information, not already included in journal publications, is presented in the Appendices. Chapter 2 presents a body of experimental work that was conducted for both SAC and Sn37Pb solder interconnects. Both constant-amplitude harmonic and random step-stress vibration durability tests were conducted at constant temperatures. The measured durability for specific SAC and Sn37Pb assemblies are empirically compared in this chapter. The results show that the Sn37Pb assemblies last longer at the same excitation level, for both harmonic and random excitation profiles used in this study. The test matrix includes test boards with different kinds of finishes, different aging conditions and different test temperatures.

Chapter 3 presents the details of the characterization of the harmonic response of the test vehicle and the associated stress and damage modeling to obtain the harmonic vibration durability model constants from the durability test results, for both SAC and Sn37Pb solder interconnects. Chapter 4 presents parametric sensitivity studies to assess the influence of the constitutive stress-strain properties of the solder on the constants in the fatigue durability model. The durability test results from harmonic study and random study have been used together in this chapter to examine the accuracy and effectiveness of the obtained durability model constants. The vibration durability investigation has been further enhanced in Chapter 5 by including the relative response of the component with respect to the PWB. This response is caused by inertial forces generated by the mass and acceleration of each component. Dynamic simulation was conducted with ABAQUS to include the transient component response when assessing the damage accumulation rates in the solder interconnect. The transient strain history was generated by dynamic FEA simulation and was compared with the results from static simulation. Significant dissimilarity between the dynamic and static stress-strain response was observed, which results in a substantial difference in the corresponding damage accumulation rates. Finally, the conclusions and main contributions are summarized in Chapter 6, including suggestions for future work.

REFERENCES

1. Amagai, M., Watanabe, M., Omiya, M., Kishimoto, K., Shibuya, T., "Mechanical Characterization of Sn-Ag-based Lead-free Solders" Microelectronics Reliability, Vol. 42, pp 951-966, 2002
2. Anand, L., "Constitutive equations for hot working of metals", Journal of Plasticity, vol. 1, pp. 213-231, 1985
3. Andrade F. A, Esat. I, Badi. M. N. M, "A New Approach to Time-Domain Vibration Condition Monitoring: Gear Tooth Fatigue Crack Detection and Identification by the Kolmogorov-Smirnov Test", Journal of sound and vibration, vol. 245, pp 909-919, 2001
4. Arra. Minna, Xie Dongji, Shangguan. Dongkai, "Performance of Lead-free Solder Joints under Dynamic Mechanical Loading", Electronic Components and Technology Conference, pp 1256-1262, 2002
5. Barker D. B, Sidharth. B, "Local PWB and Component Bowing of and Assembly Subjected to a Bending Moment", ASME Journal of Electronic Packaging, vol. 116, pp 92-97, 1994
6. Barker D. B, Chen Y. S and Dasgupta A, "Estimating the Vibration Fatigue Life of Quad Leaded Surface Mount Components", Journal of Electronic Packaging, vol. 115, pp 195-199, June, 1993
7. Boresi. A, Schmidt. R and Sidebottom. O, "Advanced Mechanics of Materials", John Wiley and Sons, 1993
8. Basaran Cemal, Chandaroy Rumpa, "Mechanics of Pb40/Sn60 Near-eutectic Solder Alloys Subjected to Vibrations", Applied Mathematical Modelling, vol. 22, pp 601-627, 1998
9. Basquin, OH, "The Experimental Law of Endurance Tests", Proc. ASTM, 1910

10. Bonte, M. H. A., and De Boer, A., "Prediction of Mechanical Fatigue Caused by Multiple Random Excitations", Proceedings of ISMA, pp 697-708, 2004
11. Che F. X, Pang H. L. J, Wong F. L, Lim G. H, Low T. H, "Vibration Fatigue Test and Analysis for Flip Chip Solder Joints", Electronics Packaging Technology Conference, pp 107-113, 2003
    1. Coffin, L.F., 1954, *Transactions of the ASME*, Vol. 76, pp. 931-950.
12. Commission of the European Communities, "Proposal for a Directive of the European Parliament and of the Council on Waste Electrical and Electronic Equipment, Document No. 500PC0347(01)," June 13, 2000, <http://europa.eu.int/eur-lex/en/com/dat/2000/en_500PC0347_01> accessed March 16, 2001.
13. Cuddalorepatta. G and Dasgupta. A, "Cyclic Mechanical Durability of Sn3.0Ag0.5Cu Pb-Free Solder Alloy", Published at ASME International Mechanical Engineering Congress and Exposition, Orlando, FL, Nov, 2005
14. Darveaux R, Banerji K, "Constitutive Relations for Tin-Based Solder Joint", IEEE Transactions on Components, Hybrid and Manufacturing Technology, vol. 15, No. 6, pp 1013-1023, 1992
15. Darveaux, R., Banerji, K., Mawer, A., Dody, G., 1995, "Durability of Plastic Ball Grid Array Assembly," Ball Grid Array Technology, Lau, J., Editor, McGraw-Hill, Inc., New York.
16. Dasgupta. A, et al, "Material Failure Mechanisms and Damage Models", A tutorial series containing 14 articles in IEEE Transactions on Reliability, Lead Article Appeared, vol. 40, No. 1, pp 531, 1999

17. Dasgupta, A., Oyan, C., Barker, D., and Pecht, M., “Solder Creep Fatigue Analysis by an Energy-Partitioning Approach”, ASME Journal of electronic Packaging, vol. 114, pp 152-160, 1992
18. Darveaux, R., Banerji, K., “Constitutive Relations for Tin-Based Solder Joints,” IEEE Transactions on Components, Hybrids, and Manufacturing Technology, Vol. 15 (6), pp 1013-1024, 1992
19. Deepak Dhar, Sharan A. M, Rao J. S, “Transient Stress Analysis and Fatigue Life Estimation of Turbine Blades”, Journal of Vibration and Acoustics, vol. 126, pp 485-495, Oct, 2004
20. Downing S. D and Socie D. F, “Simplified Rainflow Counting Algorithms”, International Journal of Fatigue, vol. 4, No. 1, 1982
21. Hall, P.M., “Creep and Stress relaxation in solder joints. In: Lau JH, editor. Solder Joint Reliability Theory and Applications” New York: Van Nostrand Reinhold, pp. 313, Chapter 10, 1991
22. Hamblin. M, “Fatigue of Cantilevered Pipe Fittings Subjected to Vibration”, Journal of Fatigue & Fracture of Engineering Materials & Structures, vol. 26, pp 695-707
23. Haswell, P. and Dasgupta, A., "Viscoplastic Constitutive Properties of Lead-Free Sn-3.9Ag-0.6Cu Alloy," *MRS Proceedings*, San Francisco, CA, 2001
24. Haswell, P. and Dasgupta, A., “Durability Properties Characterization of Sn62Pb36Ag2 Solder Alloy,” Proceedings ASME IMECE, EEP-Vol. 28, pp 181-187, Orlando, FL, 2000
25. Haterbouch, M. and Benamar, R., “The Effects of Large Vibration Amplitudes on the Axisymmetric Modes Shapes and Natural Frequencies of Clamped Thin Isotropic Circular Plates. Part II: Iterative and Explicit Analytical Solution for Non-linear Coupled Transverse and In-plane Vibrations”, Journal of Sound and Vibration, vol. 277, pp 1-30, 2004

26. Hayward, J., “Lead (Pb)-Free Packaging Strategy 2000−2003”, 2000 <www.amd.com>
27. He Xiaoling, Fulton Rober, “Modeling and Simulation of the Dynamic Response of the Electronic Packaging”, IEEE Electronic Components and Technology Conference, pp 1535-1547, 2000
28. JEDEC Solid State Technology Association, “JEDEC Announces Lead-free Definition,” <http://www.jedec.org/download/search/JESD97.pdf>, accessed September 2002.
29. Jih Edward, Jun Wayne, “Vibrational Fatigue of Surface Mount Solder Joints”, IEEE Intersociety Conference on Thermal Phenomena, pp 246-250, 1998
30. John H. L. Pang, Che F. X, Low T. H, “Vibration Fatigue Analysis for FCOB Solder joints”, Electronic Components and Technology Conference, pp 1055-1061, 2004
31. Krishna J., Mahesh P., and Andrew S., “Mechanical Bend Fatigue Reliability of Lead-free PBGA Assemblies,” International Society Conference on Thermal Phenomena, pp 915-918, 2002
32. Kariya, Y., Morihata, T., Hazawa, E., and Otsuka, M., “Assessment of Low-Cycle Fatigue Life of Sn-3.5mass%Ag-X (X=Bi or Cu) Alloy by Strain Range Partitioning Approach,” Journal of Electronic Materials, Vol. 30(9), pp. 1184-1189, 2001
33. Kim H. Y, “Vibration-Based Damage Identification Using Reconstructed FRFs in Composite Structures”, Journal of Sound and Vibration, vol.259, pp1131-1146, 2003
34. Kim Young-Bae, Noguchi Hiroshi, Amagai Masazumi, “Vibration Fatigue Reliability of BGA-IC package with Pb-free Solder and Pb-Sn Solder”, Electronic Components and Technology Conference, pp 891-897, 2003

35. Kujala, A., Reinikainen, T., Ren, W., 2002, “Transition to Pb-free Manufacturing Using Land Grid Array Packaging Technology.” 52nd Electronic Components and Technology Conference, San Diego, CA, pp 359-364, May, 2002
36. Lau. J et al, “Solder Joint Reliability of Surface Mount Connectors”, Journal of Electronic Packaging, vol. 115, pp 180-188, 1993
37. Lee. W. W, Nguyen. L. T, Selvaduray. G. S, “Solder Joint Fatigue Model: Review and Application to Chip Scale Packages”, Microelectronics Reliability, vol. 40, pp 231-244, 2000
38. Liguore Salvatore and Followell David, “Vibration Fatigue of Surface Mount Technology (SMT) Solder Joints”, IEEE Proceedings Annual Reliability and Maintainability Symposium, pp 18-26, 1995
39. Liu X, Sookala V. K, Verges M. A and Larson M. C, “Experimental Study and Life Prediction on High Cycle Vibration Fatigue in BGA Packages”, Journal of Microelectronics Reliability, vol. 46, pp 1128-1138, 2006
40. Low K. H, Chai G. B, Lim T. M, Sue S. C, “Comparisons of Experimental and Theoretical Frequencies for Rectangular Plates with Various Boundary Conditions and Added Masses”, International Journal of Mechanical Sciences, vol. 40, No. 11, pp 1119-1131, 1998
41. Luan. Jing-En, Tee. Tong Yan, Pek. Eric, Lim. Chwee Teck, Zhong. Zhaowei, “Modal Analysis and Dynamic Responses of Board Level Drop Test”, Electronics Packaging Technology Conference, pp 233-243, 2003

    2. Manson, S. S., 1965, *Experimental Mechanics*, Vol. 5, No. 7, pp. 193-226.

42. Matsuiski, M. & Endo, T., Fatigue of metals subjected to varying stress, Japan Soc. Mech. Engrg, 1969

43. Moussaoui F., Benamar R., and White R. G., “The Effects of Large Vibration Amplitudes on the Mode Shapes and Natural Frequencies of Thin Elastic Shell, Part I: Coupled Transverse-Circumferential Mode Shapes of Isotropic Circular Cylindrical Shells of Infinite Length”, Journal of Sound and Vibration, vol. 232, pp 917-943, 2000
44. Pang JHL, Tan T, Sitaraman SK, “Thermo-mechanical analysis of solder joint fatigue and creep in a flip chip on board package subjected to temperature cycling loading”, electronic Components and Technology Conference, pp. 878-883, 1998
45. Park, T.-S., and Lee, S.-B., 2002, “Isothermal Low Cycle Fatigue Tests of Sn/3.5Ag/0.75Cu and 63Sn/37Pb Solder Joints under Mixed-mode Loading Cases**,”** *ECTC 2002*, pp. 979-984, Las Vegas, NV.
46. Pitarresi J. M, Akanda A, “Random Vibratoin Response of a Surfance Mount Lead/Solder Joint”, Proceedings of the ASME International Electronics Packaging Conference, Binghamton, New York, 1993
47. Qian, Z., Liu, S., “On the Life Prediction and Accelerated Testing of Solder Joints” EPP Thermo-Mechanical Characterization of Evolving Packaging Materials and Structures Proceedings of the 1998 ASME International Mechanical Engineering Congress and Exposition, vol. 24, pp 1-11, Nov 15-20, 1998
48. Schubert, A., Dudek, R., Doring, R., Walter, H., Auerswald, E., Gollhardt, A., Schuch, B., Sitzmann, H. and Michel, B., 2002b, “Lead-free Solder Interconnects: Characterization, Testing, and Durability,” 3rd Int. Conf. On Benefiting from Thermal and Mechanical Simulation in Micro- Electronics, EuroSIME2002, pp. 74-84, Paris, France, 2002

49. Shah K, Mello M, “Ball Grid Array Solder Joint Failure Envelope Development for Dynamic Loading”, Proceeding of the Electronic Components and Technology Conference, pp 1068-1074, 2004
50. SOLDERTEC, 1999, “Lead-Free Alloys - The Way forward”, <www.lead-free.org>.
51. Song J. M, Lui T. S, Chen L. H and Tsai D. Y, “Resonant Vibration Behavior of Lead-free Solders”, Journal of Electronic Materials, vol. 32, No. 12, 1501-1508
52. Soong, T.T., Grigoriu, Mircea, “Random Vibration of Mechanical and Structural Systems”, Prentice Hall, 1993
53. Steinberg, Dave S, “Vibration Analysis for Electronic Equipment”, John Wiley & Sons, New York, 1998
54. Stolkarts, V., Moran, B, Keer, L.M., “Constitutive and damage model for solders”, Electronic Components and Technology Conference, pp 379-385, June, 1998
55. Susmel. L, Tovo. R, Lazzarin. P, “The Mean Stress Effect on the High-cycle Fatigue Strength from a Multiaxial Fatigue Point of View”, International Journal of Fatigue, vol. 27, pp 928-943, 2005
56. Tu K. N, Zeng. K, “Reliability Issues of Pb-free Solder Joints in Electronic Packaging Technology”, Electronic Components and Technology Conference, pp 1194-1200, 2002
57. Tu P. L, Chan Y. C and Lai K. L, “Effect of intermetallic compounds on Vibration Fatigue of μBGA Solder Joint”, IEEE Transactions on Advanced Packaging, vol. 24, No. 2, pp197-205, 2001
58. Vaynman, S., McKeown, S. A., “Energy-Based Methodology for the Fatigue Life Prediction of Solder Materials,” IEEE Transactions on Components, Hybrids and Manufacturing Technology, Vol. 16, No. 3, pp. 317-323, 1993

59. Wang Hongfang, Zhao Mei, Guo Qiang, “Vibration Fatigue Experiments of SMT Solder Joint”, Journal of Microelectronics Reliability, vol. 44, pp 1143-1156, 2004
60. Whitten, G., “Lead-free Solder Implementation for Automotive Electronics,” ECTC, pp 1410-1415, 2000
61. Wiese, S., Schubert, A., Walter, H., Dudek, R., Feustel, F., 2001a, “Constitutive Behavior of Lead-free Solders vs. Lead-containing Solders – Experiments on Bulk Specimens and Flip-Chip Joints,” ECTC, pp 890-902, Las Vegas, NV, 2001
62. Wirsching, P.H., Paul, H, Paze, Tomas L, Ortiz, Keith, “Random Vibration: Theory and Practice”, New York: John Wiley & Sons, Inc, 1995
63. Wong T. E, Palmieri F. W, Reed B. A, “Durability/Reliability of BGA Solder Joints under Vibration Environment”, Electronic Components and Technology Conference, pp 1083-1088, 2000
64. Yang Q. J, Lim G. H, Lin R. M, Yap F. F, Pang H. L. J and Wang Z. P, “Experimental Modal Analysis of PBGA Printed Circuit Board Assemblies”, IEEE/CPMT Electronic Packaging Technology Conference, pp 290-296, 1997
65. Yu Q, Kikuchi H, Ikeda S, Shiratori M, Kakino M, and Fujiware N, “Dynamic Behavior of Electronics Package and Impact Reliablity of BGA Solder Joints”, Proceedings of the Intersociety Conference on Thermomechanical Phenomena in Electronic Systems, pp 953-960, 2002
66. Zeng, K., Tu, K.N., “Six Cases of Reliability Study of Pb-free Solder Joints in Electronic Packaging Technology,” Materials Science and Engineering R, Vol. 273, pp 1–51, 2002
67. Zhang, Q., “Isothermal Mechanical and Thermo-mechancial Durability Characterization of Selected Pb-free Solders”, PHD Dissertation, University of Maryland, 2004

68. Zhang. Q, Dasgupta. A and Haswell. P, “Isothermal Mechanical Durability of Three Selected Pb-free Solders: Sn3.9Ag0.6Cu, Sn3.5Ag and Sn0.7Cu”, Transaction of the ASME, Vol. 127, pp 512-522, 2005
69. Zhang, Q., Dasgupta, A., Haswell, P., “Viscoplastic Constitutive Properties and Energy-Partitioning Model of Lead-Free Sn3.9Ag0.6Cu Solder Alloy”, ECTC New Orleans, Louisiana, USA, 2003
70. Zhang Q, Dasgupta A and Haswell Peter, “Viscoplastic Constitutive Properties and Energy-Partitioning Model of Lead-free Sn309Ag0.6Cu Solder Alloy”, IEEE Electronic Components and Technology Conference, pp 1862-1868, 2003

Chapter 2 Experimental Investigation for Vibration Durability

This chapter describes vibration experiments which have been conducted to identify the cyclic durability of both SAC and SnPb solder interconnects. The test vehicles are subjected to both harmonic vibration and random vibration excitations. The purpose of the harmonic durability test results is to calibrate the durability model constants. The purpose of the random vibration test results is to verify if they are compatible with the same durability constants obtained from harmonic tests. The durability tests have been conducted both on campus and in a third party test lab. This chapter will focus on the harmonic test results and the random durability test results from the third party test lab. The details of all the test results can be found in Appendix B. The experimental program and the test results are presented in this paper and the post-processing for the durability model constants is deferred to a later paper.

This part of the study has been accepted to the Journal of the Institute of Environmental Sciences and Technology (IEST). The details of post-processing of the test results, to extract the durability properties of the solder alloys, are presented in Chapter 3.

Vibration Durability of SnAgCu (SAC) Solder Interconnects: Random & Harmonic Excitation

Y. Zhou, G. Plaza, M. Osterman, and A. Dasgupta

CALCE Electronic Products and Systems Center

Mechanical Engineering Department, University of Maryland,

College Park, MD, 20742

Tel: 301-405-5231, Fax: 301-314-9262, Email: Easily@umd.edu

ABSTRACT

In this study, the durability of SAC and SnPb solder interconnects, under constant amplitude narrow-band (harmonic) excitation and under step-stress broad-band ('random') excitation, is investigated. The durability for SAC and SnPb solder materials are compared in this chapter. The results show that SnPb assemblies last longer than SAC assemblies at similar excitation levels, for both harmonic and random excitations used in this study. The test vehicles are identical for both harminc and random vibration tests, and consist of a PWA with ball grid array, flat packs, and leadless resistors. The test matrix includes test boards with different kinds of finishes and different aging conditions. The harmonic vibration is conducted on a single specimen at a time on an electrodynamic shaker. The random vibration excitation is applied on an electrodynamic shaker simultaneously to twenty test specimens at a time, with all twenty specimens mounted on a single test fixture on the shaker table. The response of the each test vehicle mounted in the fixture is first characterized before conducting the durability experiment. The strain histories are measured for different excitation conditions, at different sites on the PWA, for all possible PWA locations on the test fixtures. These measured strain histories are used to compare the performance of the assemblies at different excitation conditions and also as inputs in future studies for stress analysis to quantify the damage in the solder joints [1]. The durability tests are then conducted and time-to-failure is documented for the entire test matrix. The random durability tests are conducted at three temperatures: 125^{o}C, 25^{o}C (RT) and -40^{o}C. Destructive failure analysis (cross-sectioning, polishing and microscopy) has been used to confirm the failure modes.

I. INTRODUCTION

Vibration loading is encountered in the service life of many electronic products; therefore, its contribution to fatigue damage accumulation throughout the lifetime of a solder interconnect must be investigated. High-cycle fatigue (HCF) durability of SAC solders under vibration excitation has not been investigated to the same extent as SnPb solder [2] [3] [4], especially as a function of temperature. This is a first essential step towards understanding the interaction between thermal cycling damage and vibration damage [5] [6]. The characteristics of the stress from vibration loading are low amplitude and high frequency, while those from thermal cycling loading are high amplitude and low frequency [7] [8]. Recently, Lau, et al. [9] studied mechanical and vibration responses of plastic ball grid array assemblies due to overload environmental stress factors. In his paper, the flip-chip solder joints' thermal fatigue life was estimated with the Coffin-Manson and fracture mechanics methods. Darbha, et al. [10] investigated stress distribution of surface mount interconnections due to vibration loading. Barker, et al. [11] proposed some analytical methods to estimate the vibration fatigue lives of leaded surface mount components. Lau, et al. conducted vibration reliability testing [12] [13] [14] using sweep sinusoidal excitations and studied vibration fatigue properties based on linear assumption. Yang, et al. [15] investigated the reliability of a PBGA assembly under a sinusoidal excitation. Most failures were due to cracks near the copper pad on the PCB side in Yang's [15] work. It was also found that the dynamic displacement of the PBGA assembly under the out-of-plane excitation was highly nonlinear. Che et al. [17] conducted fatigue tests and analysis for flip chip solder joint under sinusoidal sweep test with a narrow band near the fundamental resonant frequency. Wong and Fenger [17] overviewed the applications of vibration and thermo-mechanical analyses in advanced electronic packaging design. The methodologies, combined with analytical work and experimental validation to determine the reliability in various

configurations of electronic interconnects were developed. Barker, et al [18] investigated the solder joint life under thermal and vibration loading using Miner's rule. The thermal damage was calculated using a Coffin-Manson model while the vibration damage was estimated with Basquin's high-cycle fatigue relation.

The results from a set of vibration durability tests are presented in this paper, as listed below:

- Harmonic vibration at room temperature (25 ^{o}C)
- Random vibration at room temperature (25^{o}C)
- Random vibration at high temperature (125^{o}C)
- Random vibration at low temperature (-40^{o}C)

The details of the test, the results and failure analysis are presented in this paper. The vibration durability is compared between different solders, different plating systems, different aging conditions and different test conditions.

II. TEST SPECIMEN AND MATRIX

A photograph of the test assembly used in this study is shown in Figure 1. Each test assembly includes four 256-I/O PBGAs, four 44-I/O ceramic leadless chip carriers (CLCC) (only on some test assemblies), sixteen 100-I/O quad flat packs (QFPs) and ninety-six (forty-eight 2515 and forty-eight 1210) leadless ceramic resistors, assembled on an FR4 printed wiring board (PWB). The parts are non-functional and are daisy-chained to facilitate continuous monitoring of failures in the interconnects between the component and the PWB. Failure under the test load is determined by monitoring the resistance of each net in the daisy-chains.

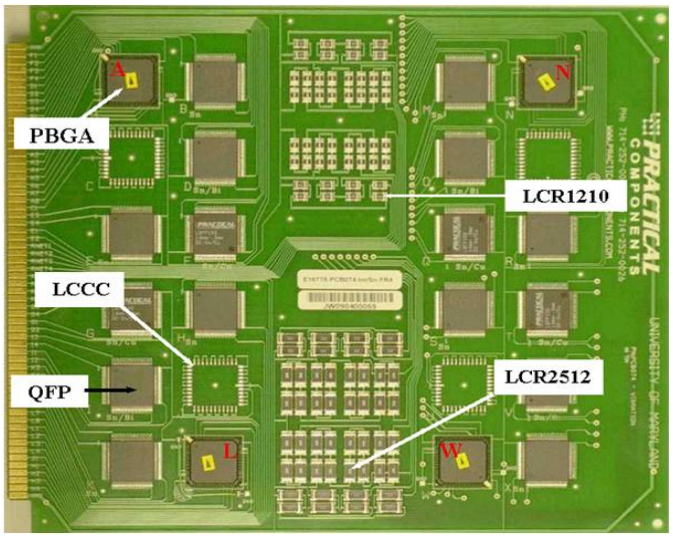

Figure 1: Test vehicle

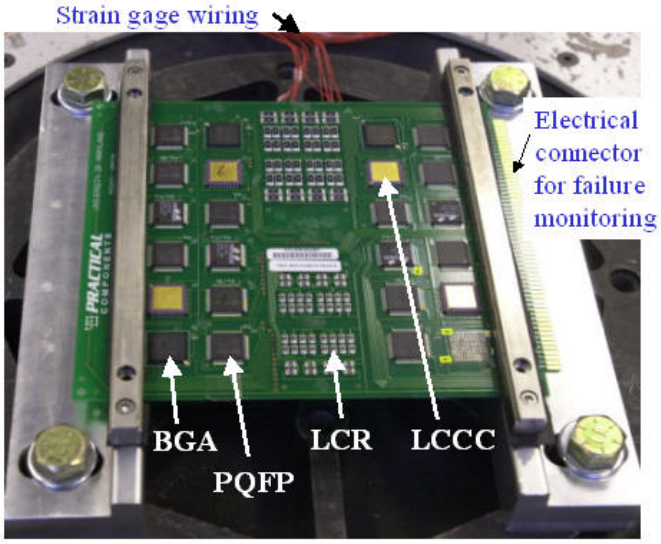

Figure 2: Test set up for harmonic vibration

The SnPb assemblies are made with no-clean-type 3-Kester 256 paste (Sn37Pb) and the PWB finish is Sn37Pb solder hot air solder level (HASL). The lead-free assemblies were made with no clean-type 3-Kester R905 solder paste (Sn3Ag0.5Cu) and the PWB finish is organic solderability preservative (OSP).

All the test specimens were pre-aged at 125^0 C before the vibration test. Some were aged for 100 hours and some for 350 hours. The test vehicle features are summarized in Table 1 and the test matrix is provided in Table 2. In this paper, the narrow-band ('harmonic') test and results are

first presented in Section III, followed by broad-band ('random') vibration test results in section IV. The effect of pre-aging conditions and test temperature are also presented in section IV.

Table 1: Test vehicle characteristics

Aging condition	Solder Paste	Pad Finish
125°C, 100 hours	SAC305	OSP
	Sn37Pb	HASL
125°C, 350 hours	SAC305	OSP
	Sn37Pb	HASL

Table 2: Durability test matrix

	Harmonic vibration	Random vibration	Random vibration	Random vibration
	(room)	(room)	(high)	(low)
SAC305	3	2	2	2
Sn37Pb	2	2	2	2

III. HARMONIC DURABILITY TEST

In this part of the study, constant-amplitude harmonic vibration excitation was applied to the test vehicles. The constant-amplitude, harmonic tests have several advantages compared to the step-stress, broad-band vibration durability tests:

- The dynamic response of the test vehicle consists only of a single mode response, and not the coupling of several modes. This facilitates data post-processing and analysis of accelerated durability tests.

- The constant-amplitude, harmonic strain response eliminates the need for complicated cycle counting algorithms to quantify the damage accumulation rate.
- The damage accumulation rate is relatively constant throughout the whole test procedure.

The harmonic durability test and corresponding results are explained in this section.

A. TEST SETUP

A single test board was clamped along the two opposite long edges on a fixture and mounted on the table of an electrodynamic, single-axis vibration shaker, for excitation in the out-of-plane direction, as shown in Figure 2. A multi-channel data-logger was used to monitor the daisy chain resistance for each component. A Labview based software and hardware was used to collect the real time strain history for PWB response characterization. The test was conducted at different excitation levels to obtain enough fatigue data points so that fatigue S-N curves can be extracted in future studies. The harmonic test matrix is listed in Table 2. All harmonic tests were run at a constant room temperature.

B. TEST SETUP CHARACTERIZATION

Three strain gages were attached to the PCB for strain characterization, as shown in Figure 3. The red numbers indicate the location and identifier number for each strain gage. All strain gages were mounted on the bottom side of the PWB which is the unpopulated side.

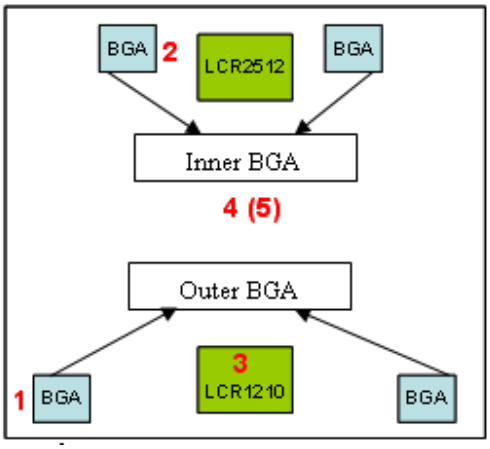

Figure 3: Strain gage attachment for harmonic test

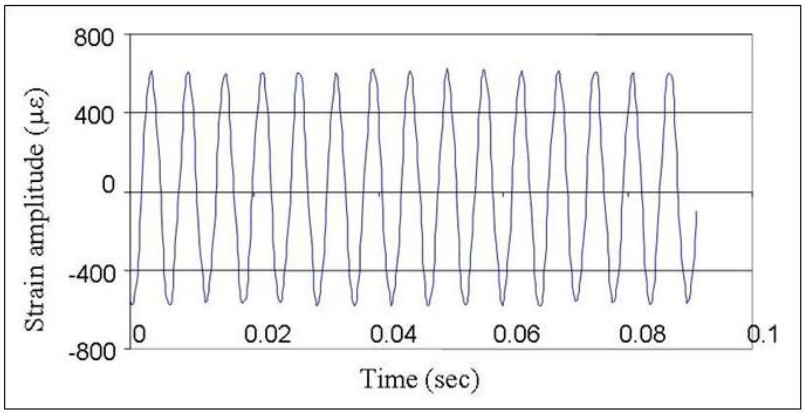

Figure 4: Typical PWB strain history under harmonic excitation

The focus of this study is on the LCR and BGA components. The BGA components are grouped into Inner BGA and Outer BGA, based on their location on the test vehicle, as shown in Figure 1. The components in the each group have two characteristics in common:

- Interconnect geometry
- Local PWB curvature

Strain gages 1 to 3 are used to collect the PWB response strain history near the foot of the outer BGA, Inner BGA and LCR components. The assumption here is that LCR2512 and LCR1210 damage history can be characterized approximately in terms of a common PWB strain history,

since the difference between their locations is very small. The output strain clearly shows that the PWB experiences a harmonic response at the excitation frequency. A typical strain history is shown in Figure 4.

C. DURABILITY TEST

Constant-amplitude, harmonic excitation at the first natural frequency of the PWB was applied to the test specimens in this study. The natural frequency was measured with an accelerometer under "white noise" excitation. The Fast Fourier Transform (FFT) of accelerometer response provides the information about the natural frequencies of the test vehicle. In this study, the first natural frequency was measured to be 168Hz. The harmonic durability test was conducted at this frequency until most of the components failed.

The test was conducted for both SAC and SnPb boards under different level of excitation amplitude. Table 3 and Table 4 show the detail test matrix for SAC and SnPb including the excitation G level. The input excitation amplitude was measured with accelerometers mounted on the fixture.

Table 3: Test matrix and excitation level for SAC305

	10.5G	9G
# of SAC305 PWAs	1	1

Table 4: Test matrix and excitation level for Sn37Pb

	12G	10.5G
# of Sn37Pb PWAs	1	1

The time-to-failure of every daisychain was monitored with the datalogger. The results for different components are plotted in Figure 5 to Figure 7 for SAC305 and Sn37Pb, respectively.

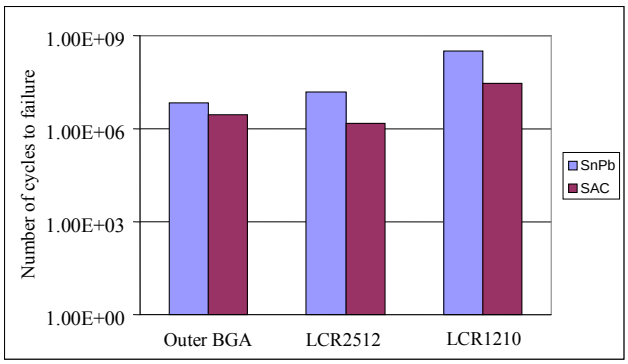

Figure 5: Durability plot for both SAC305 and Sn37Pb at 10.5G harmonic excitation

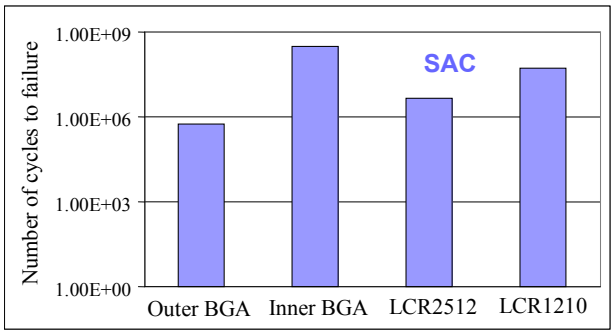

Figure 6: Durability plot for SAC305 at 9G harmonic excitation

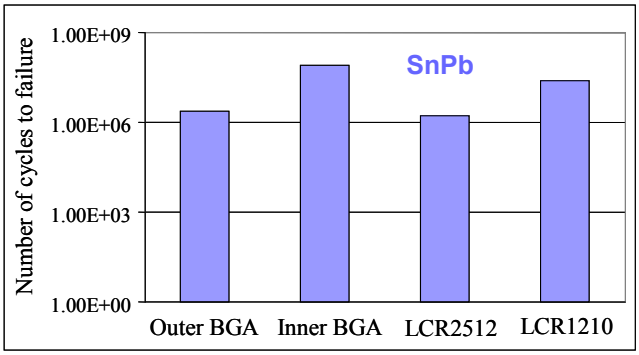

Figure 7: Durability plot for Sn37Pb interconnect at 12G harmonic excitation

The results in Figure 5 show that Sn37Pb interconnects are more durable than corresponding SAC305 interconnects, at 10.5G harmonic loading. Figure 6 and Figure 7 show that the outer BGAs fail before the inner BGAs. This is due to the fact that mode 1 response produces greater

curvature of the PWA under the outer BGAs than under the inner BGAs. Similarly, Figures 5-7 all show that LCR2512 fails before LCR1210. This is due to the fact that the larger LCRs produce higher flexural strains in the solder interconnects, at a given PWB flexure level. These durability test results, and PWA strain data will be combined with solder strain analysis in future studies [19] to obtain the model constants for a generalized strain-life durability model for both solders.

IV. "RANDOM" DURABILITY TEST

In this section, the broad-band (random) vibration test program is described in detail, including the test setup, test loading, PWB characterization and durability results.

A. TEST SETUP

Twenty test boards were clamped at a time, along two opposite long edges on a custom-built fixture, which was mounted on an electro-dynamic vibration shaker table, as shown in Figure 8. The fixture was excited in the z direction, resulting in out-of-plane excitation of the circuit card assemblies.

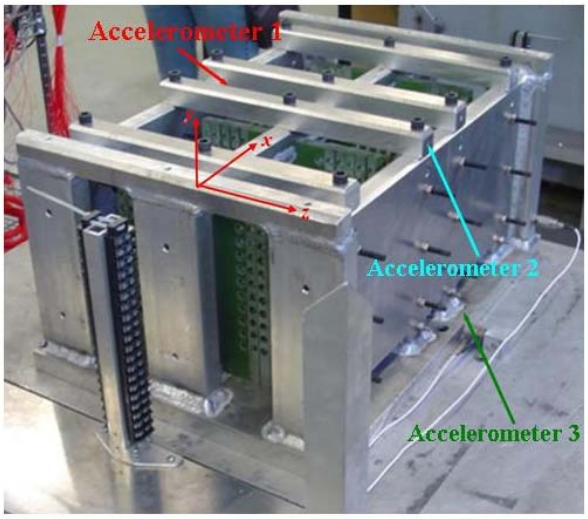

Figure 8: Broad band vibration test fixture

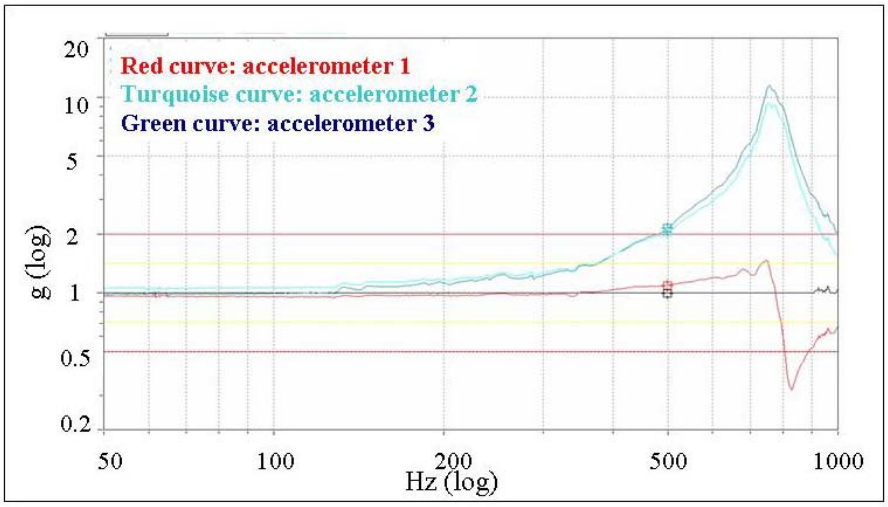

Figure 9: Fixture frequency response

The fixture is divided into four quadrants and each quadrant can hold five boards. The fixture is welded together with an aluminum plate and the plate is bolted on the slip table of an electro-dynamic shaker.

B. TEST SETUP CHARACTERIZATION

The dynamic response of the fixture was characterized before the durability test and aluminum cross bars (not shown in Figure 8) were added to increase the stiffness of the fixture. The frequency response of the fixture is very important since it influences the dynamic excitation transmitted to the test boards. To avoid the dynamics of the fixture, the highest excitation frequency should be less than the first natural frequency of the fixture. Accelerometers are used to measure the frequency response and the results are plotted in Figure 9. Three accelerometers are attached at different key locations of the fixture, as depicted in Figure 8. The characterization results show that the first natural frequency of the fixture is around 800Hz. Thus, the excitation frequencies used in the vibration test have to be well below this frequency.

C. TEST MATRIX & EXCITATION

A broad-band random vibration loading was applied in the vibration durability test. The frequency range of the broad-band excitation was from 10Hz-500Hz, with a 4dB/octave roll-off at both ends. Preliminary simulations show that this frequency range includes the first four natural frequencies of the test vehicle. As discussed in the previous section, the upper limit of the frequency range was selected to avoid significant influence of the fixture dynamics.

To compress test time, the excitation magnitude was step-stressed through four levels. The excitation level was held constant for six hours at each of the first three load level and then continued for 18 hours at the final and highest load level. The random vibration loads used in the tests, defined by power spectral density (PSD) input profiles, are shown in Figure 10. The max PSD level for the four excitation levels are: 0.02, 0.05, 0.1, and $0.2G^2/Hz$. This equates to RMS excitation levels of approximately 4, 6, 8 and 11 Gs, respectively. This broad-band vibration durability test is conducted on three sets of test assemblies at three different temperatures:

- Room temperature
- Extreme high temperature (125^oC)
- Extreme low temperature (-40^oC)

All of these test results are used to investigate the vibration durability of SAC305 and Sn37Pb solder and its dependence on temperature, aging duration and PWB pad finish.

D. TEST VEHICLE CHARACTERIZATION

The response of the test boards to the vibration excitation was characterized using strain gages, before the durability tests. Eight strain gages were attached to the rear (unpopulated) side of the test PWB, at locations shown in Figure 11. The gage locations were selected based on assumed symmetry to maximize information related to component excitation levels. The instrumented test

board was placed at different locations in the fixture. As shown in Figure 12, the fixture is divided into four quadrants. In each quadrant, PWB locations are labeled from 1 to 5.

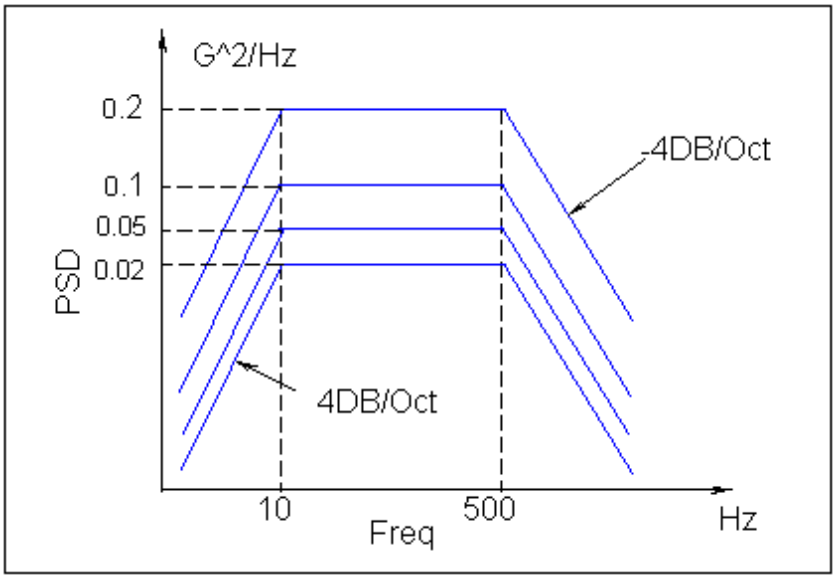

Figure 10: Broad band vibration excitation profile

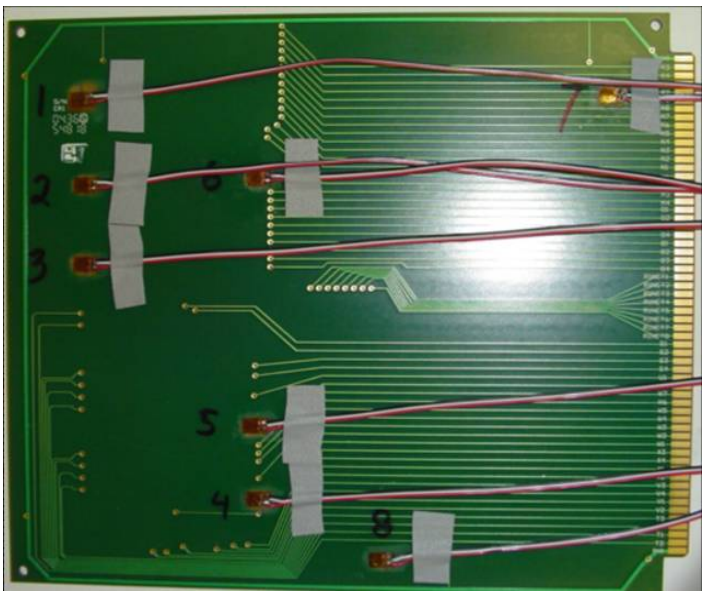

Figure 11: Strain gage locations

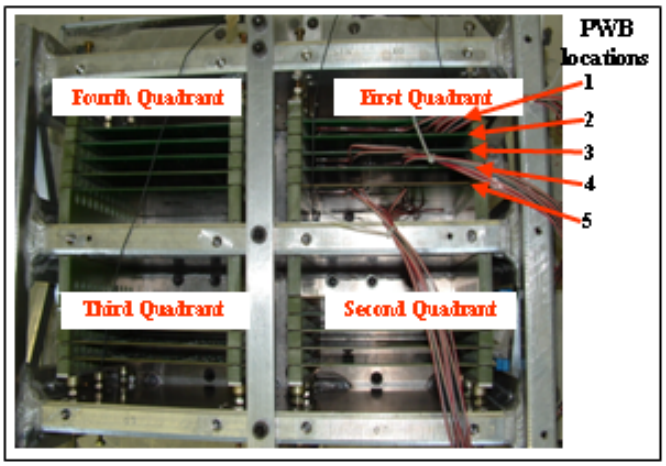

Figure 12: Test vehicle layout in the fixture profile

The instrumented board with strain gages was switched from locations 1 to 5 in different quadrants and the corresponding strain from each strain gage was collected with StrainBook/616™ software. The PWB response was found to vary slightly, depending on its location in the fixture, because of the dynamics of the fixture. The characterization was repeated under different conditions, as shown below:

- Multiple PWB locations within a quadrant: locations 1, 3, and 5
- Multiple quadrants: first and third
- Multiple PSD levels: 0.02, 0.05, 0.1, 0.2 G^2/Hz
- Multiple temperatures: 25°C, 125°C and -40°C

The measured strain results are used to compare time-to-failure for different components at different locations on the PWB, under different test conditions. In future work, these strain results, together with FEA simulations, will be used to derive strain-based durability models for SAC solder interconnects.

E. DURABILITY TEST

After both the fixture and board were characterized, the durability tests were conducted. Data loggers, shown in Figure 13, were used to measure the daisy-chain resistance and monitor the failure of each group of interconnects for each component.

Figure 13: Failure monitoring system

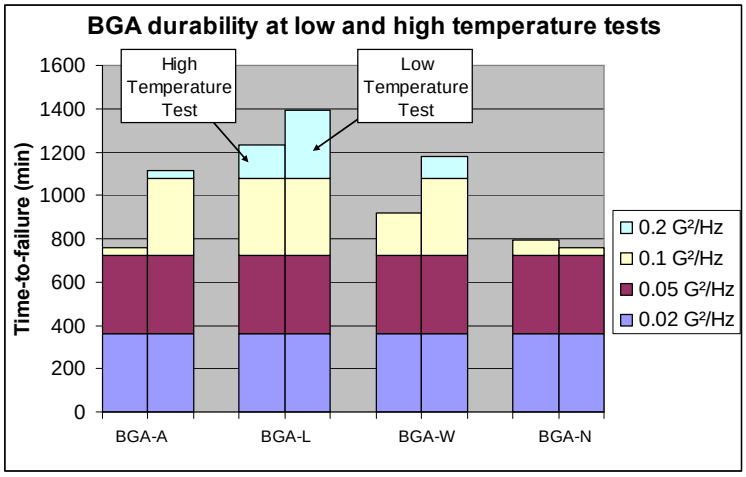

Figure 14: BGA vibration durability comparison at high and low temperatures (SAC305 solder).

As shown in Figure 14, BGAs A and N are outer BGAs, while BGAs L & W are inner BGAs)

Failure is defined to occur when the daisy-chain resistance exceeds a threshold resistance of 25Ohms. To minimize false positives due to electrical noise, at least 10 resistance spikes beyond the 25Ω threshold (with no more than 30 readings between each spike) are required, to define a hard failure. Since the durability test used step-stress excitation, different components experienced different loading histories, which makes direct durability comparison very complex. Furthermore, there are also differences in other parameters that affect the durability of each test component, such as the location of the component on the board, location of the board in the fixture, solder material, pad finish and aging conditions. Ideally, the comparison of durability should be based on identical experiment conditions. Selected durability test results and comparison between different kinds of solder joints and different loading conditions are provided in this paper.

Effect of Temperature:

The dependence of vibration durability on temperature is one of the points of interest, based on the obtained results. For example, for SAC305 solders, at room temperature 17% of the total components failed at 0.02 G^2/Hz excitation level. On the other hand, in the low-temperature durability test, most of the SAC305 components failed at higher excitation levels (i.e., 0.1 G^2/Hz and 0.2 G^2/Hz), with about 20% of the components failing at 0.2 G^2/Hz which is the highest excitation level used in this step-stress durability test program. The high temperature durability test had the largest percentage of failed interconnects at the lower excitation levels, compared to the low-temperature and room-temperature durability tests. The trend shows that the durability of test assemblies decreases as the test temperature increases. An example of this observation is shown in Figure 14. It shows time to failure for ball grid array packages and equivalent locations on equivalent test vehicles subjected to high temperature and low temperature vibration

durability tests. These test vehicles were aged at 125ºC for 100 hours prior to the test and were assembled with SAC305 solder. The focus of this comparison is on the BGA components on the PWB. There are four BGA components on each board. Two are near the clamped edges of the PWB (labeled A, N in Figure 1) Two others are close to the PWB centerline (labeled W and L in Figure 1) Except for BGA-W, all other three BGA components failed in both low-temperature and high-temperatures tests. Each histogram pair represents results for a BGA, and shows TTF (time to failure) for one low-temperature test and one high-temperature test. The histograms are segmented to illustrate the time spent at each excitation level before failure. This BGA component durability comparison shows that the durability at low temperature is generally higher than the durability at high temperature. Furthermore, as observed in Figures 6 and 7, the outer BGAs fail before the inner ones.

Effect of Load-level and Aging:

As expected, position, solder material and isothermal aging were shown to influence time to failure of Sn37Pb/HASL and SAC305/OSP test vehicles. For purposes of comparison, the durability of BGA interconnects is quantified by pseudo-fatigue curves presented in Figure 15 and Figure 16. In these curves, the vertical axis shows the highest calculated root mean square (RMS) PWB strain based on the measured strain history from strain gages close to the failed component at the maximum applied vibration loading level (0.2 G^2/Hz). Based on the location of the BGA on the PWB and the location of the PWB in the fixture, different components experienced different flexural PWB strains. It is important to remember that each component has spent several hours at the lower excitation levels. The horizontal axis shows the total TTF (time to failure) but the damage accumulation rate is clearly not constant during this time, because of the step stress excitation. Thus, while such graphs allow good qualitative comparisons,

quantitative strain-life fatigue curves can only be extracted from these after additional simulations.

In addition to the influence of load level, Figure 15 and Figure 16 also show the influence of isothermal aging as a preconditioning of the test specimens. Vibration durability of Sn37Pb assemblies appears to be more sensitive to isothermal aging compared to that of SAC305 assemblies. Furthermore, the slope of these pseudo-fatigue curves appear to be less sensitive to aging time for Sn37Pb assemblies, compared to SAC305 assemblies.

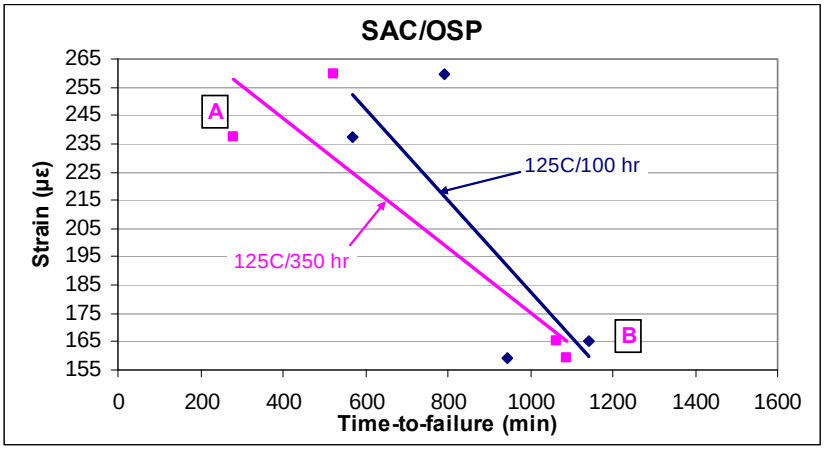

Figure 15: Influence of aging on SAC305/OSP assemblies

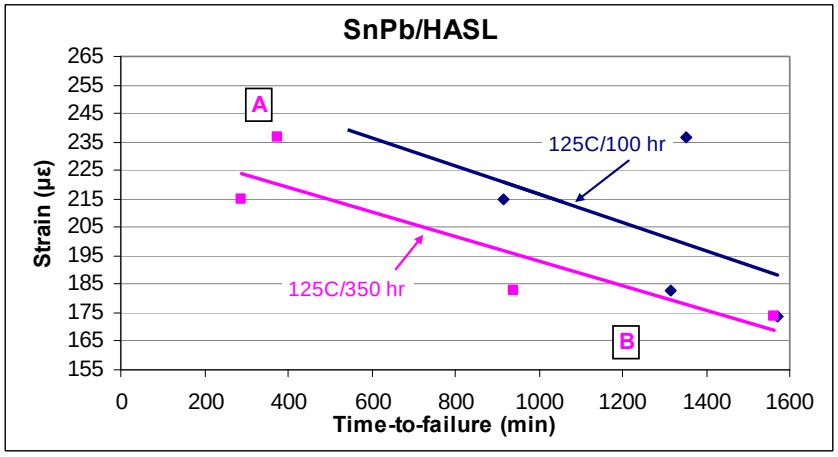

Figure 16: Influence of aging on Sn37Pb/HASL assemblies

Since the damage accumulation rates are not constant during the TTF represented on the x-axis in Figure 15 and Figure 16, it is more instructive to view the TTF as a segmented histogram. TTF for two selected BGAs (each pre-aged for 350 hrs and labeled A for the outer BGAs and B for the inner BGAs) are replotted in Figure 17 and Figure 18, respectively, as segmented histograms. The label for each histogram shows the reference RMS strain level (measured at 0.2 G^2/Hz excitation level). The segmented y axis for each histogram shows the time spent at each excitation level (in hours), before failure. Clearly the outer BGAs fail before the inner BGAs, because the PWB max flexural strain at the foot of the outer BGAs is almost 50-100με larger than that under the inner BGAs.

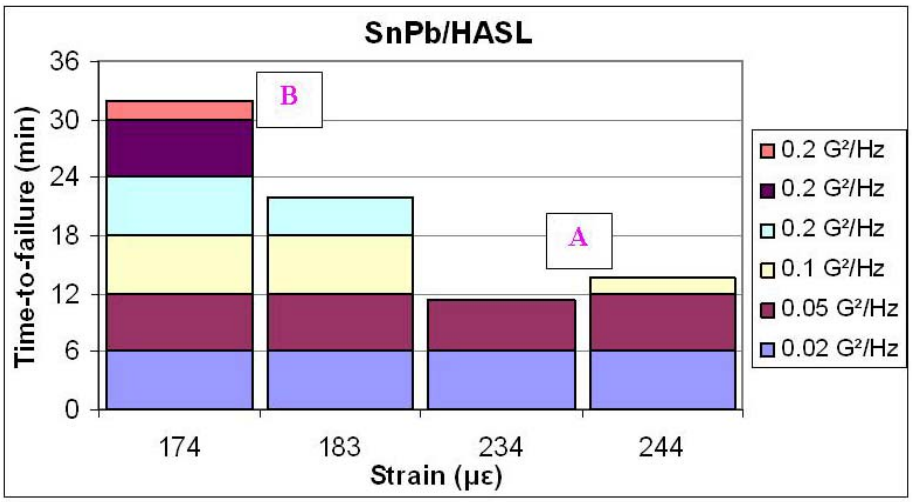

Figure 17: Effect of strain magnitude on segmented TTF for Sn37Pb/HASL assemblies

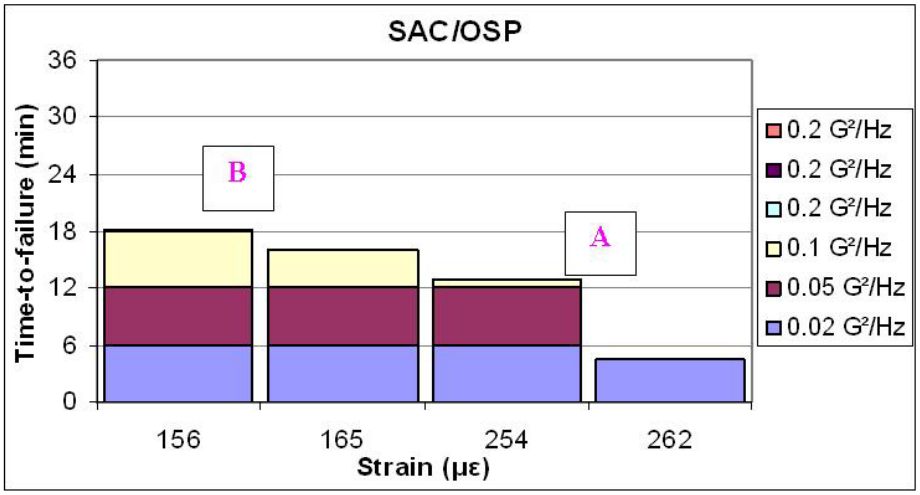

Figure 18: Effect of strain magnitude on segmented TTF for SAC305/OSP assemblies

Effect of Solder Material System:

If the results are averaged across the different room temperature tests conducted with different characteristics (such as different aging condition and different plating), Sn37Pb assemblies proved to be generally more durable than SAC305 assemblies, when exposed to the previously described vibration conditions. Figure 19 and Figure 20 illustrate the comparison between Sn37Pb/HASL and SAC305/OSP assemblies when these are exposed to the same aging conditions and excitation levels. As in Figure 15 and Figure 16, Figure 19 and Figure 20 are pseudo fatigue curves with RMS board strain calculated for the highest ($0.2G^2/Hz$) vibration load level. From these curves it can be seen that time to failure response of Sn37Pb/HASL assemblies is different than that of SAC305/OSP assemblies. The slopes of the pseudo-fatigue curves are different, implying that there is a cross-over point below which, Sn37Pb assemblies may be more durable and above which, SAC305 assemblies may be more durable.

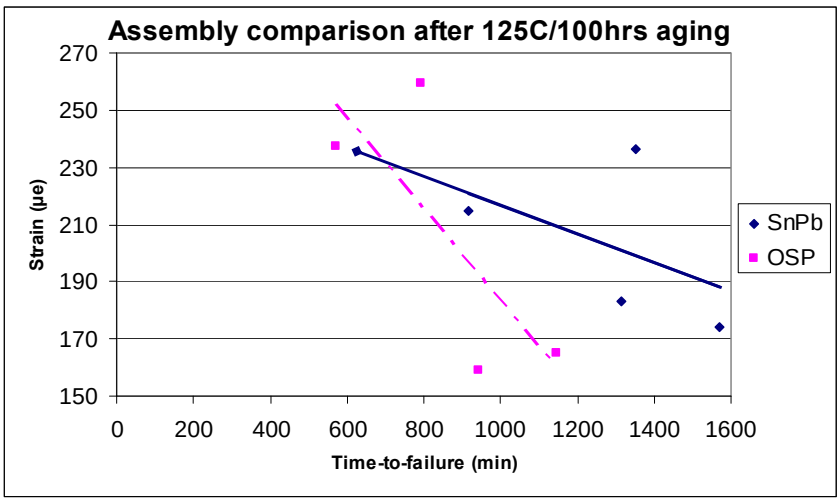

Figure 19: Comparison of vibration durability of Sn37Pb vs. SAC305 assemblies after aging at 125 ºC for 100 hours

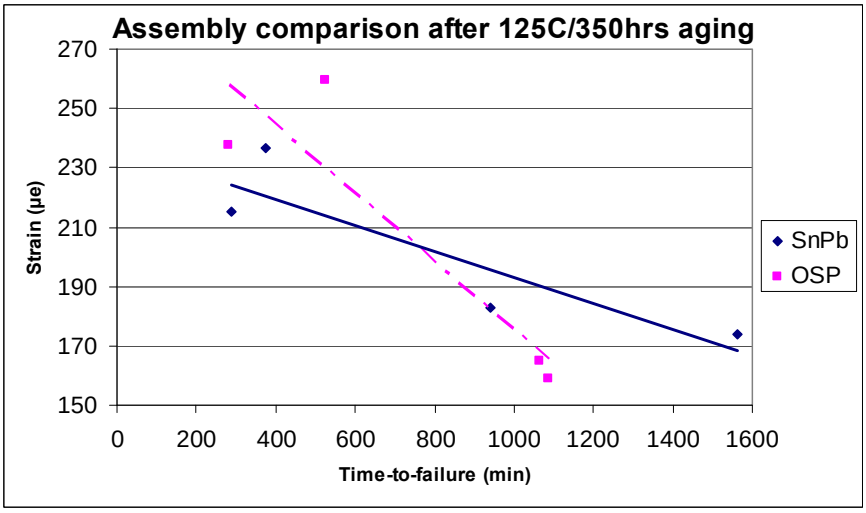

Figure 20: Comparison of vibration durability of Sn37Pb vs. SAC305 assemblies after aging at 125 ºC for 350 hours

As the exposure period to isothermal aging at 125ºC is increased, the difference in the TTF of SAC305 and Sn37Pb assemblies appears to decrease.

V. FAILURE ANALYSIS

After the accelerated vibration durability tests, destructive failure analysis is carried out for selected failed components, to confirm the failure modes and failure sites. The failure analysis is conducted by cross-sectioning and microscopy. The samples include one each, of BGA, CLCC and QFP and LCR components. We find that there are two competing failure sites. Some of the failures are in the bulk of the solder in the interconnect. Obvious fatigue cracks are found in the critical solder joint of many of the failed specimen analyzed. Figure 21 to Figure 24 show micro-sections of the failed lead-free interconnects. For the QFP, as shown in Figure 23, the failure site includes the copper lead.

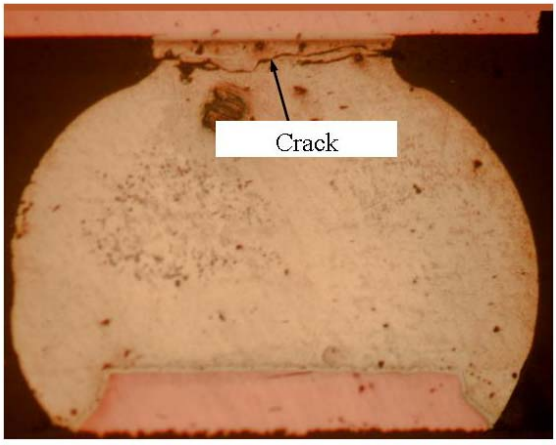

Figure 21: Crack in neck of BGA solder ball

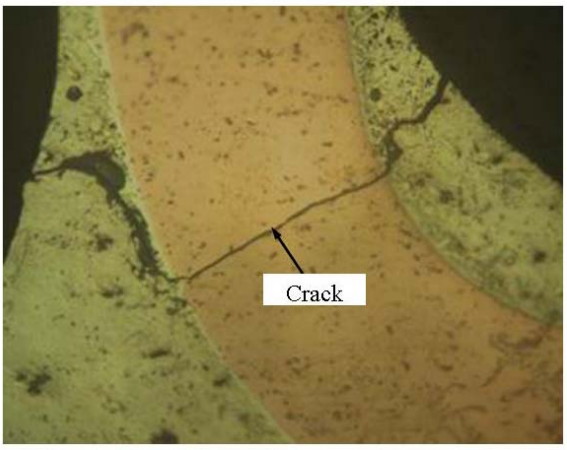

Figure 22: Crack in QFP gull wing solder joint and lead

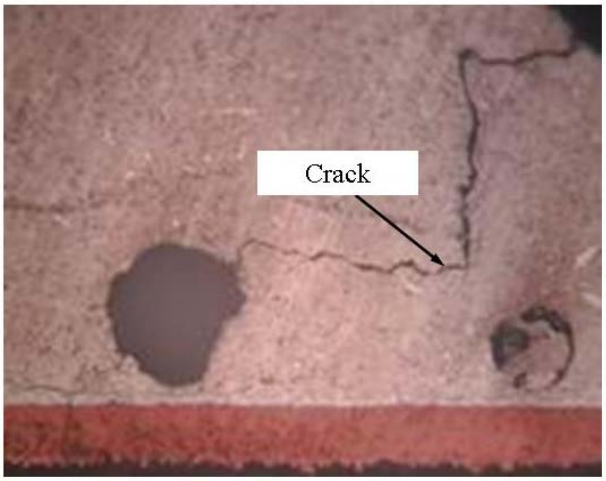

Figure 23: Crack in fillet of voided CLCC solder joint

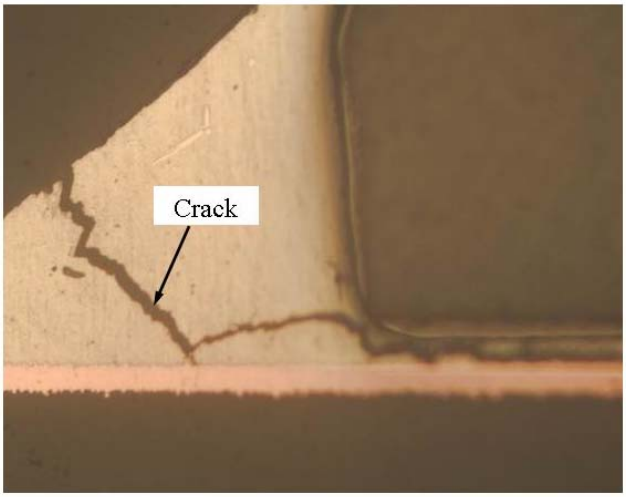

Figure 24: Crack in fillet of LCR solder joint

The competing failure site for these assemblies is fatigue cracking of the copper traces, as shown in Figure 25 and Figure 26. In general, the higher reflow temperature of the SAC305 solder consumes more of the copper pad/trace, thus weakening the copper more than in Sn37Pb assemblies. This fact partially accounts for the lower vibration durability observed in the SAC305 assemblies.

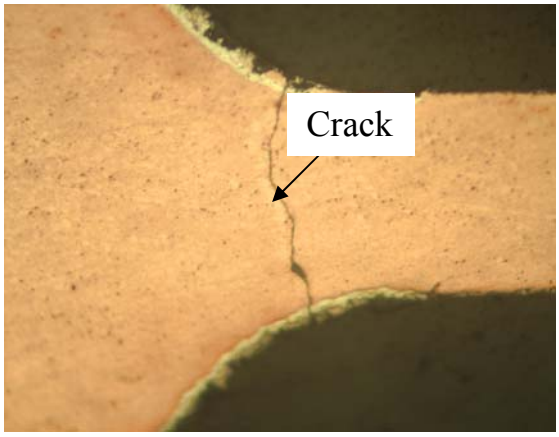

Figure 25: Copper trace crack for BGA component

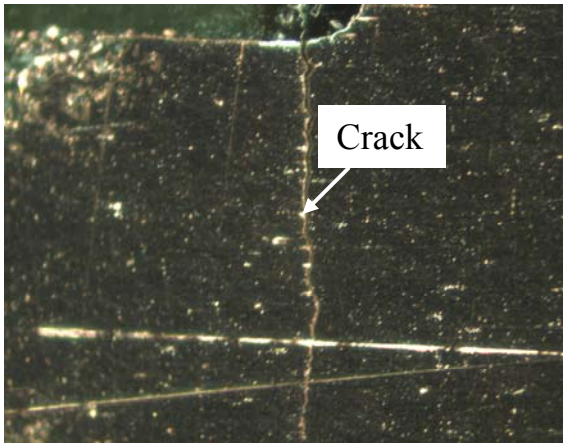

Figure 26: Copper trace crack for LCR component

VI CONCLUSIONS AND FUTURE WORK

Interconnect durability of electronic hardware was examined under harmonic and random vibration test loads. Under constant-amplitude harmonic loading, a comparison was drawn between SAC305 and Sn37Pb assemblies when similar specimens were excited at their natural frequency. Under step-stress random loading, the impact of low temperature (-40^{o}C), high temperature (125^{o}C), and room temperature (~ 25^{o}C) ambient was examined. In addition, the impact of isothermal aging preconditions of 100 hours and 350 hours at 125^{o}C on room temperature vibrations was examined. The results provide insights regarding the vibration induced fatigue failure of Sn37Pb and SAC305 assemblies. Based on these test results, the following preliminary observations can be made, in spite of the scatter in the data:

- Isothermal vibration durability generally decreases as the temperature increases, for both Sn37Pb and SAC305 assemblies.
- Increasing the duration of pre-aging at a constant elevated temperature decreases the TTF for both Sn37Pb and SAC305 assemblies when these are exposed to vibration durability testing. The influence appears to be more severe for Sn37Pb/HASL assemblies than for SAC305/OSP systems

- There are at least two competing failure sites; one in the bulk of the solder material in the join, and another in the copper trace/pad on the PWB below the solder joint.
- The SAC305 assemblies were found to be generally less durable than the Sn37Pb assemblies at the load levels examined in this study, but there appears to be a cross-over amplitude beyond which the SAC305 assemblies may be more durable..

ACKNOWLEDGMENTS

This work is sponsored by the members of the CALCE Electronic Products and Systems Consortium and the CALCE Long-term Lead Free Reliability Consortium, at the University of Maryland, College Park. We also acknowledge the help of NTS Corporation, where the broad-band tests were conducted.

REFERENCE

[1] Zhou, Y., Scanff, E., and Dasgupta, A., 2006, "Vibration Durability Comparison of Sn37Pb vs. SnAgCu Solders," *ASME International Mechanical Engineering Congress and Exposition*, Chicago, IL, paper number 13555

[2] Wang, H., Zhao, M, and Guo, Q., 2004, "Vibration Fatigue Experiments of SMT Solder Joint," *Journal of Microelectronics and Reliability*, Volume 44, Issue 7, pp 1143-1156.

[3] Basaran, C. and Chandaroy, R., 1998, "Mechanics of Pb40/Sn60 Near-eutectic Solder Alloys Subjected to Vibration," *Journal of Applied Mathematical Modeling*, Volume 22, Issue 8, pp 601-627.

[4] Zhang, Q., Dasgupta, A., and Haswell, P., 2005. "Isothermal Mechanical Durability of Three Selected Pb-Free Solders: Sn3.9Ag0.6Cu, Sn3.5Ag and Sn0.7Cu." *Transactions of the ASME*, vol. 127, pp 512-522

[5] Basaran, C. and Chandaroy, R., 2002. "Thermomechanical analysis of solder joints under thermal and vibration loading." *Transactions of the ASME*, vol. 124, pp 60-66

[6] Upadhyayula, U., 1999. "An Incremental Damage Superposition Approach for Surface Mount Electronic Interconnect Durability under Combined Temperature and Vibration Environments." *PHD Thesis*, University of Maryland

[7] Stam, F. A., Davitt, E., 2001. "Effects of Thermomechnical cycling on lead and lead-free (SnPb and SnAgCu) Surface Mount Solder Joints." *Microelectronics Reliability*, Volume 41, Issue 11, pp 1815-1822

[8] Xu, L., Pang, J. H. L., 2006. "Intermetallic growth studies on SAC/ENIG and SAC/Cu-OSP lead-free solder joints." *Thermal and Thermomechanical Phenomena in Electronics Systems.* Tenth Thermal Intersociety Conference

[9] Lau, J., 1996. “Solder joint reliability of flip chip and plastic ball grid array assemblies under thermal, mechanical and vibration conditions.” *IEEE Transactions on Components, Packaging, and Manufacturing Technology*, Vol, 19, pp. 728-735

[10] Darbha, K., Ling, S., and Dasgupta, A., 1997. “Stress Analysis of Surface-Mount Interconnections Due to Vibration Loading.” *Journal of Electronic Packaging*, Vol. 119, pp. 183-188

[11] Barker, D. B., Chen, Y. S., and Dasgupta, A., 1993. “Estimating the vibration fatigue life of quad leaded surface mount components.” *Journal of Electronic packaging*, vol. 115, pp. 195-200

[12] Lau, J., Gratalo, K., and Schneider, E., 1995. “Solder Joint Reliability of Large Plastic Ball Grid Aray Assemblies under Bending, Twisting, and Vibration Conditions.” *Circuit World*, Vol. 22, pp. 27-32

[13] Lau, J., et al., 1993. “Solder joint reliability of surface mount connectors.” *Journal of Electronic Packaging*, Vol. 115, pp. 180-188

[14] Lau, J., Schneider, E., and Baker, T., 1996. “Shock and vibration of solder bumped flip chip on organic coated copper boards.” *Journal of Electronics Packaging*, Vol. 118, pp. 101-104

[15] Yang, Q. J., Wang, Z. P., Lim, G. H., Pang, J. H. L., Yap F. F., and Lin, R. M., 2002. “Reliability of PBGA Assemblies under Out-of Plane Vibration Excitation.” *IEEE Transactions on Components and Packaging Technologies*, Vol. 25, pp. 293-300

[16] Che, F. X., Pang, H. L. J., Wong, F. L., Lim G. H., and Low, T. H., 2003. “Vibration Fatigue Test and Analysis for Flip Chip Solder Joints.” *Electronics Packaging Technology Conference*, pp 107-113

[17] Wong, T. E., and Fenger, H. S., 2004. ”Vibration and Thermo-mechanical Durability Assessment in Advanced Electronic Packaging Interconnects.” *IEEE Electronic Components and Technology Conference*, pp 1080-1087

[18] Barker, D. B., Dasgupta, A., and Pecht, M. G., 1991. “PWB solder joint life calculation under thermal and vibration loading.” *Proceedings Annual Reliability and Maintainability Symposium*, pp. 451-459

[19] Zhou. Y., and Dasgupta, A., 2007. “Vibration durability Assessment of Sn3.0Ag0.5Cu & Sn37Pb Solders under Harmonic Excitation.” *ASME International Mechanical Engineering Congress and Exposition*, Seattle, WA

Chapter 3 Vibration Durability Model for Solder Interconnects

This chapter presents the post-processing of the harmonic vibration test results that were presented in Chapter 2, to extract vibration durability model constants for both SAC305 and Sn37Pb solder materials. The durability model used in this study is a generalized strain-life model. The derivation of generalized strain-life durability model constants from random durability test results are quite complex and challenging. In Appendix A, a methodology was developed to generate a simplified secant durability model based on step-stressed random vibration durability test results. The post-processing is conducted using detailed finite element analysis of the failed interconnects, and is facilitated by characterization of the harmonic response of the PWA. The details of finite element code for ANSYS software was attached in Appendix C. Competing failure modes are found in the failure analysis of the failed components, including cracked solder joints and cracked copper traces. The occurrence of copper trace failures appears to be more prevalent in BGA components than in LCRs and also more prevalent in SAC interconnects than in SnPb interconnects. To maximize the probability of addressing solder failures, the LCR interconnects are the focus of the current analysis.

This chapter has been accepted for publication by the ASME Journal of Electronic Packaging (JEP). In Chapter 4, the dependence of the durability model constants on the stress-strain material properties will be examined with a parametric study. The accuracy of the durability model will also be tested against durability data measured from random vibration tests and from quasi-static 4-point cyclic bend tests.

Vibration durability Assessment of Sn3.0Ag0.5Cu & Sn37Pb Solders under Harmonic Excitation

Y. Zhou, B. Moustafa and A. Dasgupta*

CALCE Electronic Products and Systems Center

Mechanical Engineering Department, University of Maryland,

College Park, MD, 20742

Tel: 301-405-5231, Fax: 301-314-9262, Email: Easily@umd.edu

ABSTRACT

In this paper, the vibration durability of both SAC305 & Sn37Pb interconnects was investigated with narrow-band harmonic vibration tests conducted at the first natural frequency of the test PWB (Printed Wiring Board), using constant-amplitude excitation. A time-domain approach, reported in the literature [1], was adapted in this study for the fatigue analysis. The test board consists of daisy-chained components, to facilitate real-time failure monitoring. The response of the test specimens was characterized and accelerated fatigue tests were conducted at different loading amplitudes to obtain a mix of low-cycle fatigue (LCF) and high-cycle fatigue (HCF) data points. The SAC305 interconnects were found to have lower fatigue durability than comparable Sn37Pb interconnects, under the narrow-band harmonic excitation levels used in this study. This trend is consistent with most results from broad-band vibration tests [2] [3] [4] and from repetitive mechanical shock tests [5], but counter to findings from quasi-static mechanical cycling (LCF) studies [14]. Failure analysis revealed two competing failure modes, one in the solder and another in the copper trace under the component. Thus solder fatigue properties extracted with the help of finite element simulation of the test article should be treated as lower-bound estimates of the actual fatigue curves.

I. INTRODUCTION

Vibration loading is commonly encountered during the service life of electronic products, but durability under vibration loading has not received the same attention as thermal cycling durability. The characteristics of the stress from vibration loading are low amplitude and high frequency, while those of thermal cycling loading are high amplitude and low frequency. Recent work on fatigue effect due to vibration loading is reviewed here. Lau, et al. conducted vibration reliability testing [7] [8] [9] using sweep sinusoidal excitations and studied vibration fatigue properties based on linear assumption. Jih et al. [10] conducted 3D global/local finite element modeling combined with a fracture mechanics approach to study crack propagation along the interface of surface mount solder joint and lead frame. Liu et al [11] developed a technique and loading apparatus which allowed BGA packages to be visually inspected during high cycle vibration testing. In their study, BGA interconnect failure was observed to be the result of crack initiation and propagation along the nickel/solder interface on ENIG plating. Failure parameters were computed using a nonlinear finite element analysis, for commonly used fatigue life-prediction models, based on damage mechanics and fracture mechanics. Their results showed that the test data correlates better with fracture models than with damage models. Zhao et al [12] checked the inelastic behavior of solder joints of BGA packages under concurrent thermal and vibration loading. Laser moire interferometry was used to measure the whole deformation field of the prepared specimen surface and the corresponding inelastic strain field was then calculated. At elevated temperature, vibration and shock was found to cause the accumulation of inelastic strain and damage in solder joints, which is contrary to the popular belief that most vibration-induced strains are usually elastic.

The literature addresses many aspects of damage due to vibration loading. However, for the generalized Coffin-Manson strain-life durability model, a comprehensive set of durability model constants are not yet available. In particular there is insufficient data for the elastic HCF (Basquin) curve. Most researchers conduct experiments up to 1 million cycles for high cycle durability test, which is not enough to calibrate high cycle fatigue properties of solders. In the present study, in order to have a good understanding of HCF durability, tests were conducted for more than 10^8 cycles to failure. Elastic-plastic finite element analysis (FEA) was conducted to explore the corresponding strain level in the critical solder joint.

II. OVERVIEW OF APPROACH

The present study uses a time-domain approach for vibration fatigue characterization [1]. Constant-amplitude, harmonic durability tests were conducted at the first resonant frequency of the test PWB. Compared to broad-band step-stress vibration durability tests, this constant-amplitude harmonic test has several advantages:

- The dynamic response of the test vehicle consists only of a single mode response, and not the coupling of several modes
- The characteristic strain history is also harmonic and has a constant amplitude. Thus there is no need to use any cycle counting algorithm to quantify the loading history.
- The damage accumulation rate is constant throughout the whole test procedure, and it is hence sufficient to analyze a unit time-interval.

All these advantages make the post-processing of harmonic, constant-amplitude test results much easier and straight forward than broad-band, step-stress test results. There are less complexities and approximations in the whole procedure. Thus the vibration durability properties can be

assessed with greater accuracy, using the harmonic, constant-amplitude test. The approach is shown in Figure 1.

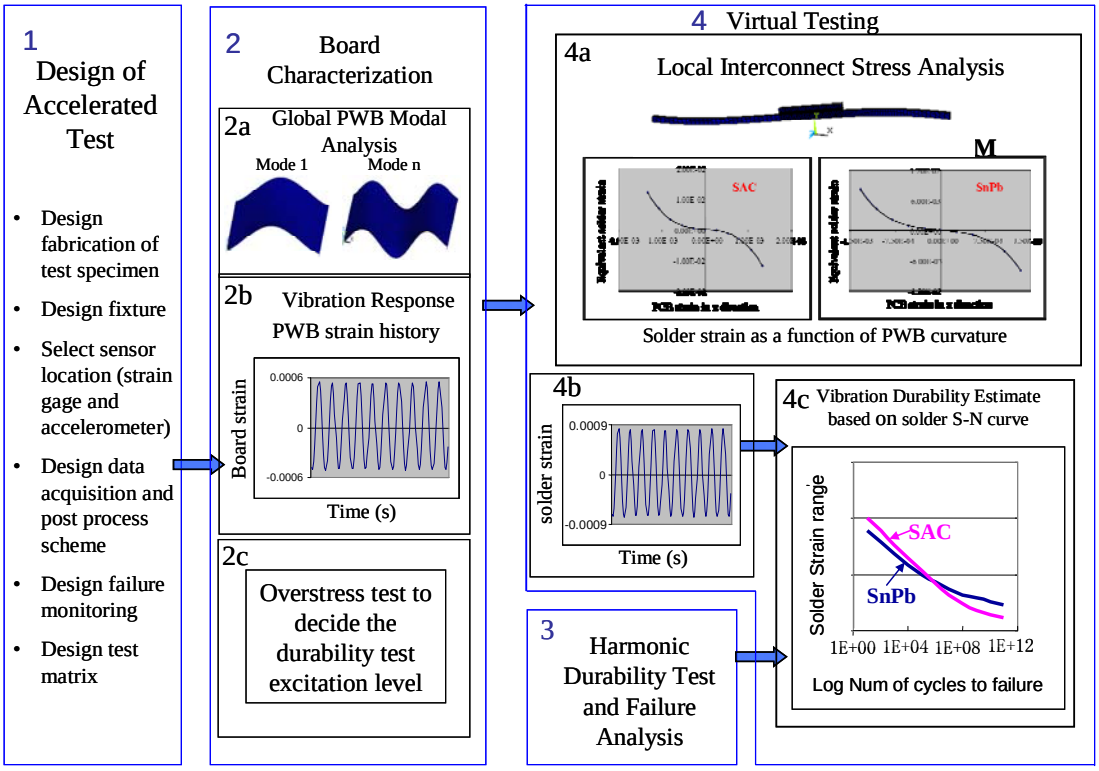

Figure 1: Time domain vibration durability approach with harmonic accelerated test

Step 1 shows the steps for designing the vibration durability test. The test specimen is a populated PWB. The test PWB is then characterized, as shown in Step 2. The outputs of the specimen characterization include natural frequency, mode shape, characteristic strain history, and overstress limit. Based on the information from the specimen characterization, the durability test is then conducted and corresponding failure analysis is carried out to obtain information about failure mode, failure site and failure mechanism, as listed in Step 3. In Step 4, detailed elastic-plastic finite element simulation is used to investigate the relationship between the flexural strain of the PWB (close to the component of interest) and the strain in the critical solder joint of the component. The PWB flexural deformation shape in the FEA is constrained to

duplicate the first mode shape (as determined from FEA modal analysis). The derived solder strain is used to obtain the durability model constants are obtained for both SAC305 and Sn37Pb. Model constants are obtained for both the HCF (Basquin) curve and the LCF (Coffin-Manson) curve, by combining the vibration fatigue data obtained from this study with mechanical cycling data obtained from earlier studies [14, 15]. The details of these steps and the relevant results are described in the remainder of this paper

III. DESIGN OF DURABILITY TEST

A special test vehicle was designed for this study, as shown in Figure 2. It's a two-layer FR4 printed wiring board (PWB) with copper metallization. Two types of solders were used for the interconnects: Sn37Pb and SAC305 (Sn3.0Ag0.5Cu).

The Sn37Pb assemblies were assembled with no-clean-type 3-Kester 256 paste (Sn37Pb) and the board finish was Sn37Pb hot air solder level (HASL). The lead-free assemblies were made with no clean-type 3-Kester R905 solder paste (Sn3.0Ag0.5Cu) and the board finish was Immersion Tin (Imm-Sn). All test assemblies were preconditioned by 100 hours of exposure to 125^{o}C temperature.

As shown in Figure 2, there are four PBGA256 components, four LCCCs, sixteen QFPs, ninety-six LCR2512 resistors and ninety-six LCR1210 resistors on each test PWB. All components are daisy-chained so they can be monitored in real-time for failures. The 96 LCRs of each type are daisy-chained into 8 nets. Four groups are mounted parallel to the PWB long edge, and four are mounted perpendicular to the long edge. The test PWB was clamped along the two opposite long edges on a fixture which was mounted on the table of a single-axis electrodynamic vibration shaker, for excitation in the out-of-plane direction.

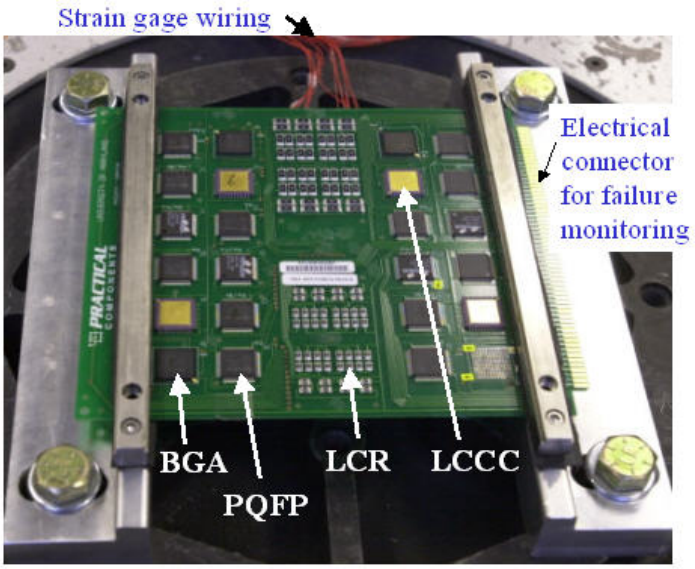

Figure 2: Vibration durability test set up

A multi channel data logger was used to monitor the daisy chain resistance for each component. The threshold resistance for failure was chosen to be 100 Ohms in this study.

Table 1: Test matrix and excitation for SAC305

SAC	Overstress test	9G	10.5G	12G
	1	1	1	1

Table 2: Test matrix and excitation for Sn37Pb

	10.5G	12G
SnPb	1	1

IV. BOARD CHARACTERIZATION

A modal test was conducted with accelerometers to measure the natural frequencies and mode shapes of the test vehicle under the boundary conditions specified in the previous section, as shown in Figure 3. The first natural frequency of the test PWB is 169Hz.

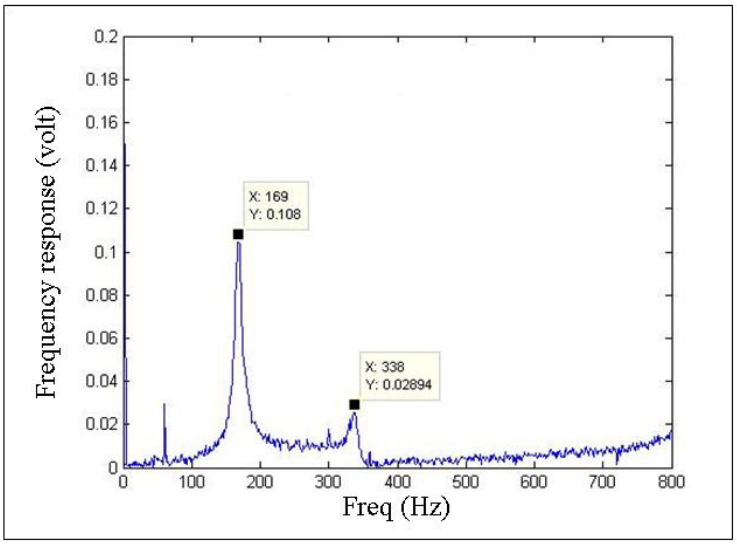

Figure 3: Frequency response from accelerometer modal test

All vibration tests were conducted at the first natural frequency. First, an "overstress" test was designed and conducted to identify the upper limit of stress allowable in the subsequent durability tests. In this study, overstress level refers to excitation that can cause component failure in the test setup in less than 10mins. The overstress limit for different components and the results are shown in Table 3.

Table 3: Overstress limit for different component

Component	LCR 2512	LCR 1210	BGA	LCCC	QFP
Overstress limit	15G	18G	15G	18G	>20G

The overstress limit of the QFP component was above 20G, which was the limit of our shaker. The overstress result was based on the first failure of each kind of component. The excitation levels for the durability test for SAC305 were chosen to be 70% and 60% of the overstress limit, which were 10.5G and 9G, respectively, as shown in Table 1. Based on previous work [2] [3] [4], Sn37Pb was found to be more durable than corresponding SAC305 solder under similar

vibration loading. To make sure the corresponding durability test can be finished in acceptable time, the excitation levels for the Sn37Pb durability test were chosen to be 80% and 70% of the overstress limit, which were 12G and 10.5G, respectively, as listed in Table 2.

The dynamic response of the PWB is characterized with 5 strain gages located as shown in Figure 4. Each strain gage is located immediately outside the footprint of a component, on the non-populated side of the PWB. This location is chosen because it has the highest curvature due to local stiffening of the PWB by the component, and hence provides the best signal-to-noise ratio.

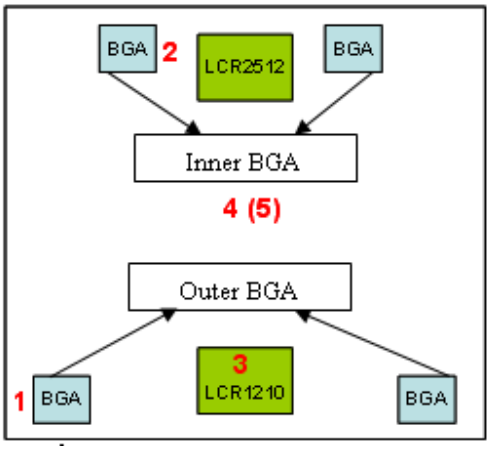

Figure 4: Strain gage attachment

A Labview-based strain-gage conditioner and DAQ system was used for board characterization to collect the strain histories. The strain histories were characterized for each of the excitation levels used in the durability tests, as per Tables 1 and 2. As expected, the output strain is harmonic at the excitation frequency. A typical strain time history is plotted in Figure 5.

The focus of this study is on LCR and BGA components. The BGA components are grouped into Inner BGA and Outer BGA based on their location on the test vehicle, as shown in Figure 4. Strain gages 1 to 3 are used to collect the strain for the outer BGA, Inner BGA and LCR

components, respectively. The assumption here is that LCR2512 and LCR1210 have the same PCB strain since the difference between their locations is small.

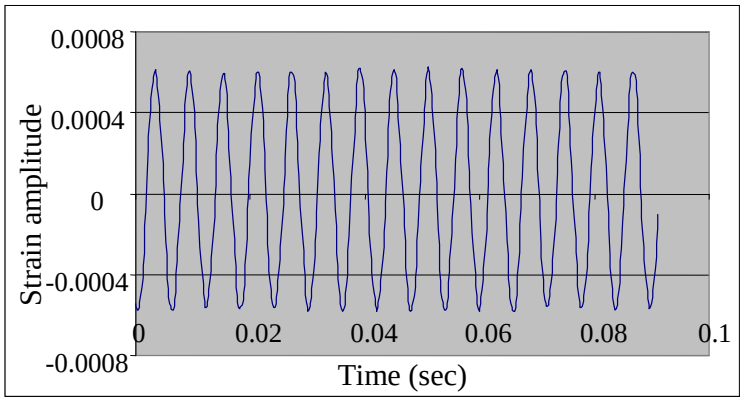

Figure 5: Characteristic strain time history

The measured strain amplitude for Outer BGA, Inner BGA and resistor under 12G, 10.5G and 9G harmonic excitation, are plotted in Figure 6. Under this clamped-clamped condition, the highest flexural strain should be at the outer edge and at the PWB center. However, the outer BGA has a larger local stiffening effect than the small LCRs. Consequently, the location of the strain gage near the outer BGA experiences the largest maximum PWB curvature (and thus, flexural strain), followed by the location of the gages near the LCR and the inner BGA.

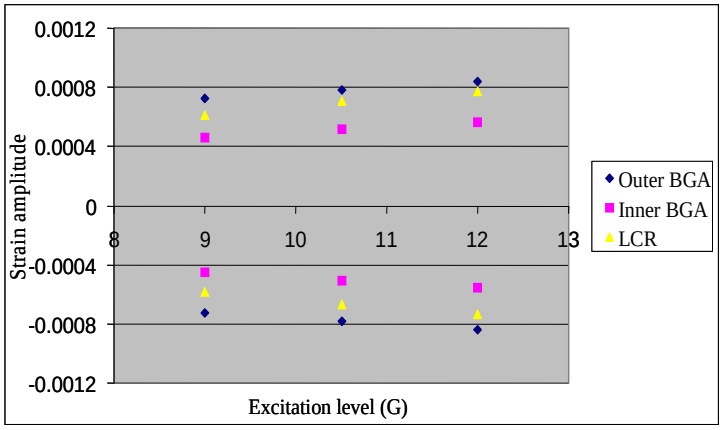

Figure 6: Strain amplitude

Strain gages 4 and 5 were attached at the center of the PCB, far away from the components. These two strain gages are used to check the membrane strain in the test board during the

durability test. The location of these two strain gages was chosen to be far away from the components to minimize the effect of the component on the PWB local stiffness. The mean of the strain reading from strain gages 4 and 5 provides the membrane strain, plotted in Figure 7. The amplitude in Figure 7 was comparable to the noise amplitude, which reveals there is no measurable membrane strain during the experiment in this study. This result is very important for accurate finite element simulations to obtain the solder strain, as explained later, in Section 6.

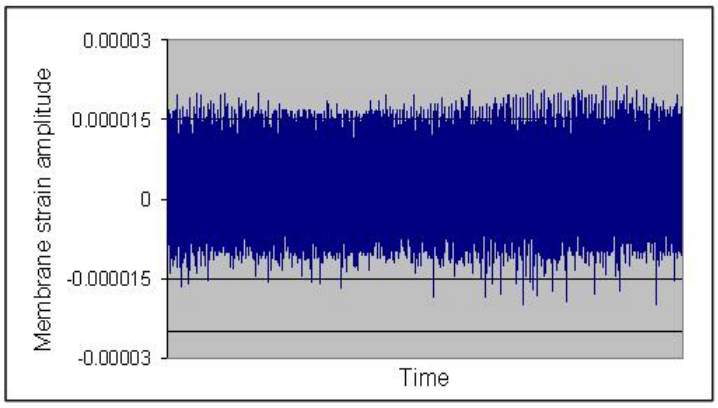

Figure 7: Membrane strain results at the center of the PCB

V. DURABILITY TEST

Constant-amplitude harmonic excitation was used in this study, at a frequency of 169Hz, which is the first natural frequency of the test vehicle. Since all joints are daisy-chained in a single net for each component, the data logger recorded the first solder joint failure (100 Ohm increase in net resistance) in each component. The test was conducted until most of the components failed. The response history for each component depends not only on the excitation, but also on the location of the component on the PWB. The components of interest in this study are LCR1210 and LCR2512. Depending on the proximity of the resistor location to the PWB centerline, they are divided into the two following groups, as shown in Figure 8:

- Center resistor

- Edge resistor

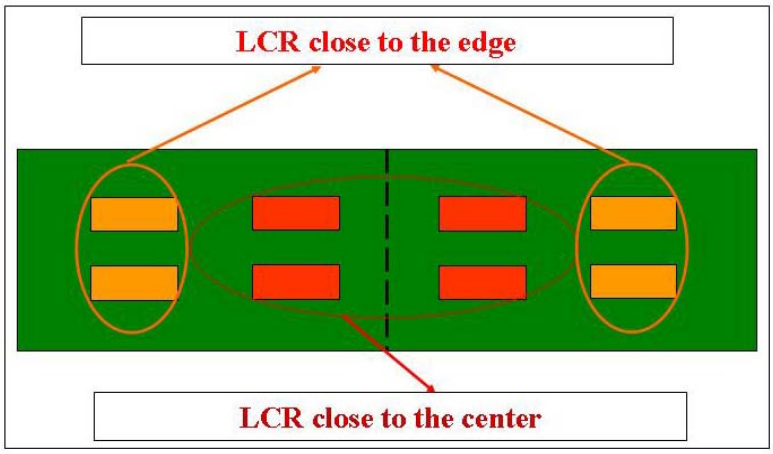

Figure 8: Resistor location on the test board

So altogether they are four types of resistor groups in this study:

- Center LCR1210
- Edge LCR1210
- Center LCR2512
- Edge LCR2512

Components in the same group have two characteristics in common:

- Same component type
- Same PWB curvature

Only the resistor groups that are assembled parallel to the long-edge of the PWB failed during the test, for both LCR2512 and LCR1210. Altogether, there are 8 durability data points for each LCR type on each test board. The durability test results for the same group of components are averaged on a log scale.

After the vibration durability test, the failure modes and sites are investigated to confirm the failure mechanism. Destructive failure analysis has been carried out for BGA and LCR

components. Obvious solder cracks have been found in many of the BGA and LCR components, as seen in Figures 9 and 10.

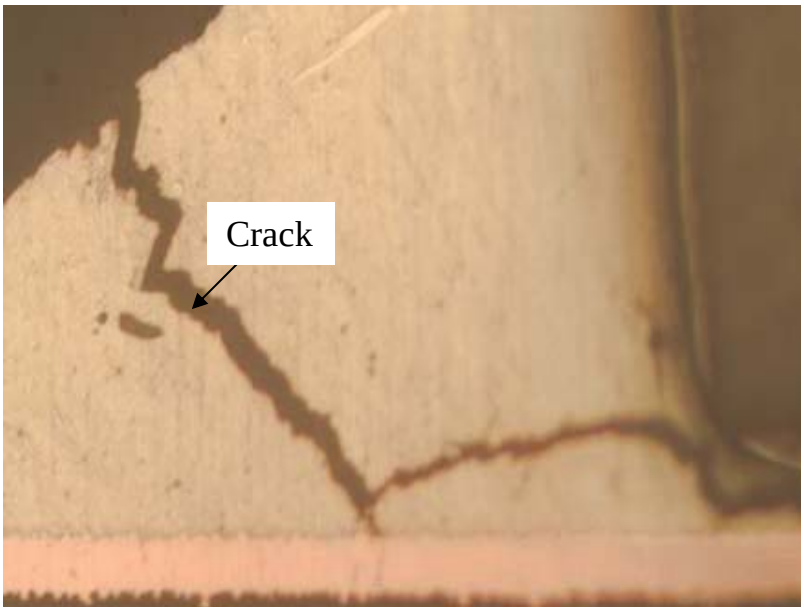

Figure 9: Crack in LCR solder joint

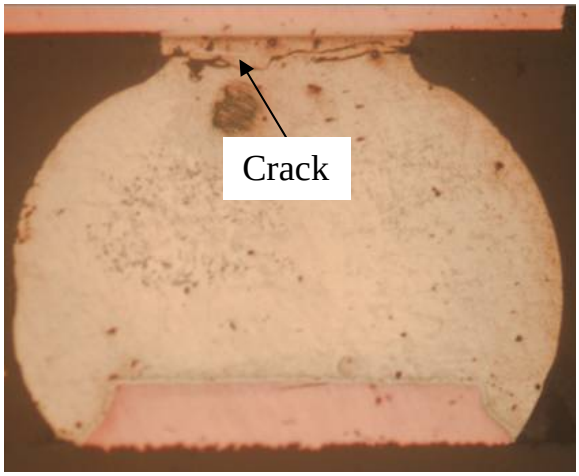

Figure 10: Crack in neck of BGA solder ball

A completing failure mechanism found for both BGA and LCR components, is fatigue cracking of the copper trace connected to the solder pad. Figures 11 and 12 show examples of the copper trace cracks.

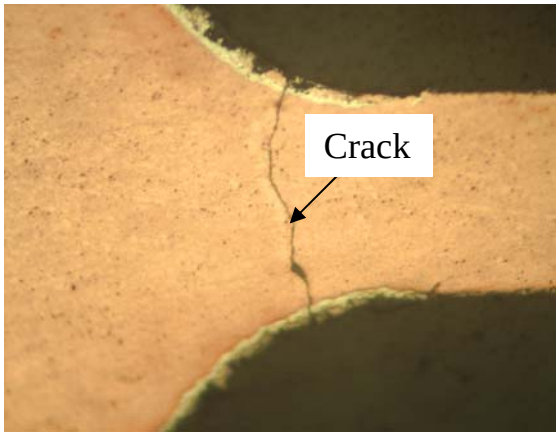

Figure 11: Copper trace crack for BGA component

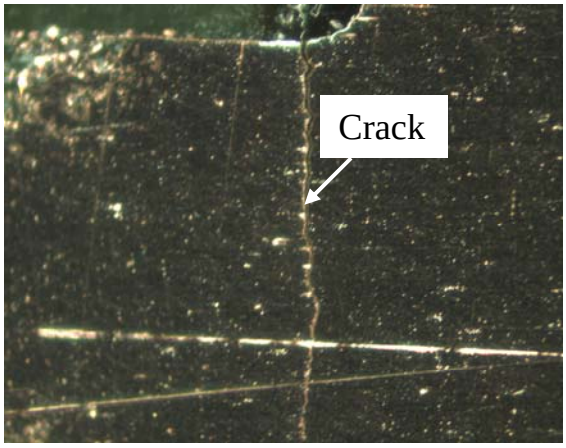

Figure 12: Copper trace crack for LCR component

Sampling of the failed specimens reveals that there are far less occurrences of copper trace failure in LCR component than in the BGA components. Failure was by solder fatigue in a larger majority of the LCR groups than in BGAs. The LCR durability data is therefore used in this study to investigate solder fatigue properties.

The measured time-to-failure of LCR components is plotted in Figures 13 to 14 for both SAC305 and Sn37Pb.

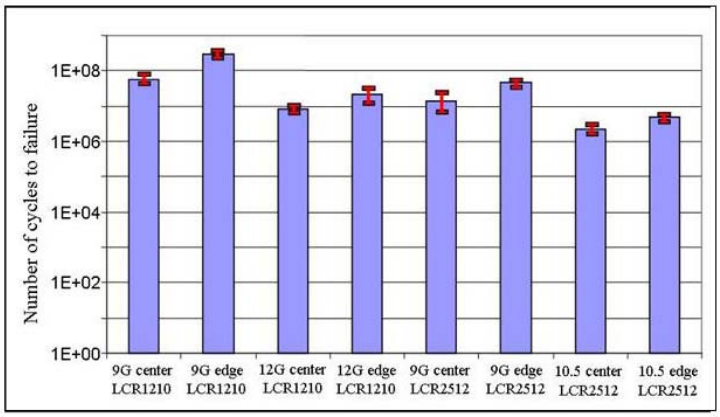

Figure 13: Durability plot for SAC LCR interconnects

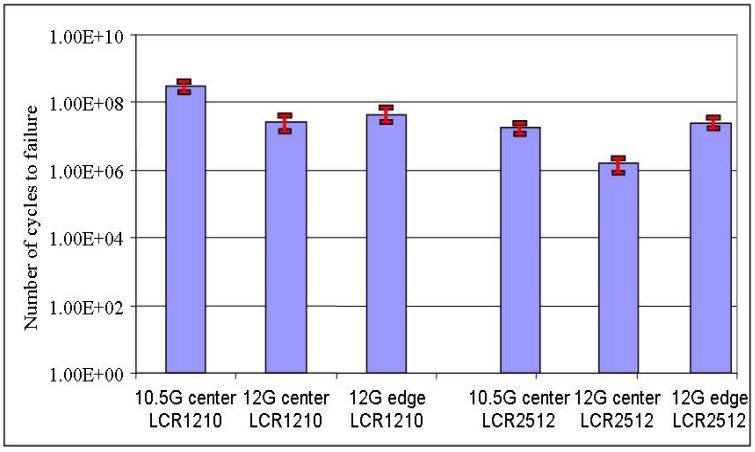

Figure 14: Durability plot for SnPb LCR interconnects

The results in Figures 13 & 14 show that Sn37Pb interconnects are more durable than corresponding SAC305 interconnects under identical amplitudes of harmonic loading. All these durability test results are used later in Sections 6 and 7 for assessing the durability model constants.

VI. VIRTUAL TESTING

In order to obtain the solder strain history, detailed local FEA modeling is conducted for both LCR components. This local FEA model is dependent not only on the component style but also on its location on the PWB. 2D models are built for LCR1210 and LCR2512 resistor assemblies.

The out-of-plane depth is scaled proportional to the relative widths of the component and the PWB.

Since the curvature of the PWB under dynamic excitation is quite different from that under static loading, modal analysis is first carried out for the local model for each component. The deformed shape for the PWB from modal analysis is then input to the FEA model using constraint equations. Details of the procedure are presented here for the LCR2512 component, for illustration.

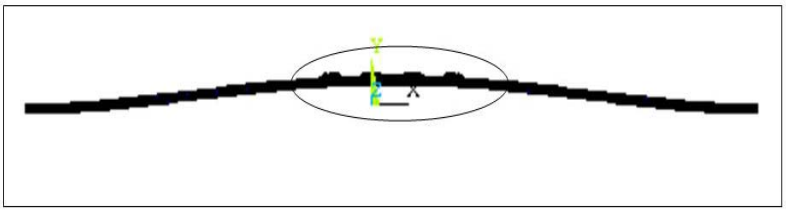

Figure 15: Local 2D model for resistor component

There are 4 resistors in the FEA model, as shown in Figure 15. The location of the strain gage is at the center of the board in Figure 16.

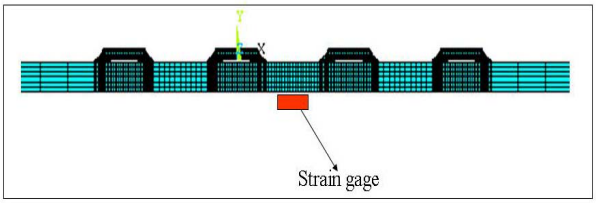

Figure 16: LCR component on the FEA

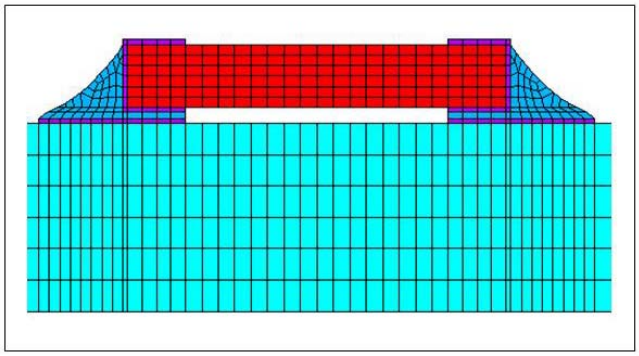

Figure 17: Detailed mesh for LCR component

The detailed finite element mesh for a LCR component is shown in Figure 17. The PWB board is modeled with plane strain elements of unit thickness, while the LCR component and the solder joint are modeled as plane-stress elements of finite thickness. The out-of-plane thickness is scaled, to preserve the dimensional ratios of the actual assembly. There are more than 3000 2D elements altogether for this local FEA. The major dimensions of the FEA model are listed in Table 4. The copper pads are modeled but the connecting traces are not modeled in detail as the copper trace cracking is not the focus of this study.

Table 4: Main dimension for LCR2512 FEA model

	Length (mm)	Height (mm)	Thickness (mm)
PCB	154	1.5	1.0
Solder	---	0.03	0.02
Copper pad	0.5	0.04	0.02
Ceramic	3.25	16	1.13

The actual boundary conditions of the test setup are very complex in our study, since rubber liners are used between the test PWB and the fixture, to protect copper traces on the surface of the test vehicle, from fretting wear. As shown earlier in Figure 7, the experiment shows no appreciable membrane strain during the dynamic response, which means that the x direction displacements are not fully constrained because of the compliant rubber liner. In this simulation, translations are constrained in the transverse direction but not in the in-plane direction (except to remove rigid body motion). Then rotational springs are used to constrain the rotation in Z direction. The stiffness of the rotational spring is determined by matching the natural frequencies to those observed in the experiment.

Modal analysis is carried out using this local model, and the normalized mode shape is shown in Figure 18.

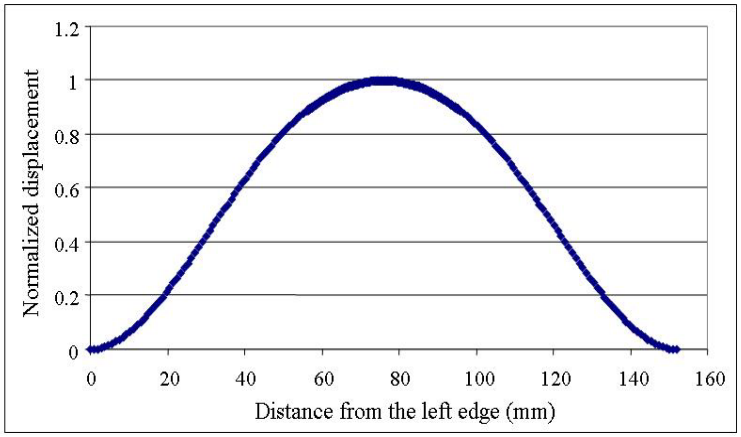

Figure 18: Normalized displacement at the center of the PCB for first mode

This mode shape is then enforced on the local finite element model using constraint equations, so that the deformation distribution during dynamic response can be captured in an equivalent static analysis. The purpose of the constraint is to make the deformed geometry consistent with the response to harmonic excitation. Since there are 537 nodes, there are 536 constraint equations

altogether. Progrssively increasing displacements are then applied at the center node of the PWB to obtain transfer functions between the PWB strains measured in the experiment and the strains in the critical location of the critical solder joint.

The elastic-plastic stress-strain properties used in this study are obtained from the literature. There is wide variation in the properties reported in the literature by different authors, because of variations in test methods and specimen microstructure. For consistency, it is desirable to use all properties from a common test method and common test specimen. Hence the properties were selected from a common reference [13]. Unfortunately, the SAC material reported in Qian's study is near-eutectic SAC, not SAC305. However, preliminary studies indicate that they can provide a reasonable approximation for SAC305 properties. The assumed stress-strain curves for both SAC305 and Sn37Pb are plotted in Figure 19.

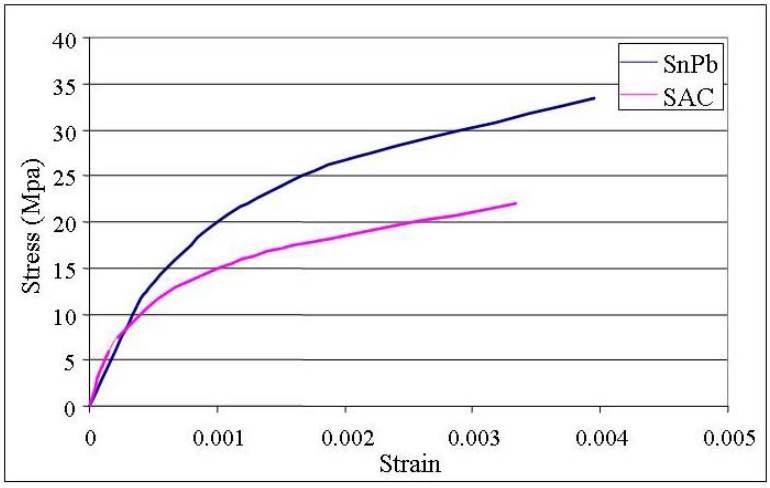

Figure 19: Stress-Strain material properties from literature [13]

To derive the strain transfer function, the PWB strains are monitored over the footprint of the strain gage, shown in Figure 16, and the solder strain is averaged in the neighborhood of the highest strain concentration, as shown in Figure 20.

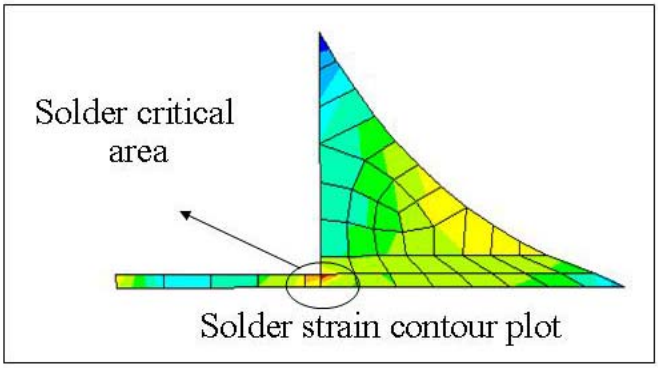

Figure 20: Local area used for averaging the strain in the critical solder joint

The strain transfer functions for both SAC305 and Sn37Pb solder, obtained from this detailed local FEA, are shown in Figure 21. This graph allows us to estimate the solder strain history for a measured strain history in the PWB.

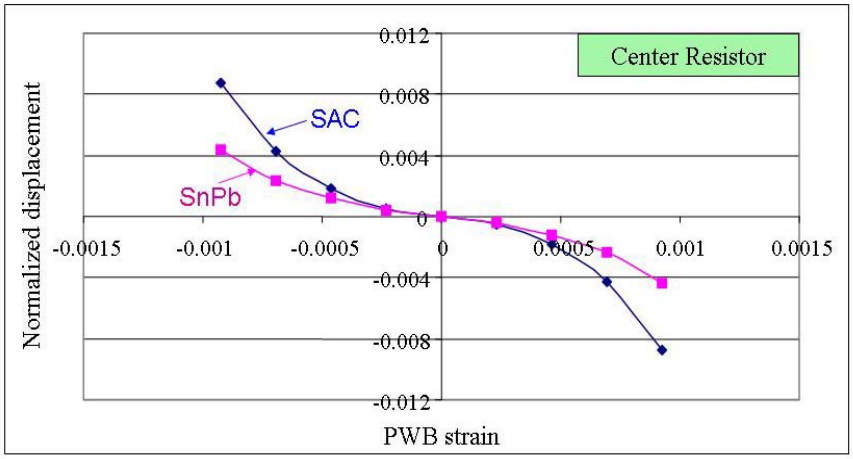

Figure 21: Strain transfer function for center resistor

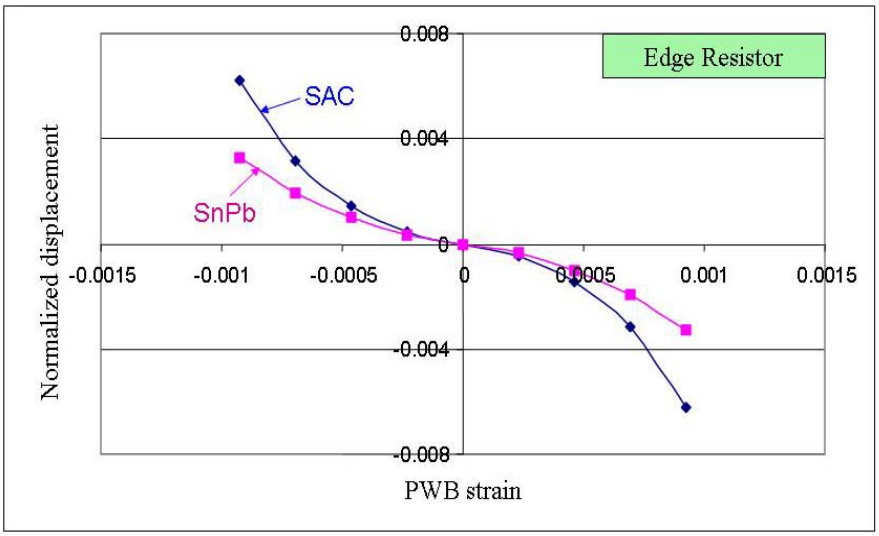

Figure 22: Strain transfer function for edge resistor

The strain transfer functions are obtained for both center and edge resistors for both SAC305 and Sn37Pb interconnects. The results show that the strain in the SAC305 joints is more sensitive to PWB curvature than in Sn37Pb joints. Similar strain transfer functions are also obtained for LCR1210.

The available data can now be summarized as follows:

- Solder strain history during vibration test, obtained from combination of FEA simulation and experimentally measured PWB strain history
- Number of cycles to failure for each component, from vibration durability experiment
- Additional durability data from previous studies [13][15][16]

This information is used to find the model constants for the generalized Coffin-Manson strain-life fatigue curve. The details are described in the next section.

VII. FAGITUE MODEL FITTING

The generalized strain-life fatigue model shown in Equation 1 is used in this study.

$$\frac{\Delta\varepsilon}{2} = \frac{\sigma_f^{'}}{E}\left(2N_f\right)^b + \varepsilon_f^{'}\left(2N_f\right)^c \quad (1)$$

$\sigma_f^{'}$: Fatigue strength coefficient

$\varepsilon_f^{'}$: Fatigue ductility coefficient

b: Fatigue strength exponent

c: Fatigue ductility exponent

E : Young's modulus

N_f : Number of cycles to failure

$\Delta\varepsilon$: Strain range

This fatigue model includes fatigue damage contributions from plastic deformation (Coffin-Manson LCF curve) and elastic deformation (Basquin HCF curve). As seen in Equation 1, there are four model constants altogether that need to be estimated. The plastic (LCF) part of the durability model has been investigated in previous studies for SAC305 [13] and for Sn37Pb [15, 16], based on 50% load-drop under quasi-static mechanical cycling on a shear specimen. In this study, the raw data from these studies is used to derive new fatigue constants for 20% load-drop.

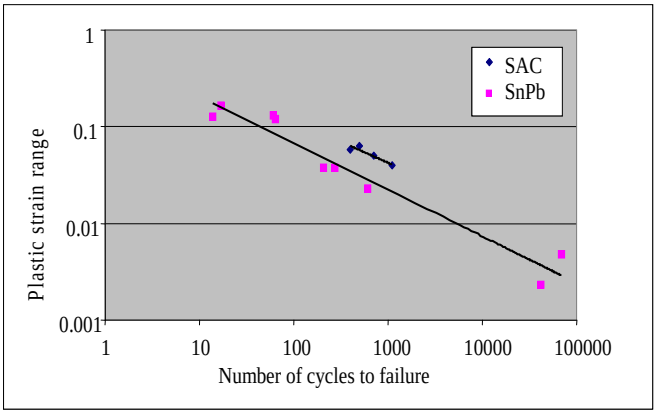

Figure 23: Plastic strain-life curves for SAC305 and SnPb [14-15]

The durability data and corresponding fitting curves are shown in Figure 23. The results show that SAC305 has better LCF resistance than Sn37Pb. The model constants $\varepsilon_f^{'}$ and c for LCF are listed in Table 5 for both SAC305 and Sn37Pb.

Then the obtained LCF model constants are used in the current study to estimate the plastic contribution in the vibration fatigue deformation. The elastic contribution is obtained by subtracting out this plastic contribution from the FEA estimate of the total deformation. The HCF model constants are then estimated by relating the elastic deformation to the measured cycles-to-failure (N_f). The results are plotted in Figure 24, and show that HCF damage dominates in most of the durability test data obtained from this vibration study. Figure 24 also shows a crossover of the HCF durability curves of these two solders. SAC305 interconnects outperformed Sn37Pb interconnects in this study for durability below 10^7 cycles, and the reverse was true above 10^7 cycles.

It is important to recognize that the failure data collected in this study contains two competing failure modes: solder fatigue and copper trace fatigue. Since it is practically impossible to segregate the two data sets, the fatigue curves presented here must be interpreted suitably as being lower-bound estimates of solder fatigue curves. In other words, the solder fatigue durability can never be less than that predicted by these fatigue curves. In that sense, these fatigue constants will provide conservative estimates of solder interconnect durability.

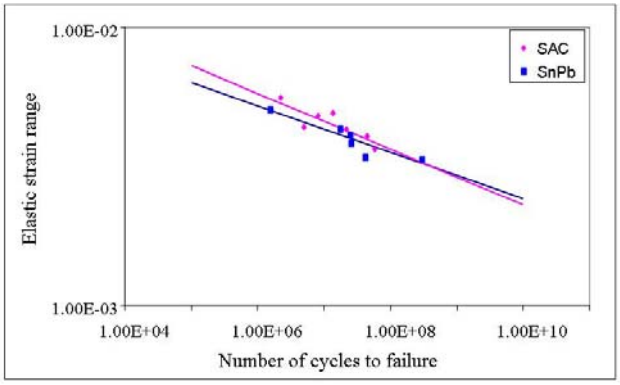

Figure 24: Elastic strain-life curves for SAC305 and SnPb

The generalized strain-life models for both SAC305 and Sn37Pb are listed in Table 5.

Table 5: Durability model fitting results for SnPb interconnect

	$\frac{\sigma_f^{'}}{E}$	b	$\varepsilon_f^{'}$	c
SnPb	0.012	0.053	0.43	-0.48
SAC	0.0087	0.073	0.59	-0.44

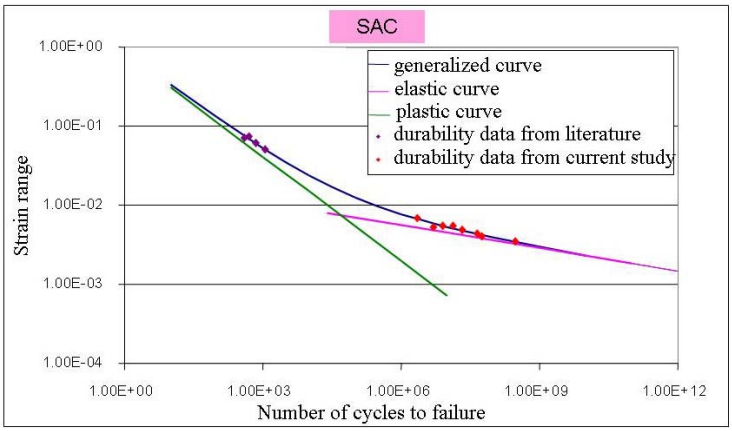

Figure 25: Durability curves and experiment data points for SAC305 interconnect

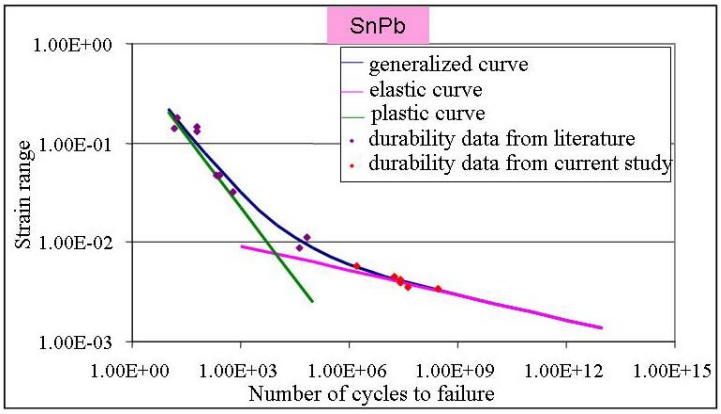

Figure 26: Durability curves and experiment data points for SnPb interconnect

The durability data and the obtained fatigue model are graphically presented in Figure 25 for SAC305 interconnects, and in Figure 26 for Sn37Pb interconnects. Both the LCF and HCF curves are included in the plots. Mechanical cycling data for these solders in the literature are found to be mostly in the LCF region, while the durability data from the current vibration study are found to be mostly in the transition and HCF area.

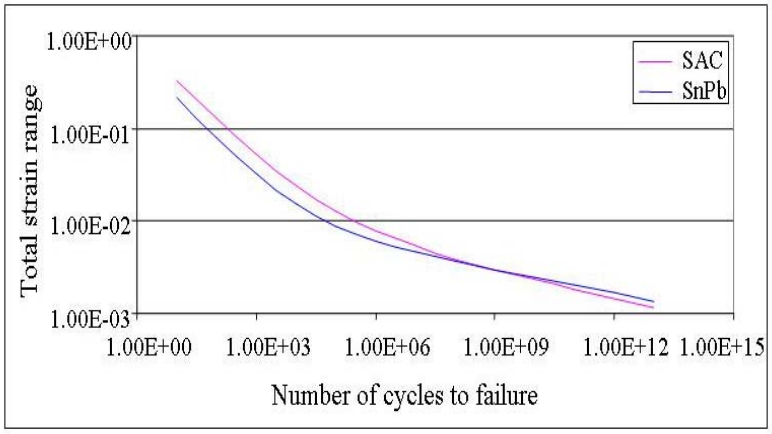

Figure 27: Fatigue curve for both SAC305 and SnPb

The generalized strain-life fatigue curves for both solders are superposed in Figure 27 for purposes of comparison. These plots clearly show that SAC305 solder material is more durable than Sn37Pb solder material in the LCF region, while Sn37Pb solder outperforms SAC305 solder

in the HCF region. Similar crossover of SAC and SnPb fatigue curves has been found by other researchers. Clech [17] found similar crossover for Sn3.9Ag0.6Cu and Sn37Pb fatigue curve under mechanical shear loading. His work showed that SAC is more durable than Sn37Pb for LCF, and less durable than Sn37Pb for HCF However, for some other Pb-free solders (eg. for Sn0.7Cu), the crossover shows the opposite trend, which is that Sn0.7Cu is more durable than Sn37Pb in the HCF region. So far the corresponding crossover for SAC305 and Sn37Pb generalized strain fatigue curves has not been adequately addressed in the literature.

SUMMARY

The vibration durability of Sn37Pb and SAC305 solders was investigated, using a combination of harmonic excitation tests and finite element modeling. The analysis was conducted using a time-domain approach, to quantify fatigue damage caused by harmonic excitation at the first natural frequency of the test vehicle. The SAC305 interconnects were found to be less durable than their Sn37Pb counterparts under the vibration loading levels in this study. This observation agrees with other publications in the literature. Based on the competing failure modes observed in the failed specimens, lower-bound fatigue properties have been estimated for both solders. Lower-bound estimates for a generalized strain-life durability model have been obtained for both Sn37Pb and SAC305 materials. These fatigue curves for Sn37Pb and SAC305 materials cross over at 10^8 cycles. In the LCF region, SAC305 solder is more durable than Sn37Pb solder, while in the HCF area, Sn37Pb solder has higher durability than SAC305 solder. Consequently, the acceleration factors for quasi-static or dynamic mechanical cyclic failures in SAC305 assemblies are expected to be generally smaller than in eutectic Sn37Pb material. The durability curves derived in this study depend on the assumed material stress-strain properties, and their sensitivity will be parametrically investigated in a future paper.

It is important to recognize that even in the LCF region where the SAC305 material is more durable, actual interconnects assembled with SAC305 solders may not outlast corresponding Sn37Pb assemblies under similar excitation levels because (i) there are competing failure mechanisms in the IMC layer and in the PWB that often make the SAC305 assemblies more vulnerable to PWB flexure; and (ii) SAC305 interconnects experience higher strain level than Sn37Pb interconnects under the same excitation level, because of different stress-strain properties.

This paper includes only the solder strains due to dynamic flexural deformation of the PWB. Further work is required to assess if there is any significant contribution from the dynamic response of the component relative to the PWB, and will be the subject of a future paper.

ACKNOWLEDGMENTS

This work is sponsored by the members of the CALCE Electronic Products and Systems Consortium at the University of Maryland, College Park.

REFERENCES

[1] Upadhyayula, K. and Dasgupta, A., "Guidelines for Physics-of-Failure Based Accelerated Stress Test", *Proceedings, Reliability and Maintainability Symposium*, pp 345-357, 1998

[2] Zhou, Y., Scanff, E. and Dasgupta, A., "Vibration Durability Comparison of Sn37Pb vs. SnAgCu Solders", Proceedings of *ASME International Mechanical Engineering Congress and Exposition*, Chicago, IL, Nov, 2006, Paper num 13555

[3] Zhou, Y. and Dasgupta, A., "Vibration Durability Investigation for SnPb and SnAgCu Solders with Accelerated Testing and Modeling" Presented at *IEEE-TC7 Conference on Accelerated Stress Testing & Reliability*, San Francisco, CA, October, 2006

[4] Woodrow, A., "JCAA/JG-PP No-Lead Solder Project: Vibration Test", *Boeing Electronics Materials and Processes Technical Report*, 2005

[5] Zhang, Q., Dasgupta, A. and Haswell, P., "Isothermal Mechanical Durability of Three Selected Pb-free Solders: Sn3.9Ag0.6Cu, Sn3.5Ag and Sn0.7Cu", *ASME Journal of Electronic Packaging*, Vol. 127, pp 512-522, 2005

[6] Dowling, N. E., "*Mechanical Behavior of Material: Engineering Methods for Deformation, Fracture, and Fatigue"* Prentice-Hall, 1999

[7] Lau, J., Gratalo, K. and Schneider, E., "Solder Joint Reliability of Large Plastic Ball Grid Array Assemblies under Bending, Twisting, and Vibration Conditions", *Circuit World*, Vol. 22, pp. 27-32, 1995

[8] Lau, J., Marcotte, T., Severine, J., Lee, A., Erasmus, S., Baker, T., Moldaschel, J., Sporer, M., and Burward-Hoy, G., "Solder joint reliability of surface mount connectors", *ASME Journal of Electronic Packaging*, Vol. 115, pp. 180-188, 1993

[9] Lau, J., Schneider, E., and Baker, T., "Shock and vibration of solder bumped flip chip on

organic coated copper boards", *ASME Journal of Electronics Packaging*, Vol. 118, pp. 101-104, 1996

[10] Jih, E., and Jung, W., "Vibration Fatigue of Surface Mount Solder Joints", *IEEE Inter Society Conference on Thermal Phenomena*, pp. 246-250, 1998

[11] Liu, X., Sookala, V. K., Verges, M. A., and Larson, M. C., "Experimental Study and Life Prediction on High Cycle Vibration Fatigue in BGA packages", *Microelectronics Reliability*, Vol. 46, pp. 1128-1138, 2006

[12] Zhao, Y., Basaran, C., Cartwright, A., and Dishongh, T., "Thermomechanical Behavior of BGA Solder Joints under Vibrations: an Experimental Observation", *IEEE Inter Society Conference on Thermal Phenomena*, pp. 349-355, 2000

[13] Darveaux, R., and Bannerji, K., "Constitutive Relations for Tin-Based Solder Joint", *IEEE Transactions on Components, Hybrid and Manufacturing Technology*, vol. 15, No. 6, pp 1013-1023, 1992

[14] Cuddalorepatta, G., and Dasgupta, A., "Cyclic Mechanical Durability of Sn3.0Ag0.5Cu Pb-Free Solder Alloy", *Proceedings, ASME International Mechanical Engineering Congress and Exposition*, Orlando, FL, Nov, 2005, Paper num 81171

[15] Haswell, P., and Dasgupta, A., "Durability Properties Characterization of Sn62Pb36Ag2 Solder Alloy" Proc. EEP-Vol. 28, pp. 181-187, *Proceedings, ASME International Mechanical Engineering Congress and Exposition*, Nov., 2000, Orlando, FL

[16] Haswell, P., "Durability Assessment and Microstructure Observations of Selected Solder Alloys", Ph.D Dissertation, University of Maryland, College Park, MD, 2001

[17] Clech, J. P., "Lead-free and Mixed Assembly Solder Joint Reliability Trends", Presented at *IPC Printed Circuits Expo, SMEMA Council APEX, Designers, Summit*, 2004

Chapter 4 Verification of Vibration Durability Model Constants: Influence of Constitutive Properties

Durability model constants were derived from harmonic vibration results in Chapter 3 for SAC305 and Sn37Pb solder materials. The accuracy of the derived fatigue curves is tested by comparing against the durability of similar LCR interconnects measured from random vibration durability tests and from quasi-static cyclic bend durability tests. All the random test results are listed in Appendix B.

The derived fatigue curves are strongly dependent on the assumed stress-strain curves. Although the stress-strain material properties of new Pb-free solder alloys have beeny investigated by many researchers, there is significant variability in the reported stress-strain material properties. This may be partly due to the wide variation in material microstructures in Pb-free test specimens. This is the motivation of the work conducted in this chapter.

A parametric study has been conducted to assess the sensitivity of the durability model dependence to the stress-strain properties of the solder materials. The resulting changes in the predicted durability are compared to test results from random vibration tests and quasi-static, 4-point cyclic bend tests.

This work has been presented at the IEEE ASTR conference in Oct 2008, and a journal paper based on this work has been submitted to the IEEE Journal of Components, Packaging and Manufacturing Technology (CPMT) for publication. In the current work, the strain history in the critical solder joint is related to the PWB flexural strain history based on quasi-static finite element analysis. Possible transient response of the component relative to the PWB due to high-frequency excitation has been neglected in this study so far, and is explored further in Chapter 5.

Harmonic and Random Vibration Durability of SAC305 and Sn37Pb Solder Alloys

Y. Zhou, M. Al-Bassyiouni and A. Dasgupta*

CALCE Electronic Products and Systems Center

Mechanical Engineering Department, University of Maryland,

College Park, MD, 20742

Tel: 301-405-5231, Fax: 301-314-9262, Email: Easily@umd.edu

ABSTRACT

In this paper, durability tests were conducted on both SAC305 and Sn37Pb solder interconnects using both harmonic and random vibration. The test articles consist of daisy-chained printed wiring boards (PWBs) with several different surface-mount component styles. Modal testing was first conducted on a test PWB to determine the natural frequencies and mode shapes. The PWB was then subjected to narrow-band excitation at its first natural frequency. Electrical continuity of the daisy-chain nets was monitored to measure the time-to-failure (and hence cycles-to-failure) of the interconnects. The response history of the PWB was recorded with strain gages located near the components of interest. Finite element analysis (FEA) was conducted for each component type, to estimate the transfer function between the flexural strain of the PWB and strain in the critical solder joint. The predicted strain transfer function was then combined with the PWB strain response history to estimate the strain history in the critical solder joints. The solder strain history was used, in conjunction with the failure history, to estimate lower bounds for the fatigue durability (S-N curves) of the solder interconnects.

In the first part of this study, the results show that the SAC305 interconnects are marginally less durable than Sn37Pb interconnects for the harmonic excitation range used in the current study.

The durability model constants are found to be very sensitive to the solder stress-strain curve assumed in the FEA. Since the stress-strain properties reported in the literature for these solder alloys vary significantly, the solder stress-strain curves were parametrically varied in the FEA, to assess the resulting effect on the estimated S-N curves.

In the second part of the study, random-vibration tests were conducted to assess durability under step-stress, broad-band excitation. Conventional cycle counting techniques were used to quantify the random excitation histories in terms of range distribution functions (RDFs). Using the same time-domain vibration fatigue analysis used earlier for narrow-band excitation, the durability trend for corresponding SAC305 and Sn37Pb solder interconnects under broad-band excitation was found to be similar to that found earlier under harmonic vibration excitation. Comparison between the durability prediction and test results provides a good understanding of the stress-strain behavior and fatigue behavior of these solder materials.

KEY WORDS:

SAC305, Sn37Pb, vibration durability, harmonic excitation, random excitation, time-domain analysis, FEA, Coffin-Manson fatigue model

I. INTRODUCTION

With the wide application of Pb-free solder materials, mechanical stress-strain constitutive properties (including elastic, plastic and creep deformation) have been the focus of a vast amount of research. However, there is wide variability in the reported material properties. For example, for the Young's modulus of Pb-free solder materials, NIST reports values varying from 11 GPa to 26 GPa [1]. Many Pb-free solder materials have no reported values for elastic modulus yet. Same applies for other material properties, such as the coefficient of thermal expansion (CTE), the plastic hardening coefficient and the plastic hardening exponent. Moreover, compared to the

constitutive properties, there are far less publications on the durability properties. Most reliability investigations for Pb-free solder alloys focus on thermal cycling durability [2], since temperature cycling was always thought of as the severest loading in the life cycle of most electronic products. In addition to thermal cycling durability, mechanical durability is another critical design issue for electronic assemblies, since they are subjected to cyclic mechanical loading during transportation and operation. Compared with thermal cycling tests, mechanical cycling tests are inexpensive and quicker to conduct in the laboratory [3]-[5]. Vibration is a commonly encountered mechanical fatigue loading during the transportation and deployment of electronic systems. The characteristics of the stress history under vibration loading are low amplitude and high frequency, while those under thermal cycling loading are high amplitude and low frequency. Among all the empirical work on vibration fatigue, Steinberg [6], who is probably the best known in the area of PWB vibration fatigue, proposed a simple rule of thumb for designing PWB's in a vibration environment. Yang, et al conducted studies on PBGA vibration reliability, including modal analysis of the board, and vibration durability characterization under out-of-plane excitation [7]-[9].

However, due to the large degree of scatter in high-cycle fatigue data, extracting the model constants for a generalized strain-life Coffin-Manson fatigue model is a challenging task. A time-domain approach has been used in the literature [10] [11]to quantify random vibration excitation and to derive strain-life fatigue model constants. This study explores the dependence of the fatigue model constants on the material constitutive properties. Young's modulus and plastic hardening exponent are parametrically varied and their influence on the fatigue model constants is presented.

Two different sets of durability tests have been conducted, including harmonic and random durability tests. The fatigue model constants are first derived from the harmonic durability test results with the help of finite element simulations. The obtained fatigue model constants are then used to predict the durability under random vibration. The comparison between the predicted and measured durability under random vibration provides better understanding of the constitutive properties of the SAC305 and Sn37Pb solder interconnects used in this study. The durability model constants are found to be more sensitive to the plastic hardening exponent than to Young's modulus. Within the parameter range examined, softer constitutive properties are found to provide better agreement between the harmonic and random durability test results.

II. APPROACH

A time-domain approach [10] [11]is used in this study to analyze the harmonic durability test results. The details of the approach are listed in Figure 1. The vibration durability test is first designed in Step 1. The outputs of the board characterization in this study include the first natural frequency, mode shape, characteristic strain history, and overstress limit, as shown in Step 2. Based on the information from the board characterization, in Step 3, the durability test is conducted and failure analysis is carried out to identify the failure mode, failure site, and failure mechanism. Detailed elastic-plastic quasi-static finite element simulation for each component is used to investigate the strain transfer function between the PWB and the critical solder joint. The fatigue durability model used here is a generalized strain-life model that includes the Basquin model for high-cycle fatigue (HCF) and the Coffin-Manson model for low-cycle fatigue (LCF). The fatigue durability model constants are obtained for both SAC305 and eutectic Sn37Pb interconnects, from a combination of the data from the vibration durability tests conducted in this study, and from LCF quasi-static mechanical cycling conducted in earlier studies [12][13].

In this paper, the elastic-plastic constitutive properties of the solders are parametrically varied and different sets of durability model constants are thus obtained. Creep response is neglected under vibration loading because of the high loading frequency. Among the constitutive model constants, Young's modulus and plastic hardening exponent are varied. The flow chart of this parametric study is shown in Figure 2. The durability model constants are derived from harmonic durability test results and selected material constitutive properties. The obtained durability model constants are used together with the response of the PWB to random excitation and FEA results, to predict durability under random vibration. Then the prediction is compared with the random durability test results.

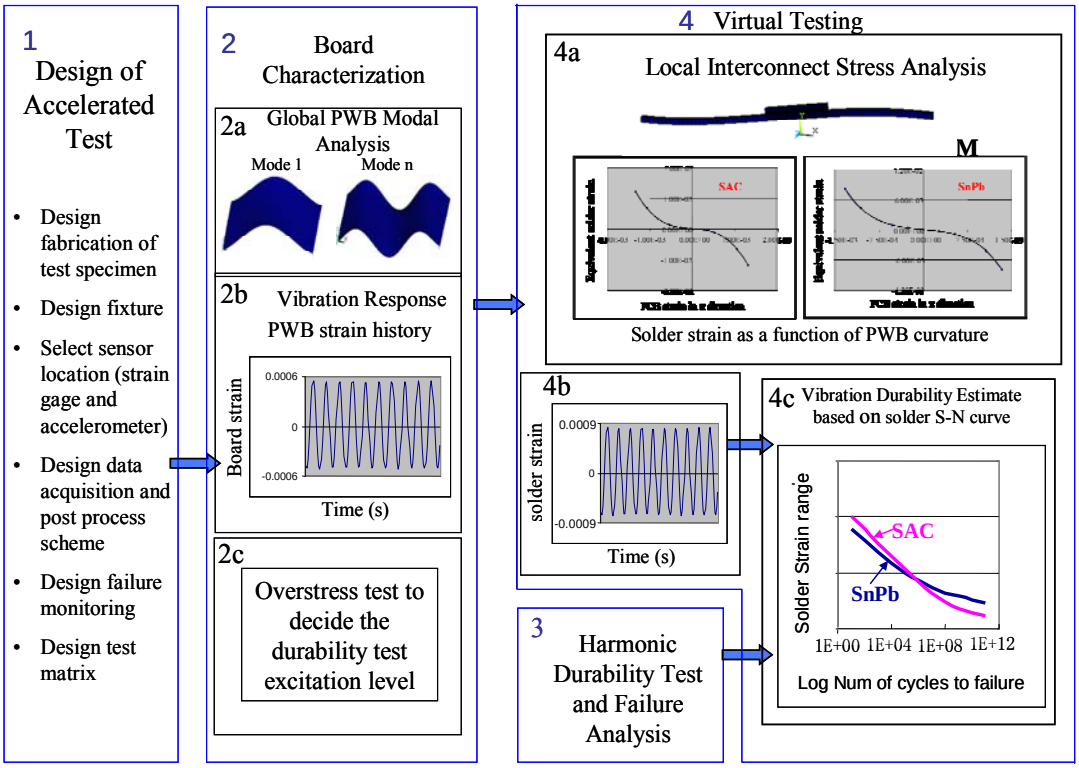

Figure 1: Time domain vibration durability approach with harmonic accelerated test

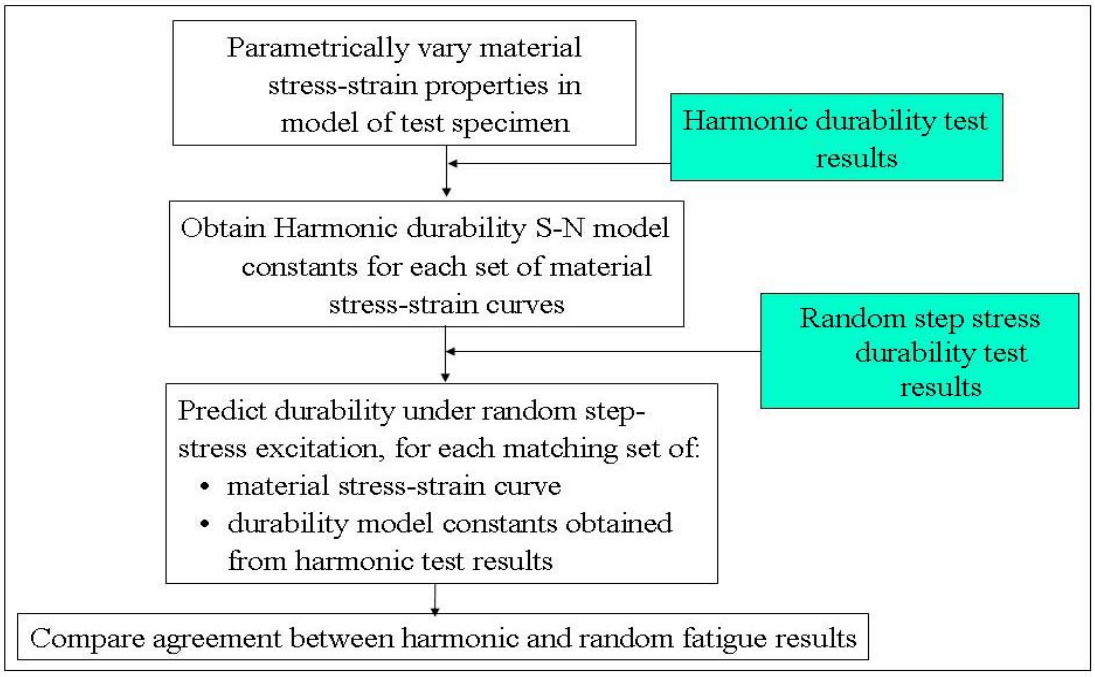

Figure 2: Flow chart for the parametric durability study

III. DESIGN OF DURABILITY TEST

A special test vehicle, shown in Figure 3, was designed and fabricated for this study. A two-layer FR4 PWB with copper metallization is used. The PWB is clamped along the two short edges to a fixture and left free at the other two edges. The fixture is connected to a uni-axial electrodynamic shaker for out-of-plane excitation. Two types of solders were investigated:

- SnPb: Sn37Pb
- SAC: Sn3.0Ag0.5Cu (SAC305)

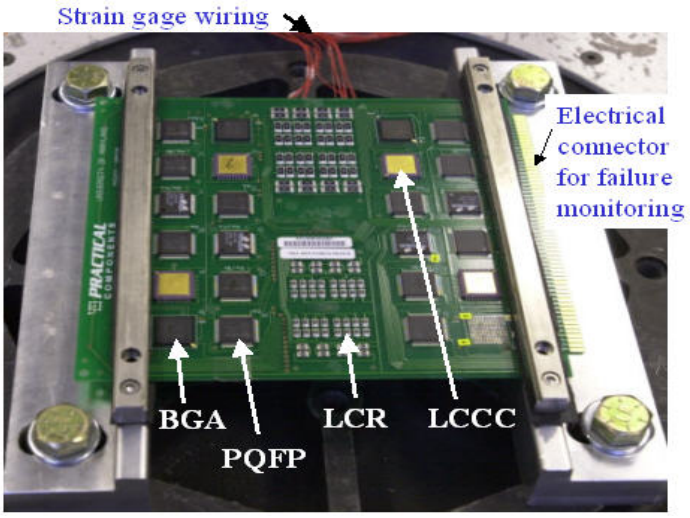

Figure 3: vibration durability test vehicle and setup

Two sets of durability tests have been conducted in this study (a) a harmonic vibration durability test under narrow-band constant-amplitude excitation and (b) a random vibration durability test under broad-band step-stress excitation. The difference between these two sets of durability tests is the excitation. Results show that harmonic durability results are less scattered than the corresponding random durability test results.

HARMONIC DURABILITY TEST

The test matrix for the durability test is listed in Table 1. The overstress test limits are used to determine excitation level for the durability test.

Table 1: Harmonic durability test matrix

Excitation	Over stress	9G	10.5G	12G
SAC	1	1	1	1
SnPb			1	1

A modal test was conducted with accelerometers to measure the natural frequencies and mode shapes of the test vehicle under the boundary conditions specified in the previous section. The

first natural frequency of the test board was found to be 169Hz. The harmonic excitation frequency was chosen to be the first natural frequency of the test vehicle, as shown in Figure 4.

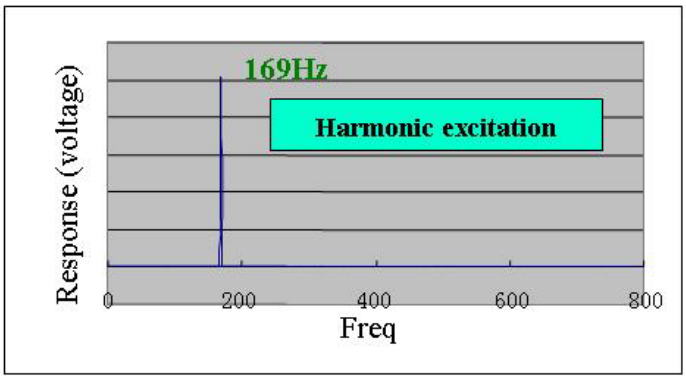

Figure 4: Excitation for harmonic durability test

Strain gages were used to characterize the PWB strain response. The locations of the strain gages, numbered 1 through 5, are shown Figure 5.

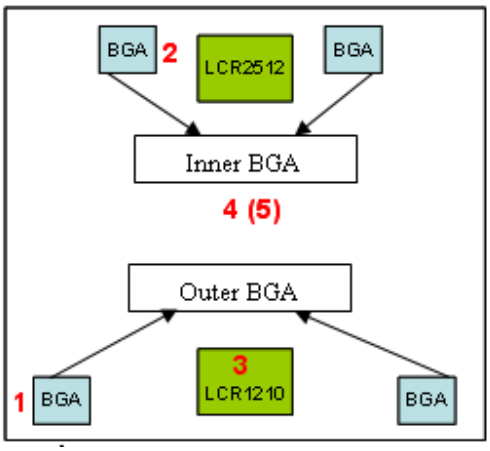

Figure 5: Locations of strain gages, numbered 1 through 5, with respect to PWB electronic components

The focus of this research effort is on Leadless Chip Resistor (LCR) interconnects. There are two types of LCRs on this test vehicle: LCR1210 and LCR2512. Half of these are aligned parallel to the direction of curvature and half are perpendicular to it. Eight LCRs are daisy-chained together in each net and there are eight such nets for each type of LCR.

The resistor layout on the board is shown in Figure 6. The resistors are assembled on the test board symmetrically, and are divided into two groups based on the distance to the center line. As a result, there are four groups of LCR components on the test board, and each group contains four resistor components.

- LCR1210 center
- LCR1210 edge
- LCR2512 center
- LCR2512 edge

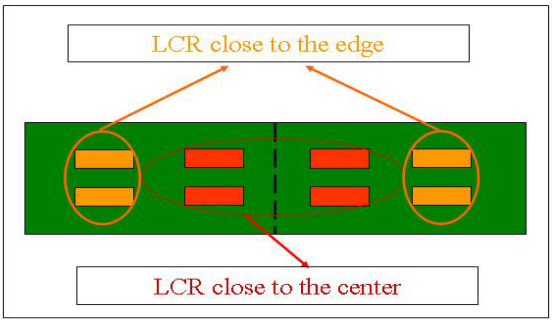

Figure 6: LCR layout on the test vehicle

Strain gage 3 was used to measure the PWB strain response near one of the LCR components. Of the 8 daisy-chain nets, failures occurred only in the 4 nets where the long axis of the LCRs is aligned parallel to the direction of the curvature.

The PWB strain in response to the harmonic excitation is a sinusoid at the excitation frequency. A typical strain response history is plotted in Figure 7.

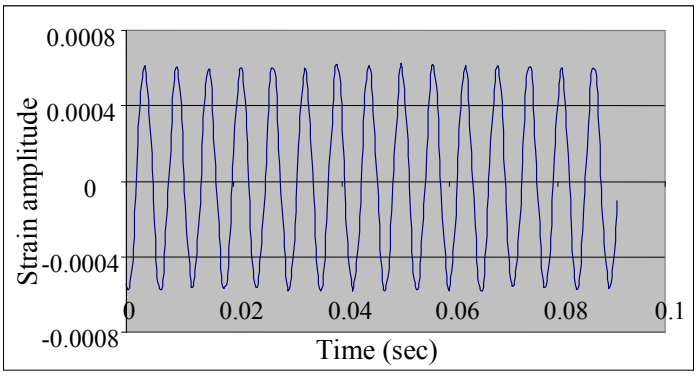

Figure 7: Characteristic strain history

The board strain amplitude for LCR components under different excitation levels is plotted in Figure 8. This result, along with that of Figure 7, shows that under our test conditions, the PWB deforms in the linear range, since the strain frequency coincides with the excitation frequency and the strain amplitude increases in proportion to the loading amplitude.

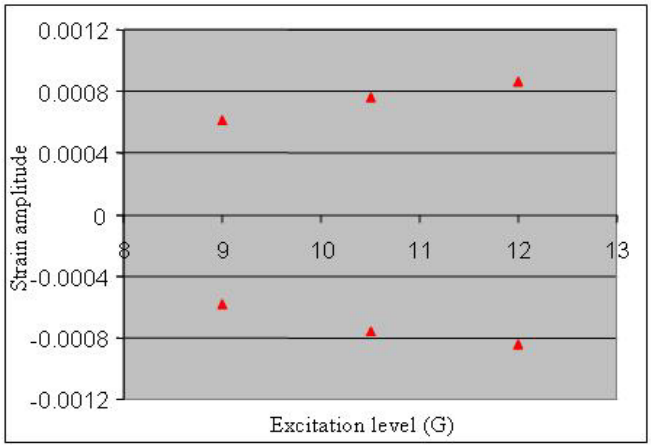

Figure 8: Board strain amplitude for LCR component

The LCR durability data is then used to investigate the solder fatigue properties. The time-to-failure for each of the LCR daisy-chain nets was monitored during the durability tests. The results for different components are plotted in Figure 9 and Figure 10 for both SAC305 and Sn37Pb assemblies.

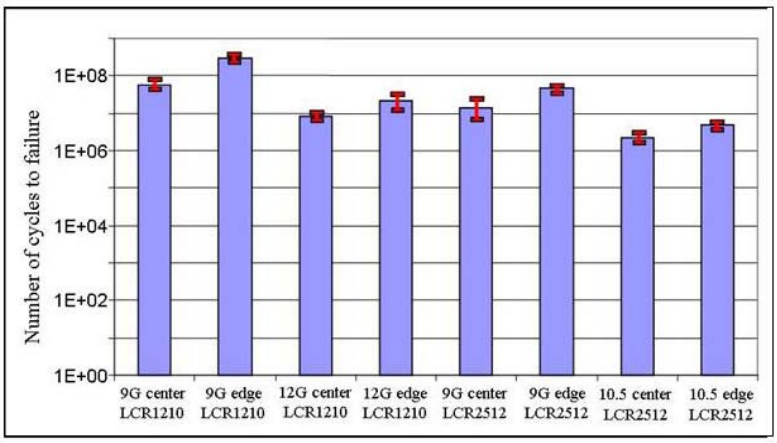

Figure 9: Harmonic vibration durability plot for SAC LCR interconnects

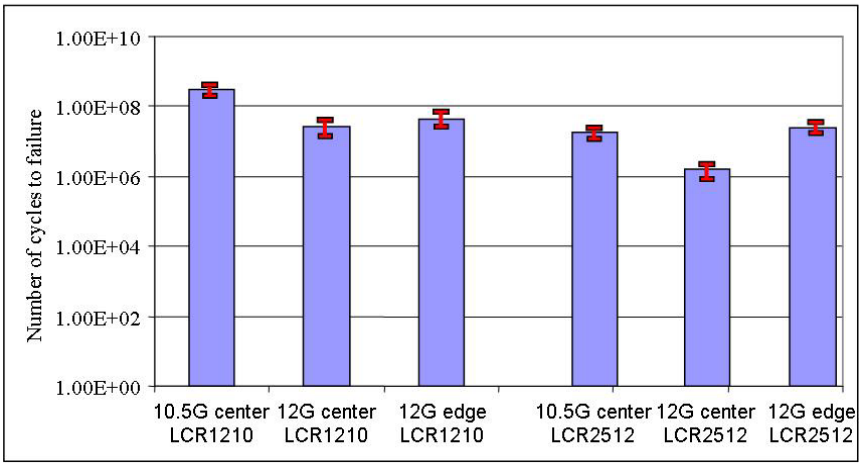

Figure 10: Harmonic vibration durability plot for SnPb LCR interconnects

RANDOM DURABILITY TEST

The technique to conduct the random durability test is very similar to that of the harmonic durability test. The test matrix for the random durability test is shown in Table 2. Step-stress loading was applied. Over a frequency range from 10 to 500 Hz, which includes four modal frequencies of the test vehicle. The PSD profile of the excitation is shown in Figure 11.

Table 2: Random durability test matrix

Step Stress	Over Stress	SAC	SnPb
Num	1	1	1

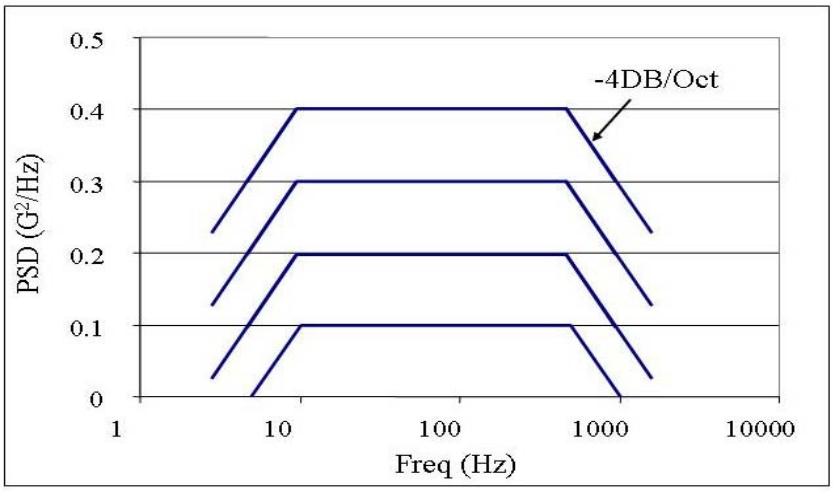

Figure 11: PSD profile for random vibration test

The loading excitation level increases from 0.1 G^2/Hz to 0.4 G^2/Hz, in successive steps. The specimens were excited for approximately 13 hours at each level. All of the LCR2512 components failed at the lowest excitation level. Some of the smaller (LCR1210) components failed at higher excitation levels. The durability histograms for LCR components for this random vibration test are provided in Figure 12 and Figure 13 for SAC305 and Sn37Pb, respectively. One SAC305 and one SnPb board have been tested. Each data point is an average for two coincident components. The histograms are segmented to show the amount of time spent at each excitation level during the step-stress test.

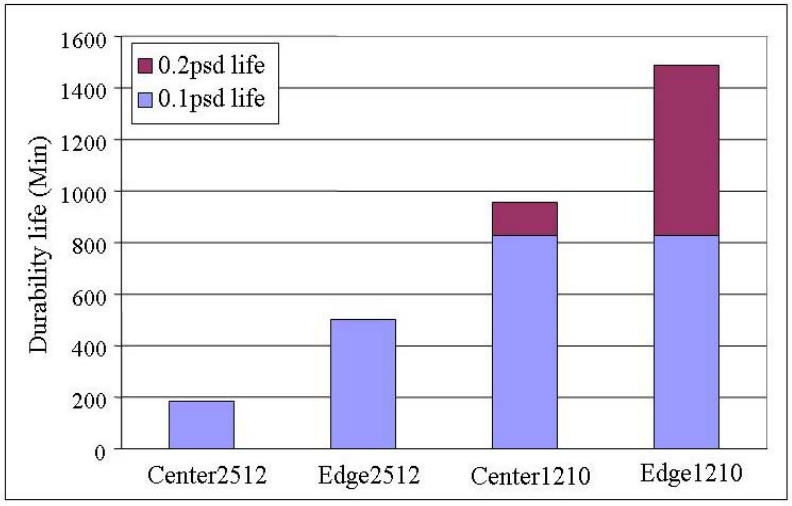

Figure 12: Random vibration durability for SAC LCR components

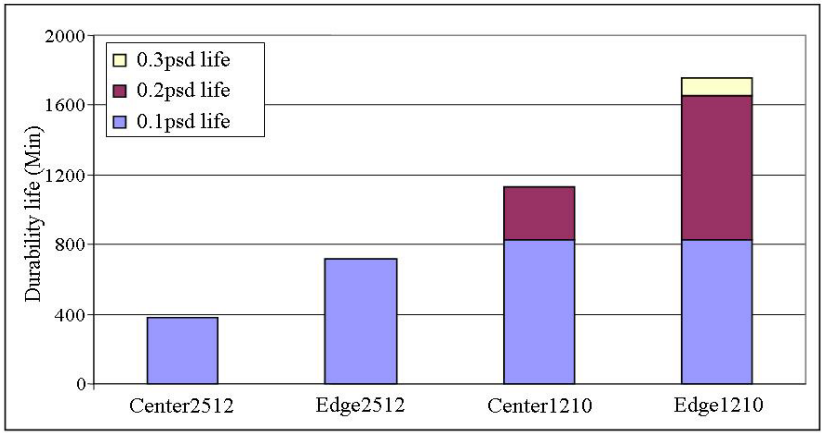

Figure 13: Random vibration durability for SnPb LCR components

IV. VIRTUAL TESTING

In order to obtain the solder strain history, detailed local FEA modeling was conducted for the LCR assemblies. The details of the simulation can be found in the literature [14]. The elastic-plastic material constitutive properties used in the FEA simulation include Young's modulus, Poisson's ratio, and the plastic model constants (C and n) defined by the relation:

$$\tau = c\gamma_{pl}^{\ n} \tag{1}$$

where τ is the shear stress and γ_{pl} is the plastic shear strain.

Young's modulus obtained from Zhang's work [15] [16] is about 18GPa for near-eutectic SAC solder alloys. However, Darveaux [17] reported Young's modulus well over 40GPa for these solders. Since the choice of material properties has a strong effect on the durability constants, Young's modulus (E) and plastic hardening exponent (n) are parametrically varied in this study for both SAC305 and Sn37Pb according to Table 3. The *c* value keeps constant for both SAC305 and SnPb for current study.

The corresponding constitutive stress-strain curves are plotted in Figure 14 and Figure 15.

Table 3: Parametric material constants

	SAC			SnPb		
	E (Gpa)	*n*	*c(Mpa)*	*E* (Gpa)	*n*	*c(Mpa)*
First set	47.5	0.28	55.6	31.6	0.25	69.8
Second set	47.5	0.2		31.6	0.17	
Third set 1 [1] [16]	18.1	0.28		17.8	0.25	
Fourth set	18.1	0.2		17.8	0.17	
Fifth set [17]	47.5	0.23				

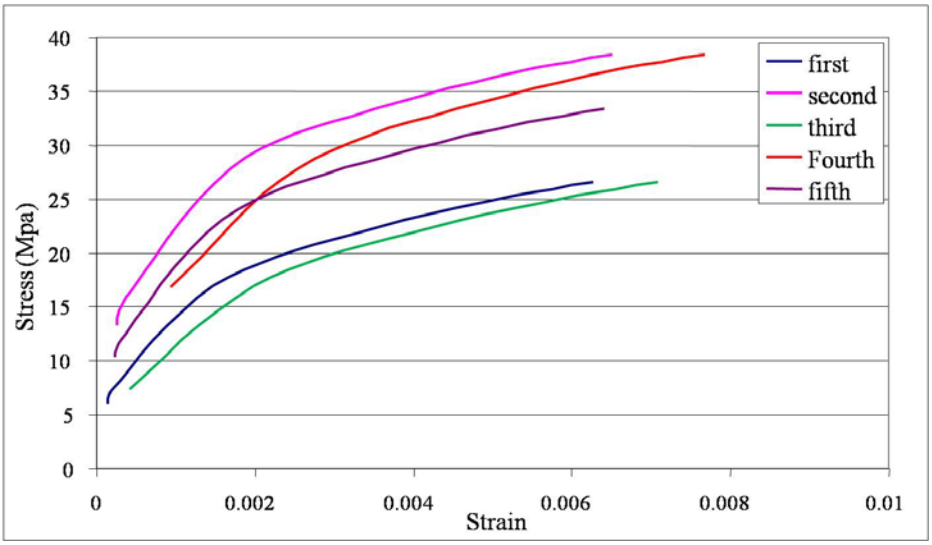

Figure 14: SAC stress-strain curves used in the FEA simulation

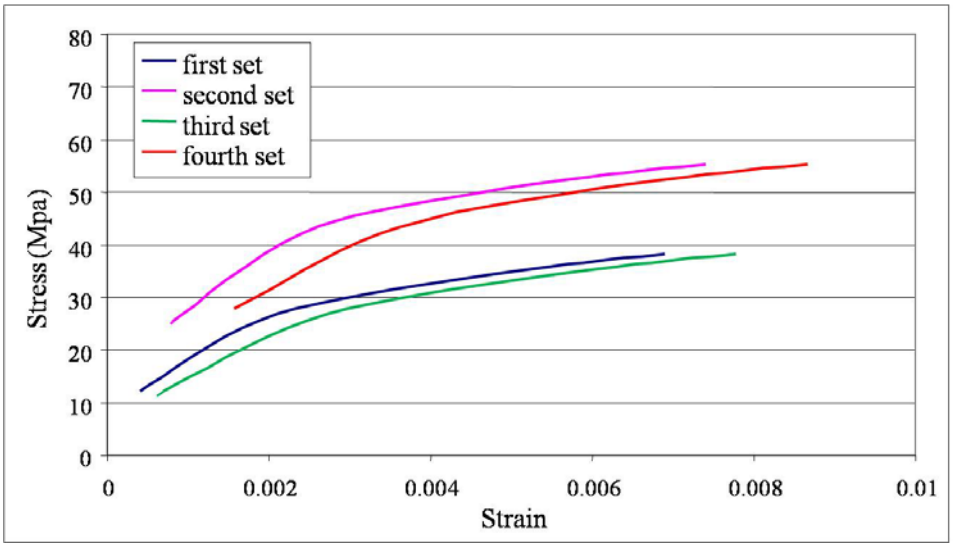

Figure 15: SnPb stress-strain curves used in the FEA simulation

These material properties are then used in FEA simulations to obtain a transfer function between the PWB flexural strain and the highest strain in the critical solder joint. Details of this analysis are described elsewhere in the literature [14]. These strain transfer functions for SAC305 and Sn37Pb solder interconnects are plotted in Figure 16 and Figure 17, respectively, for the group of LCR2512 components near the center of the PWB.

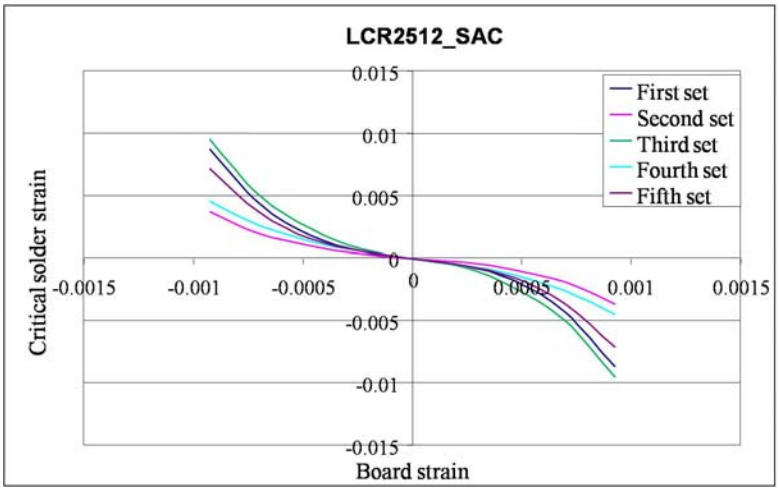

Figure 16: Strain transfer functions for center LCR2512 for SAC solder alloy

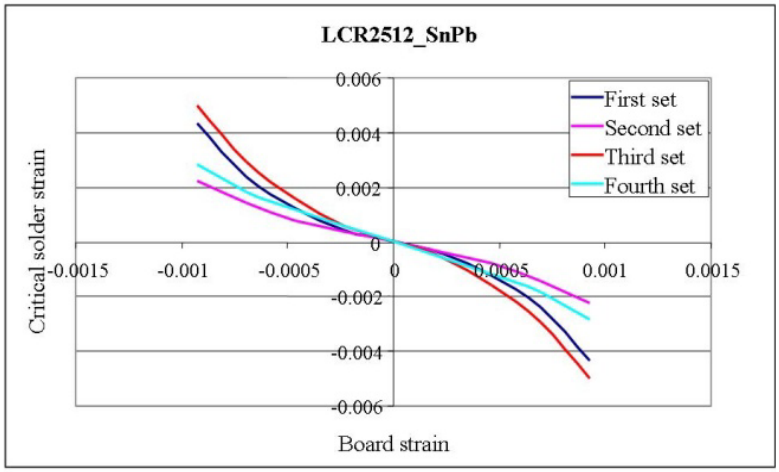

Figure 17: Strain transfer functions for center LCR2512 for SnPb solder alloy

These strain transfer functions are used to estimate the strain history in the critical solder interconnect, from the strain history measured on the PWB with strain gages. The solder strain is combined together with the durability test results, shown in Figure 9 and Figure 10, to extract the durability model constants from the test data. The generalized strain-life durability model used in this study is given as

$$\Delta\varepsilon = \frac{\sigma_f^{'}}{E} N_f^{\ b} + \varepsilon_f^{'} N_f^{\ c} \tag{2}$$

where the first term is Basquin's law for HCF and the second term is the Coffin-Manson law for LCF.

The fatigue model constants derived for both SAC305 and Sn37Pb solder alloys for different sets of material properties are listed in Table 4 and Table 5, respectively. The corresponding durability curves are plotted in Figure 18 for SAC305 and in Figure 19 for Sn37Pb. The LCF durability model constants are obtained from durability results in the literature [12] [13], and the HCF model constants are extracted in this study, using methods described in the literature [10] [14], The HCF durability model constants obtained in this study are fairly sensitive to the stress-strain properties of the solder alloy. This observation provides strong motivation for correctly identifying the stress-strain properties for both SAC305 and Sn37Pb solder materials.

Table 4: SAC Durability model constants

	$\sigma_f^{'}/E$	b	$\varepsilon_f^{'}$	c
First set	0.016	-0.09	0.86	-0.44
Second set	0.0046	-0.056	0.86	-0.44
Third set	0.023	-0.10	0.86	-0.44
Fourth set	0.0083	-0.071	0.86	-0.44
Fifth set	0.011	-0.08	0.86	-0.44

Table 5: SnPb durability model constants

	$\sigma_f^{'}/E$	b	$\varepsilon_f^{'}$	c
First set	0.0078	-0.054	0.62	-0.48
Second set	0.0056	-0.052	0.62	-0.48

Third set	0.016	-0.083	0.62	-0.48
Fourth set	0.007	-0.053	0.62	-0.48

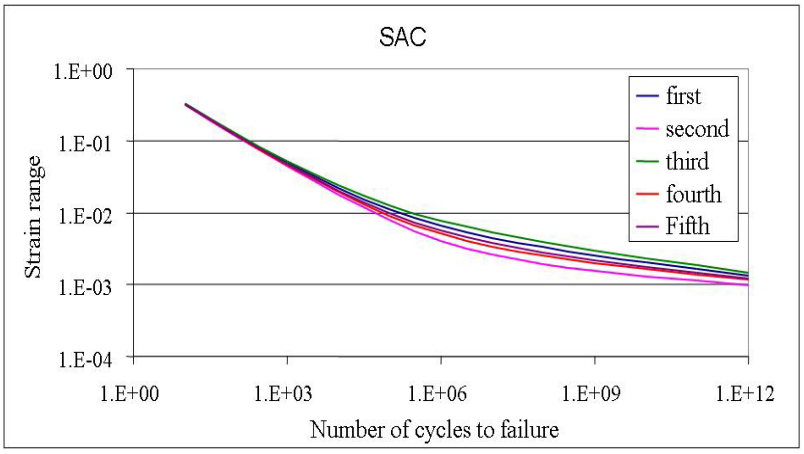

Figure 18: SAC durability S-N curves

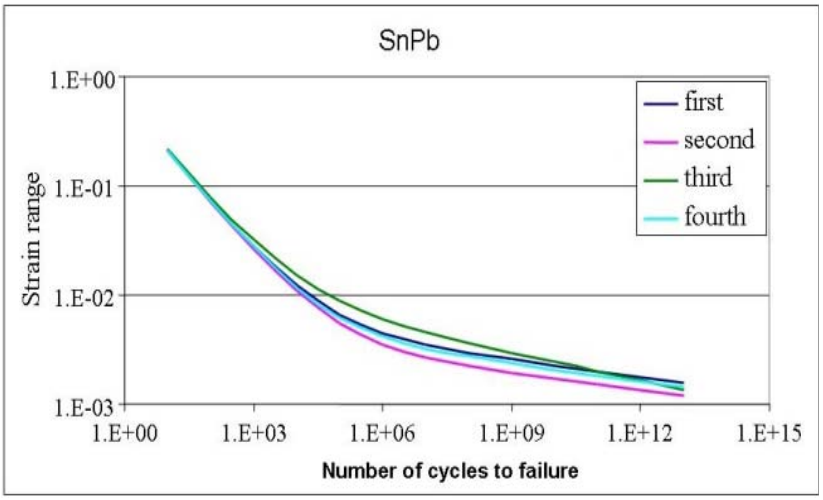

Figure 19: SnPb durability S-N curves

V. RANDOM VIBRATION DURABILITY PREDICTION

As discussed in Section II and shown in Figure 2, the durability model constants obtained from harmonic durability test results were used to predict random vibration durability, and then the predictions were compared with the experimental results. In order to perform the comparison, the

fatigue damage caused in each component by each stress level in the step-stress excitation was scaled to the first stress-level, using durability scale factors obtained from the finite element modeling and the fatigue model constants Then, the predicted random durability was normalized with respect to the experimental data for each group of LCR components. The normalized predictions are plotted in Figure 20 and Figure 21 for SAC305 interconnects and in Figure 22 and Figure 23 for Sn37Pb interconnects.

The results show that the predicted durability for random vibration is lower for:

- First and third sets of material properties, compared to the remaining sets, because of smaller plastic hardening
- Third set compared to first set because of lower stiffness
- LCR1210, compared to LCR2512, because of smaller strain magnitudes, and
- Sn37Pb, compared to SAC305 solder alloys, because of smaller plastic hardening
- Edge LCRs compared to center LCRs because of smaller flexural strains. (Sensitivity to location is weaker in Sn37Pb due to smaller strains)Since the predicted durability is higher than the measured durability for all the LCR cases studied here, lowering of the predicted durability implies better agreement with the experiments in this case.

The best-case discrepancy between the predicted and measured values for random vibration durability varies between 0% for LCR1210 to approx 400% for LCR2512. The worst-case discrepancies can be as high as 250% for LCR1210 to 1450% for LCR2512. As a reference, it is useful to remember that variability in HCF tests is commonly found to be anywhere between 200% to 1000%. The details of the sensitivity of the durability prediction to the material properties can be seen in Figures 20-23.

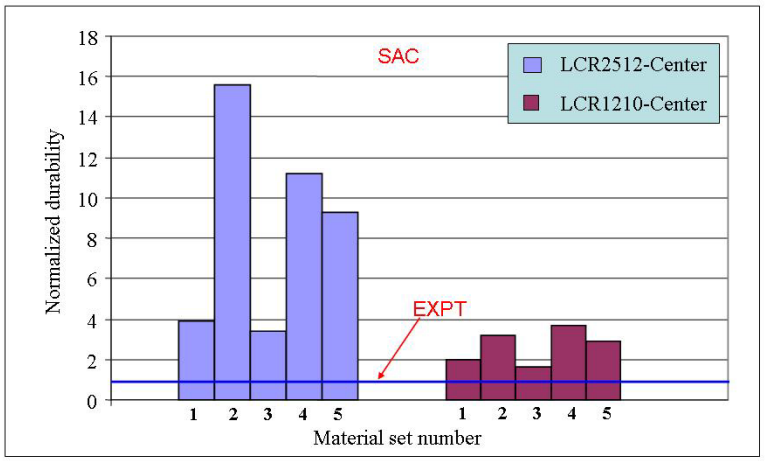

Figure 20: Random vibration durability predictions for SAC center interconnects, normalized with respect to experimental data

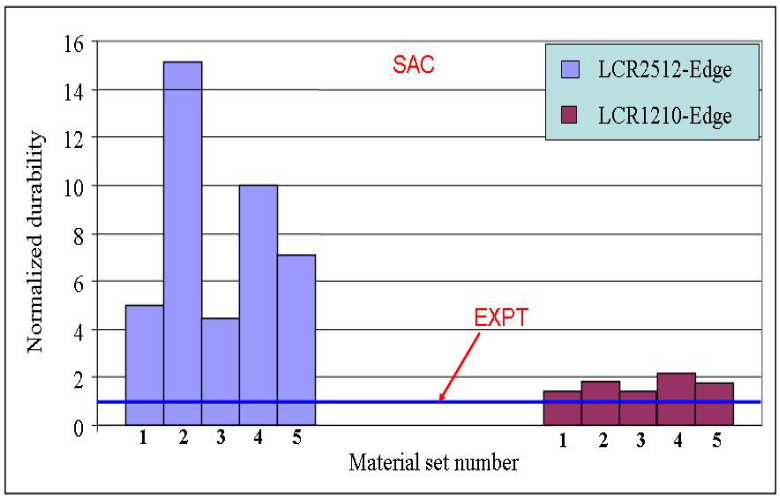

Figure 21: Random vibration durability predictions for SAC edge interconnects, normalized with respect to experimental data

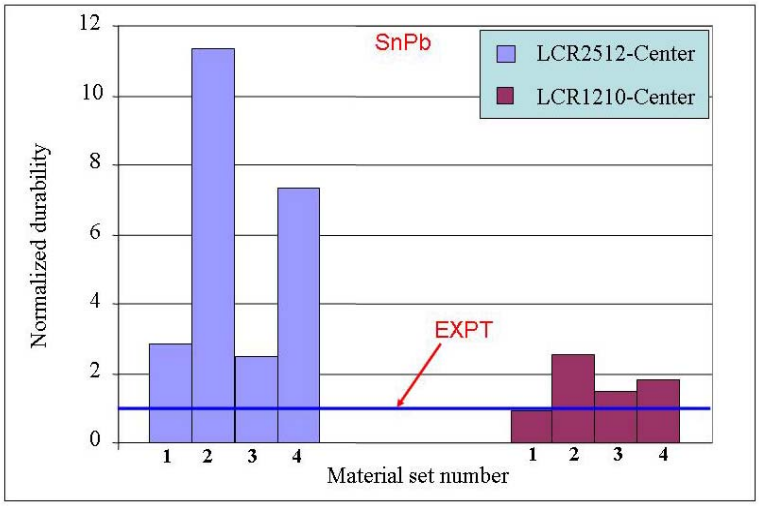

Figure 22: Random vibration durability prediction for SnPb center LCR interconnects, normalized with respect to experimental data

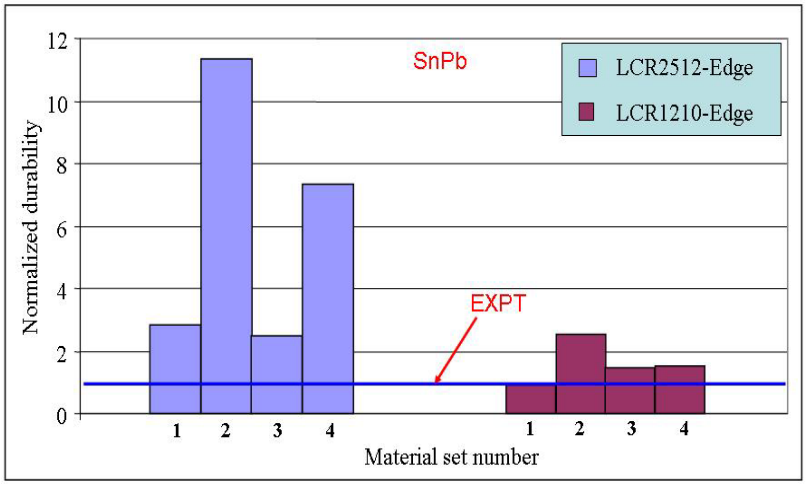

Figure 23: Random vibration durability prediction for SnPb edge LCR interconnects normalized with respect to experimental data

VI. QUASI-STATIC FOUR- POINT BENDING DURABILITY PREDICTION

The third set of material properties, which is from the literature [3], showed good agreement between harmonic and random durability results. The durability model constants obtained from this set of material properties are next used to explore the accuracy for quasi-static four-point

bending durability results from literature [20]. As in the case of the vibration durability modeling, the test specimen modeled with finite elements and the predicted durability is compared to test results.

EXPERIMENT [20]

The test vehicle used in literature [20] for quasi-static 4-point bend tests is shown in Figure 24. The 4-point bending generates a central gage region between the inner rollers that is under uniform bending moment and uniform curvature. The specimen consists of a FR-4 board of 1.6 mm thickness, with 24 LCR2512s in 3 columns within the gage region of the bend specimen. The interconnects in this study are made from eutectic Sn37Pb solder alloy.

As shown in Figure 24, a strain gage was attached within the gage region, on the top surface of the PWB, to measure the flexural strain during the experiment.

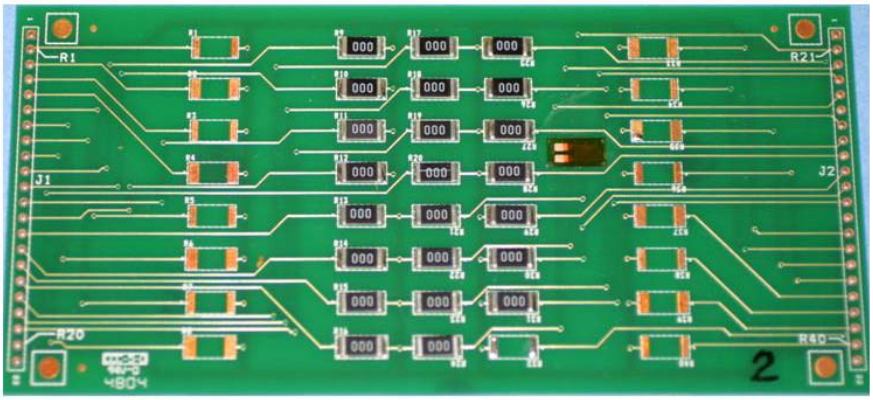

Figure 24: Test vehicle from literature [20]

The corresponding PWB flexural strain amplitude and measured cyclic durability are shown in **Table 6**.

Table 6: 4 point bending durability

Board strain (Micro strain)	Number of cycles to failure
2400	1.27E+04

1850	3.76E+04
1200	6.93E+04
1350	1.39E+05
1400	1.43E+05
1150	1.34E+06

VIRTUAL TESTING

A detailed finite element analysis was conducted to investigate the solder strain due to PWB curvature. The FEA model is shown in Figure 25.

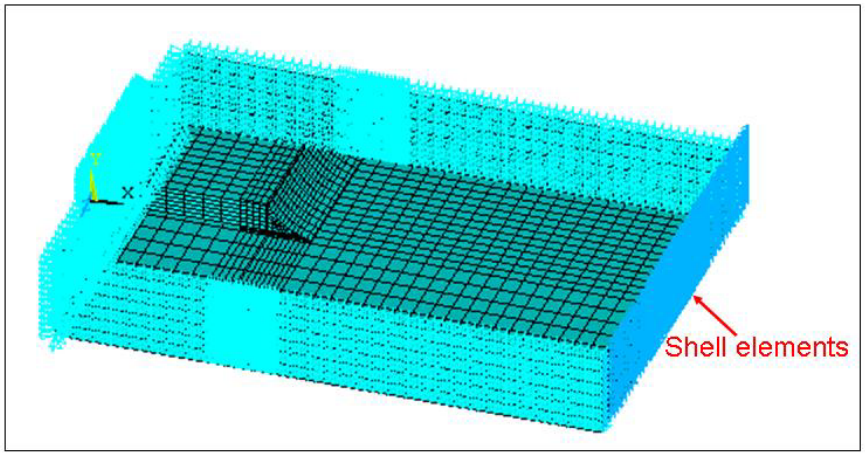

Figure 25: Finite element model for 4 point bending test vehicle

A layer of stiff shell elements were used at the end of the solid element to facilitate the application of bending moments, to mimic the loading experienced by the LCR in the 4-point bending experiment loading. The loading used was from zero to maximum, instead of being fully-reversed. Therefore, in this case, there is a non-zero mean stress which will play a role in solder fatigue damage. This simulation provided a transfer function between solder von Mises' strain (averaged over the critically stressed region) and PWB flexural strain (averaged over the foot-print of the strain gage), as shown Figure 26. Another outcome of the FEA simulation is the

transfer function relation between the hydrostatic stress in the solder joint and the PWB flexural strain, as shown in Figure 27.

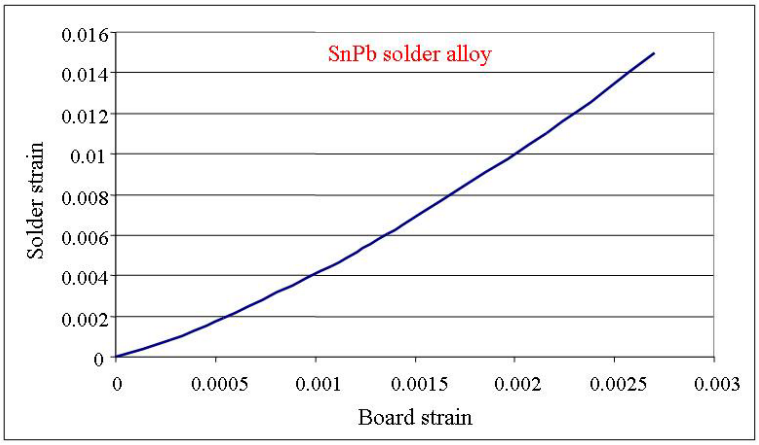

Figure 26: Strain transfer function between solder Mises' strain and PWB flexural strain for a Sn37Pb LCR2512 assembly under 4-point bending

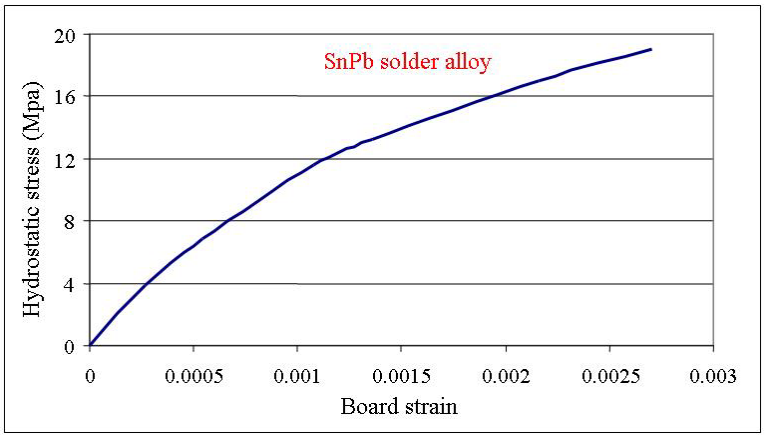

Figure 27: Strain transfer function between mean hydrostatic stress and PWB flexural strain for a Sn37Pb LCR2512 assembly under 4-point bending

DURABILITY PREDICTION

The generalized strain-life fatigue model given in Equation 2 is next modified to account for the effect of the mean hydrostatic stress, as shown in Equation 3 [21].

$$\Delta\varepsilon = \frac{\sigma_f^{'} - \sigma_m}{E} N_f^{\ b} + \varepsilon_f^{'} N_f^{\ c} \qquad 3$$

Where σ_m is the mean hydrostatic stress due to zero-to-max cyclic PWB curvature.

The model constants are derived from material property set III shown in Table 3.

Table 7: 4-point bending model prediction and experimental results

Strain (Microstrain)	mean stress (Mpa)	Predicted number of cycles to failure	experiment number of cycles to failure
2400	16.5	1.16E+04	1.27E+04
1850	14.6	6.81E+04	3.76E+04
1400	12.5	5.03E+05	1.43E+05
1350	12.2	4.81E+05	1.39E+05
1200	11.4	2.03E+06	6.93E+04
1150	11.1	2.58E+06	1.34E+06

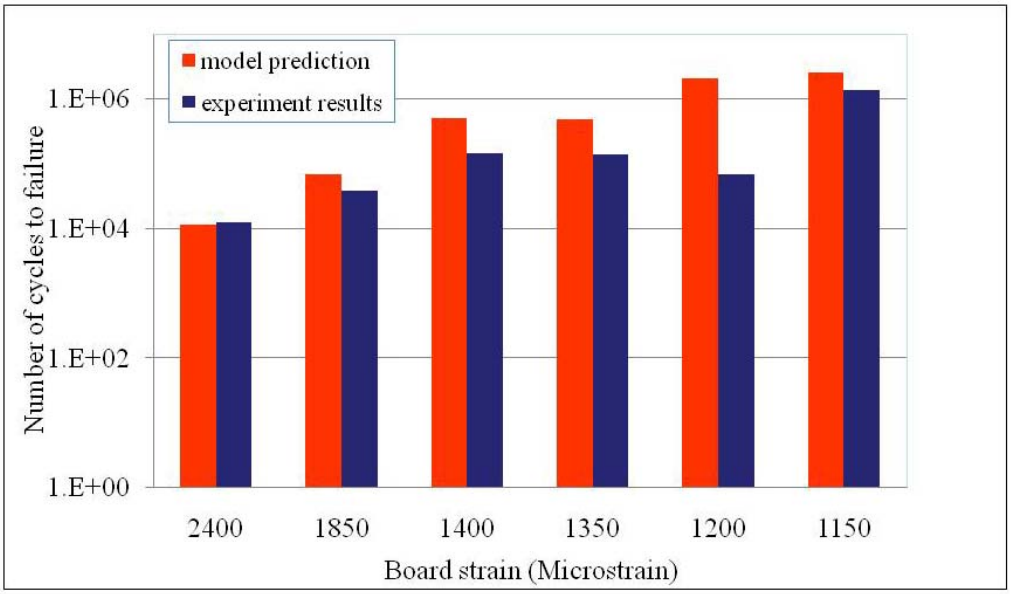

Figure 28: Comparison between model prediction and test results for quasi-static 4-point bending durability

The board strain, mean stress and durability data are listed in Table 7 and plotted in Figure 28. It shows reasonable good agreement between the model prediction and experiment results. Thereby providing confidence about the appropriateness of the material stress-strain properties used in the simulations and the corresponding durability model constants extracted from the harmonic vibration test results.

SUMMARY

In this paper, vibration durability model constants for SAC305 and Sn37Pb solder materials were extracted from harmonic vibration test results of LCR assemblies. The accompanying stress and damage analysis was performed in the time-domain with elastic-plastic finite element analysis. Parametric studies were conducted to assess the sensitivity of the durability model constants to the elastic-plastic constitutive stress-strain properties of the solder materials. The extracted durability models were used to predict the fatigue life of LCR assemblies under broad-band, step-stress vibration excitation. Increasing the hardening exponent for SAC material from 0.2 to 0.28 (40% percent) reduced the prediction for center LCR2512 interconnects about 4 times. Reducing the Young's modulus from 47.5 GPa to 18 GPa did not produce any significant changes in the durability prediction. Comparison between model predictions and experimental results showed that the predictions were non-conservative in all the cases examined. Thus, within the range of material properties studied here, the softer and more compliant material properties provide the lowest durability prediction and hence provided the best agreement between harmonic and random durability results.

Furthermore, the errors increase as the strain magnitudes increase in the solder. This produced better prediction for smaller LCRs further away from the center of the PWA and for Sn37Pb solder. However, the best-case discrepancies are still large in some cases (400% for LCR2512 at

the center of the SAC PWAs), thus leading to the conclusion that there may be additional reasons for this discrepancy.

The additional reasons for discrepancy between prediction and test result for random vibration durability may be that all the damage modeling conducted in this study is based on quasi-static stress analysis. In particular, the finite element analysis conducted to derive the strain transfer function between the PWB flexural strain and the critical strain in the LCR solder joint was a quasi-static analysis. This approximation is based on the assumption that the actual damage accumulation in the solder joint is purely due to strains generated by PWB flexure and not by inertial forces due to the component mass and acceleration. However, because of the high excitation frequencies used in the random vibration test, the solder damage maybe due to a combination of the PWB curvature and inertial loads caused by the component mass and acceleration. The contribution of the inertial forces to solder joint damage is examined in a future paper.

ACKNOWLEDGMENTS

This work is sponsored by the members of the CALCE Electronic Products and Systems Consortium at the University of Maryland, College Park.

REFERENCES

1. *http://www.boulder.nist.gov/div853/lead_free/part1.html#%201*
2. Stam, F. A. and Davitt, E., "Effects of Thermomechnical cycling on lead and lead-free (SnPb and SnAgCu) Surface Mount Solder Joints", *Microelectronics Reliability*, Volume 41, Issue 11, pp 1815-1822, 2001

3. Zhang. Q, Dasgupta. A and Haswell. P, "Isothermal Mechanical Durability of Three Selected Pb-free Solders: Sn3.9Ag0.6Cu, Sn3.5Ag and Sn0.7Cu", *Transaction of the ASME*, Vol. 127, pp 512-522, 2005
4. Kariya, Y., Morihata, T., Hazawa, E., and Otsuka, M., "Assessment of Low-Cycle Fatigue Life of Sn-3.5mass%Ag-X (X=Bi or Cu) Alloy by Strain Range Partitioning Approach," *Journal of Electronic Materials*, Vol. 30(9), pp. 1184-1189, 2001
5. Krishna J., Mahesh P., and Andrew S., "Mechanical Bend Fatigue Reliability of Lead-free PBGA Assemblies," *International Society Conference on Thermal Phenomena*, pp 915-918, 2002
6. Steinberg, Dave S, "Vibration Analysis for Electronic Equipment", John Wiley & Sons, New York, 1998
7. Yang Q. J, Lim G. H, Lin R. M, Yap F. F, Pang H. L. J and Wang Z. P, "Experimental Modal Analysis of PBGA Printed Circuit Board Assemblies", *IEEE/CPMT Electronic Packaging Technology Conference,* pp 290-296, 1997
8. Yang. Q. J, Pang. H. L. J, Wang. Z. P, Lim. G. H, Yap. F. F, Lin. R. M, "Vibration Reliability Characterization of PBGA Assemblies", *Microelectronics Reliability*, vol. 40, pp 1097-1107, 2000
9. Yang Q. J, Wang Z. P, Lim G. H, John H. L. Pang, Yap F. F, Lin R. M, "Reliability of PBGA Assemblies Under Out-of-plane Vibration Excitations", IEEE *Transactions on Components and Packaging Technologies*, vol. 25, No. 2, pp 293-300, 2002
10. Zhou, Y. and Dasgupta, A., "Vibration Durability Assessment of Sn3.0Ag0.5Cu & Sn37Pb Solders under Harmonic Excitation", *Published at ASME International*

Mechanical Engineering Congress and Exposition, Seattle, WA, Nov, 2007, Paper num 43493

11. Upadhyayula, K., and Dasgupta, A., "Accelerated Stress Testing of Surface-Mount Interconnects under Combined Temperature and Vibration Loading," Chapter 12, Pg 189, *Accelerated Stress Testing Handbook for Quality Products in a Global Market*, Eds.: H. A. Chan & P. J. Englert, Pub. IEEE Press (USA) and Wiley Blackwell (UK), 2001.
12. Cuddalorepatta, G. and Dasgupta, A., "Cyclic Mechanical Durability of Sn3.0Ag0.5Cu Pb-Free Solder Alloy", Published at *ASME International Mechanical Engineering Congress and Exposition*, Orlando, FL, Nov, 2005, Paper num 81171
13. Haswell, P. and Dasgupta, A., "Durability Properties Characterization of Sn62Pb36Ag2 Solder Alloy" Proc. EEP-Vol. 28, pp. 181-187, *ASME IMECE*, Nov., 2000, Orlando, FL
14. Y. Zhou, B. Moustafa and A. Dasgupta, "Vibration Durability Assessment of Sn3.0Ag0.5Cu & Sn37Pb solder under Harmonic Excitation", Journal of Electronic packaging, 2008, Accepted for Publication
15. Zhang, Q., Dasgupta, A. and Haswell, P., "Viscoplastic Constitutive Properties and Energy-Partitioning Model of Lead-Free Sn3.9Ag0.6Cu Solder Alloy", *ECTC New Orleans*, Louisiana, USA, 2003
16. Zhang Q, Dasgupta A and Haswell Peter, "Viscoplastic Constitutive Properties and Energy-Partitioning Model of Lead-free Sn309Ag0.6Cu Solder Alloy", *IEEE Electronic Components and Technology Conference*, pp 1862-1868, 2003
17. Darveaux, R. and Bannerji, K., "Constitutive Relations for Tin-Based Solder Joint", *IEEE Transactions on Components, Hybrid and Manufacturing Technology*, vol. 15, No. 6, pp 1013-1023, 1992

18. Amagai, M., Watanabe, M., Omiya, M., Kishimoto, K. and Shibuya, T., "Mechanical Characterization of Sn-Ag-based Lead-free Solders" *Microelectronics Reliability*, Vol. 42, pp 951-966, 2002
19. Zhou, Y., Scanff, E. and A. Dasgupta, "Vibration Durability Comparison of Sn37Pb vs. SnAgCu Solders", *Published at ASME International Mechanical Engineering Congress and Exposition*, Chicago, IL, Nov, 2006, Paper num 13555
20. Barker, D., "Experiments to validate calcePWA vibration damage model with PbSn and SAC305", CALCE project C05-04 final report, Oct, 2005
21. Norman E. Dowling, "Mechanical Behavior of Material: Engineering Methods for deformation, Fracture, and Fatigue" *Prentice-Hall*, 1999

Chapter 5 Verification of Vibration Durability Model Constants: Influence of Component Inertial Forces

Durability model constants for vibration fatigue were extracted in Chapter 3 from harmonic durability test results by quantifying the strain history in the critical solder joint with the help of quasi-static finite element simulation. The sensitivity of the durability model constants to the stress-strain properties of the solder material was parametrically investigated in Chapter 4. The accuracy of the model constants was also investigated comparing predictions with test results for durability tests under step-stress, random vibration loading and under 4-point quasi-static bending.

However, the solder strain presented in Chapters 3 and 4 was quasi-static analysis based on the first resonant mode of the dynamic flexural response of the printed wiring board (PWB). The effect of higher resonant modes of the printed wiring board (PWB) and the relative movement of the component with respect to the PWB (due to inertial forces generated by the component's mass) were ignored. The resulting approximation was reasonably accurate in the harmonic tests conducted at the low fundamental frequency of the PWB in Chapter 3, but in the case of broad-band excitation, these factors may be significant contributors to the strain and fatigue damage in the solder interconnects, because of the high-frequency energy content in the excitation. These effects may explain, in part, why the measured durability in broad-band tests in Chapter 4 was shorter than the predictions made from the fatigue constants derived in Chapter 3.

In this chapter, the significance of the latter of these two effects, viz. that due to relative motion between the component and PWB, is explored. Dynamic simulation was conducted with transient FEA for a sample PBGA256 assembly. The solder strain history from this dynamic simulation was compared with results from quasi-static simulation of the contribution due to the

fundamental mode of PWB flexure; in order to identify additional contributions such as those due to higher PWB modes and due to component inertial forces. These additional contributions were in fact found to be significant, thus making the dynamic strain magnitudes significantly higher than the quasi-static results, and resulting in a major difference in the corresponding damage accumulation rates and durability. Investigation of the contribution from higher modes of PWB flexure is deferred to a future study and this study focuses on the contribution due to relative motion of the component with respect to the PWB due to inertial forces generated by the mass of the component.

This part of the dissertation research has been submitted for publication to the International Journal of Microelectronics Reliability.

Sources of Fatigue in Random-Vibration Durability of Surface Mount Interconnects

Y. Zhou, M. Al-Bassyiouni and A. Dasgupta*

CALCE Electronic Products and Systems Center

Mechanical Engineering Department, University of Maryland,

College Park, MD, 20742

***Tel: 301-405-5251, Fax: 301-314-9677, Email: dasgupta@umd.edu**

ABSTRACT

In this paper, dynamic finite element analysis (FEA) is conducted to estimate the transient response of a PBGA256 assembly under random excitation. The dynamic strain history in the solder joint is monitored near the potential failure site. For purposes of comparison, a quasi-static FEA is also conducted to assess what fraction of the solder joint strain history is due to the fundamental mode of PWB flexure. Comparison of the results shows that the dynamic strain

magnitudes are significantly larger than the quasi-static values, resulting in much larger damage accumulation rates and smaller durability estimates from the dynamic analysis. This difference arises because the solder strain in the dynamic analysis includes additional contributions from higher modes of PWB flexure as well as from relative movement of the component with respect to the PWB due to inertial forces generated by the component mass. Investigation of the contribution from higher modes of PWB flexure is deferred to a future study and this study focuses on the contribution due to relative motion of the component with respect to the PWB due to inertial forces generated by the mass of the component. Experiments conducted on a PBGA256 assembly, with two accelerometers located at the same in-plane location, one on top of the component and the other at the bottom of the PWB, verify the dynamic relative movement between the two. The results presented in this study show the importance of the high-frequency response in the solder interconnects and help explain why broad-band durability tests, using relatively high-frequency excitation, showed higher damage accumulation rates than comparable harmonic tests at low frequency.

I. INTRODUCTION

Vibration durability estimation in the electronics industry has widely relied on Steinberg's [8] empirical equation since 1970's. However, this simple equation can only provide very approximate estimates of the durability for specific components at specific locations. Recently, more rigorous attention has been focused on this issue, since vibration is one of the commonly encountered loads during the life-cycle of electronic products. Yang et al [2][3][4] investigated vibration reliability of PBGAs, including modal analysis of the PWB, and vibration reliability characterization under out-of-plane excitation. Yu and Shah [5] simulated the dynamic response of electronic assemblies and the reliability of BGA solder joints with different commercial softwares. He [6] used nonlinear laminate theory for PWB dynamic response modeling and

analysis. Equations of motion for isotropic laminates were derived for free and forced vibration response analysis of simply supported PWBs. Results show that a nonlinear system has higher frequency oscillations with lower magnitude than a linear system. All of these studies focused on the solder strain response due to PWB flexural response, but they did not address the dynamic response of the component relative to the PWB due to its own mass and inertia.

In the present study, a hybrid experimental-numerical approach is used to examine the dynamic response of the component relative to the PWB and its effect on solder joint durability.

II. OVERVIEW OF APPROACH

The overall approach of this study is shown as a flow chart in Figure 1. The dashed lines indicate the tasks related to dynamic durability estimation; while the solid lines indicate the tasks related to estimation of the quasi-static response and durability estimation.

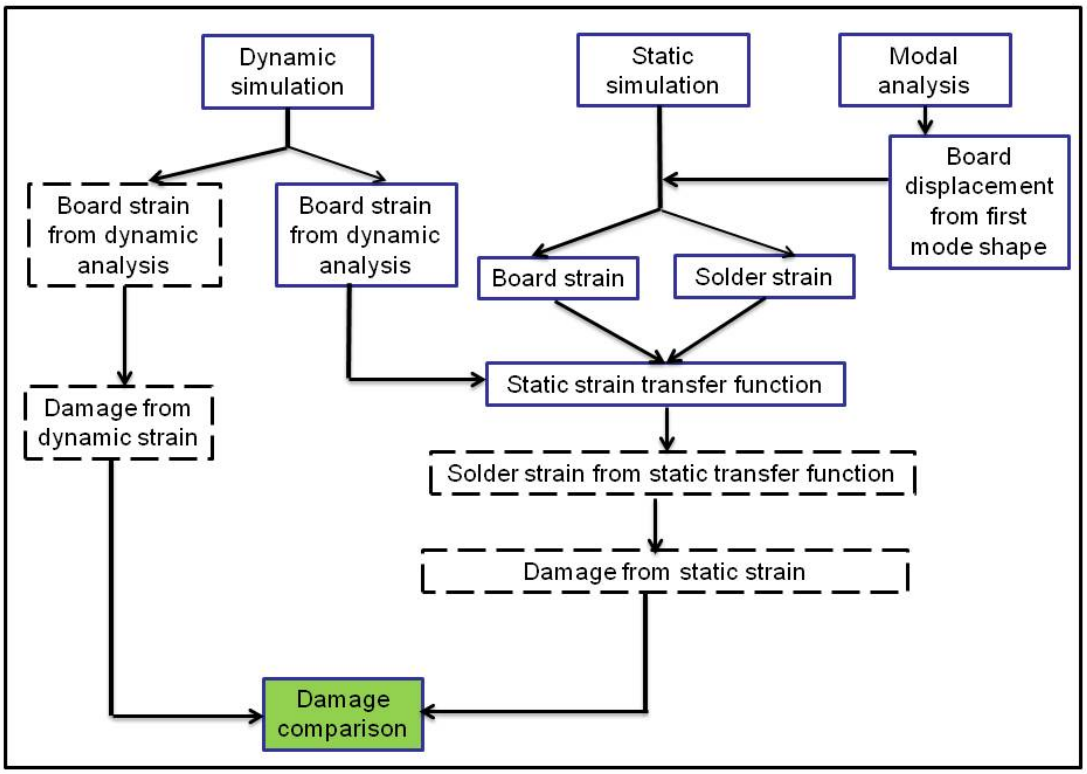

Figure 1: Approach for dynamic and quasi-static durability investigation

The excitation history was first measured with an accelerometer mounted on the fixture of the durability test specimen, and applied to a dynamic finite element model using an implicit solver. The dynamic response history of the solder joint was obtained from this simulation and used to calculate fatigue damage using an existing durability model. The results were compared with durability estimates from a quasi-static response analysis where the solder strain is caused purely by the fundamental mode of the PWB flexural deformations, as described in the next paragraph. The reason for this comparison is because this was the dominant deformation mode in the test used to derive the solder fatigue constants [7]. Experiments were conducted to verify the component relative motion with respect to PWB by characterizing the differences in amplitude and phase between the accelerations of the PBGA256 component and the accelerations of the PWB underneath, on a specially designed test vehicle.

The experiment and simulation results both revealed that the first mode of the PWB dominated its response under the random excitation used in this study [7]. So in the quasi-static stress-strain analysis, the first mode shape of the PWB was imposed on the test vehicle to obtain the theoretical transfer function between the flexural strain on the test PWB and the maximum strain in the critical solder joint. The durability model used in this study was obtained from literature [9] and [10]. The material constitutive properties are from the literature [11] and were also used in related studies by the authors [9].

III. FEA SIMULATION OF PWB RESPONSE

Generally, the components assembled on a PWB can be divided into three categories.

- Light components: chip passives (LCR, MLCC, etc), small outline transistors (SOTs), etc.
- Large surface mount active components: BGA, QFP, TSOP, etc.

- Heavy components: transformers, relays, switches, large power capacitors, etc.

Light components are typically small with negligible inertial effect, while the inertial effect of large and heavy components cannot be ignored in response analysis of the interconnects. Thus, the relative motion between SMT components and the PWB is much smaller for light, small components, than for the large heavy ones. This motion contributes to the dynamic solder strain response at higher frequencies and is explored in this study for a PBGA256 assembly.

MODELING DETAILS

In this study, a printed wiring assembly (PWA) is considered with a SMT PBGA256 component soldered on a FR4 PWB. PBGA256 is a full array BGA component with 256 solder joint (16× 16). A photograph of the component mounted on a PWB is shown in Figure 2.

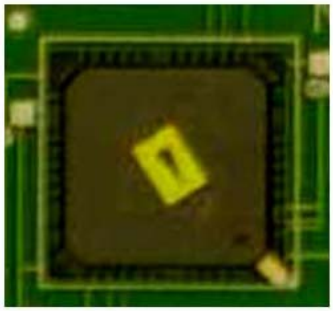

Figure 2: PBGA256 component used in this study

A schematic of the structure of the PBGA256 component is shown in Figure 3 [8], with the exception that there are no vias in our test specimen. Die attach and solder mask were not included in the current FEA model. This simplification should have minimal effect on the results, since these two layers are very thin compared to other elements in the assembly.

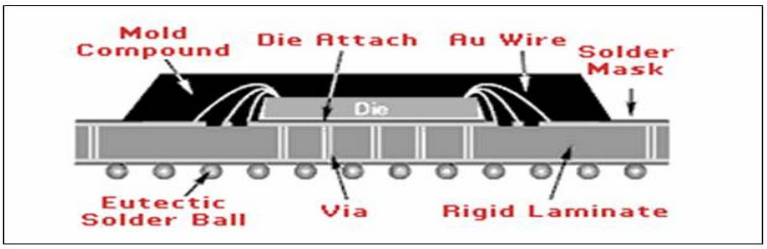

Figure 3: PBGA component structure [1]

As shown in Figure 4, the FEA model has a PBGA256 component assembled at the center of a FR4 board. The board is 120mm long, 60mm wide, and 1.5mm thick, and is clamped along the two short edges.

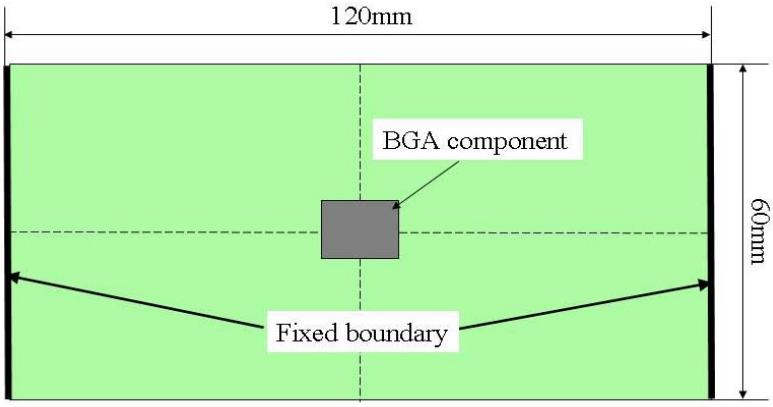

Figure 4： FEA model of a PBGA256 component attached to a FR4 Board

Due to the symmetry of the specimen, only a quarter of the model is considered with symmetric boundary conditions along the planes of symmetry. The quarter FEA model is shown in Figure 5. The detailed finite element mesh for the PBGA256 and the solder array is shown in Figure and Figure There are around 70,000 3D, eight-noded (linear interpolation) brick elements in this model.

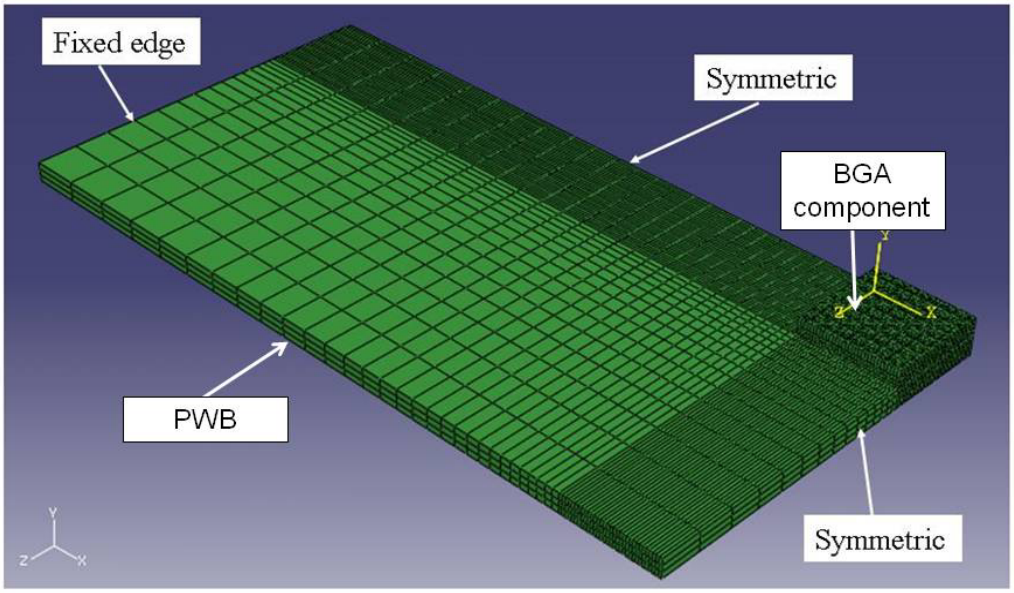

Figure 5: Quarter FEA model

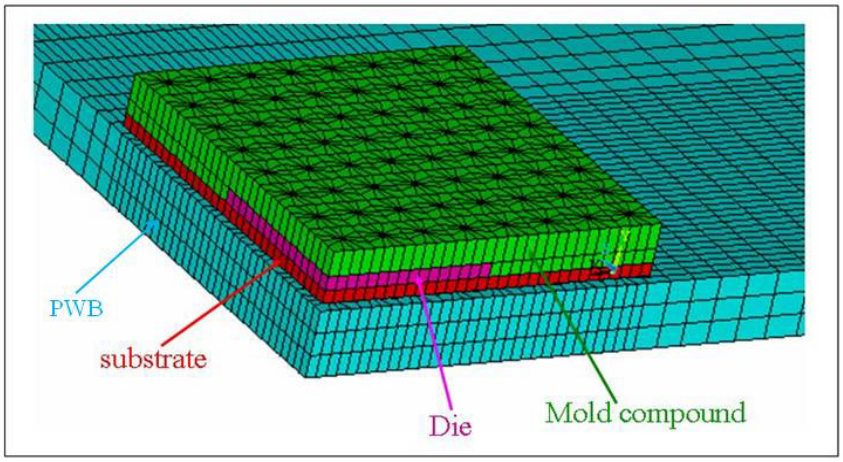

Figure 6: Detailed mesh for PBGA256 component on PWB

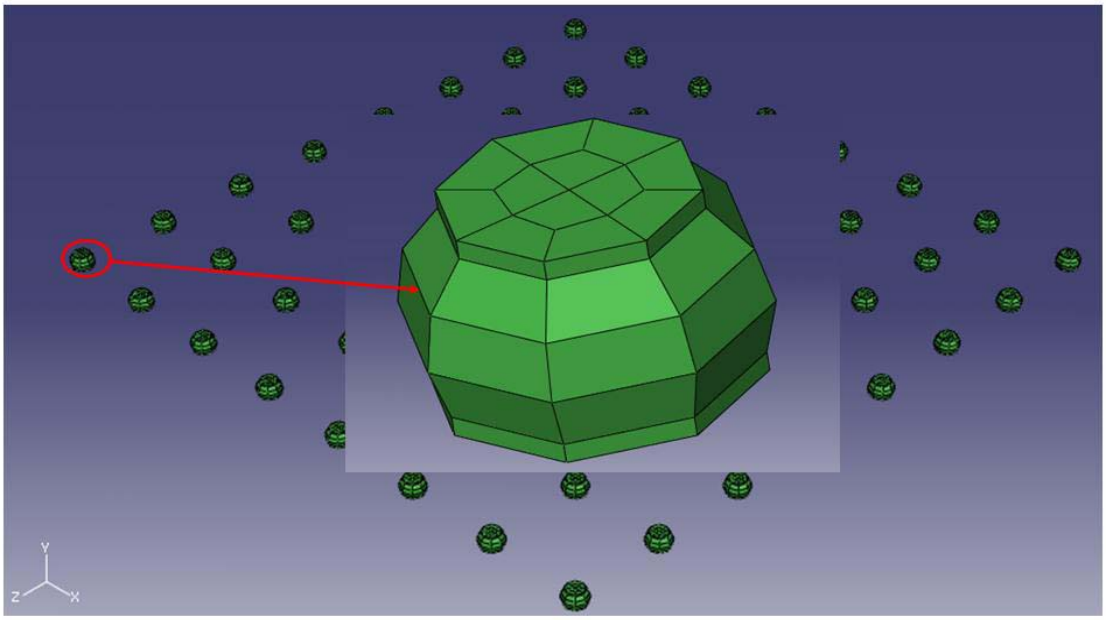

Figure 7: Detailed mesh of Solder joint

The solder is modeled as an elastic-plastic material. The elastic and plastic properties can be found in the literature [11] and have been used before by the authors [9]. The stress-strain curves for both SAC305 and Sn37Pb are plotted in Figure 8.

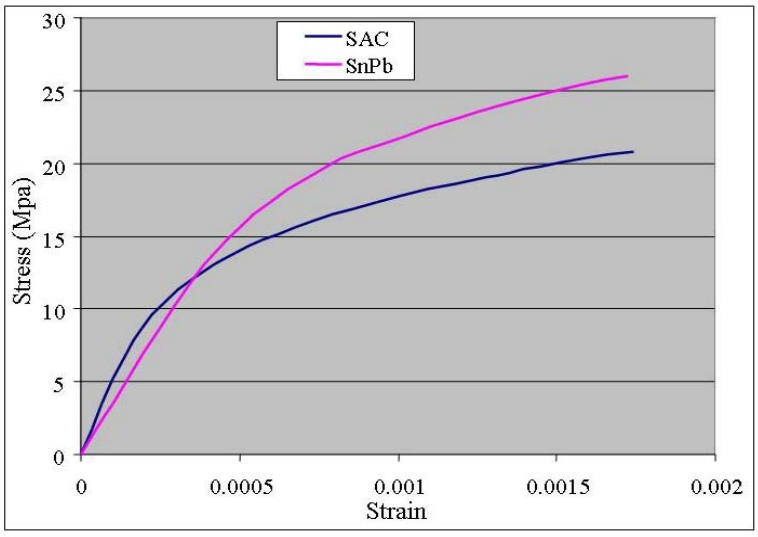

Figure 8: Stress-strain curves for SAC305 and Sn37Pb solder materials [11]

The constitutive properties for other materials in the assembly are listed in Table 1. The main dimensions of the test specimen are listed in Table 2. The FR4 PWB and PBGA-substrate are modeled as orthotropic elastic materials, while all other materials are modeled with isotropic elastic properties.

Table 1: Material properties for FEA model

	Young's modulus (Mpa)		Poisson's ratio		Density (10^3kg/mm^3)
PWB	In plane	Out of plane	In plane	Out of plane	2×10^{-9}
	17700	7710	0.28	0.11	
PBGA-Substrate	In plane	Out of plane	In plane	Out of plane	1.9×10^{-9}
	20000	4000	0.39	0.11	
Die	191000		0.28		2.3×10^{-9}
Cu pad	128750		0.35		8.9×10^{-9}
Mold compound	15900		0.3		1.2×10^{-9}

Table 2: Main dimensions for FEA model

	Length (mm)	Width (mm)
PWB	60	30
I/O pitch	1mm	
	Radius (mm)	Height (mm)
Solder	0.025	0.04

The FEA includes geometric nonlinearities to account for large-deformations caused by the high excitation magnitudes used in the response analysis later in this study. The nonlinear strain metric monitored in this FEA is logarithmic strain.

MODAL ANALYSIS

Before performing a detailed response simulation, a modal analysis was first conducted on the FEA model in order to obtain the natural frequencies and deformed mode shapes. For the current FEA model, the first natural frequency is approximately 160 Hz, with the corresponding mode shape shown in Figure .

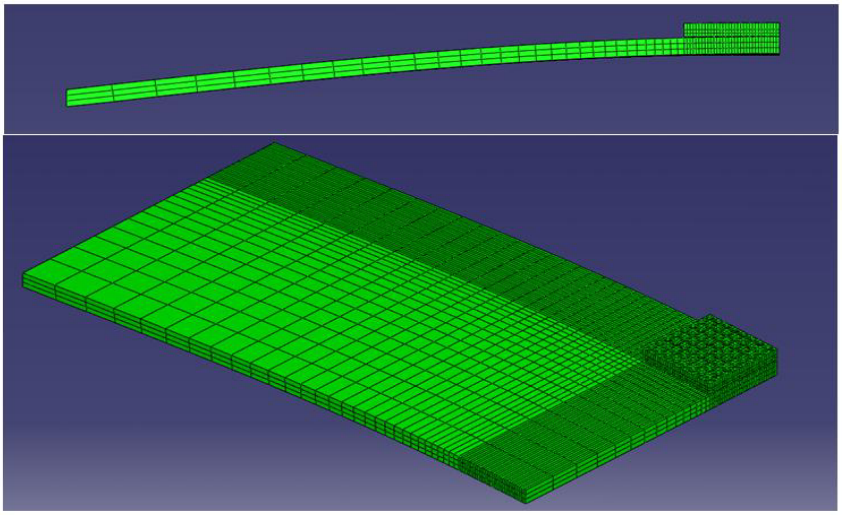

Figure 9: First mode shape from FEA model

DYNAMIC STRAIN ANALYSIS

There are two differences between the dynamic and quasi-static simulation in this study. The first is the out-of-plane inertial force of the BGA component due to its mass and acceleration, which is included in the dynamic simulation but not in the quasi-static approximation. The second is the contribution of the higher eigen-modes of the PWB, which is neglected in the quasi-static simulation. Clearly, the dynamic simulation is more representative of the real situation. The penalty for this increased accuracy is an increase in the simulation CPU time. For

example, on a 3.2G dual-CPU desktop computer with 3G RAM, it took around 30 hours to simulate a 0.1 second loading history.

The random excitation history used in this study was collected with an accelerometer during a random vibration durability study [9]. The frequency range of the random excitation is 0 to 500Hz, which covers the first three natural frequencies of the test board based on FEA results, which are 170Hz, 200Hz and 340Hz respectively. A typical 0.1s loading history with a G_{RMS} value of 6.4G is shown in Figure 10.

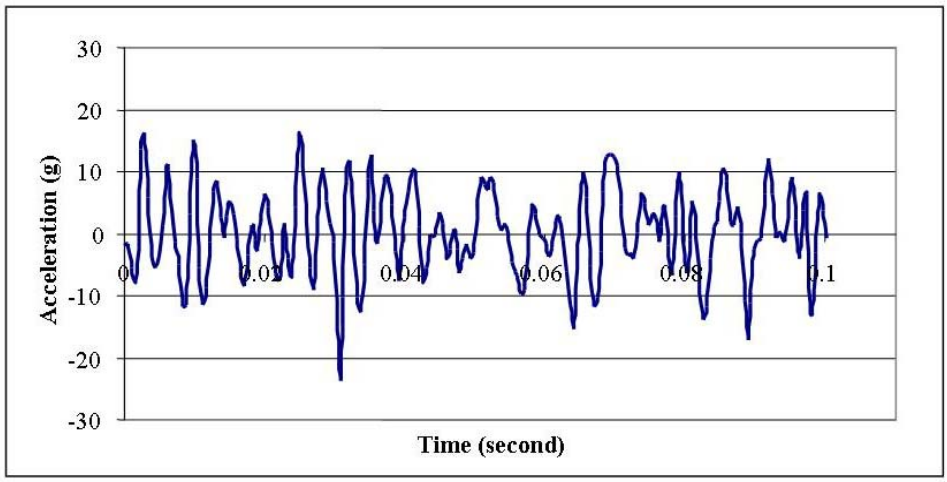

Figure 10: Random loading history for dynamic simulation, recorded from a related test by the authors [9]

The PWB primary flexural strain, ε_{xx}, due to dynamic response in the FEA model, was monitored close to the foot-print of the BGA component, on the opposite surface of the PWB. This PWB strain value was averaged over the footprint of a typical strain gage and the resulting history is shown in Figure 11. The von Mises' strain in the critical solder ball was also monitored in the FEA and locally averaged at the neck of the joint. Von-Mises' strain was calculated from individual logarithmic strain components using the formula given in the literature [12] as shown in Equation 1.

$$\varepsilon_{eq} = \frac{\sqrt{2}}{3}\sqrt{(\varepsilon_{xx}-\varepsilon_{yy})^2+(\varepsilon_{xx}-\varepsilon_{zz})^2+(\varepsilon_{zz}-\varepsilon_{yy})^2+6(\varepsilon_{xy}^2+\varepsilon_{yz}^2+\varepsilon_{xz}^2)} \quad (1)$$

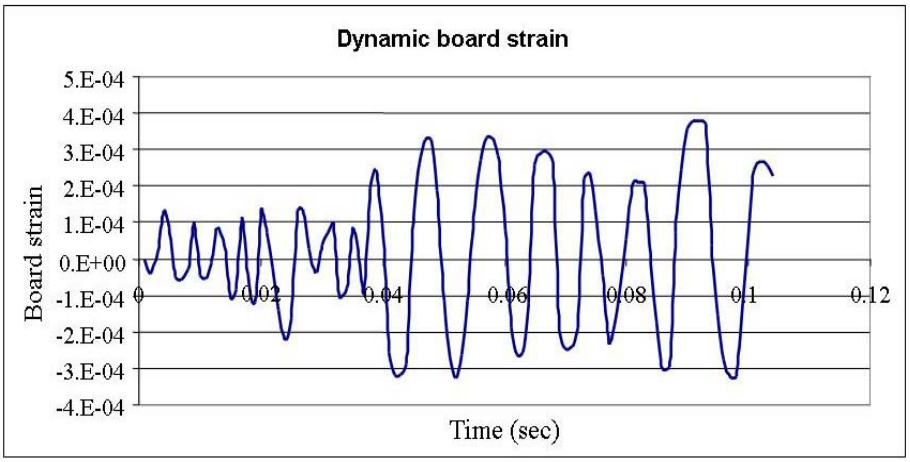

Figure 11: History of PWB flexural strain (ε_{xx}) from dynamic simulation of random excitation

The solder joint at the outer corner of the package footprint was found to be the critical one. The resulting solder strain history, shown in Figure 12, will be used later in this section to calculate the damage and durability. This dynamic durability estimate will be compared later with the durability estimated from quasi-static simulations, described later in Section V.

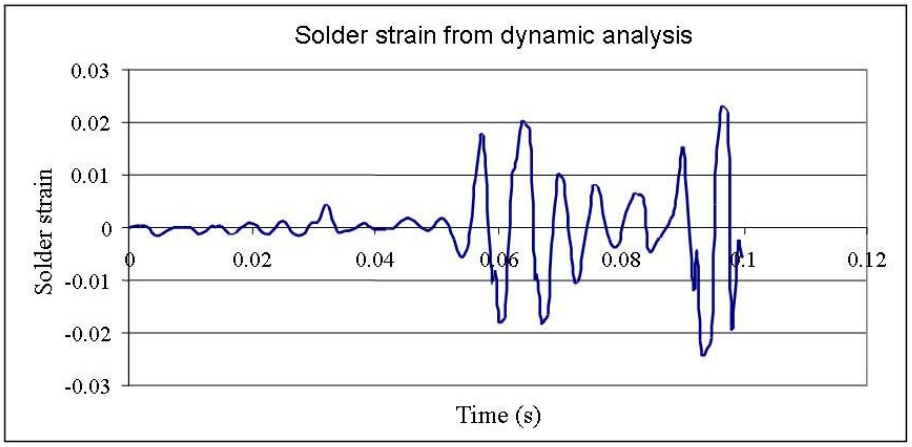

Figure 12: History of von Mises' strain, averaged in the neck of the critical solder joint from dynamic simulation of random excitation

QUASI-STATIC STRAIN ANALYSIS

This FEA model is then used to obtain the quasi-static strain response of solder joint due to PWB flexure. Following the approach used by the authors in earlier work [9, 10], the solder strain due to contribution of component inertial forces and higher PWB eigen-modes is ignored. As shown in Figure 13, the deformed mode shape of the first resonant mode is imposed with constraint equations to the top of the PWB surface. An example of the simulation results is shown in Figure

.

The critical solder joint in the quasi-static simulation was found to be the same as in the dynamic simulation. As the displacement of the PWB was progressively increased, the flexural strain ε_{xx} of the PWB adjacent to the BGA component and the locally averaged von-Mises' strain in the neck of the critical solder joint were recorded at the same locations as in the dynamic response analysis reported in the previous sub-section. The averaging techniques used here were the same as in the dynamic analysis. These averaged strains were then used to generate a transfer function between the PWB flexural strain and the von Mises' strain in the critical solder joint, as shown in Figure 15.

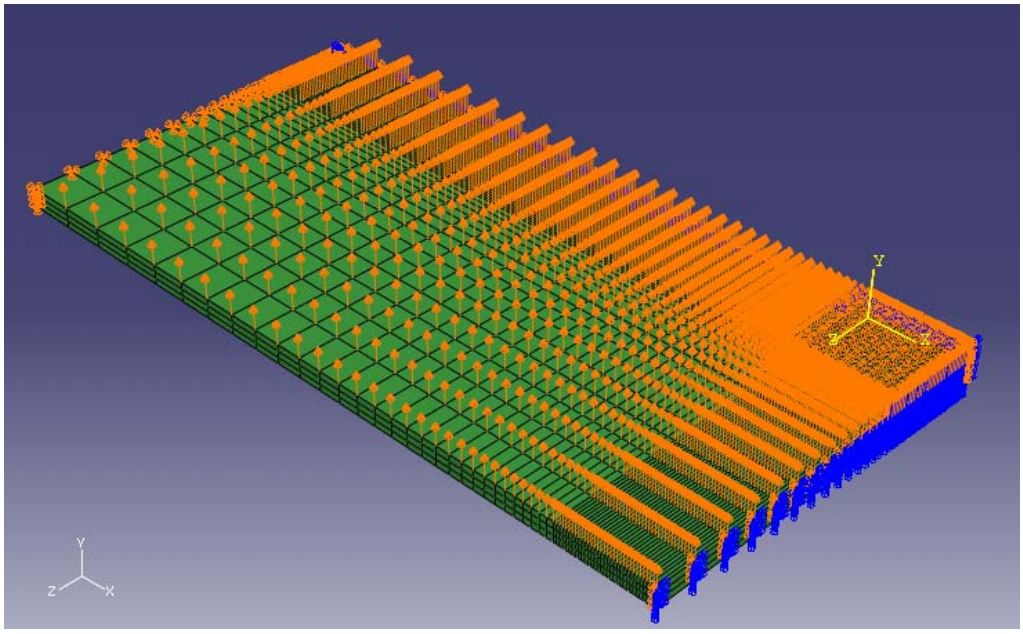

Figure 13: FEA model and boundary conditions used for static analysis

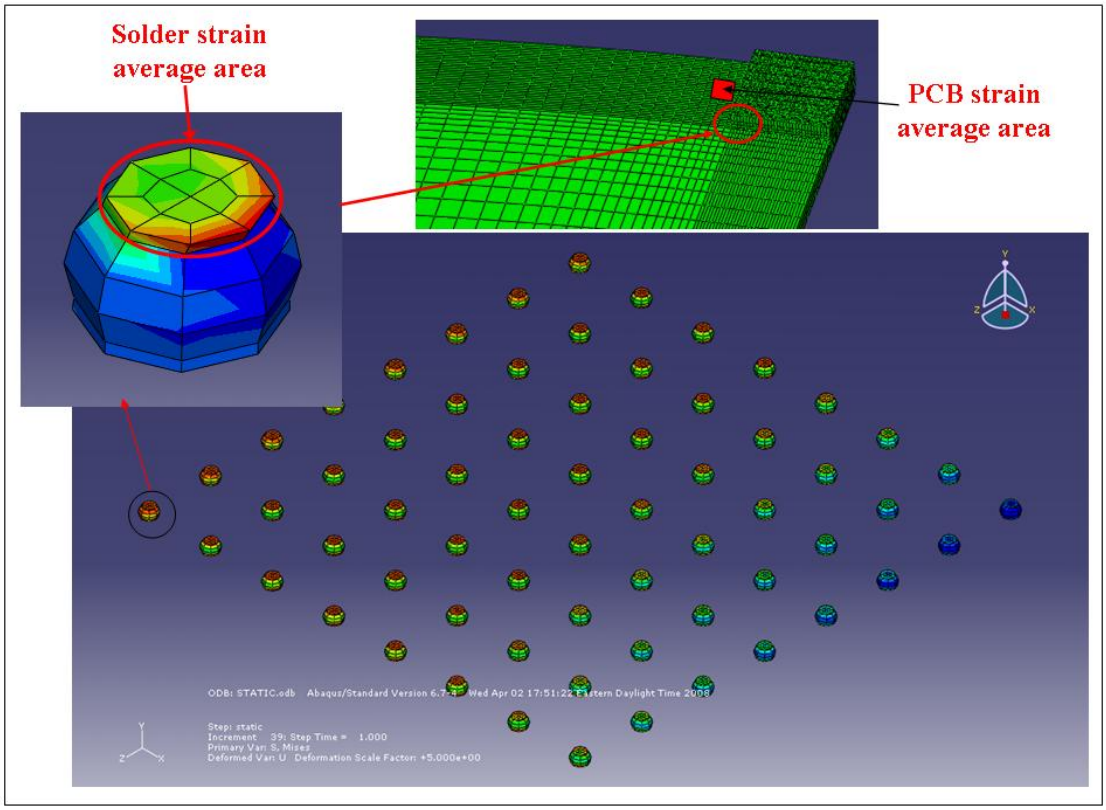

Figure 14: Contour plots of shear strain ε_{12} in solder joints, due to fundamental mode of PWB flexure

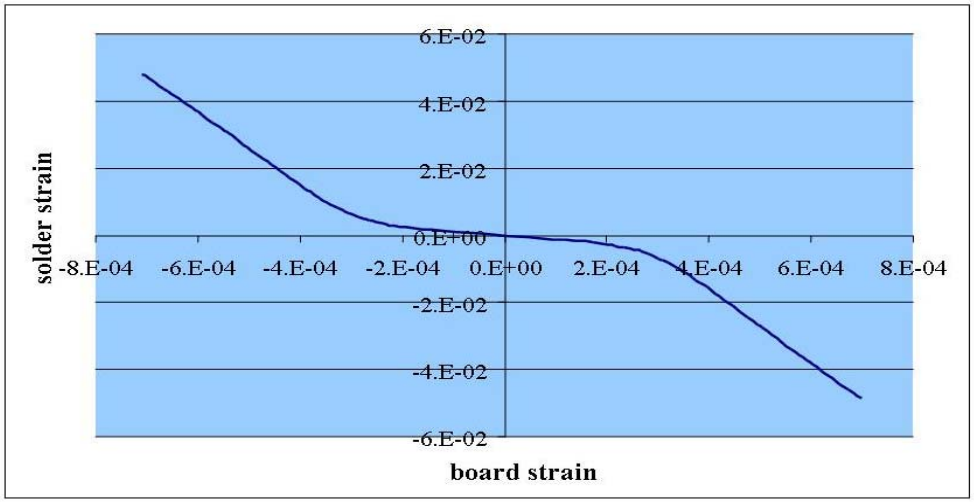

Figure 15: Quasi-static transfer function between PWB flexural strain ε_{xx} and von Mises' strain in the neck of the critical solder joint, due to the fundamental flexural mode of the PWB.

This strain transfer function shown in Figure 15 is combined with the simulated PWB strain history of Figure 11, to obtain the solder strain history due to PWB flexure, as shown in Figure .

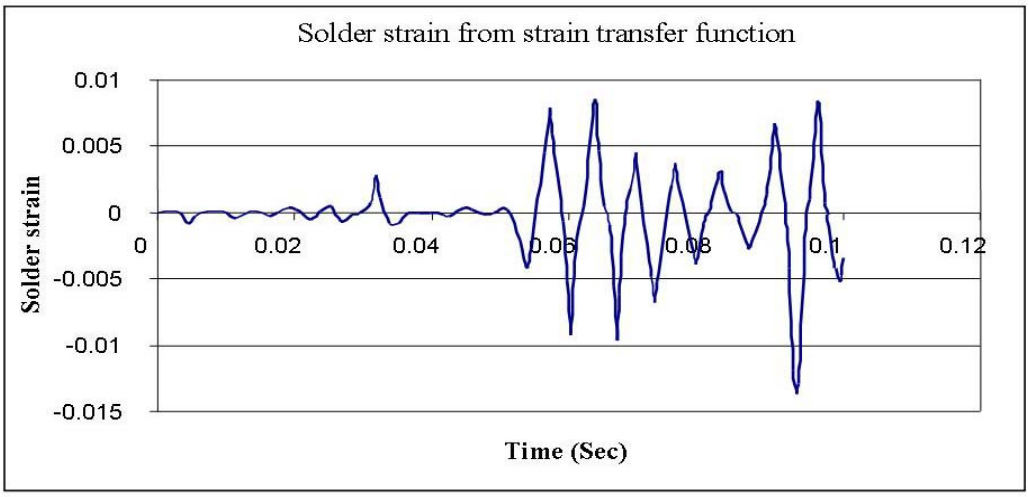

Figure 16: Solder strain history due to fundamental mode of PWB flexure

The critical solder in the dynamic simulation was found to be the same one as in the quasi-static simulation. The same averaging technique is used as in the quasi-static analysis, to obtain the dynamic history of the Von-Mises' strain in the neck of the critical solder joint. The dynamic strain plotted in Figure 12 shows similar overall history as the quasi-static strain in Figure 16. However, the amplitudes of dynamic strain in Figure 12 is almost double the quasi-static strain amplitude in Figure 16.

IV. EXPERIMENTAL VERIFICATION OF PWA RESPONSE

As hypothesized earlier, the discrepancies between the solder strain histories in Figure 12 and 16 are partly due to the higher resonant modes of PWB flexure, and partly due to relative motion motion between the component and PWB, caused by inertial forces acting due to the component mass. In this section, an experimental study is conducted to verify whether the component does indeed have large movement relative to the PWB at the frequencies used in this study.

The test vehicle and set up for this experiment, shown in Figure and Figure 18, consist of a PWA containing multiple surface mount components. The PBGA256 components, labeled as components 1 and 2 in Figure 17, are the focus of this experiment. Location 1 is close to the fixed edge while location 2 is close to the center-line of the PWA.

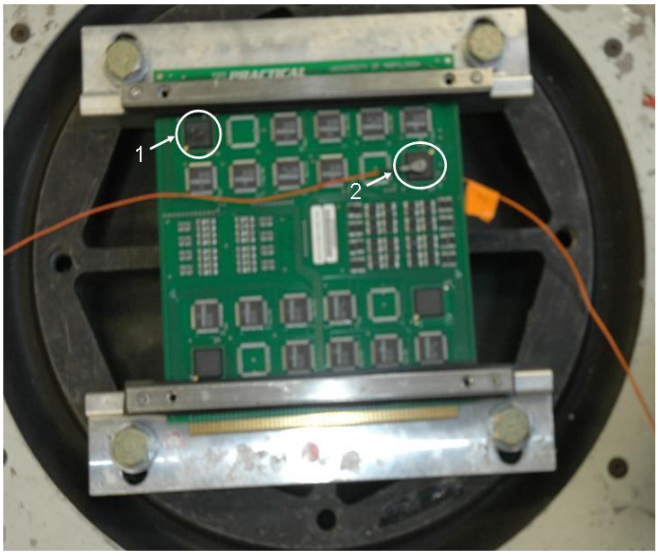

Figure 17: Test vehicle and setup

Two accelerometers are collocated in the x-y plane, one on the top surface of the component and the other on the bottom surface of the PWB, to measure the acceleration transfer function between these two BGA components and the PWB. The side view of the PWB in Figure 18, shows both accelerometers. The experiments were run twice, with the accelerometer pair located sequentially at locations 1 and 2, respectively. Each accelerometer has 1.0 mV/G nominal sensitivity.

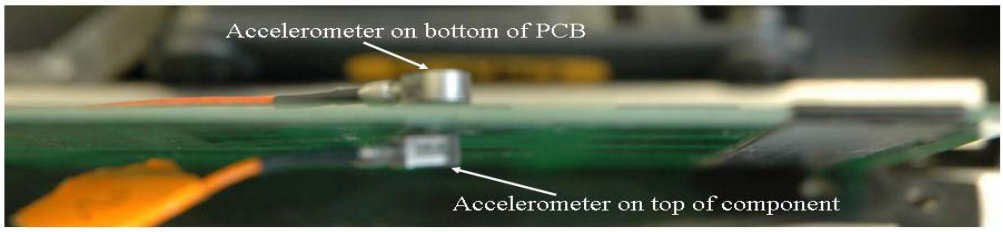

Figure 18: Accelerometer attachment

The test vehicle was then fixed along two opposite edges and excited with a white-noise random vibration in the range 20 – 800 Hz, on an electrodynamic shaker. A third accelerometer was used to acquire the acceleration of the fixture.

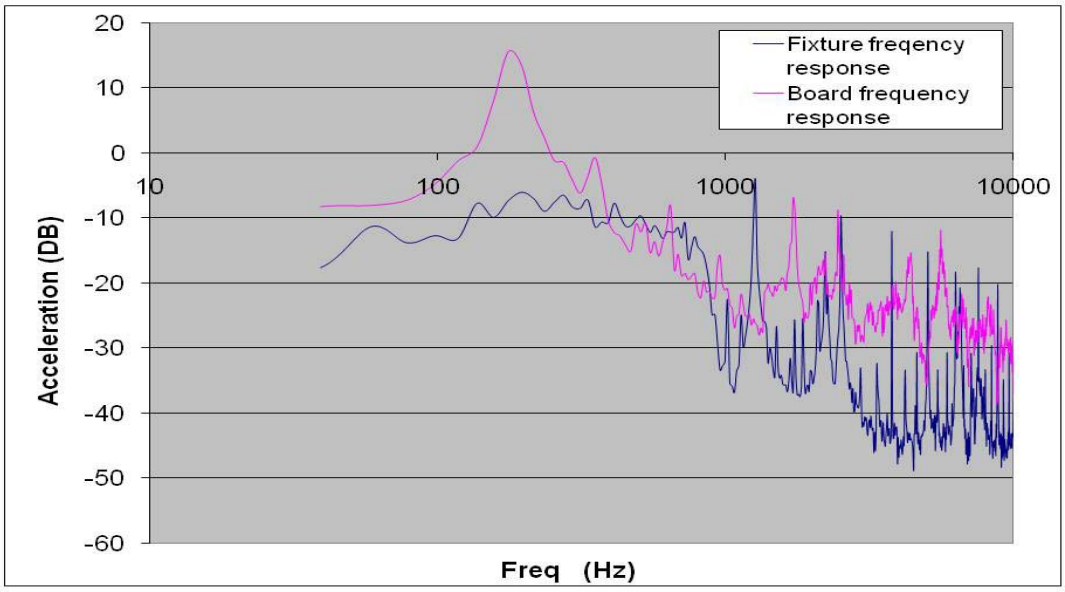

Figure 19: Fixture and PWB frequency response

The fixture and PWB frequency response are shown in Figure 19. The following observations can be made based on the acceleration measurement:

- The first natural frequency of the board is around 170Hz.
- Higher modes have insignificant acceleration amplitudes when compared with the first mode (atleast 15 dB lower).

- The natural frequency of the fixture is much higher than that of the test board, and shows dynamic response at high frequencies above 1000Hz. This high-frequency fixture response may provide excitation energy to induce component motion relative to the PWB.

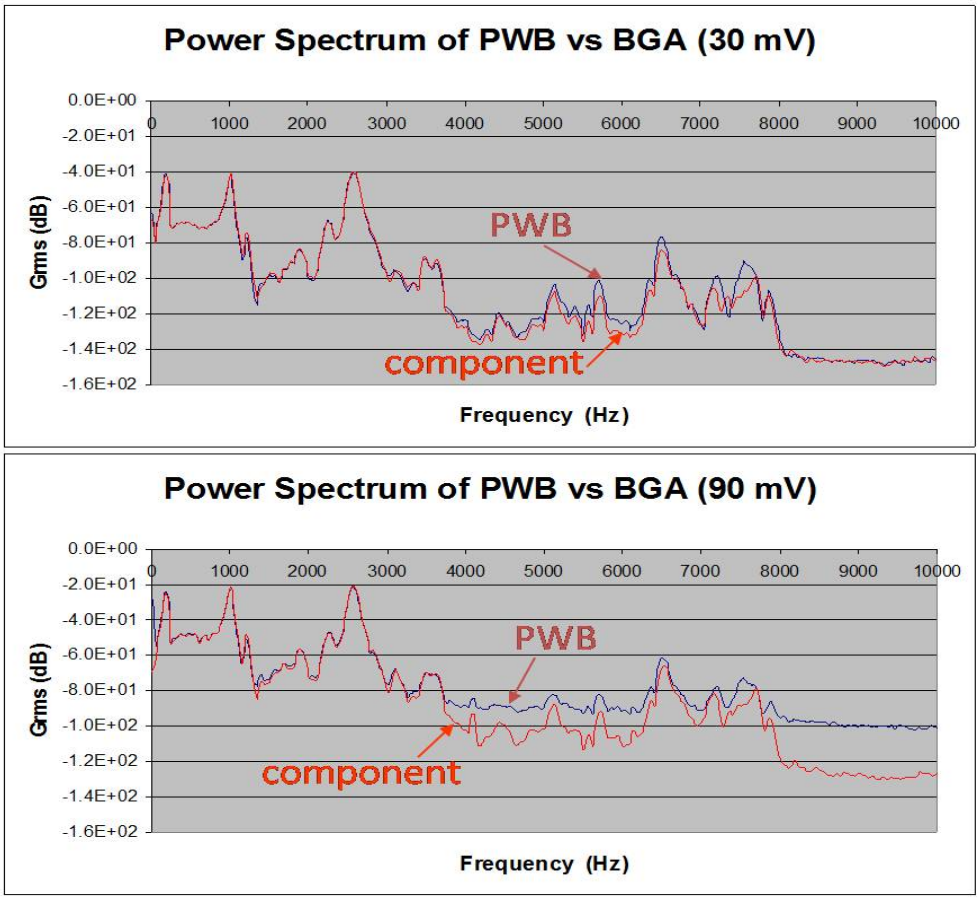

Figure 20: Acceleration frequency response plot for PWB and BGA at low excitation level

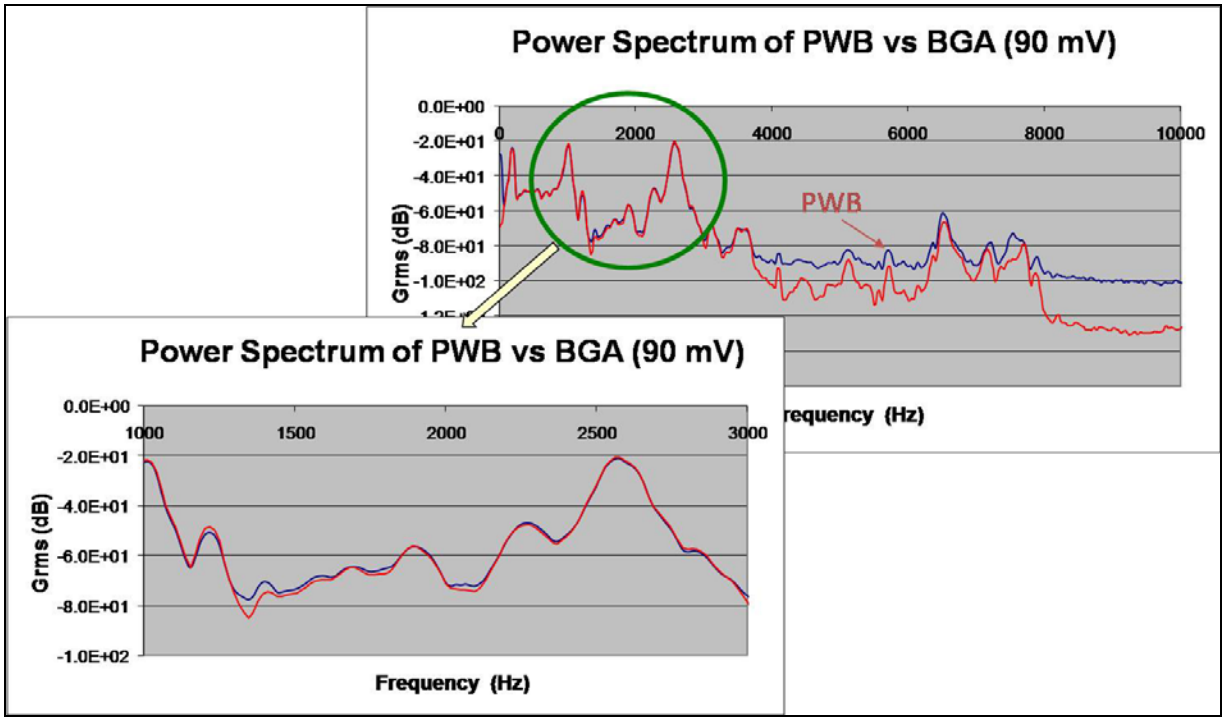

Figure 21: Acceleration frequency response plot for PWB vs BGA at high excitation level

The acceleration frequency response for accelerometers on top of the component and back of the PWB are plotted in Figure 20 and magnified in Figure 21. Significant levels of relative motion between the component and PWB was found in the following frequency ranges:

- 1 KHz < freq < 2.5 KHz
- 4 KHz < freq < 8 KHz

The corresponding phase different is shown in Figure 22. Phase difference between the PWB and component motion was found for both low (30mv) and high (90mv) excitation levels. The maximum phase difference can be seen at frequencies around 1400Hz, 3000 Hz, 3400 Hz, and 3900Hz.

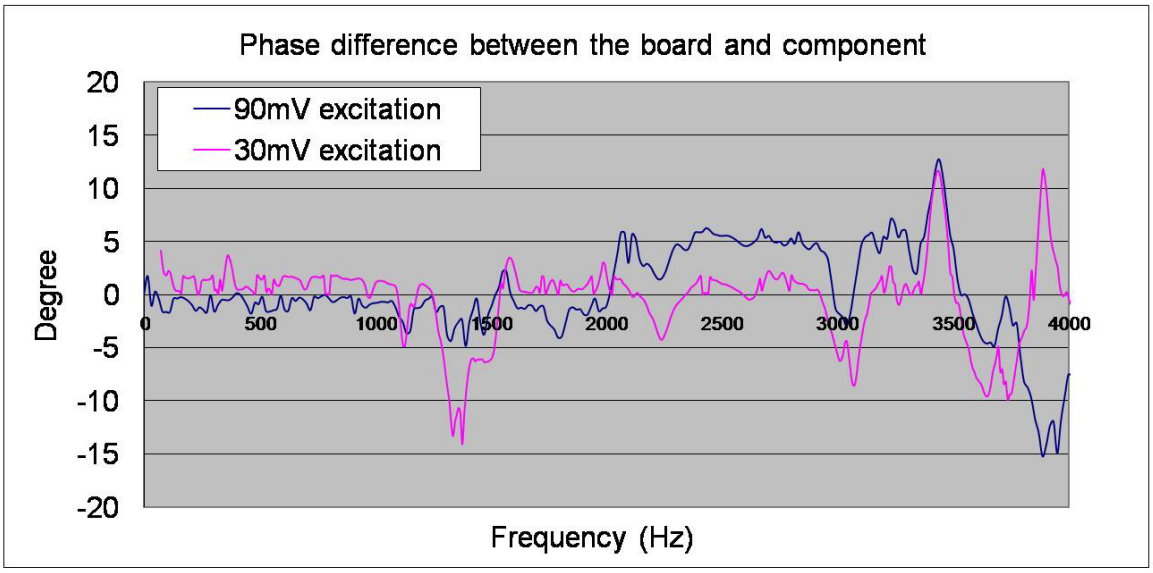

Figure 22: phase difference between PWB and component at different excitation levels

Both the amplitude difference and phase difference of the PWB response vs the component response, shown in Figures 20 to 22, can introduce additional strains in the critical solder joint, over and above the strains shown in Figure 16 due to PWB flexure. Even very small relative motion between the PWB and component can introduce large strain in the solder joint due to the very small height of the solder joints (0.15mm). Furthermore, as the plastic deformation in the solder joints increases, the magnitude and phase differences between the PWB and the component are magnified, resulting in higher strain values and, therefore, higher damage accumulation rates. In the quasi-static strain analysis presented in Figure 16, these large contributions to solder strain were ignored. This simplification may have caused a significant part of the discrepancy between the solder strain magnitudes in Figures 12 and 16.

The data in Figures 20-22 suggest that the relative motion between the component and PWB are highest at frequencies ranging from 1500 Hz to 4000 Hz. This relative motion is affected both by the input energy spectrum and by the natural frequency of the component, relative to the PWB. Figure 19 already demonstrated that the input excitation, measured at the

fixture, had a high peak at around 1500 Hz, due to the dynamic characteristics of the fixture. It is also instructive to examine the natural frequency for motion of the component, relative to the PWB. This natural frequency is clearly a function of the solder modulus and will significantly decrease as the solder starts to deform plastically. Thus FEA simulation for the BGA component is used to parametrically explore the relationship between the natural frequency and solder young's modulus. The results, shown in Figure 23, suggest that the natural frequency for motion of the PBGA256 will be at most 200 KHz for elastic deformation of the solder for the young's modulus used in current study and will be significantly smaller as the solder deforms into the plastic range and the effective tangent stiffness becomes very small. Thus, although the excitation rolls off after the resonant peak at 1500 Hz, there may be sufficient energy to cause relative motion, seen in Figures 21 and 22, at frequencies between 2000-4000 Hz.

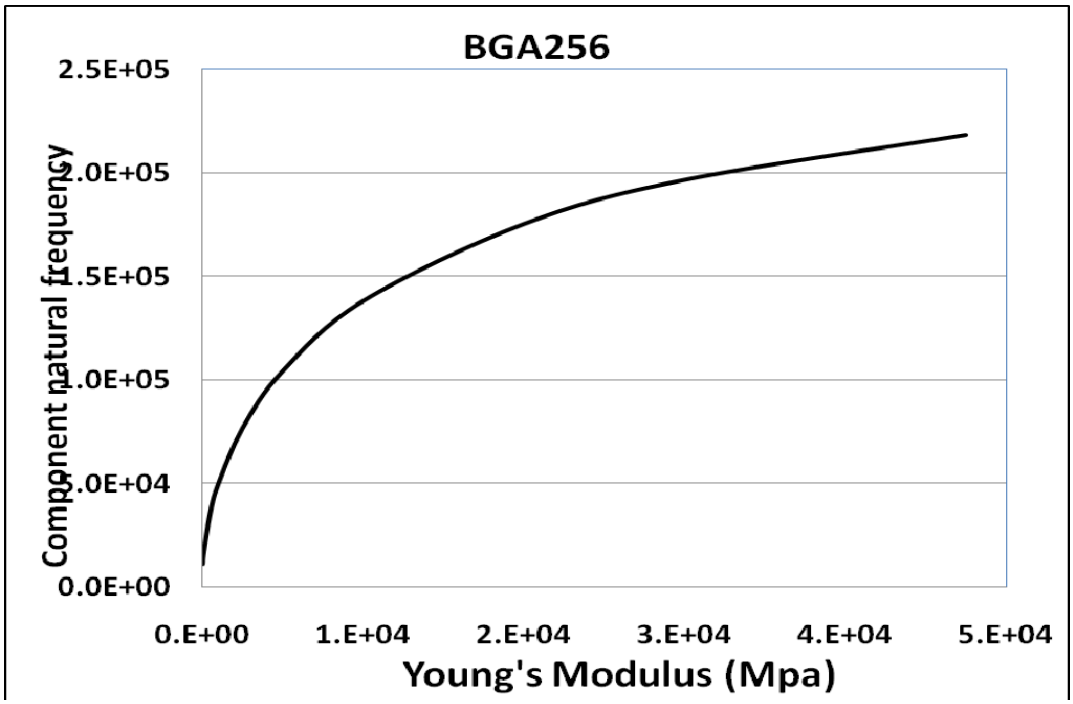

Figure 23: Relationship between natural frequency and solder young's modulus for motion of PBGA256 component

The observation from this dynamic testing and simulation shows that quasi-static simulation of just the first fundamental frequency of the PWB is not adequate to obtain the solder strain history under random vibration loading, as it significantly under-estimates the strain in the solder joint. Therefore, the durability of the solder interconnect is over-estimated under high frequency vibration loading. This provides a probable explanation for the durability differences observed between harmonic and random vibration tests, reported in the literature [9].

V. FATIGUE DAMAGE CONTRIBUTION DUE TO FUNDAMENTAL MODE OF PWB FLEXURE

The durability model used in this study is the well-known generalized Coffin-Manson fatigue model. The model constants for SAC305 and Sn37Pb solders depend on the choice of constitutive properties and have been presented before by the authors [9]:

$$\Delta\varepsilon = 0.011 N_f^{-0.08} + 0.86 N_f^{-0.44} \qquad 2$$

The number of cycles to failure N_f, for the response histories shown in Section III, is obtained by extracting the strain range from the dynamic strain history (shown in Figure 12) and from the quasi-static strain history (shown in Figure 16) with the help of cycle counting. As mentioned earlier, the quasi-static history only contains the contribution due to the fundamental mode of PWB flexure and does not contain any contributions due to higher modes of PWB flexure or due to relative motion between the component and PWB. The cycle counting algorithm is applied to a unit record-length (eg 1 sec window) of these solder strain histories, to obtain strain range distribution functions (RDFs). A typical strain RDF is plotted in Figure 23, showing the strain range on the x-axis and the corresponding occurrence rate on the y-axis.

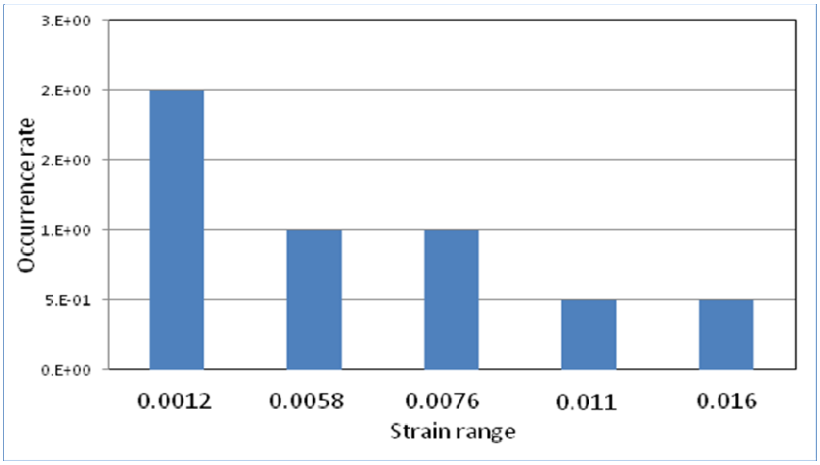

Figure 23: A typical plot for strain range distribution functions

The strain range $\Delta\varepsilon$ values shown in Figure 23 are used in Eq. 2 to calculate the number of cycles to failure, by solving the nonlinear equation. The fatigue damage (reciprocal of life) is linearly summed for the number of cycles at each of the strain levels shown in Fig 23. The resulting durability predictions are listed in Table 3 for comparison.

Table 3: Dynamic and quasi-static durability comparison

	Dynamic durability	Static durability
Durability time (Min)	10	107

These results show a significant difference between the dynamic and quasi-static durability predictions. The damage accumulation rate can be under-predicted by an order of magnitude in this case, if only the contributions due to first mode of PWB flexure are considered. This discrepancy is expected to increase even further if the bandwidth of the excitation energy is increased, since higher excitation frequency will further increase the contributions due to higher modes of PWB flexure and due to relative motion between PWB and component due to inertial forces. This observation provides a possible explanation for the high-frequency broad-band test (10-500 Hz) having a significantly higher fatigue damage accumulation rate than the low-

frequency narrow-band durability test (180 Hz), as reported elsewhere by the authors [9]. Even when the measured PWB flexural strain magnitudes were comparable under harmonic and random excitation, the solder strain amplitudes were probably much higher in the borad-band test due to the component inertial forces and due to higher participation of the higher modes of PWB flexure. Since random vibration is commonly encountered during shipping and application of electronic products, detailed dynamic investigation is clearly necessary for accurate durability estimation under such broad-band excitation.

SUMMARY

In this paper, the dynamic response of PBGA assemblies due to high-frequency excitation has been addressed with simulation and experiments. Dynamic FEA simulations of solder strain due to PWA vibration were conducted and compared to quasi-static FEA simulations that included only the effect of the first resonant mode of the PWB. Significant amount of difference has been found between the quasi-static solder strain and dynamic solder strain, thus resulting in a big difference in the dynamic and quasi-static durability predictions. This difference suggests that there are other deformation mechanisms in the solder interconnects in addition to the deformations caused by the first fundamental mode of the PWB. The possible candidates for the sources of the additional deformations are the higher resonant modes of the PWB flexure, and relative motion between the PWB and component due to inertial forces caused by the mass and acceleration of the component. Experiments revealed significant amount of relative motion between the PBGA component and the PWB at high frequencies. Therefore, the corresponding fatigue damage accumulation rates and durability are strongly sensitive to the maximum excitation frequency.

These results help explain why harmonic vibration durability tests at 160 Hz were observed [9] to accumulate fatigue damage much more slowly than broad-band random vibration durability tests with excitation frequencies as high as 500 Hz. So in order to accurately capture the mechanics of vibration fatigue durability of solder interconnects, the transient response in the solder due to component inertial forces and due to the higher fundamental modes of the PWB must be assessed.

ACKNOWLEDGMENTS

This work is sponsored by the members of the CALCE Electronic Products and Systems Consortium at the University of Maryland, College Park.

REFERENCES

[1] Steinberg, Dave S, “Vibration Analysis for Electronic Equipment”, John Wiley & Sons, New York, 1998

[2] Yang Q. J, Lim G. H, Lin R. M, Yap F. F, Pang H. L. J and Wang Z. P, “Experimental Modal Analysis of PBGA Printed Circuit Board Assemblies”, IEEE/CPMT Electronic Packaging Technology Conference, pp 290-296, 1997

[3] Yang. Q. J, Pang. H. L. J, Wang. Z. P, Lim. G. H, Yap. F. F, Lin. R. M, “Vibration Reliability Characterization of PBGA Assemblies”, Microelectronics Reliability, vol. 40, pp 1097-1107, 2000

[4] Yang Q. J, Wang Z. P, Lim G. H, John H. L. Pang, Yap F. F, Lin R. M, “Reliability of PBGA Assemblies Under Out-of-plane Vibration Excitations”, IEEE Transactions on Components and Packaging Technologies, vol. 25, No. 2, pp 293-300, 2002

[5] Yu Q, Kikuchi H, Ikeda S, Shiratori M, Kakino M, and Fujiware N, “Dynamic Behavior of Electronics Package and Impact Reliablity of BGA Solder Joints”, Proceedings of the

Intersociety Conference on Thermomechanical Phenomena in Electronic Systems, pp 953-960, 2002

[6] He Xiaoling, Fulton Rober, “Modeling and Simulation of the Dynamic Response of the Electronic Packaging”, IEEE Electronic Components and Technology Conference, pp 1535-1547, 2000

[7] Y. Zhou, M. Al-Bassyiouni and A. Dasgupta “Vibration Durability Assessment of Sn3.0Ag0.5Cu & Sn37Pb Solders under Harmonic Excitation”, Journal of Electronic Packaging (JEP), 2008, Accepted for Publication

[8] Y. Zhou, G. Plaza, M. Osterman and A. Dasgupta, “Vibration Durability of SnAgCu (SAC) Solder Interconnects”, Journal of the Institute of Environmental Sciences and Technology (IEST), 2008, Accepted for Publication

[9] Y. Zhou, M. Al-Bassyiouni and A. Dasgupta, “Harmonic and Random Vibration Durability of SAC305 and Sn37Pb Solder Alloys”, Accepted by ASME International Mechanical Engineering Congress and Exposition, Boston, MA, Nov, 2008, Paper num 67375

[10] Y. Zhou, B. Moustafa and A. Dasgupta, “Vibration Durability Assessment of Sn3.0Ag0.5Cu & Sn37Pb solder under Harmonic Excitation”, Journal of Electronic packaging, 2008, Accepted for Publication

[11] Darveaux R, Banerji K, “Constitutive Relations for Tin-Based Solder Joint”, IEEE Transactions on Components, Hybrid and Manufacturing Technology, vol. 15, No. 6, pp 1013-1023, 1992

[12] Hill, R., The Mathematical Theory of Plasticity. Oxford, Clarendon Press, 1950

Chapter 6: Summary, Contributions and Future Work

The focus of this study is the durability of surface mount Pb-free SAC305 solder interconnects under vibration loading. Vibration loading is a life-cycle environment commonly encountered during the application and transportation of electronic products, and yet has not been investigated to the same extent as durability under cyclic thermal environments. Study of vibration durability is complex when there are random and dynamic excitations histories. Before jumping to the complex study of random vibration durability, a simpler case of harmonic durability was first studied, to obtain the vibration durability fatigue model constants for SAC305 solder material. The corresponding model constants for eutectic Sn37Pb solder material were also addressed, for the purpose of comparison and bench-marking. The results of this study will be useful for the design, development and qualification of Pb-free electronics for life-cycle mechanical loading including vibration as well as combined thermal cycling and vibration.

I. SUMMARY AND CONCLUSIONS

Vibration durability tests were thoroughly conducted in this study, including constant-amplitude harmonic durability and step-stress random durability, for both SAC305 and Sn37Pb solder materials. The test results show that under comparable harmonic excitation, SAC305 interconnects were not as reliable as corresponding Sn37Pb interconnects. The sensitivity of random vibration durability to changes in the ambient temperature from low temperature (-40^{o}C) to high temperature (125^{o}C) was empirically examined. In addition, the impact of preconditioning by isothermal aging for varying lengths of time at 125^{o}C on vibration durability at RT was examined. The results provide insights regarding relative vibration durability of Sn37Pb and SAC305 assemblies under similar loading conditions.

Detailed finite element simulation was conducted for LCR components, to investigate the strain history in the solder joint under harmonic vibration loading at the first natural frequency of the test vehicle. The loading history was quantified and fatigue damage accumulation rates were analyzed using a time-domain approach. A generalized strain-life durability model was used to describe the fatigue durability of both Sn37Pb and SAC305 interconnects. The model constants were extracted from the vibration durability test results using the time-domain damage analysis method mentioned above. Failure analysis showed that most of the failures were in the solder joints but in some cases there were also failures in the copper traces. Thus, the derived durability model constants are to be treated as lower-bound estimates when predicting the durability of solder interconnects. Results show that SAC305 and Sn37Pb durability curves cross-over around 10^8 cycles. SAC305 material is more fatigue resistant than Sn37Pb material below this cross-over life, while Sn37Pb material is more fatigue resistant than SAC305 material above this cross-over life. It is important to recognize that even in the LCF region, where the SAC305 material is more durable, actual interconnects assembled with SAC305 solders may not outlast corresponding Sn37Pb assemblies under similar excitation levels because: (i) there are competing failure mechanisms in the IMC layer and in the PWB copper traces that often make the SAC305 assemblies more vulnerable than Sn37Pb assemblies to PWB flexure; and (ii) SAC305 interconnects may experience higher strain level than Sn37Pb interconnects under the same excitation level, because of different stress-strain properties.

The accuracy of the durability damage assessment method and the derived model constants was then assessed by testing the ability of the model to predict durability under step-stress broad-band vibration tests. The test conditions were simulated in the damage model and predicted life was compared to test results. The model predictions were found to be quite sensitive to the

stress-strain properties assumed for the solder. Although characterization of stress-strain curves is not the main focus of this dissertation, very useful insights were obtained about these constitutive properties by examining the sensitivity of the durability prediction to the choice of elastic-plastic constitutive properties. The mechanical stress-strain properties reported in the literature for Pb-free materials typically have a large degree of variability and scatter across different research groups. It's therefore difficult to identify the correct one to use. This sensitivity study provided some interesting insights into this choice. Comparison between the model prediction and experimental results show that the model predictions are more sensitive to the plastic hardening exponent than to the Young's Modulus. Within the range of properties investigated, the more compliant (lower Young's modulus) and softer (less plastic hardening) material properties provide better agreement between the harmonic and random durability model predictions. The optimal combination of constitutive and durability model constants (the combination that provided the best agreement between harmonic and random durability results), was also tested against a selected set of durability test results from quasi-static 4-point cyclic bending tests, reported in the literature. The model predictions were found to agree well with the 4-point bending durability test results. However, in all cases, the damage model over-predicted the random vibration durability, with the best-case discrepancy varying between 0-400% for the different LCRs and loading cases. Clearly there may be additional damage modes in the random vibration test that are not addressed in the proposed damage model, and were explored in Chapter 5 of the dissertation.

To explore the additional damage mechanisms under random vibration, a dynamic FEA simulation was conducted for a selected PBGA assembly. The damage accumulation rate in the dynamic simulation was found to be an order of magnitude larger than that from quasi-static

simulation of solder damage due to the fundamental mode of PWB flexural deformation. One of the possible reasons for the discrepancy between the dynamic and quasi-static results is the contribution of the inertial forces caused by the component mass and acceleration. In the earlier chapters of this study, the effects of this force on solder joint damage were neglected in comparison to the damage caused by PWB flexural deformations. The natural frequency for this effect is fairly high and cannot be ignored in the case of random excitation, because of the higher excitation frequencies.

It is instructive to note that if this dynamic adjustment-factor is applied to the time-to-failure of PBGA256 observed earlier in chapter 4 for the quasi-static model prediction for LCR2512, for this material property set (Set 5 in Chapter 4), then the model prediction closely matches the test results. This is not unreasonable, since the strain level in the PBGA256 critical solder joint is found to be close to the strain in the LCR2512 critical solder joint. As expected, both the LCR2512 and PBGA256 assemblies exhibit similar durability under similar vibration excitation. A further implication is that the Material Set 5 used in used in Chapters 4 and 5 is a reasonably accurate representation of the actual solder properties for simulation of vibration response and durability.

II. CONTRIBUTIONS OF THIS DISSERTATION

As described above in the summary of the dissertation, the central focus is on the vibration durability investigation for Pb-free solder interconnects using comprehensive vibration durability experiment and numerical simulation. The main contributions of this study include:

1. Insight into the fact that random vibration can be an order of magnitude more damaging than harmonic vibration for solder interconnects, due to:
    - Inertial forces due to component mass

- Higher response modes of PWB

2. A systematic study to extract HCF properties of solder material from harmonic vibration testing of electronic assemblies:
    - Generalized strain-life durability model constants for both SAC305 and eutectic Sn37Pb solder alloys
    - Quantitative insights into sensitivity of vibration durability model constants on stress-strain properties, in SAC305 and Sn37Pb solder alloy
    - Modeling improvements for strain transfer-function between PWB and solder joint
3. First study to provide comprehensive evidence that under vibration excitation copper trace failure can be a dominant failure mode, competing strongly with solder joint failure. This is consistent with previous studies that have shown copper trace failures in SAC assemblies during quasistatic mechanical cycling and drop loading. This observation is very critical for future vibration durability studies, since root cause analysis will be needed to differentiate between copper trace failures and solder joint failures. Obviously, the solder joint durability model constants obtained in current study are therefore a lower bound for the actual constants.
4. New vibration durability database for SAC305 and eutectic Sn37Pb assemblies under harmonic and random excitation: exhaustive vibration durability tests have been conducted in this study, using harmonic excitation (at the first natural frequency) and random excitation (including first four resonant frequencies), on Sn37Pb and SAC305 assemblies with a selection of several commonly used SMT component styles. These tests have been conducted at multiple isothermal conditions as well as under thermal cycling conditions. The

SAC305 test boards generally failed faster than corresponding eutectic Sn37Pb interconnects under comparable test conditions in this study. The durability tests were carefully designed to make sure that some of the component failed under high cycle fatigue. The harmonic durability test results show less scatter and better repeatability than the random test results, due to the simpler loading and response. This database is of value to researchers who can use this knowledge-base to develop new vibration fatigue models.

III. SUGGESTIONS FOR FUTURE WORK

Based on the insights from this study, possible future work is suggested in this section to improve and extend the current work. The improvements include the current experimental and simulation approach. While, vibration durability is the focus of this study, combined thermal cycling and vibration damage will be a good extension based on available vibration and thermal durability work.

1. Sample size: due to the long duration of high-cycle fatigue tests, the sample size in this study is somewhat limited. Furthermore, obtaining low-cycle fatigue data is also somewhat challenging in vibration tests, since there is a high risk of accidental overstress failures under such high loading amplitudes. Only one PWA was investigated for each loading condition in each of the harmonic and random durability tests. Given the scatter in the test results, especially under random excitation, a larger sample size will be very useful to improve the confidence in the vibration fatigue properties obtained from this study.
2. Failure analysis to separate competing failure modes: two competing failure modes have been found from the failure analysis of the failed components (BGA and LCR): a) cracked solder joints, b) cracked copper traces. In this study, real-time resistance monitoring technique was used to detect failures. However, this technique does not distinguish between

the two failure modes or provide a history of the sequence in which they occurred. Hence the obtained durability curves do not represent the true durability for either failure mechanism, but can be used to obtain a lower bound for either, for both SAC305 and Sn37Pb. Verification of the failure mode in future studies will be very useful for improving the durability model constants. New test methods, specimen design and failure monitoring techniques that distinguish between these competing failure modes will be a very valuable area for future research.

3. Influence of multiple vibration modes on fatigue damage accumulation rates: results indicate that the PWA response was primarily due to the first dynamic mode. This should be verified using higher sampling rates for recording strain. Furthermore, even a small participation from the higher mode shapes can contribute significant fatigue damage due to the higher curvatures and higher frequencies. If higher modes are important, then new modeling techniques are needed to include their effect on fatigue damage accumulation.
4. Dynamic response in solder interconnects due to component inertial force: This study presented preliminary evidence that there is some relative motion between the PWB and the component under the random excitation used in this study.
    - improved simulation and experiment are needed to better quantify the influence of relative motion between component and PWB, on solder fatigue damage accumulation rate as a function of excitation frequency
    - This study used two different specimen configurations for the simulation and the testing to identify the relative motion, and to collect failure data. A common specimen is recommended for future studies,for better confidence.

- dynamic characterization experiment should use better methods to quantify relative motion (eliminate approximations due to accelerometer mass)
- the dynamic simulation conducted in the present study simulated only a 0.1s window to economize on computing resources. The dynamic simulation period should be significantly lengthened in future studies to provide better confidence in the results.

5. Accurate stress-strain curves and fatigue constants: guided by the parametric studies of this thesis, focused analysis is needed to identify a correct combination of stress-strain curves and fatigue constants to permit accurate high-cycle fatigue analysis of solder interconnects.

Appendix

Appendix A:

Vibration Durability Investigation for Sn37Pb and Sn3.9Ag0.6Cu Solders with Accelerated Testing and Modeling

In this chapter, a methodology was proposed to quantify the random vibration fatigue durability based on step-stress test results for both SAC and SnPb surface mount interconnects. A least-square fit was used to obtain fatigue model constants for these two solders, based on the test results. The model constants are useful for vibration fatigue design. The goodness of the fit is examined in this paper. This paper was presented at IEEE-TC7 conference on Accelerated Stress Testing & Reliability, San Francisco, CA, Oct, 2006

Vibration Durability Investigation for Sn37Pb and Sn3.9Ag0.6Cu Solders with Accelerated Testing and Modeling

Yuxun Zhou, Abhijit Dasgupta

CALCE Electronic Products and Systems Center

Mechanical Engineering Department

University of Maryland, College Park, MD 20742 USA Phone: 301- 405-5231

Email: easily@wam.umd.edu

ABSTRACT

The vibration fatigue durability of eutectic Sn37Pb and near-eutectic Sn3.9Ag0.6Cu solders is quantified, based on test data available from the literature [1]. The tests use random broad-band excitation (between 20Hz & 2000Hz) on both SAC and SnPb surface mount interconnects. In the test, step-stress excitation was applied to printed wiring assemblies (PWAs) by increasing the

RMS excitation levels from 10G to 28G to fail most of the components on the board. The tests were conducted on five identical test vehicles for repeatability. Fatigue damage was quantified for 10 BGA 225 components located at various positions on the test PWA, using a time-domain approach, reported in the literature [2]. The test results show that the tested SAC solder has lower fatigue durability than eutectic SnPb solder, under the applied vibration excitation. This result is consistent with mechanical cycling studies [3] and repetitive mechanical shock, conducted earlier. A least-square fit was used to obtain fatigue model constants for these two solders, based on the test results. The model constants are useful for vibration fatigue design. The 'goodness' of the fit is examined for all 10 BGA components.

KEY WORDS

Vibration durability, SAC, SnPb, time-domain analysis, PSD analysis, rain-flow cycle counting, empirical power-law durability model

INTRODUCTION

Legislation has been passed in Europe to ban the use of lead (and other materials) starting 1 July 2006. Many of the major electronics companies have announced lead reduction targets and the move to lead-free electronics. The search for a replacement solder alloy has been conducted imminent by several industrial and academic consortia [5] [6].

Vibration loading is commonly encountered in the service life of electronic packaging. Therefore the fatigue performance of lead-free materials under vibration loading must be investigated. Compared to thermal cycling durability data, there is scarcity of vibration durability data for lead-free materials. The characteristics of the stress history caused by vibration loading are low amplitude and high frequency. Recently, Lau et al. [7] studied mechanical and vibration

responses of plastic ball grid array assemblies due to overload environmental stress factors. Darbha et al. [8] investigated stress distribution of surface mount interconnections due to vibration loading. Barker et al. [9] [10] proposed some analytical methods to estimate the vibration fatigue lives of leaded surface mount components. Liguore et al. [11] developed a simple vibration fatigue life prediction technique for the LLCC solder joints. Lau et al. conducted vibration reliability testing [12]-[14] using sweep sinusoidal excitations and studied vibration fatigue properties based on linear assumption. In their study, a linear model is used to characterize the vibration response of the test vehicle. Yang et al. [15] investigated the reliability of a PBGA assembly under a sinusoidal excitation. In his study, the dynamic displacement of the PBGA assembly was found to be highly nonlinear under out-of-plane excitation. Most failures were due to cracks near the copper pad on the PCB, in Yang's [15] work. Che et al. [16] conducted fatigue tests and analysis for flip chip solder joint under sinusoidal sweep test within a narrow frequency band near the fundamental resonant frequency.

In this paper, modeling and simulation was conducted, in order to obtain vibration durability models from reported failure data using step-stress vibration durability tests [1]. A time domain strategy [2] is used in this paper to post-process the test results. An empirical durability model is obtained for both SAC and SnPb solder joints.

APPROACH

In accordance with fatigue literature [4], a power law relation between cyclic strain range and number of cycles to failure is used, to derive an empirical vibration durability model, as shown in Equation 1.

$$N_f = A(\Delta\varepsilon)^b \tag{1}$$

N_f : Number of cycles to failure

$\Delta\varepsilon$: Solder strain range

A, b: model constants (material fatigue properties of the selected solders)

The final goal of this paper is to obtain the model constants in Equation 1, for both eutectic SnPb solder as well as the near-eutectic SAC solder. The approach to accomplish this goal is listed in following bullets:

- Characterize the PCB flexural strain at a specific location with strain gage
- Extrapolate the measured PCB strain to key locations (site of components of interest) over the PCB, using global (PCB-level) FEA
- Obtain the max solder strain from the PCB flexural strain, using local (component level) FEA
- Estimate the exponent *b* using a least-square fit of the damage ratio for selected components
- Estimate the coefficient *A* using a least-square fit of the damage for selected components

The fatigue life estimated for each component with the durability model is compared with the durability test results to assess the "goodness" of the fit.

TEST SETUP AND LOADING

The durability test setup used in the test [1] is shown in Figure 2.

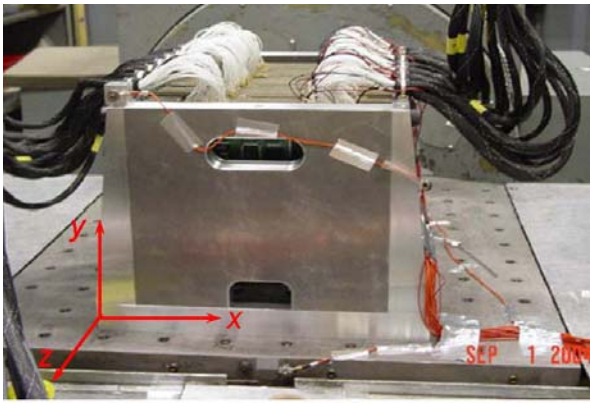

Figure 1: Durability test setup used in the test program [1]

15 test boards were mounted in card guides, in a specially designed fixture, as shown in Figure 1. This fixture was mounted on a vibration shaker and loaded in the Z direction. An event detector, combined with labview-based data collection software was used to monitor failure and strain history. The threshold for failure was set to be 300 Ohm for each joint.

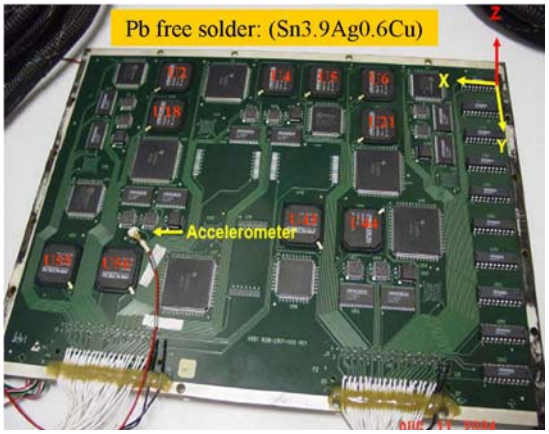

Figure 2: Test vehicle [1]

The test vehicles included both near-eutectic Sn3.9Ag0.6Cu (SAC) and eutectic Sn37Pb assemblies. Figure 2 shows the SAC board in card-guides. There are several kinds of components assembled on the test board, including BGA, TQFP, CLCC, CSP, TSOP and so on. The focus of this study is on the 10 BGA225s.

The test boards were loaded in the out-of-plane direction. The excitation level shown in Figure 3 was increased from 10Grms to 20Grms in increments of 2Grms. A final 28Grms excitation was applied to fail more components. The test lasted for one hour at each excitation level.

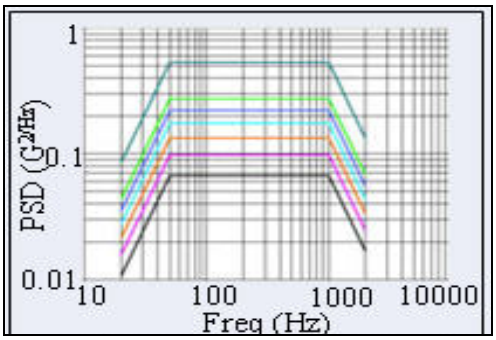

Figure 3: Excitation PSDs used for random, step-stress vibration durability test [1]

The test matrix is listed in Table 1. On the 10 SAC PWAs, only half of the BGA225s use pure SAC interconnects. The remaining use mixed solder systems with SAC ball and SnPb paste. The mixed-solder interconnects are not our focus in this study.

Table 1: Test matrix

Solder	PWB Finish	Number of components in one test board	Number of test board
SAC	SAC	5	5
SnPb	SnPb	10	5

PWB STRAIN CHARACTERIZATION

A strain gage attached between components U4 and U5, on the back side of the test board, was used to characterize the PCB flexure at that location, as shown in Figure 4. The locations of the 10 BGA225s are also included in this figure. The PCB response at this location was recorded for each excitation level shown in Figure 3.

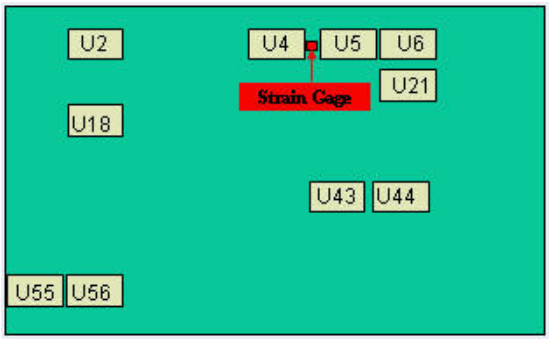

Figure 4: Strain gage and BGA component locations

A global FEA model of the PCB was used to extrapolate the strain gage readings to other locations of interest on the PCB. The global FEA will be described in the next section.

GLOBAL FINITE ELEMENT ANALYSIS OF PCB

The test vehicle is modeled as a uniform plate, as shown in Figure 5. The dimensions of the test PCB are 324 by 228 mm and the thickness is 2.28 mm. The board is meshed with 1178 shell elements. The PCB material is assumed to behave in a linear, isotropic elastic manner, with a Young's modulus of 17.7 Gpa, Poisson's ratio of 0.39, and dynamic damping factor of 0.03. The card-guide boundary conditions applied to the circuit card assembly along the two short edges consist of simple translational support in the out-of-plane (z) direction and rotational springs about the y axis. The stiffness of the rotational spring is calibrated to be 9N-m/Rad by matching the first natural frequency with experimental measurements.

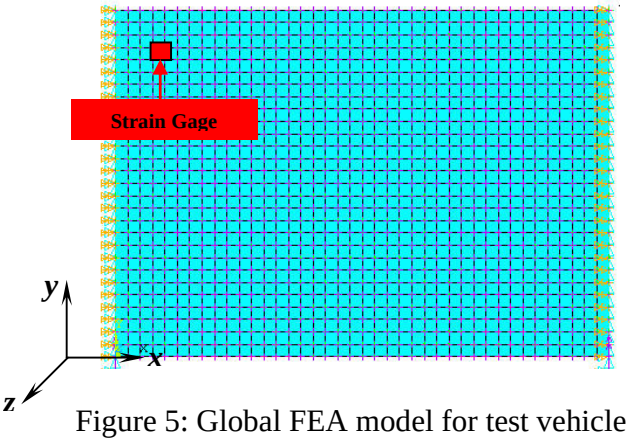

Figure 5: Global FEA model for test vehicle

The measured and predicted modal frequencies and mode shapes in the 20-2000 Hz range are compared in Figure 6. The simulation results have a good agreement with the measured results for the dominant modes.

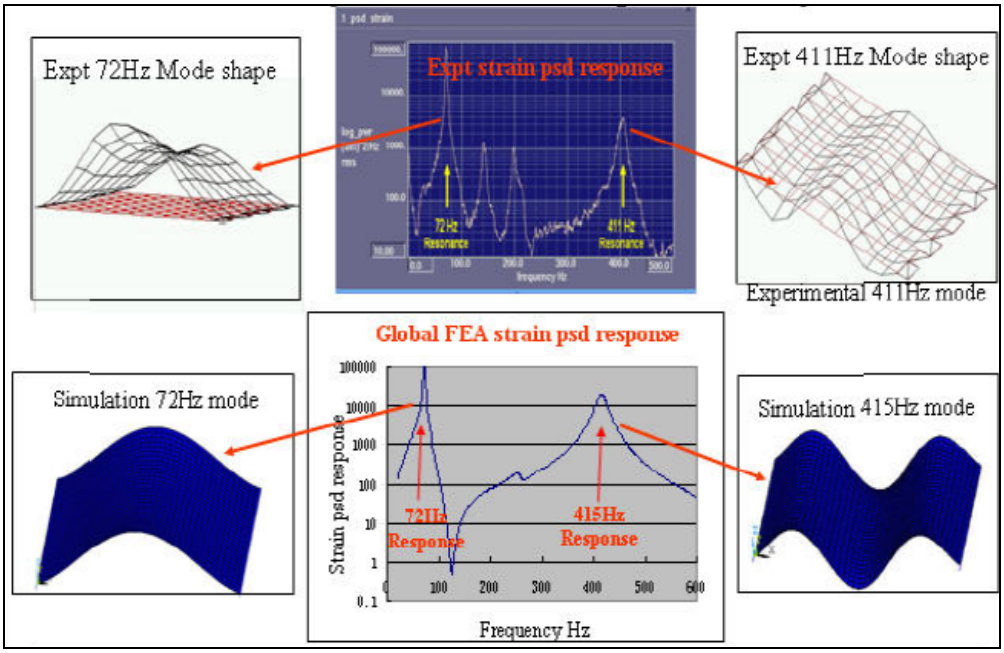

Figure 6: Experimental and simulation modal analysis results for the test vehicle

The first mode shape, which dominates in the response, produces flexural strains predominantly in the x direction, as shown in Figure 6. Clearly, BGAs along the short edges and along the

center of the PCB experience the highest flexural curvatures, and are hence at greatest risk of vibration fatigue.

The loading applied to the test vehicle is shown in Figure 3. The output of this global FEA is the corresponding strain response everywhere on the PCB. Figure 7 shows the contour plot of the 1-sigma value of the strain variable ε_{xx} obtained from the random vibration PSD analysis. This 1-sigma response is based on the assumption of a Gaussian response to the broad-band excitation, and contains contributions from modes 1-5. However, mode 1 provides the dominant contribution.

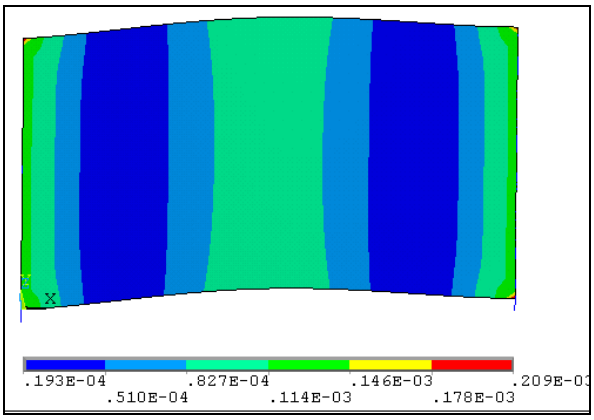

Figure 7: Contour plot for 1-sigma strain ε_{xx} under 10Grms excitation

From the FEA results, the strain scaling factors at the location of each BGA component can be obtained. The strain scaling factors are defined as the ratio of the strain ε_{xx} on the PCB near each component, to the strain ε_{xx} on the PCB at the site of the strain gage. The PCB strain scaling factor (SSF_{PCB}) results are listed in Table 2. With these strain scaling factors, the measured strain from the strain gage can be extrapolated to the site of all components on the entire PCB. As expected, component U55 experiences the maximum flexure among all the BGAs because it is closest to the clamped edge.

Table 2: PCB strain scaling factor for BGA components

U55	U4	U5	U43	U6	U44	U21	U56	U2	U18
1.03	1.0	0.99	0.88	0.70	0.69	0.65	0.32	0.30	0.28

LOCAL FINITE ELEMENT ANALYSIS OF BGA225

The purpose of the local finite element analysis is to estimate the strain transfer function between local PCB flexural strain and the equivalent strain at the critical location in the critical solder joint. Figure 8 shows the detailed FEA model for the BGA225 component. Only half of the component is modeled because of symmetry. This is a 2D model with quadrant 2D plant element.

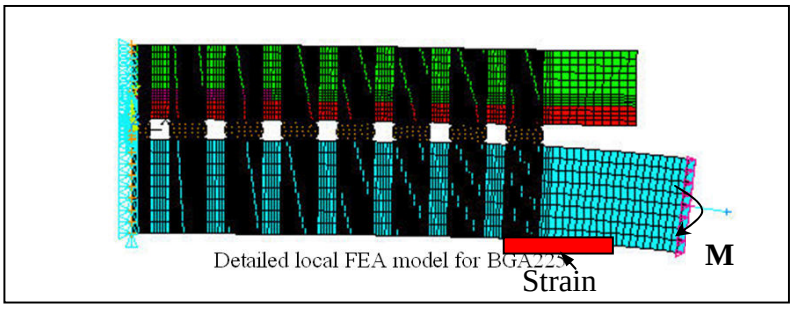

Figure 8: Detailed local FEA model for BGA225 component

Solders are modeled as elastic-plastic materials with power-law hardening [17]. All other materials are modeled as linear elastic. A bending moment is applied at the edge of the PCB and the resulting deformed shape is also shown in Figure 8. The PCB strain was monitored at the nodes along the bottom of the PCB. As shown in Figure 8, the strain gage was attached at the bottom of the PCB, adjacent to the component foot-print, where the PCB curvature is highest. The PCB strain was then averaged over the area covered by the strain gage.

From the simulation results, the outer most solder joint was found to be the most critical one. In this study, the maximum solder strains were averaged over a local neighborhood, that is 2% of

the total solder joint area, as shown in Figure 9. The resulting strain transfer functions for both SAC and SnPb solders were obtained from this detailed local FEA, as shown in Figure 10.

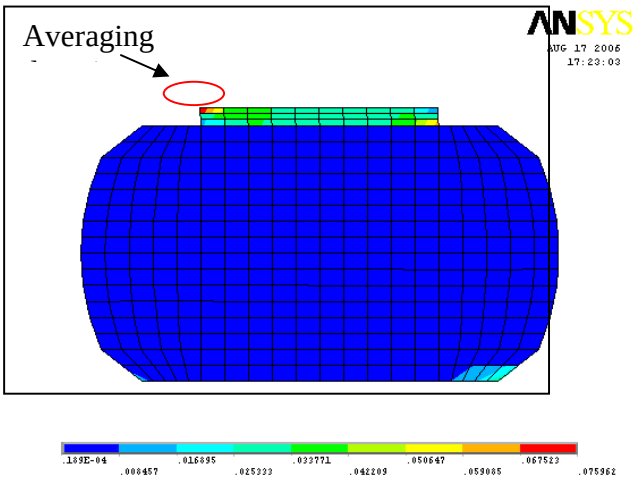

Figure 9: Solder joint mesh and domain for averaging the critical strain value

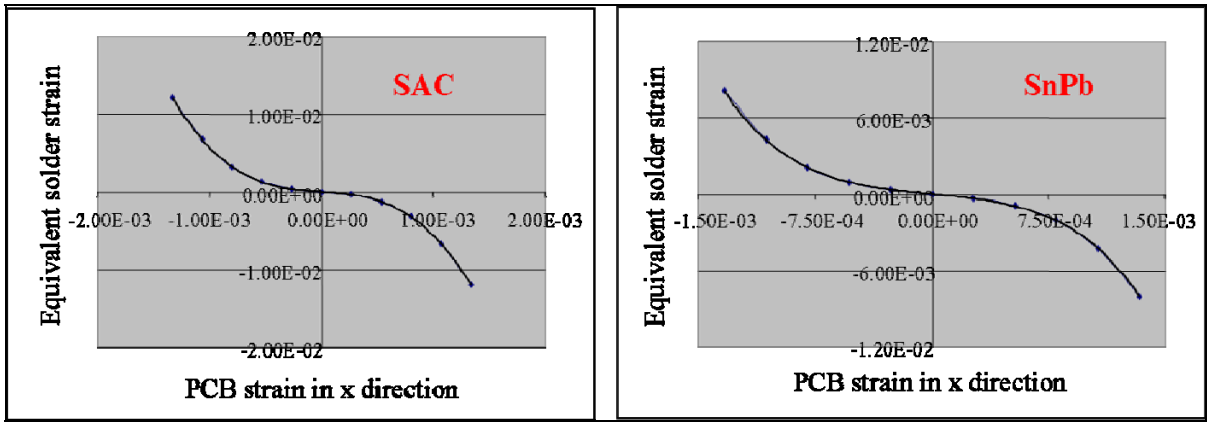

Figure 10: Strain transfer function in BGA225 for both SAC and SnPb from local FEA

The strain history at critical solder joints for each component can be estimated with the help of global FEA, local FEA and measured PCB strain history. The strain history was collected for unit time (1 second in this study). The results were averaged over many such time history records.

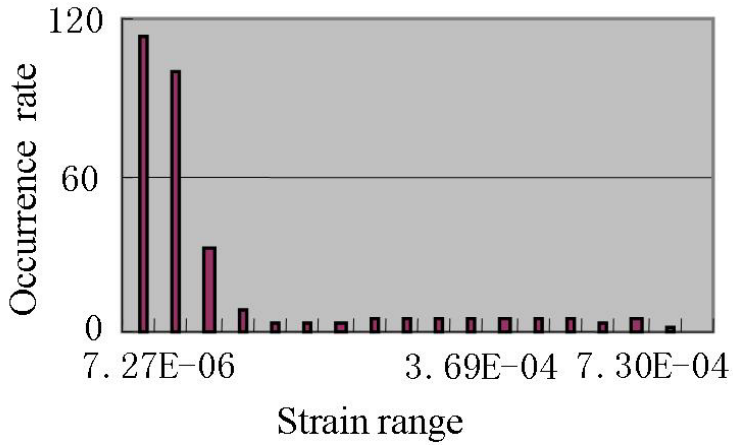

Figure 11: A typical range distribution function (RDF) for solder maximum strain

Finally rain-flow cycle counting technique [4] has been used to obtain the strain range distribution functions (RDFs) for each component, under different excitation levels. A typical strain range distribution functions is presented in Figure 11. Most of the vibration damage accumulates from the few events with the largest strain ranges, shown in the RDF.

ESTIMATION OF EXPONENT *b*

The damage ratio between selected BGA components is used to estimate the exponent *b* of the durability model, presented in Equation 1. The component is assumed to fail when the accumulated damage index approaches 1. The time to failure for each component is shown in Equation 2, where *j* is the number of the step stress level from 10Grms to 28Grms, as shown in Figure 3.

$$t_{total} = \sum_{j=1}^{7} t_j \tag{2}$$

The procedure to calculate damage rate for the averaged solder strain history is shown in Table 3. The number of cycles to failure for each strain range is calculated with the empirical durability model shown in Equation 1.

Table 3: Procedure to estimate damage

Strain range	Number of cycle	Number of cycles to failure	Damage
$\Delta\varepsilon_1$	n_1	$N_1 = A(\Delta\varepsilon_1)^b$	$D_1 = n_1/N_1$
$\Delta\varepsilon_2$	n_2	$N_2 = A(\Delta\varepsilon_2)^b$	$D_2 = n_2/N_2$
⋮	⋮	⋮	⋮
$\Delta\varepsilon_n$	n_n	$N_n = A(\Delta\varepsilon_n)^b$	$D_n = n_n/N_n$

The damage accumulated in one second is calculated in Equation 3.

$$D = \sum_{i=1}^{n} D_i = \sum_{i=1}^{n} \frac{n_i}{A(\Delta\varepsilon_i)^b} \tag{3}$$

The damage accumulated at each excitation level is calculated as the multiplication of damage rate and time spent at this excitation level, as shown in Equation 4.

$$D_j = t_j \cdot \sum_{i=1}^{n} D_i = t_j \cdot \sum_{i=1}^{n} \frac{n_i}{A(\Delta\varepsilon_i)^b} \tag{4}$$

Finally the totally damage accumulated over all the excitation levels for each component are obtained as the summation of the damage at each excitation level, as shown in Equation 5.

$$D = \sum_{j=1}^{7} D_j = \frac{1}{A} \sum_{j=1}^{7} t_j \sum_{i=1}^{n} \frac{n_{ij}}{(\Delta\varepsilon_{ij})^b} \tag{5}$$

The ratio of damage between two components, scales as shown in Equation 6. It's important to note that coefficient A does not affect the damage ratio as it cancels out. One of the components (U4 in this study, because of its proximity to the strain gage) is chosen as the reference component, for estimating the damage ratios. For example, the damage ratio for component U5 (DR_{U5}) is defined as Equation 6.

$$DR_{U5} = \frac{D_{U5}}{D_{ref}} = \frac{\left[\frac{1}{A}\sum_{j=1}^{7} t_j \sum_{i=1}^{n} \frac{n_{ij}}{\left(\Delta\varepsilon_{ij}\right)^b}\right]_{U5}}{\left[\frac{1}{A}\sum_{j=1}^{7} t_j \sum_{i=1}^{n} \frac{n_{ij}}{\left(\Delta\varepsilon_{ij}\right)^b}\right]_{Uref}} = f(b) \tag{6}$$

In the ideal case, the damage ratio for each component should also approach to 1. However, there is some experimental scatter. The resulting residual for each damage ratio is specified in Equation 7.

$$\left(residual\right)_{DR_{Ui}} = 1 - DR_{Ui} \tag{7}$$

The square of this residue is minimized, to obtain the best value of *b* that provides a least-square fit to the test data. This minimization is shown in Equation 8.

$$Min\left(\sum_{i=1}^{k} residual_{DR_{Ui}}^2\right) = Min\left(\sum_{i=1}^{k}\left(1 - DR_{Ui}\right)^2\right) = Min\left(f(b)\right) \tag{8}$$

A Matlab code was developed to solve the problem shown in Equation 8. The results for the exponent *b* for both SAC/SAC and SnPb/SnPb solders were obtained and the values are listed in Table 4.

Table 4: Exponent *b* for SAC and SnPb solders

Solder/Finish	*b*
SnPb/SnPb	-2.43
SAC/SAC	-1.85

ESTIMATION OF COEFFICIENT *A*

After the estimation of exponent *b*, the coefficient *A* can be calculated similarly, by least square fit to the damage index of each component. The residual for the damage, shown in Equation 5 for component U_k, is expressed in Equation 9.

$$residual_{Uk} = 1 - D_{Uk} = 1 - \left(\sum_{j=1}^{7} t_j \sum_{i=1}^{n} \frac{n_{ij}}{A(\Delta\varepsilon_{ij})^b} \right)_{Uk} = f(A) \quad (9)$$

Similarly, the least-square fit algorithm is used to minimize the residual shown in Equation 10.

$$Min\left(\sum resudial_{D_{Uk}}{}^2\right) = Min\left(\sum (1 - D_{Uk})^2\right) = Min(f(A)) \quad (10)$$

The coefficient results for both SnPb and SAC solders are listed in Table 5.

Table 5: Coefficient *A* for SAC and SnPb solders

Solder/finish	*A*
SnPb/SnPb	0.031
SAC/SAC	0.45

Using these coefficients, the S-N fatigue curves for both SAC and SnPb solders are plotted in Figure 12 in the range of the vibration test.

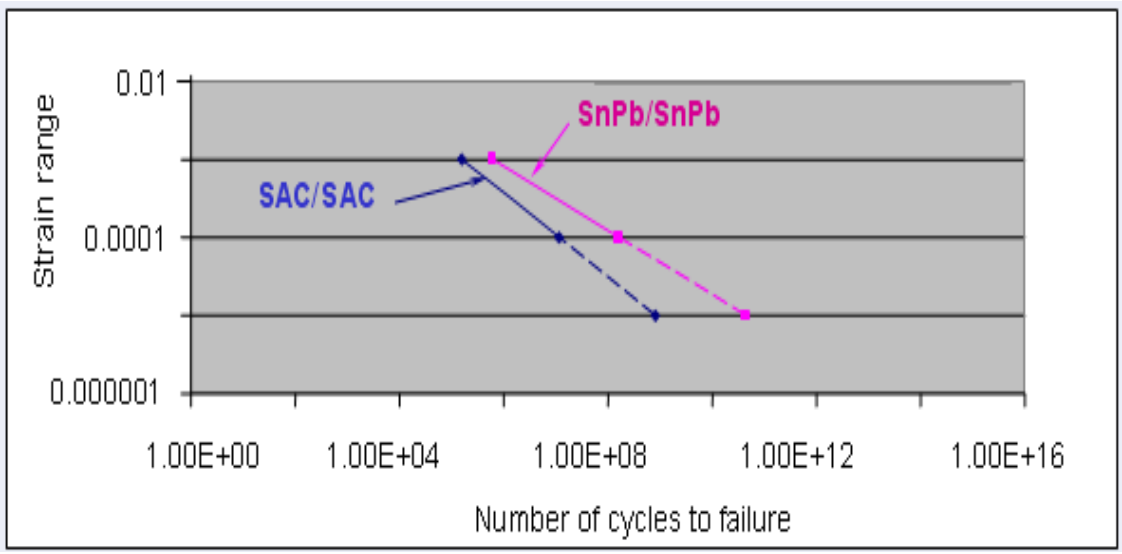

Figure 12: S-N curves for SAC and SnPb solders

The plot shows that SnPb solder outperforms SAC solder in the vibration loading which is opposite of most thermal cycling results for BGAs [18]. On the other hand, the SAC fatigue

curve is steeper than that of SnPb solder, which agrees with the thermal cycling results reported in literature 18.

”GOODNESS” OF MODEL FIT:

The obtained empirical durability model is used to estimate the durability of each component. The estimation is compared with experimental results to check the “goodness” of the fit. Figure 13 shows the comparison for SnPb solder and Figure 14 for SAC solder. The comparison shows that the model estimated life has good agreement with experimental durability, except for components U56, U2 and U18 for SnPb solder. Figure 2 shows that mode 1 does not produce much flexure at the site of these three components. The possible reason for the disagreement could be that the fatigue damage here is dominated by contributions from higher modes. The higher mode has a much higher natural frequency which is not captured in the current analysis.

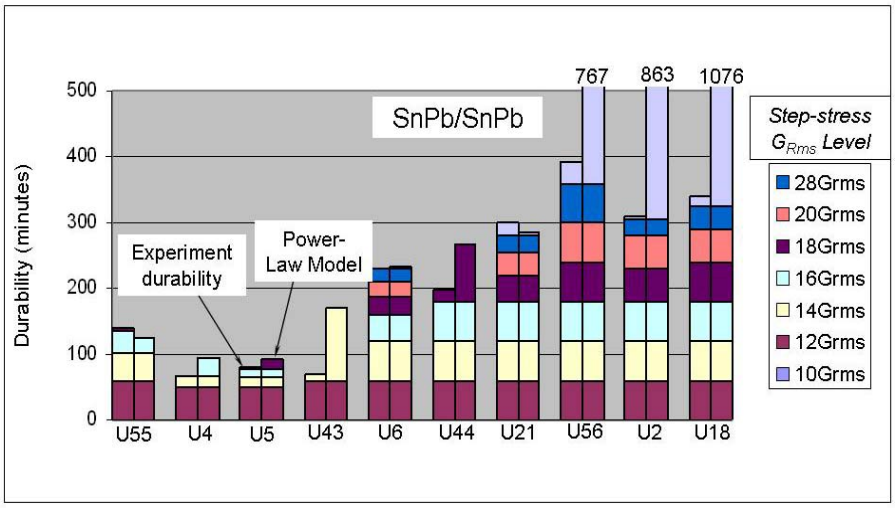

Figure 13: Durability comparison between experiment results and model estimation for SnPb solder

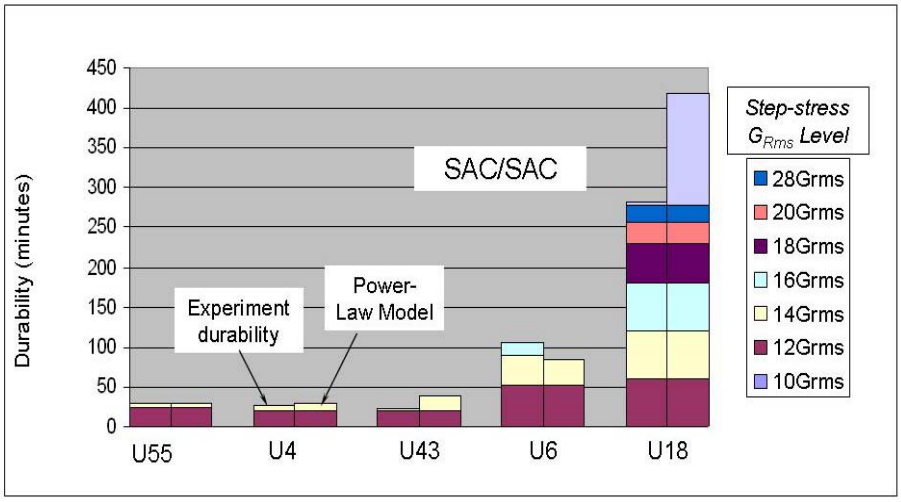

Figure 14: Durability comparison between experiment results and model estimation for SAC solder

SUMMARY AND FUTURE WORK

In this study, an approach to post-process the step-stress durability test data is provided. An empirical durability model is obtained based on the test results for both SAC and SnPb solder. The goodness of this empirical durability model is verified with the experiment results. The major conclusions from this study are summarized as follows:

1. The durability model obtained from the least-square fit algorithm is found to fit the test date reasonably well, except for 3 BGAs with the lowest strain scaling factors (U2, U18 and U56), which are located near the point of inflection for the dominant first mode of the PCB.
2. The study shows that SnPb solder is more durable then SAC solder in the test range of this study. This observation is opposite of the thermal cycling durability results for BGAs.
3. The slope of the SAC S-N curve is sleeper than that of SnPb solder, which implies a smaller acceleration factors in the test range.

To improve the accuracy of the least-square fitting, a weighted least-square fitting algorithm will be used to obtain the slope and coefficient of the durability model. In addition, constant amplitude durability tests will be conducted to improve the confidence of the power-law durability model. These constant level durability test results will be used to generate the model constants for a generalized strain-life durability model.

ACKNOWLEDGEMENT

This work is sponsored by the members of the CALCE Electronic Products and Systems Consortium at the University of Maryland, College Park. We greatly acknowledge help from Dr. A. Woodrow of Boeing Company, for providing detailed experimental results [1].

REFERENCE

1. T. Woodrow, “JCAA/JG-PP No-Lead Solder Project: Vibration Test”, Boeing Electronics Materials and Processes Report, 2005
2. K Upadhyayula, A Dasgupta, “Guidelines for Physics-of-Failure Based Accelerated Stress Test”, Reliability and Maintainability Symposium, pp 345-357, 1998
3. Q Zhang, A Dasgupta, P Haswell, “Isothermal Mechanical Durability of Three Selected Pb-Free Solders: Sn3.9Ag0.6Cu, Sn3.5Ag and Sn0.7Cu”, Transctions of the ASME, vol. 127, pp 512-522, 2005
4. N. E. Dowling, “Mechanical Behavior of Material: Engineering Methods for Deformation, Fracture, and Fatigue” Prentice-Hall,1999
5. J. Hwang, “Overview of Lead-free Solders for Electronics and Microeletronics”, Surface Mount Int., Edina, MN, USA, pp 405-421, 1994
6. Directive on Waste of Electronic Equipment (WEEE), 2001
7. J. Lau, K. Gratalo, and E. Schneider, “Solder Joint Reliability of Large Plastic Ball Grid

Aray Assemblies under Bending, Twisting, and Vibration Conditions", Circuit World, Vol. 22, pp. 27-32, 1995

8. K. Darbha, S. Ling, and A. Dasgupta, "Stress Analysis of Surface-Mount Interconnections Due to Vibration Loading", Journal of Electronic Packaging, Vol. 119, pp. 183-188, 1997
9. D. B. Barker, A. Dasgupta and M. G. Pecht, "PWB solder joint life calculation under thermal and vibration loading", Proceedings Annual Reliability and Maintainability Symposium, pp. 451-459, 1991
10. D. B. Barker, Y. S. Chen, and A. Dasgupta, "Estimating the vibration fatigue life of quad leaded surface mount components", Journal of Electronics packaging, vol. 115, pp. 195-200, 1993
11. S. Liguore, S. Fields, D. Followell, and R. Perez, "Vibration fatigue of leadless chip carrier solder joints", ASMe paper 92-WA/EEP-25, 1992
12. J. Lau et al., "Solder joint reliability of surface mount connectors", Journal of Electronic Packaging, Vol. 115, pp. 180-188, 1993
13. J. Lau, "Solder joint reliability of flip chip and plastic ball grid array assemblies under thermal, mechanical and vibration conditions", IEEE Transactions on Components, Packaging, and Manufacturing Technology, Vol, 19, pp. 728-735, 1996
14. J. Lau, E. Schneider, and T. Baker, "Shock and vibration of solder bumped flip chip on organic coated copper boards", Journal of Electronics Packaging, Vol. 118, pp. 101-104, 1996
15. Q. J. Yang, Z. P. Wang, G. H. Lim, John H. L. Pang, F. F. Yap and R. M. Lin, "Reliability of PBGA Assemblies Under Out-of Plane Vibration Excitation", IEEE Transactions on Components and Packaging Technologies, Vol. 25, pp. 293-300, 2002

16. F. X. Che, H. L. J. Pang, F. L. Wong, G. H. Lim and T. H. Low, “Vibration Fatigue Test and Analysis for Flip Chip Solder Joints”, Electronics Packaging Technology Conference, pp. 107-113, 2003
17. R. Darveaux and K. Banerji “Constitutive Relations for Tin-Based Solder Joint”, IEEE Transaction on components, Hybrid and Manufacturing Technology, vol. 15, No. 6, pp 1013-1023, 1992
18. Q. Zhang, A. Dasgupta, D. Nelson, H. Pallavicini, “Systematic Study on Thermo-Mechanical Durability of Pb-Free Assemblies: Experiments and FE Analysis”, Journal of Electronic Packaging, Vol. 127, pp. 415-429, 2005

Appendix B: List of All Durability Test Results

In this section, all the durability test data will be listed, including harmonic and step-stress random vibration durability data.

Harmonic Durability Test Results

The harmonic durability test conducted will be summarized in this section. Four test boards, two SAC and two SnPb boards, have been tested. The excitation level was varied from 9G to 12G with increasing interval of 1.5G.

Table 1: SAC305 harmonic durability test results

Excitation	9G	10.5G	12G
Center LCR 1210 (cycle)	5.73E+07		8.07E+06
Edge LCR 1210 (cycle)	2.92E+08		2.16E+07
Center LCR 2512 (cycle)	1.37E+07	2.22E+06	
Edge LCR2512 (cycle)	4.53E+07	5.04E+06	

Table 2: SnPb harmonic durability test results

Excitation	10.5G	12G
Center LCR 1210 (cycle)	3.00E+08	2.59E+07
Edge LCR 1210 (cycle)		4.26E+07
Center LCR 2512 (cycle)	1.78E+07	1.58E+06
Edge LCR2512 (cycle)		2.50E+07

Random vibration durability test results conducted in CALCE

For the random vibration conducted on campus. Step-stressed excitation was utilized to fail more test components on the board. The test frequency range was from 10Hz to 500Hz. The PSD level

increased from $0.1G^2/Hz$ to $0.4G^2/Hz$ with 0.1 increment interval each time. The durability results for SAC and SnPb at each excitation level are listed in following table 8 & 9.

Table 3: SAC random durability test results

Excitation (G^2/Hz)	0.1	0.2	0.3	0.4
Center LCR2512 (min)	47			
	64			
Edge LCR2512 (min)	91			
	134			
Center LCR1210 (min)	830	124		
	830	525		
Edge LCR1210 (min)	830	657		
	830	827	860	14

Table 4: SnPb random durability test results

Excitation (G^2/Hz)	0.1	0.2	0.3	0.4
Center LCR2512 (min)	379			
	254			
Edge LCR2512 (min)	683			
	746			
Center LCR1210 (min)	830	163		
	830	304		
Edge LCR1210 (min)	830	827	104	
	830	827	89	

Random vibration durability test results conducted in third lab

The layout for the durability test conducted in the third lab is shown in Figure 15, including the solder and PCB material.

	(QUADRANT TWO)				(QUADRANT THREE)			
	S/N	Dummy	10		S/N	SAC-ImSn-Fr4	11	
	S/N	Dummy	9		S/N	SAC-ImSn-Fr4	12	
	S/N	Dummy	8		S/N	Dummy	13	
	S/N	Dummy	7		S/N	Dummy	14	
	S/N	Dummy	6		S/N	Dummy	15	
	S/N	Dummy	5		S/N	Dummy	16	
	S/N	SAC-ImSn-Fr4	4		S/N	Dummy	17	
	S/N	SAC-ImSn-Fr4	3		S/N	Dummy	18	
	S/N	SnPb-Fr4	2		S/N	Dummy	19	
	S/N	SnPb-Fr4	1		S/N	Dummy	20	
	(QUADRANT ONE)				(QUADRANT FOUR)			

Figure 15: Board layout on the fixture for the room temp random durability test

The durability results for board 1, 2, 3, 4, 11 and 12 will be listed in this section.

Table 5: Durability test results for SnPb Fr4 board at location 1

SnPb-Fr4 board at location 1							
channel	component	0.02 (G^2/Hz)	0.05 (G^2/Hz)	0.1 (G^2/Hz)	0.2 (G^2/Hz)	0.2 (G^2/Hz)	0.2 (G^2/Hz)
227	N5	360	24				
307	R1NET4	360	18				
221	R1	360	360	227			
223	P1	360	360	100			
224	N8	360	360	195			
228	N4	360	360	148			
229	N3	360	360	300			
305	R1NET2	360	360	280			
310	R1NET7	360	360	20			
311	R1NET8	360	360	42			
102	F2	360	360	360	216		

120	A8	360	360	360	29		
121	C1	360	360	360	31		
126	RNET1	360	360	360	211		
130	RNET5	360	360	360	345		
139	I4	360	360	360	291		
203	K4	360	360	360	36		
204	K1	360	360	360	357		
222	R2	360	360	360	360		
226	N6	360	360	360	83		
230	N2	360	360	360	145		
231	N1	360	360	360	176		
101	F1	360	360	360	360	173	
103	F3	360	360	360	360	178	
104	F4	360	360	360	360	178	
105	D1	360	360	360	360	176	
106	D2	360	360	360	360	193	
107	D3	360	360	360	360	180	
108	D4	360	360	360	360	178	
109	B1	360	360	360	360	179	
110	B2	360	360	360	360	178	
111	B3	360	360	360	360	178	
112	B4	360	360	360	360	178	
113	A1	360	360	360	360	178	
114	A2	360	360	360	360	127	
115	A3	360	360	360	360	125	
116	A4	360	360	360	360	128	
117	A5	360	360	360	360	33	
118	A6	360	360	360	360	31	
119	A7	360	360	360	360	172	
122	E3	360	360	360	360	178	
123	E4	360	360	360	360	178	
124	E1	360	360	360	360	179	
125	E2	360	360	360	360	178	
127	RNET2	360	360	360	360	177	
128	RNET3	360	360	360	360	177	
129	RNET4	360	360	360	360	181	
201	I2	360	360	360	360	82	
202	K3	360	360	360	360	89	
205	K2	360	360	360	360	84	
206	L5	360	360	360	360	82	
207	L6	360	360	360	360	84	
208	L7	360	360	360	360	87	
209	L8	360	360	360	360	83	
210	L1	360	360	360	360	83	
211	L2	360	360	360	360	83	
212	L3	360	360	360	360	83	
213	L4	360	360	360	360	79	
214	J1	360	360	360	360	86	

215	H1	360	360	360	360	83	
216	H2	360	360	360	360	78	
217	H3	360	360	360	360	81	
218	H4	360	360	360	360	87	
219	R3	360	360	360	360	21	
220	R4	360	360	360	360	81	
225	N7	360	360	360	360	78	
232	M1	360	360	360	360	85	
233	M2	360	360	360	360	88	
234	M3	360	360	360	360	81	
235	M4	360	360	360	360	81	
236	O1	360	360	360	360	84	
237	O2	360	360	360	360	84	
238	O3	360	360	360	360	81	
239	O4	360	360	360	360	88	
240	Q1	360	360	360	360	85	
301	Q2	360	360	360	360	82	
302	Q3	360	360	360	360	84	
303	Q4	360	360	360	360	81	
304	R1NET1	360	360	360	360	81	
306	R1NET3	360	360	360	360	80	
308	R1NET5	360	360	360	360	83	
309	R1NET6	360	360	360	360	84	
312	S1	360	360	360	360	84	
313	S2	360	360	360	360	15	
314	S3	360	360	360	360	85	
315	S4	360	360	360	360	82	
316	U1	360	360	360	360	81	
317	W8	360	360	360	360	89	
318	W7	360	360	360	360	88	
319	W6	360	360	360	360	88	
320	W5	360	360	360	360	82	
321	W4	360	360	360	360	85	
322	W3	360	360	360	360	84	
323	W2	360	360	360	360	83	
324	W1	360	360	360	360	81	
325	X3	360	360	360	360	79	
326	X4	360	360	360	360	79	
327	X1	360	360	360	360	86	
328	X2	360	360	360	360	86	
329	V3	360	360	360	360	79	
330	V4	360	360	360	360	78	
331	V1	360	360	360	360	84	
332	V2	360	360	360	360	84	
333	T3	360	360	360	360	84	
334	T4	360	360	360	360	85	
335	T1	360	360	360	360	85	
336	T2	360	360	360	360	85	

131	RNET6	360	360	360	360	360	206
132	RNET7	360	360	360	360	360	201
133	RNET8	360	360	360	360	360	206

Table 6: Durability test results for SnPb Fr4 board at location 2

SnPb-Fr4 board at location 2							
channel	component	0.02 (G^2/Hz)	0.05 (G^2/Hz)	0.1 (G^2/Hz)	0.2 (G^2/Hz)	0.2 (G^2/Hz)	0.2 (G^2/Hz)
121	C1	360	205				
223	P1	360	241				
227	N5	360	117				
228	N4	360	40				
115	A3	360	360	114			
116	A4	360	360	264			
117	A5	360	360	115			
118	A6	360	360	114			
310	R1NET7	360	360	125			
311	R1NET8	360	360	125			
113	A1	360	360	360	64		
120	A8	360	360	360	120		
126	RNET1	360	360	360	310		
127	RNET2	360	360	360	309		
128	RNET3	360	360	360	87		
129	RNET4	360	360	360	82		
130	RNET5	360	360	360	82		
131	RNET6	360	360	360	226		
132	RNET7	360	360	360	226		
133	RNET8	360	360	360	234		
134	G3	360	360	360	278		
136	G1	360	360	360	323		
210	L1	360	360	360	80		
220	R4	360	360	360	317		
221	R1	360	360	360	261		
225	N7	360	360	360	261		
226	N6	360	360	360	204		
229	N3	360	360	360	141		
336	T2	360	360	360	199		
101	F1	360	360	360	360	160	
102	F2	360	360	360	360	160	
103	F3	360	360	360	360	159	
104	F4	360	360	360	360	161	
105	D1	360	360	360	360	158	
106	D2	360	360	360	360	158	
107	D3	360	360	360	360	158	

108	D4	360	360	360	360	160	
109	B1	360	360	360	360	158	
110	B2	360	360	360	360	159	
111	B3	360	360	360	360	158	
112	B4	360	360	360	360	158	
114	A2	360	360	360	360	159	
119	A7	360	360	360	360	161	
122	E3	360	360	360	360	158	
123	E4	360	360	360	360	138	
124	E1	360	360	360	360	138	
125	E2	360	360	360	360	158	
135	G4	360	360	360	360	155	
219	R3	360	360	360	360	31	
224	N8	360	360	360	360	199	
230	N2	360	360	360	360	71	
231	N1	360	360	360	360	191	
235	M4	360	360	360	360	1	
236	O1	360	360	360	360	1	
308	R1NET5	360	360	360	360	153	
309	R1NET6	360	360	360	360	157	
333	T3	360	360	360	360	18	
201	I2	360	360	360	360	360	38
202	K3	360	360	360	360	360	37
203	K4	360	360	360	360	360	37
204	K1	360	360	360	360	360	37
205	K2	360	360	360	360	360	36
206	L5	360	360	360	360	360	35
207	L6	360	360	360	360	360	35
208	L7	360	360	360	360	360	35
209	L8	360	360	360	360	360	38
211	L2	360	360	360	360	360	36
212	L3	360	360	360	360	360	37
213	L4	360	360	360	360	360	37
214	J1	360	360	360	360	360	35
215	H1	360	360	360	360	360	44
216	H2	360	360	360	360	360	37
217	H3	360	360	360	360	360	37
218	H4	360	360	360	360	360	37
222	R2	360	360	360	360	360	35
232	M1	360	360	360	360	360	38
233	M2	360	360	360	360	360	36
234	M3	360	360	360	360	360	38
237	O2	360	360	360	360	360	36
238	O3	360	360	360	360	360	36
239	O4	360	360	360	360	360	36
240	Q1	360	360	360	360	360	37

301	Q2	360	360	360	360	360	37
302	Q3	360	360	360	360	360	37
303	Q4	360	360	360	360	360	37
304	R1NET1	360	360	360	360	360	38
305	R1NET2	360	360	360	360	360	39
306	R1NET3	360	360	360	360	360	35
307	R1NET4	360	360	360	360	360	37
312	S1	360	360	360	360	360	35
313	S2	360	360	360	360	360	36
314	S3	360	360	360	360	360	36
315	S4	360	360	360	360	360	38
316	U1	360	360	360	360	360	38
317	W8	360	360	360	360	360	37
318	W7	360	360	360	360	360	37
319	W6	360	360	360	360	360	38
320	W5	360	360	360	360	360	38
321	W4	360	360	360	360	360	36
322	W3	360	360	360	360	360	37
323	W2	360	360	360	360	360	38
324	W1	360	360	360	360	360	45
325	X3	360	360	360	360	360	38
326	X4	360	360	360	360	360	36
327	X1	360	360	360	360	360	37
328	X2	360	360	360	360	360	37
329	V3	360	360	360	360	360	36
330	V4	360	360	360	360	360	38
331	V1	360	360	360	360	360	38
332	V2	360	360	360	360	360	37
334	T4	360	360	360	360	360	36

Table 7: Durability test results for SAC-ImSn-Fr4 board at location 3 (the date for this board was missing after 0.2

SAC-ImSn-Fr4 board at location 3							
channel	component	0.02 (G^2/Hz)	0.05 (G^2/Hz)	0.1 (G^2/Hz)	0.2 (G^2/Hz)	0.2 (G^2/Hz)	0.2 (G^2/Hz)
332	V2	322					
305	R1NET2	360	74				
310	R1NET7	360	118				
223	P1	360	360	121			
227	N5	360	360	14			
304	R1NET1	360	360	0			
311	R1NET8	360	360	9			
316	U1	360	360	352			

Table 8: Durability test results for SAC-ImSn-Fr4 board at location 4 (the date for this board was missing after 0.2

SAC-ImSn-Fr4 board at location 3							
channel	component	0.02psd	0.05psd	0.1psd	0.2psd	0.2psd	0.2psd
228	N4	52					
305	R1NET2	173					
310	R1NET7	281					
223	P1	360	41				
227	N5	360	64				
304	R1NET1	360	34				
311	R1NET8	360	80				
316	U1	360	235				
120	A8	360	360	65			

Table 9: Durability test results for SAC-ImSn-Fr4 board at location 11

SAC-ImSn-Fr4 board at location 11							
channel	component	0.02psd	0.05psd	0.1psd	0.2psd	0.2psd	0.2psd
135	G4	360	315				
116	A4	360	360	351			
117	A5	360	360	243			
137	G2	360	360	84			
203	K4	360	360	56			
305	R1NET2	360	360	257			
113	A1	360	360	360	377		
120	A8	360	360	360	25		
123	E4	360	360	360	4		
139	I4	360	360	360	34		
202	K3	360	360	360	29		
204	K1	360	360	360	335		
213	L4	360	360	360	360		
224	N8	360	360	360	41		
227	N5	360	360	360	128		
228	N4	360	360	360	360		
304	R1NET1	360	360	360	245		
127	RNET2	360	360	360	360	256	
132	RNET7	360	360	360	360	91	
140	I1	360	360	360	360	138	
201	I2	360	360	360	360	176	
207	L6	360	360	360	360	116	
220	R4	360	360	360	360	41	
122	E3	360	360	360	360	360	43
126	RNET1	360	360	360	360	360	100

133	RNET8	360	360	360	360	360	43
134	G3	360	360	360	360	360	113
136	G1	360	360	360	360	360	38
210	L1	360	360	360	360	360	102
212	L3	360	360	360	360	360	99
229	N3	360	360	360	360	360	42

Table 10: Durability test results for SAC-ImSn-Fr4 board at location 12

SAC-ImSn-Fr4 board at location 12							
channel	component	0.02psd	0.05psd	0.1psd	0.2psd	0.2psd	0.2psd
117	A5	360	35				
135	G4	360	88				
304	R1NET1	360	86				
305	R1NET2	360	87				
310	R1NET7	360	121				
311	R1NET8	360	276				
116	A4	360	360	351			
137	G2	360	360	84			
203	K4	360	360	56			
101	F1	360	360	360	143		
113	A1	360	360	360	7		
118	A6	360	360	360	314		
120	A8	360	360	360	1		
122	E3	360	360	360	109		
126	RNET1	360	360	360	72		
127	RNET2	360	360	360	28		
129	RNET4	360	360	360	290		
134	G3	360	360	360	102		
204	K1	360	360	360	106		
210	L1	360	360	360	64		
227	N5	360	360	360	7		
228	N4	360	360	360	22		
229	N3	360	360	360	283		
307	R1NET4	360	360	360	114		
315	S4	360	360	360	108		
317	W8	360	360	360	296		
319	W6	360	360	360	107		
326	X4	360	360	360	72		
327	X1	360	360	360	104		
331	V1	360	360	360	132		
335	T1	360	360	360	122		
115	A3	360	360	360	360	17	
130	RNET5	360	360	360	360	14	
131	RNET6	360	360	360	360	156	

133	RNET8	360	360	360	360	192	
136	G1	360	360	360	360	224	
208	L7	360	360	360	360	100	
320	W5	360	360	360	360	29	
328	X2	360	360	360	360	243	
330	V4	360	360	360	360	199	
332	V2	360	360	360	360	58	
333	T3	360	360	360	360	30	
334	T4	360	360	360	360	17	
336	T2	360	360	360	360	244	
114	A2	360	360	360	360	360	42
138	I3	360	360	360	360	360	62
224	N8	360	360	360	360	360	259
240	Q1	360	360	360	360	360	84
301	Q2	360	360	360	360	360	179
302	Q3	360	360	360	360	360	717
309	R1NET6	360	360	360	360	360	318
314	S3	360	360	360	360	360	92
318	W7	360	360	360	360	360	120
321	W4	360	360	360	360	360	82
329	V3	360	360	360	360	360	286

Appendix C: ANSYS Input File for Strain Transfer Simulation

```
/prep7
!material number 1--pcb
MP,REFT,1,298
MP,EX,1,19700
MP,EY,1,7709.3
MP,EZ,1,19700
MP,NUXY,1,0.19
MP,NUYZ,1,0.19
MP,NUXZ,1,0.30
MP,GXY,1,6312.4
MP,GYZ,1,6312.4
MP,GXZ,1,3456.2
MPTEMP,,,,,,,,
MPTEMP,1,0
MPDATA,DENS,1,,1.8E-9
!material number 2--cu pad
MP,REFT,2,298
MP,EX,2,1.2875E+5
MP,PRXY,2,0.35
MPTEMP,,,,,,,,
MPTEMP,1,0
MPDATA,DENS,2,,8.9E-9
!material number 3--ceramic
MP,REFT,3,298
MP,EX,3,21334
MP,PRXY,3,0.3
MPTEMP,,,,,,,,
MPTEMP,1,0
MPDATA,DENS,3,,1.9E-9
!material number 7--solder ball
MP,REFT,4,298
MP,EX,4,47500
MP,PRXY,4,0.35
MPTEMP,,,,,,,,
MPTEMP,1,0
MPDATA,DENS,4,,8.4E-9
!power model: power law relationship "Darveaux material properties"
TB,MISO,4,1,21
TBPT,,9.18913E-05,4.365425829
TBPT,,0.000142863,6.016542934
TBPT,,0.000196147,7.305255652
TBPT,,0.001474931,16.90144427
TBPT,,0.003300642,21.84474705
TBPT,,0.006276047,26.52378012
```

```
TBPT,,0.012157192,32.20503813
TBPT,,0.018004055,36.0769131
TBPT,,0.023834896,39.10319255
TBPT,,0.029656166,41.62430739
TBPT,,0.035470975,43.80440333
TBPT,,0.041281085,45.73649401
TBPT,,0.047087601,47.47889636
TBPT,,0.052891266,49.07082071
TBPT,,0.058692605,50.54002111
TBPT,,0.11663274,61.36543508
TBPT,,0.174507552,68.74314073
TBPT,,0.232351836,74.50959736
TBPT,,0.290177882,79.31348265
TBPT,,0.347991616,83.46756981
TBPT,,0.405796396,87.14909271
!define the element type
ET,1,plane183
ET,2,PLANE82
!parameter definition unit: mm
!pcb parameters
pcbh=1.50
!cu pad parameters
padl=0.522              !from the cross section picture
padh=0.04
padll=0.775
!ceramic parameters
ceramicl=3.25-padh      !from vishay website
ceramich=0.5
partw=3.2
!solder parameters
solderh=0.03
!modeling a part of the ceramic
k,1,0,0,0
k,2,ceramicl-padl+padh,0,0
k,3,ceramicl-padl+padh,ceramich,0
k,4,0,ceramich,0
l,1,2
l,2,3
l,3,4
l,4,1
Al,1,2,3,4
!modeling a small part of the pwb
k,5,0,-2*padh-solderh,0
k,6,ceramicl-padl+padh,-2*padh-solderh,0
k,7,0,-2*padh-solderh-pcbh,0
k,8,ceramicl-padl+padh,-2*padh-solderh-pcbh,0
```

```
l,5,6
l,6,8
l,7,8
l,5,7
AL,5,6,7,8
!modeling a small part of the ceramic
k,9,ceramicl,0,0
k,10,ceramicl,ceramich,0
l,2,9
l,9,10
l,3,10
AL,2,9,10,11
!modeling a small part of the pcb
k,11,ceramicl,-2*padh-solderh,0
k,12,ceramicl,-2*padh-solderh-pcbh,0
l,6,11
l,11,12
l,12,8
AL,6,14,12,13
!modeling a small part of the cu pad
k,13,ceramicl-padl+padh,ceramich+padh,0
k,14,ceramicl,ceramich+padh,0
l,10,14
l,14,13
l,3,13
AL,11,15,16,17
!modeling a small part of the cu pad
k,15,ceramicl-padl+padh,-padh,0
k,16,ceramicl,-padh,0
l,9,16
l,16,15
l,15,2
AL,9,18,19,20
!modeling a small part of the cu pad
k,17,ceramicl-padl+padh,-padh-solderh,0
k,18,ceramicl,-padh-solderh,0
l,6,17
l,17,18
l,18,11
AL,12,21,22,23
!modeling a small part of the solder
l,15,17
l,16,18
AL,24,19,25,22
!modeling a small part of the cu pad
k,19,ceramicl+padh,ceramich,0
```

```
k,20,ceramicl+padh,ceramich+padh,0
l,10,19
l,19,20
l,14,20
AL,15,26,27,28
!modeling a small part of the cu pad
k,21,ceramicl+padh,0,0
l,19,21
l,9,21
AL,10,26,29,30
!modeling a small part of the cu pad
k,22,ceramicl+padh,-padh,0
l,21,22
l,22,16
AL,30,31,32,18
!modeling a small part of the solder
k,23,ceramicl+padh,-padh-solderh,0
l,22,23
l,23,18
AL,32,33,34,25
!modeling a small part of the cu pad
k,24,ceramicl+padh,-padh-solderh-padh,0
l,23,24
l,24,11
AL,34,35,36,23
!modeling a small part of the pcb
k,25,ceramicl+padh,-padh-solderh-padh-pcbh,0
l,24,25
l,25,12
AL,36,37,38,13
!modeling a small part of the pcb
k,26,ceramicl+padh+padll,-padh-solderh-padh,0
k,27,ceramicl+padh+padll,-padh-solderh-padh-pcbh,0
l,24,26
l,26,27
l,25,27
AL,37,39,40,41
!modeling a small part of the cu pad
k,28,ceramicl+padh+padll,-padh-solderh,0
l,26,28
l,23,28
AL,35,39,42,43
!modeling a small part of the pcb
!k,29,pcbl-1,-padh-solderh-padh,0
!k,30,pcbl-1,-padh-solderh-padh-pcbh,0
!l,26,29
```

```
!l,29,30
!l,30,27
!AL,40,44,45,46
!modeling the last part of the pcb
!k,31,pcbl,-padh-solderh-padh,0
!k,32,pcbl,-padh-solderh-padh-pcbh,0
!l,29,31
!l,31,32
!l,32,30
!AL,45,47,48,49
!modeling a small part of the solder
k,33,ceramicl+padh+0.7,-padh,0
l,28,33
l,33,22
AL,33,43,44,45
!modeling a small part of the solder
k,34,ceramicl+padh+0.58,0,0
l,33,34
l,21,34
AL,31,45,46,47
!modeling a small part of the solder
k,35,ceramicl+padh+0.35,0.125,0
k,36,ceramicl+padh+0.20,0.25,0
k,37,ceramicl+padh+0.09,0.375,0
BSPLIN,19,37,36,35,34
AL,29,47,48
!*
KEYOPT,1,1,0
KEYOPT,1,3,3
KEYOPT,1,6,0
KEYOPT,1,10,0
!*
!*
KEYOPT,2,1,0
KEYOPT,2,3,2
KEYOPT,2,6,0
KEYOPT,2,10,0
!*
!/////////////////////////meshing the areas
ASEL,S,AREA,,1,,,1          !mesh the ceramic
LESIZE,1,,,8
LESIZE,3,,,8
LESIZE,2,,,6
LESIZE,4,,,6
TYPE,1
R,2,0.02,
```

```
AATT,3,2,1,,
AMESH,1
ASEL,S,AREA,,2,,,1          !mesh the pcb
LESIZE,5,,,8
LESIZE,7,,,8
LESIZE,6,,,6
LESIZE,8,,,6
TYPE,2
AATT,1,,2,,
AMESH,2
ASEL,S,AREA,,3,,,1          !mesh the  ceramic
LESIZE,10,,,6
LESIZE,9,,,4
LESIZE,11,,,4
AATT,3,2,1,,
AMESH,3
ASEL,S,AREA,,4,,,1          ! mesh the pcb
LESIZE,13,,,6
LESIZE,12,,,4
LESIZE,14,,,4
AATT,1,,2,,
AMESH,4
ASEL,S,AREA,,5,,,1          !mesh the cu pad
LESIZE,16,,,4
LESIZE,17,,,1
LESIZE,15,,,1
AATT,2,2,1,,
AMESH,5
ASEL,S,AREA,,6,,,1          !mesh the cu pad
LESIZE,19,,,4
LESIZE,20,,,1
LESIZE,18,,,1
AATT,2,2,1,,
AMESH,6
ASEL,S,AREA,,7,,,1          !mesh the cu pad
LESIZE,22,,,4
LESIZE,21,,,1
LESIZE,23,,,1
AATT,2,2,1,,
AMESH,7
ASEL,S,AREA,,8,,,1          !mesh the solder
LESIZE,24,,,1
LESIZE,25,,,1
AATT,4,2,1,,
AMESH,8
ASEL,S,AREA,,9,,,1          !mesh the cu pad
```

```
LESIZE,27,,,1
LESIZE,28,,,1
LESIZE,26,,,1
AATT,2,2,1,,
AMESH,9
ASEL,S,AREA,,10,,,1      !mesh the cu pad
LESIZE,29,,,6
LESIZE,30,,,1
AATT,2,2,1,,
AMESH,10
ASEL,S,AREA,,11,,,1      !mesh the cu pad
LESIZE,31,,,1
LESIZE,32,,,1
AATT,2,2,1,,
AMESH,11
ASEL,S,AREA,,12,,,1      !mesh the solder
LESIZE,33,,,1
LESIZE,34,,,1
AATT,4,2,1,,
AMESH,12
ASEL,S,AREA,,13,,,1      !mesh the cu pad
LESIZE,35,,,1
LESIZE,36,,,1
AATT,2,2,1,,
AMESH,13
ASEL,S,AREA,,14,,,1      !mesh the pcb
LESIZE,37,,,6
LESIZE,38,,,1
TYPE,2
AATT,1,,2,,
AMESH,14
 ASEL,S,AREA,,15,,,1      !mesh the pcb
LESIZE,40,,,6
LESIZE,39,,,8
LESIZE,41,,,8
AATT,1,,2,,
AMESH,15
ASEL,S,AREA,,16,,,1    !mesh the cu pad
LESIZE,42,,,1
LESIZE,43,,,8
AATT,2,2,1,,
AMESH,16
ASEL,S,AREA,,17,,,1    !mesh the solder
LESIZE,45,,,8
LESIZE,44,,,1
AATT,4,2,1,,
```

```
AMESH,17
ASEL,S,AREA,,18,,,1    !mesh the solder
LESIZE,47,,,8
LESIZE,46,,,1
AATT,4,2,1,,
AMESH,18
ASEL,S,AREA,,19,,,1    !mesh the solder
LESIZE,48,,,10
AATT,4,2,1,,
AMESH,19
ALLSEL,ALL
NUMMRG,ALL
ARSYM,X,ALL, , , ,0,0
ALLSEL,ALL
NUMMRG,ALL
! FORM THE SECOND RESISTOR
pcbmiddle=2.5
pcbright=1.2
pcbleft=66.8-pcbmiddle-8.05
AGEN,2,1,38,1,-pcbmiddle-8.05,0,0,0,0,0
A,86,85,59,60
LESIZE,190,,,10
LESIZE,189,,,10
AATT,1,,2,,
AMESH,77
ALLSEL,ALL
NUMMRG,ALL
! model the left part of the pcb
ALLSEL,ALL
KGEN,2,112, , ,-pcbleft, , , ,0
KGEN,2,111, , ,-pcbleft, , , ,0
A,111,112,116,117
LESIZE,192,,,6
LESIZE,191,,,30
LESIZE,193,,,30
AATT,1,,2,,
AMESH,78
! MODEL THE RIGHT PART OF THE PCB
KGEN,2,26, , ,pcbright, , , ,0
KGEN,2,27, , ,pcbright, , , ,0
A,26,27,119,118
LESIZE,195,,,6
LESIZE,196,,,10
LESIZE,194,,,10
AATT,1,,2,,
AMESH,79
```

```
ALLSEL,ALL
NUMMRG,ALL
! the other symmetry
NWPAVE,    4342
csys,4
ARSYM,X,ALL, , , ,0,0
ALLSEL,ALL
NUMMRG,ALL
!//////////////////////////boundary condition
NSEL,S,NODE,,3808
D,ALL,UY,0
D,all,UX,0
NSEL,S,NODE,,8323
D,ALL,UY,0
ALLSEL,ALL
!NSEL,S,LOC,X,5.225
!DSYM,SYMM,X,
allsel,all
csys,0
ALLSEL,ALL
NUMSTR,NODE,10000
N       ,       10000 ,       -70.825       ,       -1.61   ,       0
N       ,       10001 ,       -70.825       ,       -1.36   ,       0
N       ,       10002 ,       -70.825       ,       -1.11   ,       0
N       ,       10003 ,       -70.825       ,       -0.86   ,       0
N       ,       10004 ,       -70.825       ,       -0.61   ,       0
N       ,       10005 ,       -70.825       ,       -0.36   ,       0
N       ,       10006 ,       -70.825       ,       -0.11   ,       0
Nsel,s,node,,10000,10006
D,all,all,0
ET,4,COMBIN14
R,3,500
!*
KEYOPT,4,1,0
KEYOPT,4,2,1
KEYOPT,4,3,0
!*
TYPE,4
REAL,3
E       ,       3802  ,       10000
E       ,       3812  ,       10001
E       ,       3810  ,       10002
E       ,       3808  ,       10003
E       ,       3806  ,       10004
E       ,       3804  ,       10005
E       ,       3742  ,       10006
```

```
allsel,all
! constrain equation for left and right edge
CE,1,0,3802,UX,1,8317,UX,-1,8323,UX,1,
CE,2,0,3812,UX,1,8327,UX,-1,8323,UX,1,
CE,3,0,3810,UX,1,8325,UX,-1,8323,UX,1,
CE,4,0,3806,UX,1,8321,UX,-1,8323,UX,1,
CE,5,0,3804,UX,1,8319,UX,-1,8323,UX,1,
CE,6,0,3742,UX,1,8257,UX,-1,8323,UX,1,
! There are more than 100 constraint equations used in this simulation. 6 of them are listed here as example.
allsel,all

/SOL
ANTYPE,0
NLGEOM,1
AllSEL,ALL

NSEL,S,node,,4368
D,ALL, ,2.0, , , ,UY, , , , ,
allsel,all
solve
```

REFERENCES

1. Amagai, M., Watanabe, M., Omiya, M., Kishimoto, K., Shibuya, T., "Mechanical Characterization of Sn-Ag-based Lead-free Solders" Microelectronics Reliability, Vol. 42, pp 951-966, 2002
2. Anand, L., "Constitutive equations for hot working of metals", Journal of Plasticity, vol. 1, pp. 213-231, 1985
3. Andrade F. A, Esat. I, Badi. M. N. M, "A New Approach to Time-Domain Vibration Condition Monitoring: Gear Tooth Fatigue Crack Detection and Identification by the Kolmogorov-Smirnov Test", Journal of sound and vibration, vol. 245, pp 909-919, 2001
4. Arra. Minna, Xie Dongji, Shangguan. Dongkai, "Performance of Lead-free Solder Joints under Dynamic Mechanical Loading", Electronic Components and Technology Conference, pp 1256-1262, 2002
5. Barker, D., "Experiments to validate calcePWA vibration damage model with PbSn and SAC305", CALCE project C05-04 final report, Oct, 2005
6. Barker, D. B., Chen, Y. S., and Dasgupta, A., 1993. "Estimating the vibration fatigue life of quad leaded surface mount components." *Journal of Electronic packaging*, vol. 115, pp. 195-200
7. Barker, D. B., Dasgupta, A., and Pecht, M. G., 1991. "PWB solder joint life calculation under thermal and vibration loading." *Proceedings Annual Reliability and Maintainability Symposium*, pp. 451-459
8. Barker D. B, Sidharth. B, "Local PWB and Component Bowing of and Assembly Subjected to a Bending Moment", ASME Journal of Electronic Packaging, vol. 116, pp 92-97, 1994

9. Boresi. A, Schmidt. R and Sidebottom. O, “Advanced Mechanics of Materials”, John Wiley and Sons, 1993
10. Basaran C, Chandaroy R, “Mechanics of Pb40/Sn60 Near-eutectic Solder Alloys Subjected to Vibrations”, Applied Mathematical Modelling, vol. 22, pp 601-627, 1998
11. Basaran, C. and Chandaroy, R., “Thermomechanical analysis of solder joints under thermal and vibration loading.” *Transactions of the ASME*, vol. 124, pp 60-66, 2002
12. Basquin, OH, “The Experimental Law of Endurance Tests”, Proc. ASTM, 1910
13. Bonte, M. H. A., and De Boer, A., “Prediction of Mechanical Fatigue Caused by Multiple Random Excitations”, Proceedings of ISMA, pp 697-708, 2004
14. Clech, J. P., “Lead-free and Mixed Assembly Solder Joint Reliability Trends”, Presented at *IPC Printed Circuits Expo, SMEMA Council APEX, Designers, Summit,* 2004
15. Che F. X, Pang H. L. J, Wong F. L, Lim G. H, Low T. H, “Vibration Fatigue Test and Analysis for Flip Chip Solder Joints”, Electronics Packaging Technology Conference, pp 107-113, 2003
16. Commission of the European Communities, “Proposal for a Directive of the European Parliament and of the Council on Waste Electrical and Electronic Equipment, Document No. 500PC0347(01),” June 13, 2000, <http://europa.eu.int/eur-lex/en/com/dat/2000/en_500PC0347_01> accessed March 16, 2001.
17. Cuddalorepatta. G and Dasgupta. A, “Cyclic Mechanical Durability of Sn3.0Ag0.5Cu Pb-Free Solder Alloy”, Published at ASME International Mechanical Engineering Congress and Exposition, Orlando, FL, Nov, 2005

18. Darbha, K., Ling, S., and Dasgupta, A., 1997. "Stress Analysis of Surface-Mount Interconnections Due to Vibration Loading." *Journal of Electronic Packaging*, Vol. 119, pp. 183-188
19. Darveaux R, Banerji K, "Constitutive Relations for Tin-Based Solder Joint", IEEE Transactions on Components, Hybrid and Manufacturing Technology, vol. 15, No. 6, pp 1013-1023, 1992
20. Hill, R., The Mathematical Theory of Plasticity. Oxford, Clarendon Press, 195
21. Darveaux R, Banerji K, "Constitutive Relations for Tin-Based Solder Joint", IEEE Transactions on Components, Hybrid and Manufacturing Technology, vol. 15, No. 6, pp 1013-1023, 1992
22. Darveaux, R., Banerji, K., Mawer, A., Dody, G., 1995, "Durability of Plastic Ball Grid Array Assembly," Ball Grid Array Technology, Lau, J., Editor, McGraw-Hill, Inc., New York.
23. Dasgupta. A, et al, "Material Failure Mechanisms and Damage Models", A tutorial series containing 14 articles in IEEE Transactions on Reliability, Lead Article Appeared, vol. 40, No. 1, pp 531, 1999
24. Dasgupta, A., Oyan, C., Barker, D., and Pecht, M., "Solder Creep Fatigue Analysis by an Energy-Partitioning Approach", ASME Journal of electronic Packaging, vol. 114, pp 152-160, 1992
25. Darveaux, R., Banerji, K., "Constitutive Relations for Tin-Based Solder Joints," IEEE Transactions on Components, Hybrids, and Manufacturing Technology, Vol. 15 (6), pp 1013-1024, 1992
26. Deepak Dhar, Sharan A. M, Rao J. S, "Transient Stress Analysis and Fatigue Life Estimation of Turbine Blades", Journal of Vibration and Acoustics, vol. 126, pp 485-495, Oct, 2004

27. Dowling, N. E., "*Mechanical Behavior of Material: Engineering Methods for Deformation, Fracture, and Fatigue"* Prentice-Hall, 1999
28. Downing S. D and Socie D. F, "Simplified Rainflow Counting Algorithms", International Journal of Fatigue, vol. 4, No. 1, 1982
29. Hall, P.M., "Creep and Stress relaxation in solder joints. In: Lau JH, editor. Solder Joint Reliability Theory and Applications" New York: Van Nostrand Reinhold, pp. 313, Chapter 10, 1991
30. Hamblin. M, "Fatigue of Cantilevered Pipe Fittings Subjected to Vibration", Journal of Fatigue & Fracture of Engineering Materials & Structures, vol. 26, pp 695-707
31. Haswell, P. and Dasgupta, A., "Viscoplastic Constitutive Properties of Lead-Free Sn-3.9Ag-0.6Cu Alloy," *MRS Proceedings*, San Francisco, CA, 2001
32. Haswell, P. and Dasgupta, A., "Durability Properties Characterization of Sn62Pb36Ag2 Solder Alloy," Proceedings ASME IMECE, EEP-Vol. 28, pp 181-187, Orlando, FL, 2000
33. Haterbouch, M. and Benamar, R., "The Effects of Large Vibration Amplitudes on the Axisymmetric Modes Shapes and Natural Frequencies of Clamped Thin Isotropic Circular Plates. Part II: Iterative and Explicit Analytical Solution for Non-linear Coupled Transverse and In-plane Vibrations", Journal of Sound and Vibration, vol. 277, pp 1-30, 2004
34. Hayward, J., "Lead (Pb)-Free Packaging Strategy 2000−2003", 2000 <www.amd.com>
35. He Xiaoling, Fulton Rober, "Modeling and Simulation of the Dynamic Response of the Electronic Packaging", IEEE Electronic Components and Technology Conference, pp 1535-1547, 2000
36. JEDEC Solid State Technology Association, "JEDEC Announces Lead-free Definition," <http://www.jedec.org/download/search/JESD97.pdf>, accessed September 2002.

37. Jih Edward, Jun Wayne, “Vibrational Fatigue of Surface Mount Solder Joints”, IEEE Intersociety Conference on Thermal Phenomena, pp 246-250, 1998
38. John H. L. Pang, Che F. X, Low T. H, “Vibration Fatigue Analysis for FCOB Solder joints”, Electronic Components and Technology Conference, pp 1055-1061, 2004
39. Krishna J., Mahesh P., and Andrew S., “Mechanical Bend Fatigue Reliability of Lead-free PBGA Assemblies,” International Society Conference on Thermal Phenomena, pp 915-918, 2002
40. Kariya, Y., Morihata, T., Hazawa, E., and Otsuka, M., “Assessment of Low-Cycle Fatigue Life of Sn-3.5mass%Ag-X (X=Bi or Cu) Alloy by Strain Range Partitioning Approach,” Journal of Electronic Materials, Vol. 30(9), pp. 1184-1189, 2001
41. Kim H. Y, “Vibration-Based Damage Identification Using Reconstructed FRFs in Composite Structures”, Journal of Sound and Vibration, vol.259, pp1131-1146, 2003
42. Kim Young-Bae, Noguchi Hiroshi, Amagai Masazumi, “Vibration Fatigue Reliability of BGA-IC package with Pb-free Solder and Pb-Sn Solder”, Electronic Components and Technology Conference, pp 891-897, 2003
43. Kujala, A., Reinikainen, T., Ren, W., 2002, “Transition to Pb-free Manufacturing Using Land Grid Array Packaging Technology.” 52nd Electronic Components and Technology Conference, San Diego, CA, pp 359-364, May, 2002
44. Lau. J et al, “Solder Joint Reliability of Surface Mount Connectors”, Journal of Electronic Packaging, vol. 115, pp 180-188, 1993
45. Lau, J., 1996. “Solder joint reliability of flip chip and plastic ball grid array assemblies under thermal, mechanical and vibration conditions.” *IEEE Transactions on Components, Packaging, and Manufacturing Technology*, Vol, 19, pp. 728-735

46. Lau, J., Gratalo, K., and Schneider, E., 1995. “Solder Joint Reliability of Large Plastic Ball Grid Aray Assemblies under Bending, Twisting, and Vibration Conditions.” *Circuit World*, Vol. 22, pp. 27-32

47. Lau, J., Schneider, E., and Baker, T., 1996. “Shock and vibration of solder bumped flip chip on organic coated copper boards.” *Journal of Electronics Packaging*, Vol. 118, pp. 101-104

48. Lee. W. W, Nguyen. L. T, Selvaduray. G. S, “Solder Joint Fatigue Model: Review and Application to Chip Scale Packages”, Microelectronics Reliability, vol. 40, pp 231-244, 2000

49. Liguore Salvatore and Followell David, “Vibration Fatigue of Surface Mount Technology (SMT) Solder Joints”, IEEE Proceedings Annual Reliability and Maintainability Symposium, pp 18-26, 1995

50. Liu X, Sookala V. K, Verges M. A and Larson M. C, “Experimental Study and Life Prediction on High Cycle Vibration Fatigue in BGA Packages”, Journal of Microelectronics Reliability, vol. 46, pp 1128-1138, 2006

51. Low K. H, Chai G. B, Lim T. M, Sue S. C, “Comparisons of Experimental and Theoretical Frequencies for Rectangular Plates with Various Boundary Conditions and Added Masses”, International Journal of Mechanical Sciences, vol. 40, No. 11, pp 1119-1131, 1998

52. Luan. Jing-En, Tee. Tong Yan, Pek. Eric, Lim. Chwee Teck, Zhong. Zhaowei, “Modal Analysis and Dynamic Responses of Board Level Drop Test”, Electronics Packaging Technology Conference, pp 233-243, 2003

53. Manson, S. S., 1965, *Experimental Mechanics*, Vol. 5, No. 7, pp. 193-226.

54. Matsuiski, M. & Endo, T., Fatigue of metals subjected to varying stress, Japan Soc. Mech. Engrg, 1969

55. Moussaoui F., Benamar R., and White R. G., “The Effects of Large Vibration Amplitudes on the Mode Shapes and Natural Frequencies of Thin Elastic Shell, Part I: Coupled Transverse-Circumferential Mode Shapes of Isotropic Circular Cylindrical Shells of Infinite Length”, Journal of Sound and Vibration, vol. 232, pp 917-943, 2000
56. Norman E. Dowling, “Mechanical Behavior of Material: Engineering Methods for deformation, Fracture, and Fatigue” *Prentice-Hall*, 1999
57. Pang JHL, Tan T, Sitaraman SK, “Thermo-mechanical analysis of solder joint fatigue and creep in a flip chip on board package subjected to temperature cycling loading”, electronic Components and Technology Conference, pp. 878-883, 1998
58. Park, T.-S., and Lee, S.-B., 2002, “Isothermal Low Cycle Fatigue Tests of Sn/3.5Ag/0.75Cu and 63Sn/37Pb Solder Joints under Mixed-mode Loading Cases**,”** *ECTC 2002*, pp. 979-984, Las Vegas, NV.
59. Pitarresi J. M, Akanda A, “Random Vibratoin Response of a Surfance Mount Lead/Solder Joint”, Proceedings of the ASME International Electronics Packaging Conference, Binghamton, New York, 1993
60. Qian, Z., Liu, S., “On the Life Prediction and Accelerated Testing of Solder Joints” EPP Thermo-Mechanical Characterization of Evolving Packaging Materials and Structures Proceedings of the 1998 ASME International Mechanical Engineering Congress and Exposition, vol. 24, pp 1-11, Nov 15-20, 1998
61. Schubert, A., Dudek, R., Doring, R., Walter, H., Auerswald, E., Gollhardt, A., Schuch, B., Sitzmann, H. and Michel, B., 2002b, “Lead-free Solder Interconnects: Characterization, Testing, and Durability,” 3rd Int. Conf. On Benefiting from Thermal and Mechanical Simulation in Micro- Electronics, EuroSIME2002, pp. 74-84, Paris, France, 2002

62. Shah K, Mello M, “Ball Grid Array Solder Joint Failure Envelope Development for Dynamic Loading”, Proceeding of the Electronic Components and Technology Conference, pp 1068-1074, 2004

63. SOLDERTEC, 1999, “Lead-Free Alloys - The Way forward”, <www.lead-free.org>.

64. Song J. M, Lui T. S, Chen L. H and Tsai D. Y, “Resonant Vibration Behavior of Lead-free Solders”, Journal of Electronic Materials, vol. 32, No. 12, 1501-1508

65. Soong, T.T., Grigoriu, Mircea, “Random Vibration of Mechanical and Structural Systems”, Prentice Hall, 1993

66. Stam, F. A., Davitt, E., 2001. “Effects of Thermomechnical cycling on lead and lead-free (SnPb and SnAgCu) Surface Mount Solder Joints.” *Microelectronics Reliability*, Volume 41, Issue 11, pp 1815-1822

67. Steinberg, Dave S, “Vibration Analysis for Electronic Equipment”, John Wiley & Sons, New York, 1998

68. Stolkarts, V., Moran, B, Keer, L.M., “Constitutive and damage model for solders”, Electronic Components and Technology Conference, pp 379-385, June, 1998

69. Susmel. L, Tovo. R, Lazzarin. P, “The Mean Stress Effect on the High-cycle Fatigue Strength from a Multiaxial Fatigue Point of View”, International Journal of Fatigue, vol. 27, pp 928-943, 2005

70. Tu K. N, Zeng. K, “Reliability Issues of Pb-free Solder Joints in Electronic Packaging Technology”, Electronic Components and Technology Conference, pp 1194-1200, 2002

71. Tu P. L, Chan Y. C and Lai K. L, “Effect of intermetallic compounds on Vibration Fatigue of μBGA Solder Joint”, IEEE Transactions on Advanced Packaging, vol. 24, No. 2, pp197-205, 2001

72. Upadhyayula, U., 1999. “An Incremental Damage Superposition Approach for Surface Mount Electronic Interconnect Durability under Combined Temperature and Vibration Environments.” *PHD Thesis*, University of Maryland

73. Upadhyayula, K. and Dasgupta, A., “Guidelines for Physics-of-Failure Based Accelerated Stress Test”, *Proceedings, Reliability and Maintainability Symposium*, pp 345-357, 1998

74. Upadhyayula, K., and Dasgupta, A., "Accelerated Stress Testing of Surface-Mount Interconnects under Combined Temperature and Vibration Loading,” Chapter 12, Pg 189, *Accelerated Stress Testing Handbook for Quality Products in a Global Market*, Eds.: H. A. Chan & P. J. Englert, Pub. IEEE Press (USA) and Wiley Blackwell (UK), 2001

75. Vaynman, S., McKeown, S. A., “Energy-Based Methodology for the Fatigue Life Prediction of Solder Materials,” IEEE Transactions on Components, Hybrids and Manufacturing Technology, Vol. 16, No. 3, pp. 317-323, 1993

76. Wang Hongfang, Zhao Mei, Guo Qiang, “Vibration Fatigue Experiments of SMT Solder Joint”, Journal of Microelectronics Reliability, vol. 44, pp 1143-1156, 2004

77. Whitten, G., “Lead-free Solder Implementation for Automotive Electronics,” ECTC, pp 1410-1415, 2000

78. Wiese, S., Schubert, A., Walter, H., Dudek, R., Feustel, F., 2001a, “Constitutive Behavior of Lead-free Solders vs. Lead-containing Solders – Experiments on Bulk Specimens and Flip-Chip Joints,” ECTC, pp 890-902, Las Vegas, NV, 2001

79. Wirsching, P.H., Paul, H, Paze, Tomas L, Ortiz, Keith, “Random Vibration: Theory and Practice”, New York: John Wiley & Sons, Inc, 1995

80. Wong T. E, Palmieri F. W, Reed B. A, "Durability/Reliability of BGA Solder Joints under Vibration Environment", Electronic Components and Technology Conference, pp 1083-1088, 2000

81. Woodrow, A., "JCAA/JG-PP No-Lead Solder Project: Vibration Test", *Boeing Electronics Materials and Processes Technical Report*, 2005

82. Xu, L., Pang, J. H. L., 2006. "Intermetallic growth studies on SAC/ENIG and SAC/Cu-OSP lead-free solder joints." *Thermal and Thermomechanical Phenomena in Electronics Systems.* Tenth Thermal Intersociety Conference

83. Yang Q. J, Lim G. H, Lin R. M, Yap F. F, Pang H. L. J and Wang Z. P, "Experimental Modal Analysis of PBGA Printed Circuit Board Assemblies", IEEE/CPMT Electronic Packaging Technology Conference, pp 290-296, 1997

84. Yang. Q. J, Pang. H. L. J, Wang. Z. P, Lim. G. H, Yap. F. F, Lin. R. M, "Vibration Reliability Characterization of PBGA Assemblies", *Microelectronics Reliability*, vol. 40, pp 1097-1107, 2000

85. Yang, Q. J., Wang, Z. P., Lim, G. H., Pang, J. H. L., Yap F. F., and Lin, R. M., "Reliability of PBGA Assemblies under Out-of Plane Vibration Excitation." *IEEE Transactions on Components and Packaging Technologies*, Vol. 25, pp. 293-300, 2002

86. Yu Q, Kikuchi H, Ikeda S, Shiratori M, Kakino M, and Fujiware N, "Dynamic Behavior of Electronics Package and Impact Reliablity of BGA Solder Joints", Proceedings of the Intersociety Conference on Thermomechanical Phenomena in Electronic Systems, pp 953-960, 2002

87. Zeng, K., Tu, K.N., "Six Cases of Reliability Study of Pb-free Solder Joints in Electronic Packaging Technology," Materials Science and Engineering R, Vol. 273, pp 1–51, 2002

88. Zhang, Q., “Isothermal Mechanical and Thermo-mechancial Durability Characterization of Selected Pb-free Solders”, PHD Dissertation, University of Maryland, 2004

89. Zhang. Q, Dasgupta. A and Haswell. P, “Isothermal Mechanical Durability of Three Selected Pb-free Solders: Sn3.9Ag0.6Cu, Sn3.5Ag and Sn0.7Cu”, Transaction of the ASME, Vol. 127, pp 512-522, 2005

90. Zhang, Q., Dasgupta, A., Haswell, P., “Viscoplastic Constitutive Properties and Energy-Partitioning Model of Lead-Free Sn3.9Ag0.6Cu Solder Alloy”, ECTC New Orleans, Louisiana, USA, 2003

91. Zhang Q, Dasgupta A and Haswell Peter, “Viscoplastic Constitutive Properties and Energy-Partitioning Model of Lead-free Sn309Ag0.6Cu Solder Alloy”, IEEE Electronic Components and Technology Conference, pp 1862-1868, 2003

92. Zhao, Y., Basaran, C., Cartwright, A., and Dishongh, T., “Thermomechanical Behavior of BGA Solder Joints under Vibrations: an Experimental Observation”, *IEEE Inter Society Conference on Thermal Phenomena*, pp. 349-355, 2000

93. Zhou, Y., Scanff, E., and Dasgupta, A., 2006, “Vibration Durability Comparison of Sn37Pb vs. SnAgCu Solders,” *ASME International Mechanical Engineering Congress and Exposition*, Chicago, IL, paper number 13555

94. Zhou. Y., and Dasgupta, A., 2007. “Vibration durability Assessment of Sn3.0Ag0.5Cu & Sn37Pb Solders under Harmonic Excitation.” *ASME International Mechanical Engineering Congress and Exposition*, Seattle, WA

95. Zhou, Y. and Dasgupta, A., “Vibration Durability Investigation for SnPb and SnAgCu Solders with Accelerated Testing and Modeling” Presented at *IEEE-TC7 Conference on Accelerated Stress Testing & Reliability*, San Francisco, CA, October, 2006

96. Zhou, Y., Moustafa, B. and Dasgupta, A., “Vibration Durability Assessment of Sn3.0Ag0.5Cu & Sn37Pb solder under Harmonic Excitation”, Journal of Electronic packaging, 2008, Accepted for Publication
97. Zhou, Y., Plaza, G., Osterman, M. and Dasgupta, A., “Vibration Durability of SnAgCu (SAC) Solder Interconnects”, Journal of the Institute of Environmental Sciences and Technology (IEST), 2008, Accepted for Publication